



Faculty of Science and Technology

MASTER'S THESIS

Study program/ Specialization: Offshore Technology – Marine and Subsea Technology	Spring semester, 2014 Open
Writer: Lise Eide Wold (Writer's signature)
Faculty supervisor: Professor Ove Tobias Gudmestad	
Thesis title: A study of the changes in freeboard, stability and motion response of ships and semi-submersible platforms due to vessel icing	
Credits (ECTS): 30	
Key words: - Sea-spray icing - Atmospheric icing - Freeboard - Stability - Motion response	Pages: 104 + appendix: 53 Stavanger, 02.06.14

Abstract

There is an increasing demand for energy in the world, and as the traditional fossil fuel supplies are diminishing, it is pushing the oil and gas industry to seek for natural resources in remote and harsh environments. One of these distant and tough environments is in the Arctic region. Vessel icing from both sea-spray icing and atmospheric icing are common in these waters and can impact the safety of a platform or a ship in different ways.

Ice accumulation on vessels contributes to an extra load on the vessel and consequently there will be a change in the freeboard and stability. A reduction in one or both of these parameters can cause a vessel to capsize and sink. There have been numerous accidents in the past where small fishing vessels have capsized due to heavy icing. Scientists have discussed for years whether or not vessel icing is going to be a problem for larger vessel when considering the change in freeboard and stability.

Four different types of vessels were analysed in order to study the effect the ice has on dissimilar vessels, which are a fishing boat, a platform supply vessel, a drillship and a semi-submersible platform. Further, a case study and a parameter study have been undertaken for these vessels. The case study examines an icing event that could occur in the Barents Sea under a winter storm. The parameter study reveals the exact amount of sea-spray ice needed in order to make the vessels unsafe.

The calculated results revealed that icing accumulations had a significant impact on the freeboard, stability and motion response for the vessels. It was also calculated that the smallest ship, the fishing boat, was much more likely to lose its freeboard and stability due to vessel icing. This boat has a length of 23.10 m, which was three times shorter than the platform supply ship and almost ten times shorter than the drillship. However, the calculated amount of ice needed in order to make the two larger ships and the semi-submersible unsafe was so immense that such a situation is considered as highly unlikely to occur.

Further, this work also includes a proposal for further studies that can be done on this subject.

Acknowledgement

This Thesis was done during the spring semester 2014 at the University of Stavanger. There are several people I would like to thank that have helped me and encouraged me throughout the process of writing the report.

First of all I would like to express my thanks and gratitude to my adviser Professor Ove Tobias Gudmestad, who offered me guidance and help throughout the entire work of my Thesis. I would also like to thank Charles Ryerson for being helpful by answering my emails with comprehensive answers.

I would also like to thank my family for helping me during my years of studying and for always being supportive for me. I would also like to thank all of my friends who have motivated me and supported me throughout my education.

Last but not least; I would like to thank my dear boyfriend Espen Knoph, for his support and encouragement during my work with this Thesis.

Table of Contents

Abstract	I
Acknowledgement	II
Table of Contents	III
List of Figures	VII
List of Tables	XI
Abbreviations	XII
Nomenclature	XIII
1. Introduction	1
1.1. Background and Motivation	1
1.1.1. Types of Vessel Icing	3
1.1.2. Ice Accretion on Offshore Vessels	3
1.1.3. Past Incidents with Semi-submersibles and Ships	4
1.2. Scope of Work	5
1.3. Organization of the Thesis	5
2. Literature Review	6
2.1. The Development of the Ship	6
2.2. The Development of the Semi-submersible Platform	8
3. Description of Vessels	9
3.1. Lady of Grace	9
3.2. MV Viking Fighter	10
3.3. DrillMax Ice	11
3.4. West Alpha	12
4. Theoretical Subjects	13
4.1. Icing Literature	13
4.1.1. Types of Ice Accretion	13
4.1.1.1. Sea-Spray Ice, Snow and Sleet Ice	15
4.1.1.2. Frost, Glaze and Rime	15
4.1.2. Vessel Components and Functions	17
4.1.2.1. Stability, Integrity and Fire and Rescue Equipment	17

4.1.2.1. Communication Equipment, Ventilation and Helicopter Pad	17
4.1.2.2. Flare Boom, Handles, Valves and Windows	18
4.1.3. Conditions for Icing and Icing Intensity	18
4.1.4. Area of Ice Accretion on Offshore Vessels	24
4.1.4.1. Area of Icing on Ships	24
4.1.5. Area of Icing on Semi-submersibles	27
4.1.6. Area of Icing on the Four Vessels	28
4.1.6.1. Ice Accumulation on the Lady of Grace Boat	30
4.1.6.2. Ice Accumulation on the Viking Fighter Vessel	31
4.1.6.3. Ice Accumulation on the Drillmax Ice Drillship	32
4.1.6.4. Ice Accumulation on the West Alpha Rig	33
4.1.7. Ice Protection, Prevention and Detection Technologies.....	35
4.1.7.1. Chemicals, Coatings and Design	35
4.1.7.2. Electrical Techniques, Mechanical De-icing and Ice Detection.....	36
4.2. Freeboard of Vessels	37
4.2.1. Freeboard and Buoyancy of a Floating Object.....	37
4.2.2. Freeboard of the Ships	39
4.2.3. Freeboard of the Semi-submersible.....	39
4.2.4. Freeboard of a Vessel With Accumulated Ice.....	41
4.3. Stability of Vessels.....	42
4.3.1. Intact Stability at Small Angles of Heel	42
4.3.1.1. Intact Stability of the Ships	43
4.3.1.2. Intact Stability of the Semi-submersible	43
4.3.1.3. Intact Stability of a Vessel With Accumulated Ice.....	49
4.3.2. Intact Stability at High Angles of Heel	50
4.3.3. Static Heel Angle of a Vessel Due to Asymmetric Load of Ice	51
4.4. Vessel Motion Characteristics.....	54

4.4.1.	The General Vessel Motions	54
4.4.2.	Heave Motion	55
4.4.3.	Pitch Motion	55
4.4.4.	Coupled Heave and Pitch Motion.....	56
4.4.5.	Roll Motion.....	56
4.5.	Natural Periods	58
4.5.1.	General Information About Natural Periods	58
4.5.2.	Natural Period in Heave	58
4.5.2.1.	Natural Period in Heave for the two Ships	59
4.5.2.2.	Natural Period in Heave for the Semi-submersible	60
4.5.3.	Natural Period in Pitch	61
4.5.3.1.	Natural Period in Pitch for Ships.....	62
4.5.3.2.	Natural Period in Pitch for the Semi-submersible	62
4.5.4.	Natural Period in Roll.....	64
4.5.4.1.	Natural Period in Roll for the Two Ships	64
4.5.4.2.	Natural Period in Roll for the Semi-submersible	65
4.6.	Response Amplitude Operators.....	66
5.	Requirements	67
5.1.	Stability Requirements for Ships.....	67
5.2.	Stability Requirements for Semi-submersibles	67
6.	Conditions of the Barents Sea	68
6.1.	General Description.....	68
6.2.	Changes in the Ice Cover	69
6.3.	Environmental Characteristics	69
6.3.1.	Waves	70
6.3.2.	Wind	71
6.3.3.	Air Temperature	73
6.3.4.	Sea Temperature	74

6.4. Polar Lows.....	75
7. Results.....	76
7.1. Freeboard, Stability, Righting arm and Heeling Angle Results.....	76
7.1.1. Results from the Lady of Grace Boat.....	76
7.1.2. Results from the Viking Fighter Vessel.....	78
7.1.3. Results from the DrillMax Ice Drillship.....	79
7.1.4. Results from the West Alpha Semi-submersible Rig.....	81
7.2. Summarization of the Stability Results.....	83
7.3. Motion Response.....	84
7.3.1. Motion Response for the Lady of Grace.....	84
7.3.2. Motion Response for the Viking Fighter.....	87
7.3.3. Motion Response for the DrillMax Ice.....	90
7.3.4. Motion Response for the West Alpha.....	93
7.4. Summarization of the Motion Response Results for the Vessels.....	97
8. Discussion.....	98
8.1. Assumptions.....	98
8.2. Freeboard and Stability Results.....	99
8.3. Righting Arm Results.....	100
8.4. Static Heeling Angle.....	101
8.5. Comparison of the Vessels.....	101
8.6. Motion Response Results.....	102
9. Conclusion.....	104
List of References.....	105
Appendix A - General Arrangement.....	A-1
Appendix B - Added Mass Coefficients.....	A-3
Appendix C - RAO Tables for the Vessels.....	B-4
Appendix D – Conference in Narvik.....	C-8
Appendix E – Calculations.....	D-11

List of Figures

Figure 1.1-1 The countries and seas of the Arctic region (Ernst and Young, 2013)	1
Figure 1.1-2 The sea ice extent averaged in the period from 1979 – 2000 in March and September (Perovich and Richter-Menge, 2009)	2
Figure 1.1-3 Accumulated ice and snow on a ship (Hamilton, 2006).....	3
Figure 2.1-1 The world's oldest ship (Gould, 2011)	6
Figure 3.1-1 The fishing vessel Lady of Grace (USCG, 2008)	9
Figure 3.2-1 The platform supply vessel Viking Fighter (Eidesvik, 2012)	10
Figure 3.3-1 The drilling ship Drillmax Ice (Stena, 2011)	11
Figure 3.4-1 The drilling rig West Alpha (Offshore-technology.com, 2013).....	12
Figure 4.1-1 Rime accumulation on a lattice steel structure (Ryerson, 2013).....	16
Figure 4.1-2 The relationship between the freezing point and maximum density for water with different values of salinity (Bowditch, 2002).....	19
Figure 4.1-3 The dependency of sea temperature and icing rate (Overland, 1990).....	20
Figure 4.1-4 A plot of the calculated algorithm for accumulated ice for four different sea temperatures (Overland, 1990).....	21
Figure 4.1-5 The locations of the Shtokman, Skrugard and Norne fields (Hansen, 2012).....	23
Figure 4.1-6 Icing rates for total wind and wave-spray icing at three different locations (Hansen, 2012)	23
Figure 4.1-7 The direction of the freezing fraction of sea-spray accretion on a ship (Ryerson, 2008) ..	24
Figure 4.1-8 The velocity field over the ship Geosund, measured in m/s (Shipilova et al., 2012).....	25
Figure 4.1-9 The velocity field over the ship Skandi Mongstad, measured in m/s (Shipilova et al., 2012)	25
Figure 4.1-10 Estimated ice accretion rate given in cm/hr (Shipilova et al., 2012).....	25
Figure 4.1-11 Accumulation of ice on a Norwegian fishing boat (Abrahamsen and Johansen, 2000) ..	26
Figure 4.1-12 Areas of icing on a semi-submersible rig (Ryerson, 2011).....	27
Figure 4.1-13 Sea spray icing the columns of a semisubmersible (Ryerson, 2013)	28
Figure 4.1-14 Side view of the assumed ice and snow thickness on the Lady of Grace	30
Figure 4.1-15 Top view of the assumed ice and snow thickness on the Lady of Grace	30
Figure 4.1-16 Side view of the assumed ice and snow thickness on the Viking Fighter vessel	31
Figure 4.1-17 Top view of the assumed ice and snow thickness on the Viking Fighter vessel.....	31
Figure 4.1-18 Side view of icing accretion on the Drillmax Ice	32

Figure 4.1-19 Top view of the Drillmax Ice vessel with the assumed thickness of ice and snow.....	32
Figure 4.1-20 Front view of the West Alpha rig with the assumed ice and snow loads.....	33
Figure 4.1-21 Top view of West Alpha	34
Figure 4.1-22 Side view from the windward side.....	34
Figure 4.1-23 Side view from the opposite side of the wind	35
Figure 4.1-24 Manual de-icing on a crab fishing boat (Deadliest Catch. Man vs. Ice, 2006).	37
Figure 4.2-1 A submerged body in water (Tupper, 2004)	38
Figure 4.2-2 Draft and freeboard of a rectangular vessel.....	38
Figure 4.2-3 The submerged part of the hull structure of West Alpha under operating conditions (Erik Falkenberg, Xu and Odor, 2001).....	40
Figure 4.3-1 Front view of a ship with angles and stability parameters (Tupper, 2004).....	42
Figure 4.3-2 Showing the different vertical parameters.....	44
Figure 4.3-3 The waterline area of the semi-submersible.....	45
Figure 4.3-4 Parameters used in the formula for the centre of gravity, KG	47
Figure 4.3-5 The waterline area of the semi-submersible.....	48
Figure 4.3-6 Figure of a vessel with masses of ice and snow	50
Figure 4.3-7 Stability of a vessel at large angles (Tupper, 2004)	51
Figure 4.3-8 Static heeling angle due to the asymmetric load of sea-spray ice	52
Figure 4.3-9 Parameters of the KG formula before the heeling moment.....	53
Figure 4.4-1 Vessel motion characteristics in a coordinate system (Faltinsen, 1993).....	54
Figure 4.4-2 Roll motion of a ship (Tupper, 2004).....	56
Figure 4.5-1 Different axes for roll and pitch motions	61
Figure 4.5-2 The plane area of the pontoons for the pitch motion.....	63
Figure 4.5-3 The plane area of the pontoons for the roll motion	65
Figure 6.2-1 Time series of the ice area in the Barents Sea from January 1967 to June 2012 (Iden et al., 2012).....	69
Figure 6.3-1 The position of the points from the NORA10 database in the Barents Sea which are used in the study (Iden et al., 2012).....	70
Figure 6.3-2 Wind directions and degrees (BP, 2007).....	72
Figure 6.3-3 The maximum, middle and minimum, as well as 99, 90 and 10 per centile on yearly basis for the period of 1958 – 2011 (Iden et al., 2012).....	73
Figure 6.3-4 The maximum, middle and minimum, as well as 99, 90 and 10 per centile on yearly basis	

for the period of 1958 – 2011 (Iden et al., 2012).....	74
Figure 6.4-1 Frequency point of polar low formations in the Norwegian region (Iden et al., 2012)	75
Figure 7.1-1 Varying freeboard for different thicknesses of sea-spray ice.....	76
Figure 7.1-2 Varying stability for different thicknesses of sea-spray ice	77
Figure 7.1-3 Varying righting arm for different thicknesses of sea-spray ice	77
Figure 7.1-4 Varying freeboard for different thicknesses of sea-spray ice.....	78
Figure 7.1-5 Varying stability for different thicknesses of sea-spray ice	78
Figure 7.1-6 Varying stability for different thicknesses of sea-spray ice	79
Figure 7.1-7 Varying freeboard for different thicknesses of sea-spray ice.....	79
Figure 7.1-8 Varying stability for different thicknesses of sea-spray ice	80
Figure 7.1-9 Varying righting arm for different thicknesses of sea-spray ice	80
Figure 7.1-10 Varying freeboard for different thicknesses of sea-spray ice.....	81
Figure 7.1-11 Varying stability for different thicknesses of sea-spray ice	81
Figure 7.1-12 Varying heeling angle for different thicknesses of sea-spray ice.....	82
Figure 7.3-1 Coupled heave and pitch motion for the Lady of Grace in head sea (0°); blue line is when ice is included, red line when there is no ice	85
Figure 7.3-2 Coupled heave and pitch motion for the Lady of Grace in waves with direction of 45° with the vessel; blue line is when ice is included, red line when there is no ice.....	85
Figure 7.3-3 Coupled heave and pitch motion for the Lady of Grace in beam sea (90°); blue line is when ice is included, red line when there is no ice	86
Figure 7.3-4 Roll motion for the Lady of Grace in waves with direction of 45° with the vessel; blue line is when ice is included, red line when there is no ice.....	86
Figure 7.3-5 Roll motion for the Lady of Grace in beam sea (90°); blue line is when ice is included, red line when there is no ice	87
Figure 7.3-6 Coupled heave and pitch motion for the Viking Fighter in head sea (0°); blue line is when ice is included, red line when there is no ice	88
Figure 7.3-7 Coupled heave and pitch motion for the Viking Fighter in waves with direction of 45° with the vessel; blue line is when ice is included, red line when there is no ice.....	88
Figure 7.3-8 Coupled heave and pitch motion for the Viking Fighter in beam sea (90°); blue line is when ice is included, red line when there is no ice	89
Figure 7.3-9 Roll motion for the Viking Fighter in waves with direction of 45° with the vessel; blue line is when ice is included, red line when there is no ice.....	89
Figure 7.3-10 Roll motion of the motion for the Viking Fighter in beam sea (90°); blue line is when ice is included, red line when there is no ice.....	90
Figure 7.3-11 Coupled heave and pitch motion for the DrillMax Ice in head sea (0°); blue line is when	

ice is included, red line when there is no ice	91
Figure 7.3-12 Coupled heave and pitch motion for the DrillMax Ice in waves with direction of 45° with the vessel; blue line is when ice is included, red line when there is no ice	91
Figure 7.3-13 Coupled heave and pitch motion for the DrillMax Ice in beam sea (90°); blue line is when ice is included, red line when there is no ice	92
Figure 7.3-14 Roll motion for the DrillMax Ice in waves with direction of 45° with the vessel; blue line is when ice is included, red line when there is no ice.....	92
Figure 7.3-15 Roll motion for the DrillMax Ice in beam sea (90°); blue line is when ice is included, red line when there is no ice	93
Figure 7.3-16 Coupled heave and pitch motion for West Alpha in head sea (0°); blue line is when ice is included, red line when there is no ice	94
Figure 7.3-17 Coupled heave and pitch motion for West Alpha in waves with direction of 45° with the rig; blue line is when ice is included, red line when there is no ice	94
Figure 7.3-18 Heave motion for West Alpha in 90° sea; blue line is when ice is included, red line when there is no ice.....	95
Figure 7.3-19 Roll motion for West Alpha in waves with direction of 45° with the rig; blue line is when ice is included, red line when there is no ice.....	95
Figure 7.3-20 Roll motion for the West Alpha rig in beam sea (90°); blue line is when ice is included, red line when there is no ice	96

List of Tables

Table 4.1-1 Joint safety impacts by rig component and ice type (Ryerson, 2009)	14
Table 4.1-2 Different ice action cases (NORSOK N003, 2007)	19
Table 4.1-3 Rate of icing (Overland, 1990)	22
Table 5.1-1 Stability requirements for a ship (DNV, 2005)	67
Table 5.2-1 Stability requirements for semi-submersible (DNV, 2013).....	67
Table 6.3-1 Wave height frequency with corresponding peak periods in the Barents Sea (Iden et al., 2012).....	71
Table 6.3-2 Wind speed frequencies in the Barents Sea (Iden et al., 2012)	72
Table 6.3-3 The maximum and minimum temperatures in °C (Iden et al., 2012)	73
Table 6.3-4 The maximum and minimum temperatures (Iden et al., 2012)	74
Table 7.2-1 Results from the case study	83
Table 7.2-2 Results from the parameter study showing the amount of ice (given in m) needed in order to make to no longer fulfil DNVs requirements	83
Table 7.3-1 Calculated natural periods for the Lady of Grace boat	84
Table 7.3-2 Calculated natural periods for the Viking Fighter vessel	87
Table 7.3-3 Calculated natural periods for the DrillMax Ice	90
Table 7.3-4 Calculated natural periods for West Alpha.....	93
Table 7.4-1 Maximum displacement and angle results for the vessels	97
Table 8.6-1 Analytical added mass coefficients	B-3
Table 8.6-1 Detemining the <i>CA</i> coefficient.....	B-3
Table 8.6-2 The added mass coefficient and formula for <i>AR</i>	B-3
Table 8.6-1 The displacement RAOs at 0° for a standard flat-bottom ship	C-4
Table 8.6-2 The displacement RAOs at 45° for a standard flat-bottom ship	C-5
Table 8.6-3 The displacement RAOs at 90° for a standard flat-bottom ship	C-5
Table 8.6-4 Displacement RAO at 0° for a standard semi-submersible	C-6
Table 8.6-1 Displacement RAO at 45° for a standard semi-submersible	C-7
Table 8.6-2 Displacement RAO at 90° for a standard semi-submersible	C-7

Abbreviations

CFD	Computational Fluid Dynamics
DNV	Det Norske Veritas
PSV	Platform Supply Vessel
NCS	Norwegian Continental Shelf
NSG	NorSea Group
RAO	Response Amplitude Operator

Nomenclature

A_{33}	Added mass in heave
A_{330}	Added mass for a flat plate
A_{44}	Roll added moment of inertia
A_{55}	Pitch added moment of inertia
A_p	Area of submerged part of object that is projected on a horizontal plane
A_W	Water plane area of the vessel
\overline{BM}	Distance from the point of buoyancy to the metacentre (transverse)
\overline{BM}_{ice}	Distance from the point of buoyancy to the metacentre when ice and snow loads are included (transverse)
\overline{BM}_{pitch}	Distance from the point of buoyancy to the metacentre (longitudinal)
b_p	Breadth of the pontoons
$b_{r.c}$	Breadth of the rectangular columns
b_v	Breadth of the vessel
$b_{x.ice}$	Breadth of the ice
$b_{x.snow}$	Breadth of the snow
d_{ice}	Draft of the vessel when the ice and snow loads are included
d_{semi}	Draft of the semi-submersible
d_v	Draft of the vessel
F_B	Buoyancy force
F_G	Gravitational force
f_{semi}	Freeboard of the semi-submersible
f_v	Freeboard of the vessel
g	Gravitational acceleration
GG_1	Difference in KG horizontally due to the sea-spray ice
\overline{GM}	Metacentric height (transverse)
\overline{GM}_{ice}	Metacentric height when ice and snow loads are included

	(transverse)
\overline{GM}_{pitch}	Metacentric height (longitudinal)
\overline{GZ}	Righting arm
h_{all}	Total height of the columns
h_{level}	Height from the keel to where the ice has accreted
$h_{maindeck}$	Height of the main deck
h_p	Height of the pontoons
h_v	Height of the vessel
$h_{c.wl}$	Submerged height of the columns
I_r	Roll mass moment of inertia (transverse)
I_{semi}	Second moment of inertia for the semi
k	Stiffness
\overline{KB}	Center of buoyancy (vertically)
\overline{KG}	Center of gravity (vertically)
\overline{KG}_{ice}	Center of gravity when ice and snow loads are included (vertically)
$KG_{H.old}$	Initial center of gravity (horizontally)
$KG_{H.new}$	New center of gravity (horizontally)
l_b	Length of the bracings
l_p	Length of the pontoons
$l_{r.c}$	Length of the rectangular columns
l_v	Length of the vessel
$l_{x.ice}$	Length of the ice
$l_{x.snow}$	Length of the snow
M_r	Righting moment
m_{semi}	Mass of the semi-submersible
m_v	Mass of the vessel
$m_{x.ice}$	Total mass of ice on the vessel

r_b	Radius of the bracings
$r_{c.c}$	Radius of the cylindrical columns
r_r	Mass radius of gyration
$u_{coupled}$	Coupled heave and pitch displacement
u_{heave}	Heave displacement
u_{pitch}	Pitch displacement
$V_{c.c}$	Volume of one cylindrical column
V_{deck}	Volume of the deck
$V_{derrick}$	Volume of one of the four plates of the derrick
$V_{r.c}$	Volume of one rectangular column
T_a	Air temperature
T_f	Freezing point of seawater
T_{heave}	Natural period in heave
$T_{heave.ice}$	Natural period in heave when ice and snow loads are included
$T_{0,p}$	Natural period in pitch
$T_{0,r}$	Natural period in roll
t_{ice}	Thickness of the sea-spray ice
t_{snow}	Thickness of the snow
T_w	Sea temperature
$x_{BM.c.c}$	Distance from the center to the middle of the column
$x_{BM.r.c}$	Distance from the center to the middle of the column
$x_{c.c}$	The horizontal distance from the center of the cylindrical column and the y-axis
$x_{derrick}$	Horizontal distance from the center of the derrick to the y-axis
$x_{r.c}$	Horizontal distance from the center of the rectangular column and the x-axis
y_{all}	Vertical gravity distance from the pontoons to the columns
y_b	Vertical gravity height of the braces
y_{deck}	Vertical gravity distance from the pontoons to the deck

$y_{derrick}$	Vertical distance from the center gravity of the derrick to the bottom of the rig
y_{subm}	Vertical distance from the center of gravity of the submerged part of the component
y_p	Vertical distance from the center gravity of the pontoons
z_x	Vertical distance from the keel of the vessel and to the center of the gravity of the ice or snow load
∇	Submerged volume of the vessel
$\nabla_{Bracings}$	Submerged volume of the bracings
$\nabla_{c.c}$	Submerged volume of the cylindrical columns
$\nabla_{Pontoons}$	Submerged volume of the pontoons
$\nabla_{r.c}$	Submerged volume of the rectangular columns
∇_{semi}	Submerged volume of the semi-submersible
λ	Factor between height of object and area of submerged part
ρ_w	Density of the sea water
ρ_{ice}	Density of the ice
ρ_{snow}	Density of the snow
$\omega_{0.h}$	Natural frequency in heave
$\omega_{0.h.ice}$	Natural frequency in heave when ice and snow loads are included
$\omega_{0.p}$	Natural frequency in pitch
$\omega_{0.p.ice}$	Natural frequency in pitch when ice and snow loads are included
$\omega_{0.r}$	Natural frequency in roll
$\omega_{0.r.ice}$	Natural frequency in roll when ice and snow loads are included
$\varphi_{p.amplitude}$	Amplitude of pitch motion
φ_r	Roll angle
$\varphi_{r.amplitude}$	Amplitude of roll motion

1. Introduction

This Thesis deals with vessel icing and changes in freeboard, stability and motion response due to accumulated ice. The purpose was to reveal whether or not vessel icing could be dangerous because of the changes in freeboard and stability. Another aim of the report was to discover and compare the different results from several types of vessels.

In the following section, background and motivation for the Thesis will be given, followed by information on types of vessel icing, ice accretion on offshore vessels, past incidents with semi-submersibles and ships due to heavy icing, scope of work, and lastly there will be a description of the organization of the report.

1.1. Background and Motivation

There is an increasing demand for energy in the world, and as the traditional fossil fuel supply are diminishing, it is pushing the oil and gas industry to seek for natural resources in remote and harsh environments. One of these distant and tough environments is the Arctic region, where recent estimates has shown that this area can hold 13% of the world's undiscovered oil reserves, and 30% of the worlds unexplored natural gas. In the report by Ernst and Young (2013), it is mentioned that the total estimate of the potential Arctic oil and gas resources is 412 billion barrel of oil equivalent, where the Norwegian Barents Sea is estimated to comprise 12% of these reserves. It is also estimated that Russia holds more than half of the total oil and gas resources in the Arctic. Some of the greatest challenges in operating in the Arctic will be the winter darkness, vast distances, moving sea-ice and inclement weather.

Ernst and Young (2013) mentioned that the Arctic region consists of eight countries in total: Norway, Denmark, Sweden, Finland, Russia, Iceland, the United States and Canada. However, Sweden and Finland are the only countries out of these without jurisdictional claims in the Arctic Ocean, as these countries do not border the ocean. This can also be seen in Figure 1.1-1 below.



Figure 1.1-1 The countries and seas of the Arctic region (Ernst and Young, 2013)

Norway is the fifth-largest oil exporter and the second-greatest exporter of natural gas in the world. The Norwegian authorities opened the Barents Sea in the Arctic for exploration in 1981, which was the same year that the Snøhvit natural gas field was discovered (Ernst and Young, 2013).

In the 1990's, Statoil participated in exploration drilling activities in the Russian sector of the Barents Sea. In more recent years, Statoil has participated in exploring the Shtokman gas field, situated 600 km from the Kola Peninsula, with Total and Gazprom. Ernst and Young (2013) wrote that both the Russian Government and the Norwegian Government has yet not agreed on the border at the south side Barents Sea. Both countries would like to own this area, as potential oil and gas reserves have been estimated near this border. About two-thirds of the Arctic region consists of ocean waters, and the remaining part is covered by land. Half of the ocean waters are typically deeper than 500 meters; the other part comprises of the offshore continental shelf with waters generally less than 500 meters.

The polar ice cap is at its maximum extent in March and at its minimum extent in September. Seen from Figure 1.1-2, the Barents Sea is not covered by the polar ice cap any time of the year, which allows a great area of open waters. Open waters increase the risk of the unfavourable phenomenon of sea-spray icing on vessels.

Sea-spray icing depends largely on the temperature, wave height and wind speed. The distance from the Norwegian shore to the polar ice cap is much larger than some other areas in the Arctic, representing a longer fetch length¹, and therefore the wind speeds and waves can be greater in this area. This again will intensify the vessel icing by sea-spray in this area.

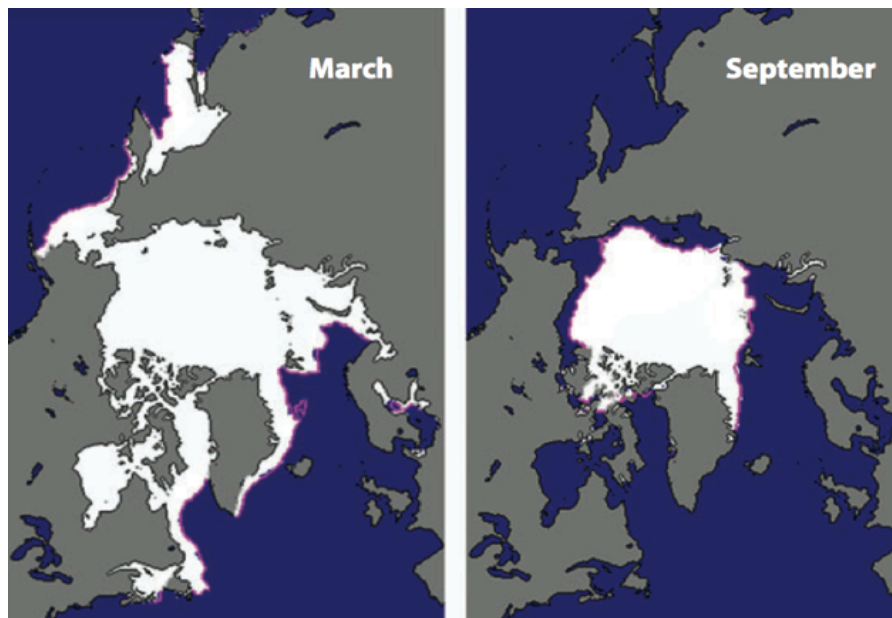


Figure 1.1-2 The sea ice extent averaged in the period from 1979 – 2000 in March and September (Perovich and Richter-Menge, 2009)

¹ The horizontal distance along open water over which the wind blows and generates waves.

Another issue regarding sea-spray icing in the Arctic is the decrease of the polar ice cap. A research paper written by Stroeve et al. (2012) stated that the global climate changes has caused the polar ice cap to decrease significantly the recent years. This could cause an even greater probability of marine icing in the future, due to the enlarged fetch length (Young, Zieger and Babanin, 2011).

1.1.1. Types of Vessel Icing

There are essentially two main categories of vessel icing; atmospheric icing and sea-spray icing. The atmospheric icing consists of freshwater and is a result from precipitation and lay upon the vessel in the shape of snow, moisture or freezing rain. The sea-spray icing is the most dangerous source of icing, and is produced by the breaking waves against the vessels hull. Mentioned by Andreas and Jones (2009), the main source of ice accumulations on offshore installations comes normally from sea-spray. It consists of seawater with lower density than atmospheric icing, and is generated from the sea under environmental conditions with strong winds, cold air temperature, waves and low sea temperature (NORSOK N-003, 2007). Sea-spray ice and snow accumulation on a ship is shown in the Figure 1.1-2 below.



Figure 1.1-3 Accumulated ice and snow on a ship (Hamilton, 2006)

1.1.2. Ice Accretion on Offshore Vessels

Superstructure icing can result in great accumulation of ice on marine vessels, where most of the accreted ice is usually generated by sea-spray. The sea-spray is usually generated under pitching and heaving movement of the vessel moving through the waves. Vessel icing can also cause great heeling when most of the ice accretes on the windward side. It is a highly unfavourable phenomenon that can cause hazardous situations such as loss of vessel stability, loss of freeboard, navigation trouble, blocked and frozen escape routes, slippery gangways and ladders, frozen valves and equipment, and more. It is also expected to reduce the efficiency of an operation. These situations could lead to the loss of a vessel, loss of lives, personal injuries, asset damages and even damage to the environment.

1.1.3. Past Incidents with Semi-submersibles and Ships

Nauman (1984) provided information about an icing incident for a semi-submersible, Ocean Bounty, during the winter of 1979 – 1980, when it experienced six storms during a 121-day period offshore. The sea-spray caused ice as high as 30 meters on the structure, in waves between 3.0 to 9.4 m, and in varying temperatures from - 2.2 C° to - 20.5 C°. The indicated accumulations of ice thickness varied from 5 – 25 cm each day. At one point, the weight of the accumulated ice, estimated to be 500 tons, was so immense that drilling mud had to be offloaded to prevent the vessel from losing its freeboard (Andreas and Jones, 2009).

Another incident with heavy icing on a semi-submersible was on the Sedco 708 in January 1983. The incident occurred during a storm lasting for five days on the North Aleutian Shelf outside Alaska. It was mentioned in a report by Minsk (1984) that the estimated ice load was 30 tons. It had a maximum ice thickness of 13 cm on the diagonal trusses on the under-structure, while on the main columns there were only measured an ice thickness of 3 cm.

In September 2012 there was an incident in the Barents Sea where a semi-submersible, named Scarabeo 8, heeled 5.7 degrees because seawater had unintentionally entered a ballast tank. Within an hour the tank was emptied and the semi-submersible was stabilized. This was reported to be a very frightening experience for the personnel who also had prepared for evacuation. However, the Norwegian Petroleum Safety Authority claimed that it was no danger that this rig would capsize and sink as it was designed to stand 21 degrees listing if the rig was undamaged, and 17 degrees if the rig was damaged (Hovland, 2012).

There are many documented incidents caused by heavy icing on ships, especially small fishing boats. An example of this is the tragedy that occurred in the U.S. in 2007 with the small fishing boat, Lady of Grace, claiming the lives of all four persons aboard (USCG, 2008). There was so much accumulated ice on the boat that the stability was lost and therefore she capsized and sank. This boat will also be used in the analysis in this report due to its history, and the amount of sea-spray ice needed to make it unstable will be calculated.

Another occurrence involving icing on a bigger ship was the M/S Anna Broere, which was abandoned in the Baltic on New Year's Eve in 1978 due to heavy icing. Another event where a vessel were lost is the British trawler Gaul, which went down in 1974, off the North Cape of Norway, claiming the lives of 36 people onboard (Perez-Rojas, 2008). Some researchers believe that heavy icing caused this accident, and others believe there were other reasons.

Bowditch (2002) writes that water splashing near shore is increased by two to four times compared to open seas. According to Kultashev (1976, cited in Efimov 2012, p.23), an investigation on lost vessels shows that 71 % of the incidents happened near shore, while 26 % of the occurrences happened in open seas. This indicates that there is a greater danger for heavy ice accumulations on vessels in waters close to the shore.

Some scientists believe that vessel icing is not going to be a problem for larger vessels that will be used in cold climate areas such as the Barents Sea or the Arctic in general, while others believe that icing could be a great danger for these vessels.

1.2. Scope of Work

The scope of this Thesis was to discover whether or not vessel icing is likely to be a problem when considering the changes in the freeboard, stability and motion response due to this. Four different types of vessels have been analysed for that purpose. A case study and a parameter study will be calculated for these vessels. The case study will examine an icing event that is considered as likely to occur in the Barents Sea. The parameter study will discover the exact amount of sea-spray ice needed in order to make the vessels unsafe.

In this report the drawing program SketchUp Pro, has been used to make some drawings of the vessels. For the calculations, both Excel and Maplesoft have been used. There will not be performed any experimental tests like field test or a tank test due to the limiting working time of one semester.

1.3. Organization of the Thesis

In chapter 2, a review of the development of ships and semi-submersibles will be presented.

In chapter 3, the four different vessels will be described and some technical dimensions will be presented.

Theoretical subjects will be presented in chapter 4, where the section is divided into six main parts; icing literature, freeboard of vessels, stability of vessels, vessel motion characteristics, natural periods and the response amplitude operators.

Chapter 5 shall provide information about requirements given by Det Norske Veritas (DNV) regarding the minimum freeboard and stability for ships and semi-submersibles. These requirements are essential to this Thesis, as they will be used to determine whether the vessels are considered safe or not to use.

The different challenges due to the meteorological conditions of the Barents Sea will be presented in chapter 6. There will also be provided a set of statistical data of the different air and water temperatures, wind speeds, wave heights and wave periods to be used in the calculations.

The results of the calculations will be presented in chapter 7. A discussion of these results will be done in chapter 8.

Finally, in chapter 9, concluding remarks are given which would highlight the most important findings.

2. Literature Review

In this chapter there will be a review of the development of the ship and the semi-submersible platform.

The chapter is divided into two sections. The first section regards the development of the ship from the first ones built and to those built today. There will also be a description of future ship projects. The second section will describe the development of the semi-submersible platform.

2.1. The Development of the Ship

Marine archaeologists have found evidence that ships were built in Egypt for as long as 4500 years ago (Gould, 2011). The ships were assembled with a hull made of wooden planks, and the planks were lashed together by woven straps. The world's oldest ship yet known is the royal ship of Cheops, which was made around 1600 BC, see Figure 2.1-1 below.



Figure 2.1-1 The world's oldest ship (Gould, 2011)

In the 14th century, the use of wooden ships was common in many countries around the world. During the 15th century, one of the world's first iron-clads, named Tekkosen, was developed in Japan (Gould, 2011).

Until the late 19th century, ship design was fairly unchanged. It was during the Second Industrial Revolution, in the transition years from 1840 to 1870, that new mechanical methods were introduced on ships. Some of these methods were the propulsion system and the ability to construct ships from metal, which triggered an immense growth in different ship design, and ships were then built for entirely new functions. These could be ships made for rescue, fire extinguishing, supplying services, research, drilling and more.

In the late 1940s the first drillship was built. It was a surplus U.S Navy Patrol craft produced to overcome water depth challenges in the Pacific Ocean. The vessel was equipped with cantilevered drilling equipment. The next drillship that was built was constructed with a moon pool and an on-board drilling derrick.

In 1972 the first dynamic positioning drillship was used, which was a European drillship named Pelican. The drillship had success in drilling and testing of several wells in different seas; the Mediterranean, Labrador and the North Sea, which led to the design of higher performance ships in the same family (Steel, 2004). From that time the use of drillships around the world were comprehensively taken into use, and many more were constructed.

Another type of vessel that is often used in the oil and gas industry is the platform supply vessel (PSV). The PSVs are usually 45 – 76 m long, but some also exceed 100 m in length. The supply vessels are used to supply offshore platforms and for most of these vessels their primary function is to transport personnel and goods from and to offshore platforms (Ryerson, 2008).

It was mentioned by Ryerson (2008) that both fishing and supply vessels are the type of boats which have the highest risk of superstructure icing, and may experience the greatest danger due to ice accretion. The reason for this is the great amounts of equipment on decks, which lower the center of gravity and the freeboard.

The drillship, Noble Discoverer, was made in 1979 and later winterized for service in the Arctic. In recent years, the need for vessels to be used in cold areas has increased and winterization of vessels has become more common.

Several ships have also been designed and built specifically to operate in icy areas such as the Arctic Ocean. The DrillMax Ice, which is owned by Stena Drilling, is an example of this (Stena, 2011). It is a quite new vessel that was taken into use in 2012. It is also one of the four vessels that will be analysed in this report.

Aleksey Chirikov is an offshore supply vessel which was specially designed for the extreme environmental conditions in the Arctic (Mainwaring, 2013). It should be capable to operate in drifting ice up to 1.7 meters and in environments as cold as -35°C . Another example of a ship that is specifically built to operate in icy areas is the Polarcus Amani, which is a 3D seismic vessel with ice class ICE 1A. This means that it is prepared for extreme ice conditions with floating ice up to 1.0 meter. It was delivered in March 2012 by the Norwegian ship constructor Ulstein.

Another supply vessel that was delivered in 2012 and planned to operate in the Barents Sea is the Viking Fighter, which is owned by NorSea Group (NSG). This vessel will also be analysed in this Thesis.

There are many future projects regarding Arctic ships, one of them is a Statoil-owned arctic drilling vessel, Inocean CAT-1. It shall have an ice-strengthened hull suitable to operate in ice-infested waters, with ice up to 1.2 meters high (Mainwaring, 2013). Two other vessels, NanuQ 5000 DP and NanuQ 5000, turret moored, are two drilling vessels that will be built to operate in the Arctic (Taraldsen, 2013). They are going to be winterized and suitable for year-round operations in the Arctic, and shall be able to be operated in waters in depths up to 1500 meters.

2.2. The Development of the Semi-submersible Platform

The first semi-submersible rig, named Blue Water Rig No.1, arrived by coincidence in 1961, where the Blue Water Drilling Company was the owner. It had four columns, and was used for drilling in the Gulf of Mexico for Shell. It carried too much weight and was not able to carry the topside at the designed draft due to insufficient buoyancy. Some of the main advances discovered by this semi-submersible were the large deck area with the ability to carry heavy topside and the favourable motion characteristics (Gallala, 2013). The Ocean Driller was the first purpose-built drilling semi-submersible, and was launched in 1963. In 1966 and 1967 three more semi-submersibles were made by ODECO (Maung, 1974).

The first self-propelled semi-submersible was constructed in 1971 by ODECO, and due to the success of these platforms, the development of this type of rig increased rapidly (Ismail et al., 2014).

An ice resistant semi-submersible was developed and a model was tested in a model tank in 1983 (Maung, 1974). The test revealed that the ice loads were underestimated, and to minimize the ice interaction and accumulation, attention was brought to induce no bracings through the water plane area.

The Ocean Bounty was a drilling rig made to operate in cold climates, and in 1979 it was recorded so much ice accumulation on the rig that drilling mud had to be offloaded in order to maintain the rig stability. Another semi-submersible that was purposely built for drilling in cold areas is the Kulluk, a conical-shaped rig owned by Shell, which was built in 1983 and was in use in the Chukchi Sea in the Arctic in 2012.

Today, there are several semi-submersibles in use in cold areas in the north, and the need for more rigs in these areas is increasing. It is an issue that can be solved by building more rigs purposely for icy areas, or to winterize old ones.

Winterizations of rigs can be done in different shipyards around the world. In Norway, winterizations have been done in a shipyard near Ølen. This was done for the semi-submersible Scarabeo 8, in 2011, which is now capable of operating in temperatures down to -20°C . Another rig they winterized in the spring of 2014 is the West Alpha, which also will be analysed in this report (Wright, 2000).

In 2009, Aker solutions delivered two semi-submersibles, type Aker H-6e, named Aker Spitsbergen and Aker Barents. Mentioned by Økland (2012), these platforms are likely the world's biggest and most advanced drilling semisubmersibles. They were specially designed to meet the high environmental standards in the Barents Sea, and are able to drill at depths from 100 to 3000 m in harsh environments.

3. Description of Vessels

In this chapter there will be a description of four different vessels that will be analysed for situations with ice accumulations. One of these vessels has been used for fishing purposes before it sank due to heavy icing in 2007. The other three vessels that are described are used in the oil and gas industry.

In section 3.1, will be a description of the fishing vessel Lady of Grace. Information about a platform supply vessel, Viking Fighter, will be given in the next section. Section 3.3 provides information about Drillmax Ice, a drillship with an ice class that makes it suitable to operate in the Arctic, which includes the Barents Sea. In the last section of the chapter (in section 3.4) will be provided information about a semi-submersible drilling platform, West Alpha.

3.1. Lady of Grace

The Lady of Grace (shown in Figure 3.1-1) was a fishing boat owned by the Santos Fishing Corporation. In January 2007, it sank due to heavy icing in the Nantucket Sound, outside the U.S. coast, claiming the lives of all four persons aboard (USCG, 2008).



Figure 3.1-1 The fishing vessel Lady of Grace (USCG, 2008)

Principal dimensions (USCG, 2008):

Length o.a.	25.50 m
Length w.l.	23.10 m
Height to main deck	3.41 m
Breadth mld	6.70 m
Deadweight	153 MT

3.2. MV Viking Fighter

The MV Viking Fighter platform supply vessel (shown in Figure 3.2-1) is owned by the NorSea Group (NSG). It is a ship that was designed by STX OSV with a deck area of 840 m², which is planned to work in the Barents Sea and the North Sea (Ship-technology, 2012). The engines, propulsion and hull are designed with advanced catalyst machineries, which result in less emission to air and a low fuel consumption. The vessel has also been developed with advanced fire-fighting equipment and equipment for recovering oil in case of a spill.



Figure 3.2-1 The platform supply vessel Viking Fighter (Eidesvik, 2012)

Principal dimensions (Eidesvik, 2012):

Length o.a.	81.70 m
Length w.l.	74.00 m
Height to main deck	7.80 m
Breadth mld	18.00 m
Deadweight	4000 MT
Maximum speed	16 knots

More technical information for this vessel is shown in the general arrangement drawing that is given in Appendix A. The general arrangement drawing has also been given on the CD in the back of the report in order to get a closer look on the vessel dimensions.

3.3. DrillMax Ice

The DrillMax Ice (shown in Figure 3.3-1) is a drilling vessel owned by Stena Drilling. It is the world's first dynamically positioned dual ice-class +1A1 drillship, which makes it capable to operate under Arctic conditions. It was constructed by Samsung Heavy Industries in South Korea and was released in the first quarter of 2012 (Iden et al., 2012).

It has a ice class hull of Polar Class 4, which means that it the hull is re-enforced with a band of steel between 6.5 and 14.0 metres above the baseline (Stena, 2011). It should be capable of surviving a significant wave height of 16.0 m and wind speeds up to 41.0 m/s.

The maximum environmental conditions for when the vessel can drill is up to a significant wave height of 6.7 m and wind speeds up to 27.0 m/s. It is also able to perform drilling operations in water depths from 250 m to 3000 m. The vessel has to be supported by icebreakers carrying out ice management in order to get a controlled environment under transit and drilling operations.



Figure 3.3-1 The drilling ship Drillmax Ice (Stena, 2011)

Principal dimensions (Stena, 2011):

Length o.a.	228.4 m
Length b.p.p	219.4 m
Breadth	42.0 m
Height	19.0 m
Operational draft, mid.	12.0 m
Displacement	98000 MT
Variable deck load drilling/survival	15000 MT
Transit speed	12 knots

3.4. West Alpha

West Alpha is a semi-submersible drilling rig (shown in Figure 3.4-1) owned by North Atlantic Drilling. It was built in 1986 and is one of the oldest drilling rigs still in use today. It is able to operate in depths between 60 to 600 m, with a drilling depth of 7000 m (Seadrill, 2009). The platform is able to accommodate up to 110 persons and move at a maximum transit speed of 5 knots.

Mentioned by Økland (2012), the Westcon Group has winterized the vessel for Arctic conditions in the Spring 2014 in Ølen, Norway.

The rig is planned to drill for ExxonMobile in the Kara Sea during fall of 2014, which is on the Russian shelf. The Kara Sea is covered in ice most times of the year where the temperature usually varies $-2\text{ }^{\circ}\text{C}$ to $-23\text{ }^{\circ}\text{C}$ during the summer.



Figure 3.4-1 The drilling rig West Alpha (Offshore-technology.com, 2013)

Principal dimensions (Offshore.no, 2014):

Breadth	66.00 m
Air gap	22.00 m
Operational draft	21.50 m
Length of pontoons	89.00 m
Width of pontoons	13.00 m
Height of pontoons	12.50 m
Length of deck structure	70.00 m
Width of deck structure	66.00 m
Total height to top derrick structure	108.50 m
Operating displacement	30731 MT

More technical information for this rig is shown in the general arrangement drawing given in Appendix A. The general arrangement drawing has also been given on the CD in the back of the report in order to get a closer look on the vessel dimensions.

4. Theoretical Subjects

In the following chapter, different theoretical subjects will be described for the purpose to get an understanding on what have been considered in the calculations and how the calculations have been conducted. For this purpose the chapter has been divided into six subjects; icing literature, freeboard of vessels, stability of vessels, vessel motion characteristics, natural periods and response amplitude operators.

4.1. Icing Literature

This section is divided into six parts where the first, section 4.1.1, describes the types of icing that accretes on offshore vessels. This is important to be aware of, as each type of ice will have different impacts on a vessel regarding the amount of ice and the location of the accretion. The most important functions of the vessel and equipment can be destroyed or deteriorated by the ice. This is further described in section 4.1.2. A description of the environmental conditions needed in order for vessel icing to occur is given in section 4.1.3. Information about different icing rates and intensities will also be given in this section. The area of ice accretion on ships and semi-submersibles will be explained in section 4.1.4. In section 4.1.5 the area of icing on the four vessels will be showed with figures. Lastly, section 4.1.6, presents the different methods for ice protection, prevention and detection technologies that are being used today.

4.1.1. Types of Ice Accretion

Vessel icing can be divided into two categories; sea-spray icing and atmospheric icing. The main difference in composition from those two is that sea-spray icing is generated by the sea, and therefore it contains saltwater, while the atmospheric icing comes from different types of precipitation and contains freshwater.

According to Cammaert (2013), sea-spray icing can be formed in two different ways. One way is when the vessel interacts with the waves and from this the sea spray is generated. Another way is when sea-spray is formed when the wind blows droplets of sea water off wave crests, which are also called spume. The amount of spume generated on deck will depend largely on wind speed and steepness of the waves.

Atmospheric icing can be described as precipitation given in different deposits. The atmospheric icing can be divided into different types of icing, which are based on the characteristics of the deposits and methods of deposition (NORSOK N003, 2007). These types of icing are snow, glaze, rime, frost and sleet, which are caused by precipitation of supercooled atmospheric water. This water is usually saturated with vapour and comes from either freezing rain or freezing drizzle snow with the influence of cold air.

It is common that both atmospheric icing and sea-spray icing are generated simultaneously, and they both need to be considered when determining the ice accretion on the vessels.

A rating of the dangers caused by different types of vessel icing is shown in Table 4.1-1, in a scale from 1 to 10, whereas 10 represent the highest threat.

Table 4.1-1 Joint safety impacts by rig component and ice type (Ryerson, 2009)

Hazard rating	Safety rating	Spray ice	Snow	Glaze	Rime	Frost	Sleet
		10	8	7	6	4	1
Stability	10	100	80	70	60	40	10
Integrity	10	100	80	70	60	40	10
Fire and rescue	9	90	72	63	54	36	9
Communications	8	80	64	56	48	32	8
Helicopter pad	8	80	64	56	48	32	8
Air vents	8	80	64	56	48	32	8
Flare boom	7	70	56	49	42	28	7
Handles, valves	6	60	48	42	36	24	6
Windows	5	50	40	35	30	20	5
Cranes	4	40	32	28	24	16	4
Winches	4	40	32	28	24	16	4
Stairs	4	40	32	28	24	16	4
Decks	3	30	24	21	18	12	3
Railings	3	30	24	21	18	12	3
Hatches	2	20	16	14	12	8	1
Cellar deck	1	10	8	7	6	4	1
Moon pool	1	10	8	7	6	4	1

Table 4.1-1 shows that the greatest threat to the stability of a vessel is by the sea-spray ice. It also shows that both snow and glaze represent a danger to the vessel's stability.

According to an analysis of 3000 vessel icing incidents performed by Borisenkov and Panov (1972, cited in ISO 19906, 2010, p. 125), sea-spray icing was the dominating cause for loss of vessels stability. The analysis showed that ocean spray icing was the sole cause of ice accretion in 86.0 % of the incidents. Drizzle, fog or rain combined with spray accounted for 6.4 % of the events. Snow combined with sea-spray accounted for only 1.1% of the incidents. Fog, rain or drizzle alone accounted for only 2.7% of the cases.

Makkonen (1984) states that it is fully possible for an offshore structure to accumulate over 1000 tons of atmospheric ice. It has been recorded several events where ships have accumulated layers of 120 mm of atmospheric ice. In some events, atmospheric icing has even formed a layer up to 600 mm (Minsk, 1980). In some situations where both sea-spray icing and atmospheric icing occurs, total ice thickness on the deck has reached as much as 1000 mm in some events.

Stated by Liljeström and Lindgren (1983, cited in Ryerson, 2008, p. 19), ice accumulation on different platforms have been reported to vary from 200 tons up to as much as 1600 tons, where the average of ice accumulation observations on these platforms were in the range of 500 – 700 tons.

4.1.1.1. **Sea-Spray Ice, Snow and Sleet Ice**

Sea-spray ice originates when the vessel hits the waves in the sea, and where the spray transforms into ice in the cold air and accumulates on the vessel. Ryerson (2008) states that superstructure icing is usually the biggest threat to the safety of the vessel. It can reduce the freeboard, raise the centre of gravity and increase the rolling moment that can lead to a decrease in the vessel's stability. It can damage the vessel and its components due to the weight loads of ice. The ice can also cause slippery surfaces and cover features such as; firefighting equipment, hatches, windows, valves and rescue equipment, making it difficult or impossible to get to or see through.

In February 1970, a severe icing event happened with a semi-submersible, Sedneth II, off the east coast of the United States. It had so much accumulated ice that the draft decreased at a rate of 300 mm per hour during the worst period of the storm (Crowley, 1988). Sea-spray icing was observed to start at 2 – 5 m above the sea level, where most of the ice accreted on the 150 mm diameter tubular braces that were supporting the platform legs.

Snow is created from ice crystals in the atmosphere. It is precipitation where the ice crystals grow to a big enough size where its weight causes it to fall down from the cloud. The snow typically coats all the horizontal surfaces on a vessel, and it has also been observed that snow can assemble on all heights on both semi-submersibles and boats (Ryerson, 2013). When the snow is wet, it has much higher adhesive and cohesive characteristics compared to when it is dry, which makes it possible to accumulate even on vertical surfaces. Normally dry snow does not accumulate on vessels at sea because the wind blows it off again, but this is not what usually happens if the surfaces are wet by for example sea-spray or spume.

The snow can cause several hazardous situations on a vessel such as slippery surfaces, prevention of operations of valves, and it may even contribute to a flare boom collapse. The frequency of snowing is also regarded as much higher compared to the occurrences with freezing drizzle or rain, also called glaze. The duration of snowing can also be much longer compared to glaze, where the snowing can last from 80 to 270 hours during some months. Glaze accretion rarely lasts for longer than 20 hours for most winter months. Ryerson (2008) states that the snow can add a significant amount of weight to a rig, contributing to instability of the vessel.

Sleet ice typically forms in warm frontal conditions, and is a transition form of precipitation between snow and freezing rain. Normally, sleet will not stick to components because it hits surfaces as a compact shape of precipitation, but it may form a sufficient layer on stairs and decks causing a slippery condition (Ryerson, 2008). The amount of sleet that forms on an offshore structure is usually not much, and is therefore not considered as danger to the vessel's stability.

4.1.1.2. **Frost, Glaze and Rime**

Frost forms a thin layer directly onto surfaces from water vapour that is continuous or discontinuous with a shape of needles oriented away from the surface. It usually forms on windless and clear nights on surfaces that are facing the sky. The coverage of frost usually varies spatially, and it is often most strongly observed on surfaces that have a convex shape that are exposed to the atmosphere (Ryerson, 2013).

On offshore structures, the frost often accretes on decks, stairs, cables, handles and railings, and at thickness of 0.5 mm it causes slipping hazards for the personnel onboard (Ryerson, 2008). The frequency and location of frost on offshore vessels has not known to be recorded at sea, and it has not been acknowledged as a major danger to a vessel's stability. It could, however, together with other types of icing, contribute to a dangerous stability situation for a vessel.

Freezing rain or freezing drizzle precipitation can form glaze on a structure, where it primarily lays upon horizontal surfaces. It is also possible that run-off² and wind can force the glaze to accumulate on vertical surfaces. The glaze is usually very clear and easy to see through, which is the result of slow rate freezing. It generates a slipping hazard on the vessel, and can disable cranes and winches by locking the cables in hard ice. A layer of glaze that is less than 1 mm thick can cause a great danger of falling on the stairways and decks. It is also regarded difficult to erase the glaze due to its high hardness and density (Ryerson, 2008). According to Liljestrom and Lindgren (1983, cited in Ryerson, 2008, p.13), incidents with up to 270 tons of glaze ice on a platform outside the Canadian coast with thicknesses up to 30 mm have been reported. The number of observations of glaze on platforms have been high in the Canadian West Coast and East Coast with a frequency of more than 10 %, while in the Barents Sea the occurrences of this has been much lower, less than 4% (Ryerson, 2013).

Rime ice is a result from cloud drops or super-cooled fog carried by the wind (Brown and Roebber, 1985). Bodies that face the wind will usually accumulate the largest rime ice thickness because of their higher efficiency of droplet collection. These accumulations usually occur on objects such as railings, lattices, cables and antennas. Rime can generate slippery conditions, and often occurs when the wind is blowing across a deck causing rime accumulation on different surfaces. This can be seen in Figure 4.1-1, where an ice thickness of 150 mm had accreted on a lattice steel structure.

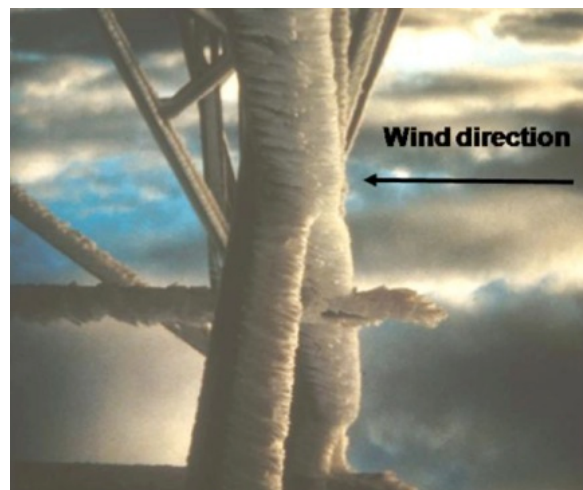


Figure 4.1-1 Rime accumulation on a lattice steel structure (Ryerson, 2013)

² The occurrence of draining away substances carried in the water from the surface of an area.

During a 12-hour storm period outside the Alaskan region, it was observed a thickness of 100 mm of rime ice on deck of a ship and 300 mm of rime ice on the ship's side at the rail lever. It resulted in approximately a total 30 tons of rime ice for 12 hours (Fett, Englebretson and Perryman, 1993).

4.1.2. Vessel Components and Functions

When ice accumulates on vessels it can create hazards due to disabled or hindered components and functions. Some of the most important components are shown above in Table 4.1-1 with different hazard ratings. The rating is based on a principle where a threat to the whole rig has a higher importance than a threat to the crew, and where the threat to each person is more important than to the working efficiency.

The ice accumulation can cause great threats to the function of some of the vessel's components. This section provides a description of what can happen to these functions of the vessel due to the icing accretion where they will be described in an order starting with the most critical elements to less critical elements.

4.1.2.1. Stability, Integrity and Fire and Rescue Equipment

The greatest danger due to vessel icing regards the stability as it can cause the vessel to capsize and thus be lost. As mentioned earlier, the stability of a vessel can decrease significantly with large masses of ice on it. The added weight due to this can also decrease the freeboard and enlarge the vessel motions.

When a ship is entering head sea (waves in direction of 0° with the vessel), it will accumulate about the same amount of ice on each side, and the ice accumulation in these situations will be generated with a symmetric load from the lateral amidships.

The second greatest threat to a vessel due to icing is the possibility of losing the vessel's integrity. There is a potential that parts of the vessel breaks off due to the icing loads. A vessel is designed to handle oscillatory stresses by the wave actions. The flexural response of components due to ice accumulation could change the vessel's capability during a design wave, which could lead to a loss of the vessel, loss of personnel and an oil and chemical spill.

If an explosion would occur, there is a possibility that the icing can encase the firefighting equipment, and thus lead to loss of its capability, the fire and gas sensors and even rescue equipment like lifeboats. The ice accretion can also decrease the possibilities to escape via davits or chutes. There may also be a danger if valves are totally frozen making them impossible to move.

4.1.2.1. Communication Equipment, Ventilation and Helicopter Pad

Another great danger due to icing is when it accumulates on communication equipment. As icing can deteriorate or destroy the communication equipment, it can be a huge hazard especially under emergency situations where the functions of the equipment can mean the difference between life and death. Events where these tools are extremely necessary are when the personnel must be rescued or if they require some assistance.

The ice typically accumulates on small diameters equipment, which can be the dipole and whip communication antennas (Ryerson, 2009). The accumulation of ice may also bridge short antennas and insulators. The water that is trapped in the ice may raise the dielectric constant causing it to block electric signals.

It is also possible under storm conditions that helicopters and supply boats can be unable to reach the platform or the ship due to the high seas, wind or fog. After the ice has ceased the communication equipment may still be destroyed or disabled by the ice accretion and making difficulties for the people involved.

The air ventilation is another critical system on the vessel. If this does not function properly it could be the cause of possible death of one or several crewmembers. Another event that may happen if the air is blocked is that it can increase the threat of stagnating and explosive gases in areas with ignition sources or in the living quarter.

The machinery also often requires proper air ventilation in order to function properly. If there is no or too little air ventilation the machinery could shut down which further under extreme situations could cause loss of the rig or ship (Ryerson, 2009).

There are also possibilities that the icing can prevent the use of the helicopter landing pad. This could be dangerous if someone is injured and needs to get onshore, or if there is a need for a supply of medical items. The icing could also cause a problem when tying down a helicopter, and a danger for the crew if the helicopter landing pad gets very slippery, as it could cause people to fall and slide off the pad.

4.1.2.2. Flare Boom, Handles, Valves and Windows

The flare boom consists typically of lattice structures, which usually have a large area for ice accumulation, and it is considered as a high threat to the safety since it is used to burn explosive gases. If ice accretes on the flare boom it could block the burner nozzles, and cause an explosion, fire, or increase the concentrations of poisonous gases.

The cold ice can make valves and handles difficult to operate, which could prevent operation of some important components that controls the safety system of the vessel.

Windows can get covered in ice making it impossible to see through. This can create problems and danger for crane operators and other personnel who are working in enclosed control stations. If a crane accident occurs, it could be hazardous to the entire personnel if a resulting fire or explosion occurs.

4.1.3. Conditions for Icing and Icing Intensity

Strong wind, low sea temperature, waves and cold air temperature is necessary in order for sea-spray icing to occur. The air temperature must generally be about -2.0 °C or colder and the sea temperature must be 7 °C or colder. The wind must typically be 9 m/s or more (Ryerson, 2013). When sea-spray is generated over the vessel, the water droplets freeze to ice in the air because of the energy loss, and form a layer of ice when they fall or blow down onto the vessel.

Atmospheric icing normally occurs when the wind speed is less than 10 m/s and the air temperature is between 0 and -20 °C (Minsk, 1980).

Another important factor for the sea-spray icing is the seawater salinity, when the seawater salinity is higher, the amount of accumulated ice on the vessel is higher (Funk, 2012). The freshwater ice at its freezing point has a density of 917 kg/m^3 . The newly formed sea ice contains usually a higher amount of salt content and is therefore denser, typically with a density of 925 kg/m^3 . When the ice freshens the density decreases, and by the time it has shed much of its salt, the freshwater ice becomes denser than the sea ice. The reason for this is that the ice formed in the sea contains a greater amount of air bubbles. Normally ice with no salt contains air to the extent of 8% of the volume, and has a density of 845 kg/m^3 (Bowditch, 2002). Also the freezing point increases when the salinity increases, which means that the higher salinity content there is in the water, the lower the potential is for icing. This can be seen in Figure 4.1-2.

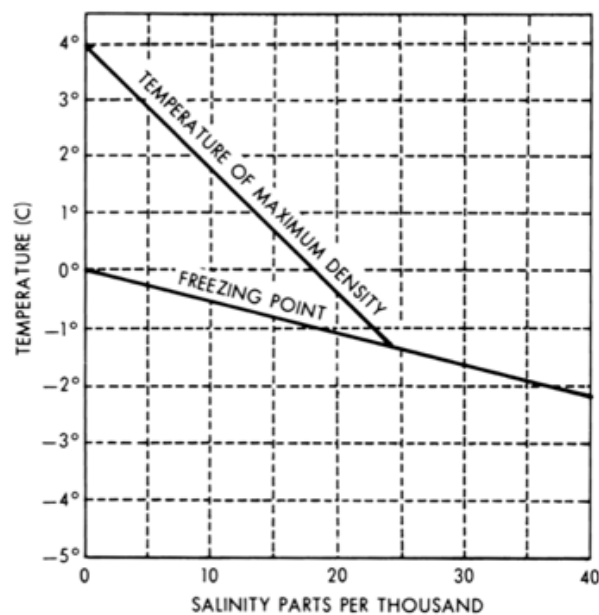


Figure 4.1-2 The relationship between the freezing point and maximum density for water with different values of salinity (Bowditch, 2002)

In order to take a value for the probable density of the ice and snow loads in the calculations, Table 4.1-2 will be used. It is a table that is based on data measured in different Norwegian seas, which makes it eligible to use for icing accretion on offshore vessels in the Barents Sea. The table shows different ice action cases of ice caused by sea-spray, and ice caused by rain or snow with an annual probability of exceedance of 10^{-2} .

Table 4.1-2 Different ice action cases (NORSOK N003, 2007)

Height above Sea level mm	ACTION CASE 1			ACTION CASE 2	
	Ice caused by sea-spray			Ice caused by rain / snow	
	56° N to 68° N mm	North of 68° N mm	Density kg/m ³	Thickness mm	Density kg/m ³
5 to 10	80	150	850	10	900
10 to 25	Linear reduction from 80 to 0	Linear reduction from 150 to 0	Linear reduction from 850 to 500	10	900
Above 25	0	0	-	10	900

It is assumed that most of the ice accumulation on the vessels will be from 10 m above sea level. This indicates from Table 4.1-2 that the density of sea-spray ice will vary from 850 kg/m^3 to 500 kg/m^3 . By assuming that the area of accretion is somewhere between 10 to 25 m above sea level, the density of sea-spray icing on the vessels is taken to be 700 kg/m^3 in the calculations. The density of the ice caused by rain/ snow, regardless of the height above sea level, has been taken from Table 4.1-2 to be 900 kg/m^3 .

Other environmental conditions that affect the amount of sea-spray icing on vessels are the wave size, direction and steepness. As sea spray icing are usually generated when the vessel hit the waves, the amount of water on the vessel and deck varies greatly. The steeper the waves are, the greater the spray from the waves will be. When an accumulation of ice has formed on the vessel, the rate of ice accumulation will speed up by itself (Fett, Englebretson and Perryman, 1993). Also the icing intensity on a vessel depends largely on the environmental conditions. The different icing rates (given in cm/hour) for various sea temperatures are shown in Figure 4.1-3. The icing rate is further defined in Table 4.1-3.

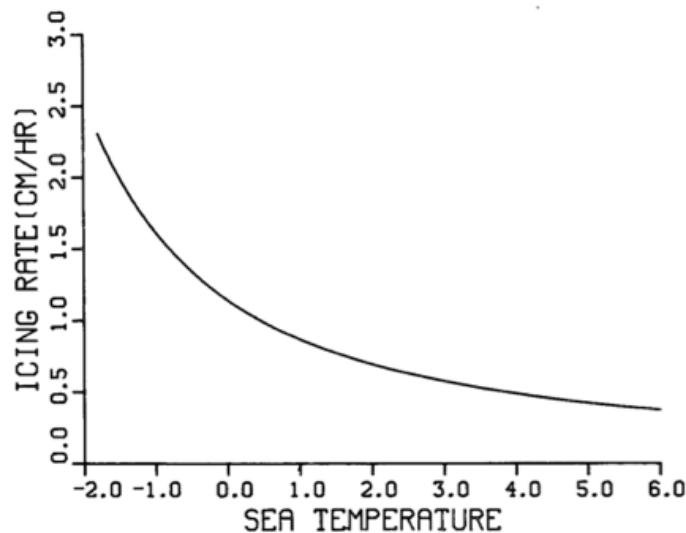


Figure 4.1-3 The dependency of sea temperature and icing rate (Overland, 1990)

Seen in Figure 4.1-3, the marine icing has a rate of 0.50 cm/hour at a sea temperature about 6°C , where the icing rate slowly increases with decreasing temperature.

The dependency on air temperature and wind speed in order for ice to form at different rates (light, moderate or heavy) is shown in Figure 4.1-4.

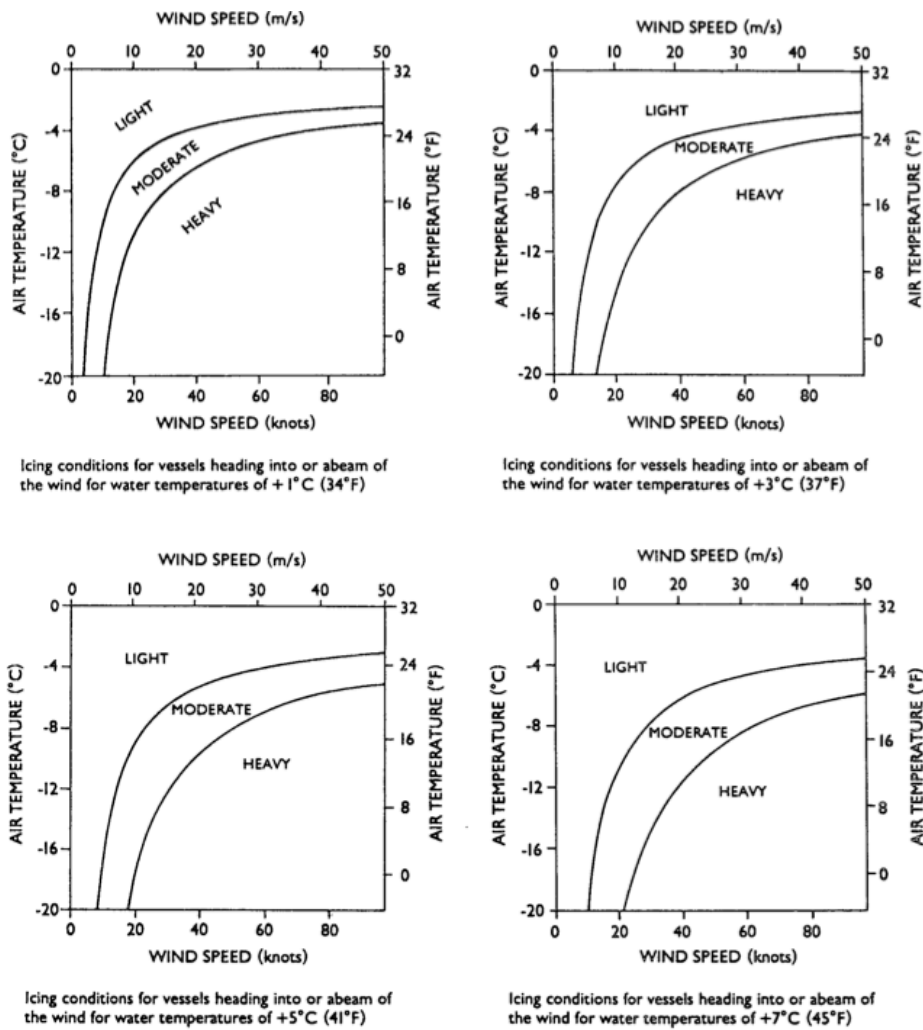


Figure 4.1-4 A plot of the calculated algorithm for accumulated ice for four different sea temperatures (Overland, 1990)

All four diagrams above prove that the higher the wind speed and air temperature is, regardless if the water temperature is + 7 °C or colder, the icing rate will increase.

In order for the weather forecasters to predict the amount of sea-spray icing, Overland (1990) has developed a formula based on algorithms, see formula (4.1-1). This formula is primarily based on reports from intermediate sized vessels between 20 to 75 m in length steaming into the wind.

$$PPR = \frac{V_a \cdot (T_f - T_a)}{1 + 0.3 \cdot (T_w - T_f)} \quad (4.1-1)$$

Where:

PPR	$[m^{\circ}Cs^{-1}]$	Icing predictor
V_a	$[ms^{-1}]$	Wind speed
T_f	$[^{\circ}C]$	Freezing point of seawater

T_a	[°C]	Air temperature
T_w	[°C]	Sea temperature

Further, the results of the ice predictor formula can be used to determine the ice rate, see Table 4.1-3.

Table 4.1-3 Rate of icing (Overland, 1990)

Icing class	Ice rate [cm/hr]	Predictor [$m^{\circ}Cs^{-1}$]
Light	0.7	< 22.4
Moderate	0.7 – 2.0	22.4 – 53.3
Heavy	> 2.0	> 53.3
Extreme		> 83.0

The table shows the results of the predictor and the corresponding result of the icing rate. This value was determined from open-ocean observations in the Alaskan seas for ships that were not heading downwind (Overland, 1990).

Other scientists have also categorized the different rates of icing. Ekeberg (2010) writes that the icing rate could be divided into three main groups; slow icing, fast icing and very fast icing. Slow icing is when the ice accumulation is less than 10 mm/hr. This occurs when the air temperature is $-3^{\circ}C$ or lower, with a wind speed of less than 7 m/s, or with air temperatures between $0^{\circ}C - 3^{\circ}C$, at any wind speed. Fast icing is ice accumulation between 10 mm/hr – 30 mm/hr, when the air temperature is between $-3^{\circ}C$ and $-8^{\circ}C$, and wind speed of 7 m/s to 15 m/s. Very fast icing is when the ice accumulates faster than 30 mm/hr, which occurs in air temperatures lower than $-8^{\circ}C$ with wind speeds of more higher than 15 m/s.

An investigation showed that for 74 % of the occurrences, the vessel icing lasted for longer than 12 hours, where the maximum duration was seven days (Minsk, 1980). Different measurements of the rate of icing in the arctic have been done, and for September it was shown that the rate of slow icing accounted for 20% - 40% of the period prior to freeze-up in the coastal areas. For the central parts of the arctic seas the occurrences ranged from 50% - 70%. In the southern parts of the arctic, the occurrence of fast icing ranged from 15 %. In October all these values increased further by 10% (Minsk, 1980).

Different icing rates for the period 1957 – 2009 has been estimated for three different locations outside the Norwegian and Russian coast, Shtokman, Skrugard and Norne field, see Figure 4.1-5.

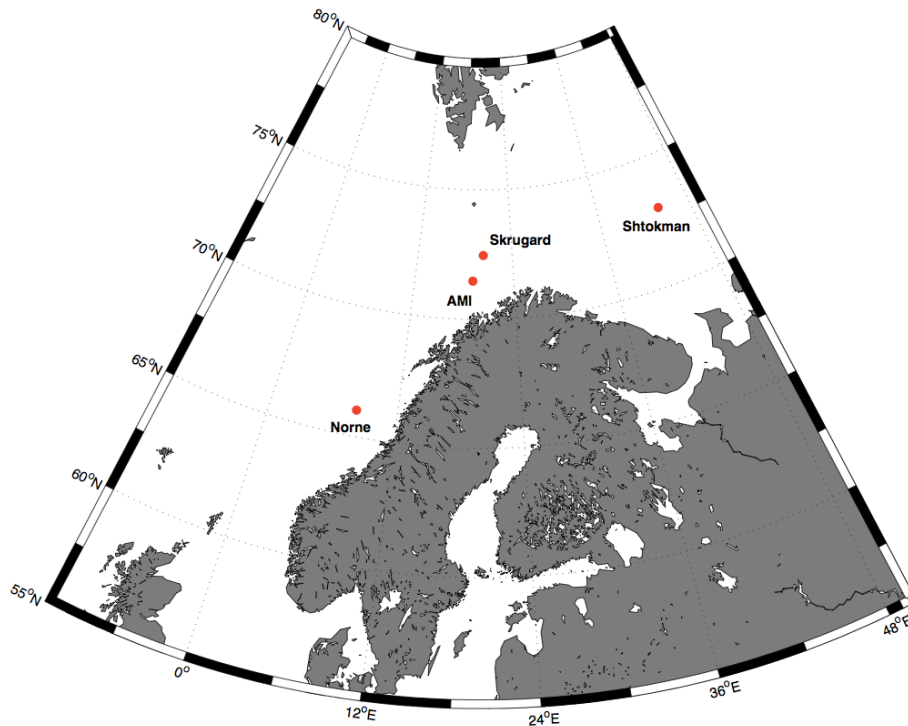


Figure 4.1-5 The locations of the Shtokman, Skrugard and Norne fields (Hansen, 2012)

In order to estimate the icing rate at these three locations, different data is taken from hindcast Nora10 throughout this period. The data has further been used in the algorithm formula by Overland (1990), formula (4.1-2). The formula is based on the wind speed, freezing point of seawater, air and sea temperature. The results of the estimation for these three fields are shown in Figure 4.1-6.

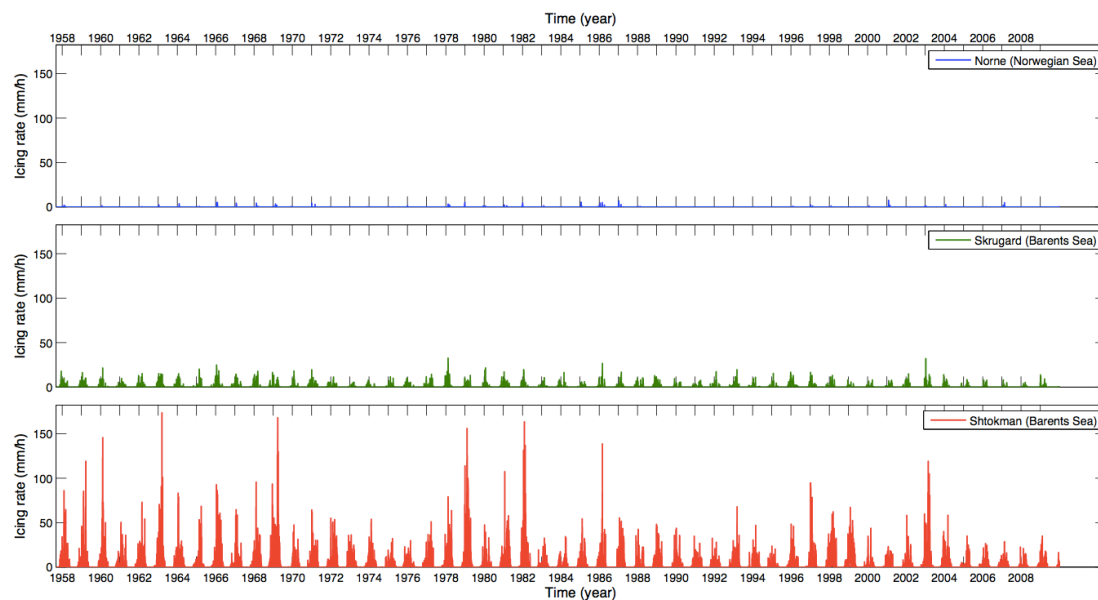


Figure 4.1-6 Icing rates for total wind and wave-spray icing at three different locations (Hansen, 2012)

According to Figure 4.1-6, the worst case of icing rate is up to 15 mm/hour at some points in the Shtokman area of the Barents Sea. This is the value that will be used in the calculations for the maximum thickness of sea-spray icing in this report.

4.1.4. Area of Ice Accretion on Offshore Vessels

In order for ice to accrete there must be some wet surfaces on the vessels that the ice can cling on to. One of the main factors for where and how much ice will accrete on a vessel is the geometry of the vessel, especially the height and the length. For example, the ice will accrete differently on a ship than a semi-submersible, as the geometries of these two vessels are quite different. Also, the height of the structure limits the amount of sea-spray icing on the deck. As mentioned earlier, the wind speed is essential for sea spray icing to occur. Typically the sea spray icing begins at wind speeds from 9 m/s, and the higher the wind speeds are; the higher the spray is lifted. The height of the sea spray icing above the sea level is usually limited to about 25 m, but there have been occurrences of sea spray icing at a height of 60 m above the sea level (Minsk, 1980).

The area and amount of sea-spray icing on a vessel also depends on the ocean wave field, structures on the vessel in the way of the sea spray, the length of the vessel, its freeboard, speed, and heading with respect to waves, wind and swells (Fett, Englebretson and Perryman, 1993). When the wavelength approaches the length of the vessel, the vertical motions of the vessel are enhanced. It is an interaction between the sea and the vessel that significantly increases the amount of spray on the vessel. It has been observed that a vessel in head sea will experience more sea spray than a vessel in beam sea.

4.1.4.1. Area of Icing on Ships

Some areas on a ship will experience greater icing than other. Figure 4.1-7 illustrates a ship with a maximum ice accretion zone, where this zone stretches in a bow from the front of the ship and backwards.

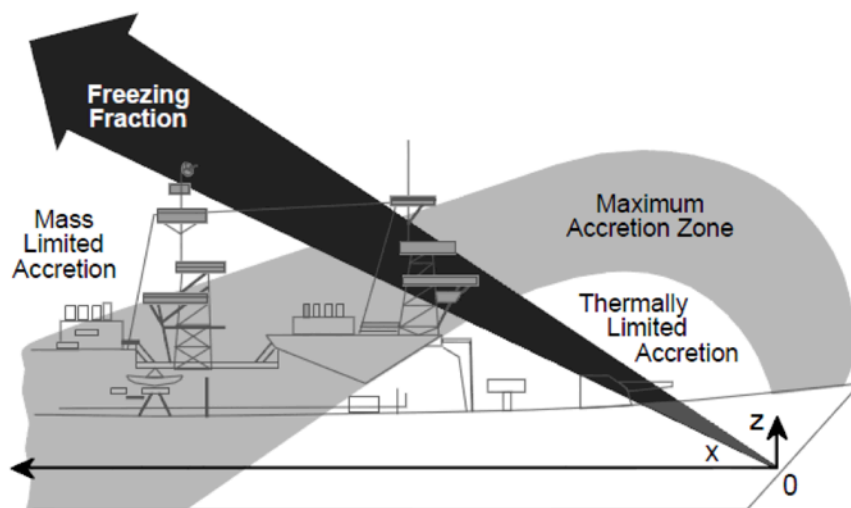


Figure 4.1-7 The direction of the freezing fraction of sea-spray accretion on a ship (Ryerson, 2008)

An analysis of the air flow for an initial wind speed of 15 m/s in the plane along the ship's centerline have been conducted for two different vessels (Shipilova et al., 2012). The two vessels used in the analysis were Geosund and Skandi Mongstad with lengths of 98.5 m and 97.0 m respectively, see Figure 4.1-8 and Figure 4.1-9.

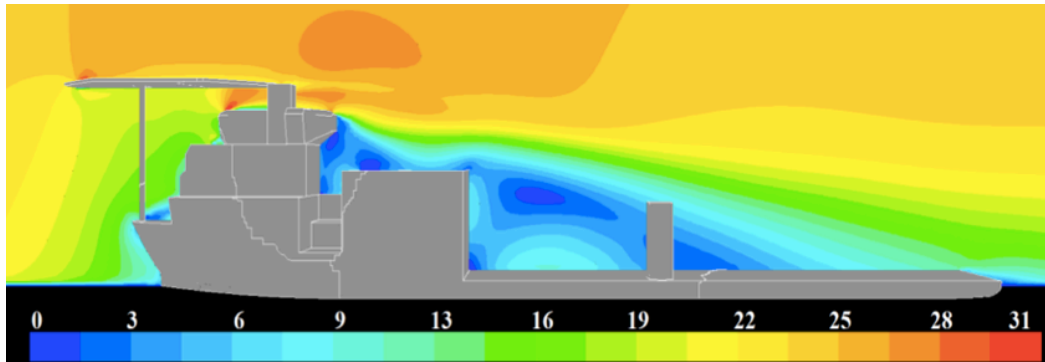


Figure 4.1-8 The velocity field over the ship Geosund, measured in m/s (Shipilova et al., 2012)

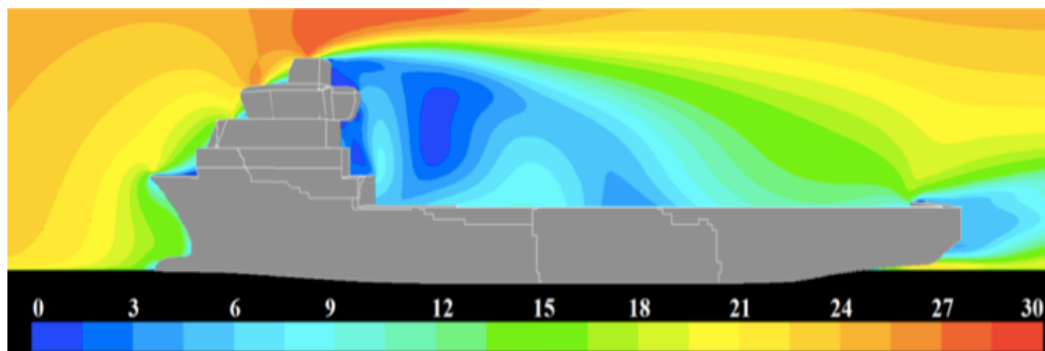


Figure 4.1-9 The velocity field over the ship Skandi Mongstad, measured in m/s (Shipilova et al., 2012)

The water flux rate on the surface of the Geosund vessel with the resulting ice accretion rate is shown in Figure 4.1-10. In that situation the wind speed was 25 m/s with an air temperature of $-15\text{ }^{\circ}\text{C}$.

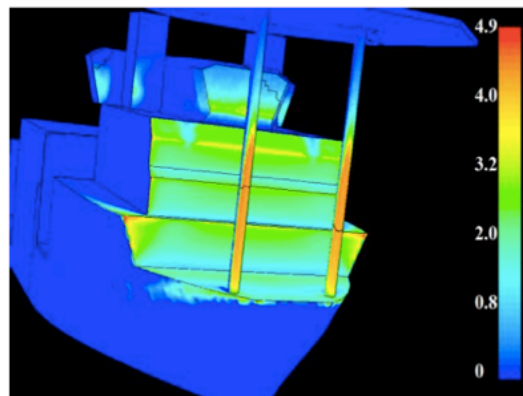


Figure 4.1-10 Estimated ice accretion rate given in cm/hr (Shipilova et al., 2012)

The figure shows that the amount of water droplets that does not impact the surface in a way that it increases the ice accretion rate, since most of the ice accretion occurs at the lower part of the bridge and not the house. Shipilova et al. (2012) explained that the reason for this is because the incoming water on the ship delivers too much energy, in which the seawater becomes a little above its freezing temperature. Another reason for this can be that the new wave washes away the ice before it is really stuck to the vessel. The situation on the legs that supports the helideck is opposite, where almost the entire amount of incoming water freezes.

There have been made several observations of snow accumulations on ships as well. An United States Coast Guard's vessel, CGC MIDGETT, accumulated a few centimetres of snow which froze immediately as a solid mass on the deck in the Bering Sea in February 1990 (Ryerson, 2013).

In the report about the Lady of Grace, a fishing vessel that sank on January 26, 2007 outside the United States due to heavy icing, there were made some observations from another fishing ship, Debbie Sue, that was out in the same area that day (USCG, 2008). This day the temperature dropped 20 °C very rapidly. The ship was 22.60 m long, and there was observed 250 mm of ice accretion on the handrails on the top deck, from the waist of the ship down to the deck she was totally covered in ice. The top of the pilothouse was fully covered by a 150 mm thickness of ice, except of the exhaust stack. On the windward side (starboard), there was ice hanging with a thickness of 150 mm from the upper deck floor to the sea level on the outer hull of the ship. The 25 mm wire hanging from the bow had accumulated between 250 – 350 mm of ice in diameter on the lower part of the wire from 1.50 m – 2.40 m to the deck.

Figure 4.1-11 show how ice had accumulated on a Norwegian fishing boat.



Figure 4.1-11 Accumulation of ice on a Norwegian fishing boat (Abrahamsen and Johansen, 2000)

Another observation of ice was made on a Norwegian fishing boat, Solveig, which went out fishing on a quiet and nice day on the 15th January 1940 outside Porsgrunn in Norway (Abrahamsen and Johansen, 2000). In a few hours the weather suddenly changed greatly, and dropped 25 °C and the wind blew up to northeast gale. When Solveig finally came back to shore the next day the guy-ropes on the fishing vessel had accumulated ice as thick as timber logs (200 – 250 mm), and on the deck the ice was flush with the railings (around 250 mm). The pilothouse was fully covered in ice. Even the windows on the pilothouse were fully covered by ice. During this period another fishing vessel, named M/S Brodrene, was lost due to heavy icing in this area.

It is mentioned earlier that in three quarters of observations of vessel icing, the icing lasted for longer than 12 hours, with a maximum duration of seven days (Minsk, 1980). According to Van De Rest (2012, cited in Lange, 2012, p.15), the average duration of a winter storm in the North Sea is about 15 hours. A winter storm can be described as an event that happens at low temperatures with varieties of precipitation such as sleet, snow and freezing rain.

4.1.5. Area of Icing on Semi-submersibles

The motion characteristics together with the high air gap of semi-submersibles makes the rigs less exposed for sea-spray ice accretion on deck. It has been observed that most of the ice accretion from sea-spray occurs under the deck of the rig, while snow, rime and frost typically form a layer on the deck and higher. Some amount of sea-spray can accrete on the deck where most of it are generated by low density spume (Ryerson, 2014). Usually the rime and frost accrete on the mast of the platform, contributing little to change the vessel's stability. The type of ice and where it accumulates on a semi-submersible is shown in Figure 4.1-12.



Figure 4.1-12 Areas of icing on a semi-submersible rig (Ryerson, 2011)

According to Baller (1988, cited in Ryerson, 2013, p.18), the sea-spray icing will accumulate in the splash zone 5.0 – 7.0 m above sea level in drilling mode on the platform legs, bracings, blowout preventer guidelines, marine riser and mooring chains. Figure 4.1-13 shows a picture of ice accumulation on a semi-submersible.



Figure 4.1-13 Sea spray icing the columns of a semisubmersible (Ryerson, 2013)

It has been observed that the most severe ice build-ups occur at the small-diameter leg elements with lattice bracing. On large diameter legs, the ice accumulation will only be a few centimetres, and then it will drop off (Ryerson, 2013). The sea spray ice will build up to a certain thickness and then break off due to vibrations and its own weight. It is believed that in extreme conditions the sea-spray icing could coat portions of the deck, but it largely depends on the wind direction in relation to any structures on the rig that could possibly block the wind. Ryerson (2014) mentions that most of the seawater ice accumulated on the deck originates from spume. He also mentions that most of the sea-spray ice will accumulate on the upwind side of the platform, which gives an asymmetric load on the structure and thus can make the structure unstable.

4.1.6. Area of Icing on the Four Vessels

A case study for the four vessels will be conducted in this report that will be based on the information given in previous sections. In the case study, it is assumed that the Barents Sea has the same average winter storm duration of 15 hours as the North Sea, and with a maximum ice accretion rate of 15 mm/hour (see Figure 4.1-6). The maximum ice thickness used in the case study will therefore be 225 mm.

The value of a maximum ice thickness of 225 mm will be used in the calculations, as it is considered as an event that may possibly happen in the Barents Sea. It is also common that sea-spray icing accretion and snow accretion formation occurs simultaneously, which is why they both will be considered in the calculations. According to Liljestrom and Lindgren (1983, cited in Ryerson, 2008, p.13), incidents where the snow load was as much as 150 tons with a depth of 300 mm on a vessel have been reported. By this reason, it is assumed that an amount of 300 mm of snow layer will cover all the horizontal surfaces of all four vessels.

It is also important to discover the amount of ice that will make the vessels unsafe, and whether this amount of ice is realistic to occur or not. A parameter study will be conducted for this purpose, where the magnitude of ice in order to not meet the requirements from DNV will be calculated.

In these calculations the snow loads are assumed to be constant at a thickness of 300 mm with a density of 900 kg/m^3 on all horizontal surfaces, with a varying layer of sea-spray ice with a density of 700 kg/m^3 . It is shown in Table 4.1-2, that the density of snow is 900 kg/m^3 which is the reason this value will be used.

The same table also regards the density of sea-spray ice at different heights above the sea. It is assumed that most of the sea-spray occurs at a level of 10 – 25 m above the sea level, and that the appropriate density value to use for all vessels is somewhere in the middle of this height. This is the reason why a constant density of 700 kg/m^3 has been chosen for the sea-spray ice.

Further in this parameter study, the different lengths and height dimensions of the vessels given in the figures below will be used in the calculations. The sea-spray ice thickness will vary from a thickness of 0 mm to several meters, where two different ice thicknesses will be used for different areas on the vessels. In the maximum ice accretion zone, the sea-spray ice thickness will be $1.0 \cdot t_{ice}$, and outside the maximum ice accretion zone the thickness will be $0.5 \cdot t_{ice}$. Here the $1.0 \cdot t_{ice}$ applies to per unit length (m) of the vessel. By increasing the value of t_{ice} to a certain value, the requirements from DNV will no longer be fulfilled.

The calculations of the resulting freeboard, stability and righting arm will be based on the assumed sea-spray ice loads, snow loads, and the dimensions of the vessels are shown in the figure of the vessels below.

Other types of atmospheric icing such as frost, rime, sleet and glaze ice have not been included in the calculations for the ships because they are assumed to have a very small impact on the stability and freeboard of the vessel. Glaze ice has under some events been contributing to a significant additional weight on vessels, but it has been disregarded in the calculations because of the few observations with glaze ice in the Barents Sea.

4.1.6.1. Ice Accumulation on the Lady of Grace Boat

It is assumed that the ship will experience sea-spray ice accumulation on all horizontal surfaces and surfaces facing the wind with a maximum ice thickness at all horizontal surfaces of the ship since it is so small. For surfaces not facing the maximum ice accretion zone or vertical surfaces, it is assumed that the ice thickness is only half the maximum ice thickness. It is also assumed that there will be a constant thickness of 300 mm snow on all horizontal surfaces of the vessel. This can be seen in Figure 4.1-14 and Figure 4.1-15.

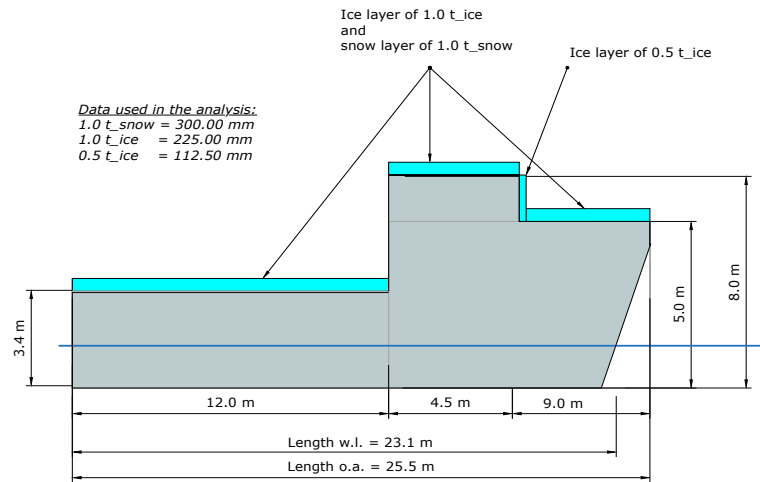


Figure 4.1-14 Side view of the assumed ice and snow thickness on the Lady of Grace

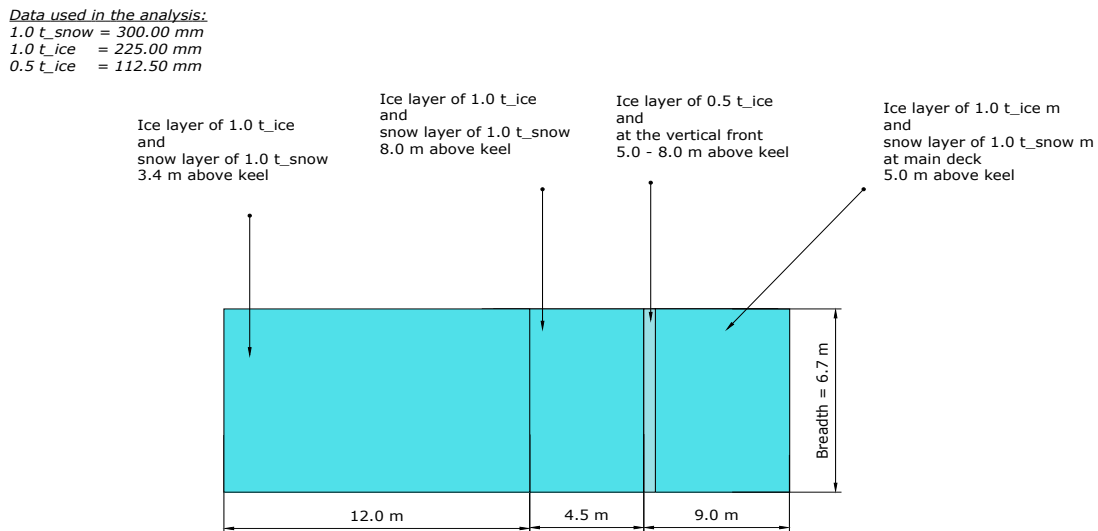


Figure 4.1-15 Top view of the assumed ice and snow thickness on the Lady of Grace

4.1.6.2. Ice Accumulation on the Viking Fighter Vessel

The assumed thickness of ice and snow on the different areas of the Viking Fighter is shown in Figure 4.1-16 and Figure 4.1-17.

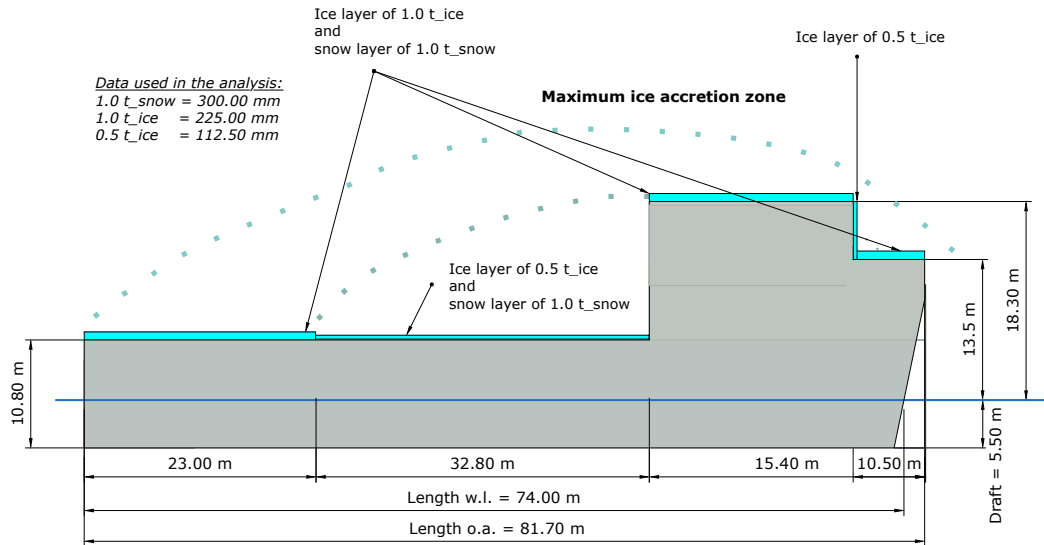


Figure 4.1-16 Side view of the assumed ice and snow thickness on the Viking Fighter vessel

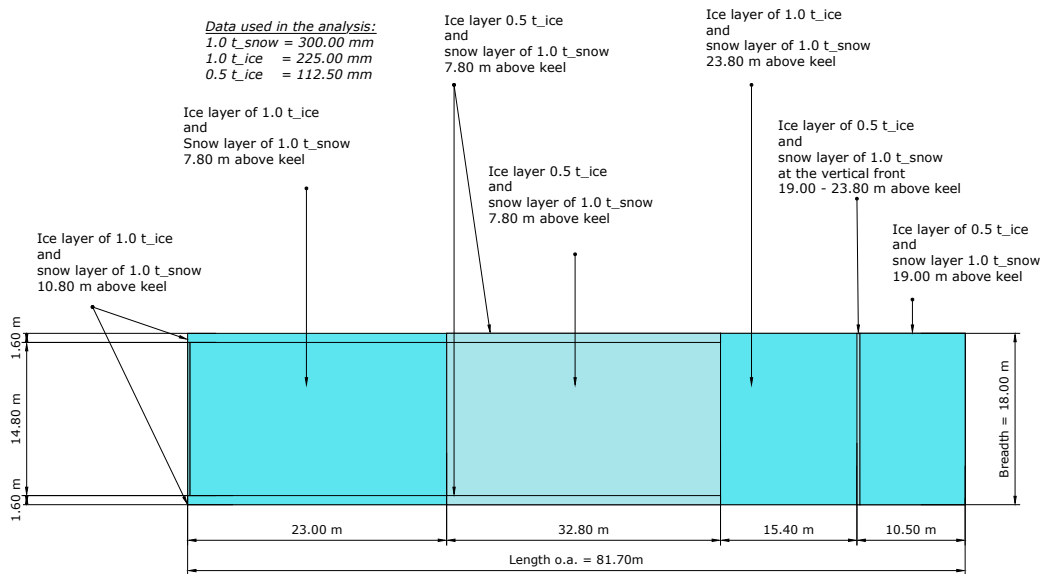


Figure 4.1-17 Top view of the assumed ice and snow thickness on the Viking Fighter vessel

4.1.6.3. Ice Accumulation on the Drillmax Ice Drillship

The Drillmax Ice vessel is more than twice the length of the Viking Fighter vessel, and it is also much taller. It is earlier mentioned that the vessel characteristics such as length and height are two important factors considering the amount of accreted sea-spray ice on the vessel. The top of the bridge of this vessel is about 40 m above the sea level, which is quite high regarding the sea-spray. There have, however, been observations of sea-spray up to 60 m, and therefore it is assumed that the spray blows over bridge of this vessel and all the way to the mid of the ship, see Figure 4.1-18 and Figure 4.1-19.

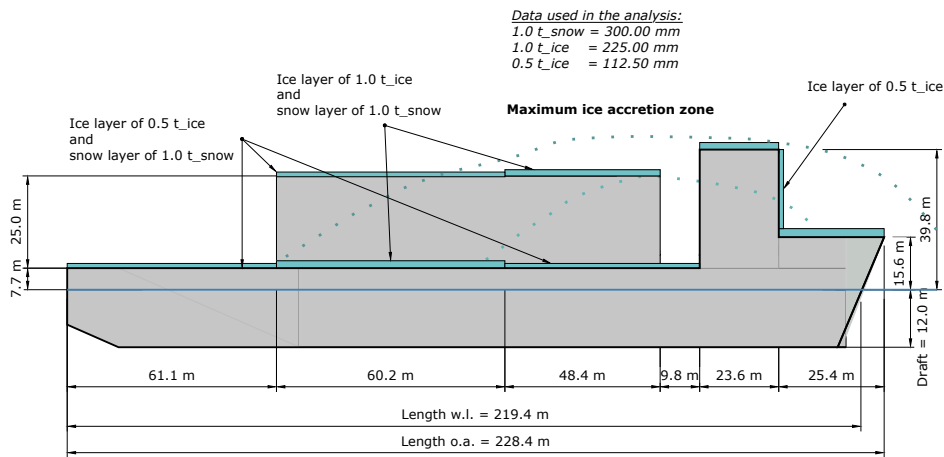


Figure 4.1-18 Side view of icing accretion on the Drillmax Ice

For this vessel it is assumed that sea-spray ice will accrete on horizontal surfaces and vertical surfaces facing the wind, and that snow will accumulate on all horizontal surfaces of the vessel.

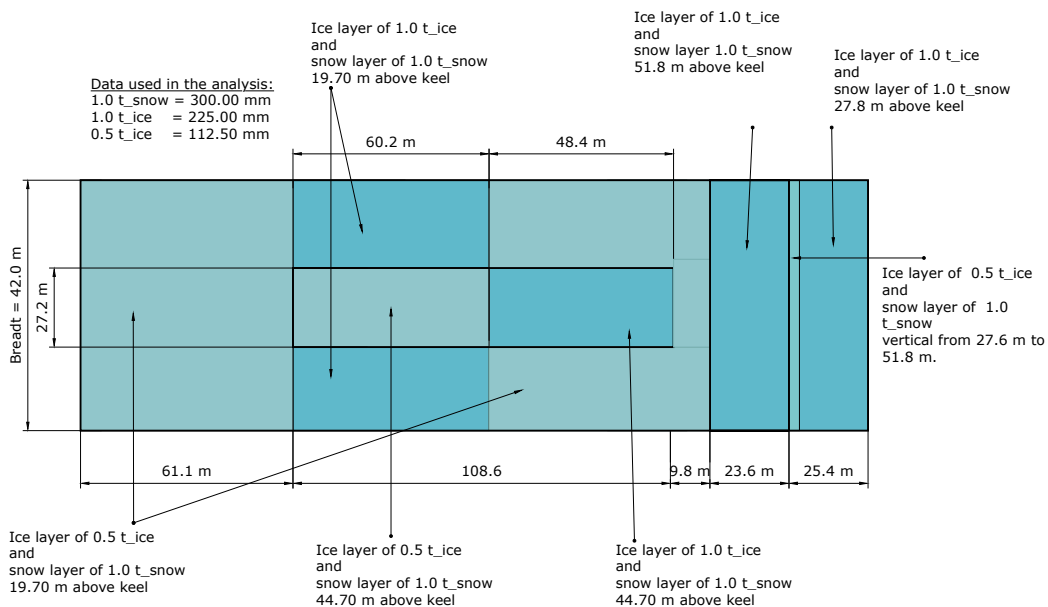


Figure 4.1-19 Top view of the Drillmax Ice vessel with the assumed thickness of ice and snow

4.1.6.4. Ice Accumulation on the West Alpha Rig

It is assumed that the maximum sea-spray accretion on the structure generates under the deck on the windward side of the vessel, on the square columns and the cylindrical columns, the hull geometry of the semi-submersible is shown in Figure 4.2-3. On the other side of the vessel where there is no wind, it is assumed that the components under the deck will experience half the thickness of sea-spray ice. The difference in ice loads from the windward side, and the other side will therefore cause the platform to heel. It is further assumed that the sea-spray icing starts at a level of 5 m above the water line, and that it covers as much as $\frac{1}{4}$ of the length of the main deck where there is no structures in the way. As there is no documentation of how large portions of the deck that sea-spray icing may cover, the value of $\frac{1}{4}$ is just assumed to be a worst-case scenario.

For the rig it has been considered that a load of 100 mm of atmospheric ice (rime, frost, snow) will accumulate on the derrick. This is an extra load together with the thickness of 225 mm sea-spray ice and the thickness of 300 mm of snow.

It is assumed that the rig is placed with the living quarter against the wind, and for safety reasons, the process area/ the flare is as far away from the living quarter area as possible. However, the wind can blow sideways from the living quarter side, as this side has very little obstacles/ equipment to prevent sea-spray ice to accrete; this is shown by the top view of the rig in Figure 4.1-21. When the wind blows in this direction there will be more accumulation of sea-spray ice, and it is considered as the worst-case scenario for this rig.

The different ice accumulations with the different dimensions on the rig can be seen in Figure 4.1-20, Figure 4.1-21, Figure 4.1-22 and Figure 4.1-23.

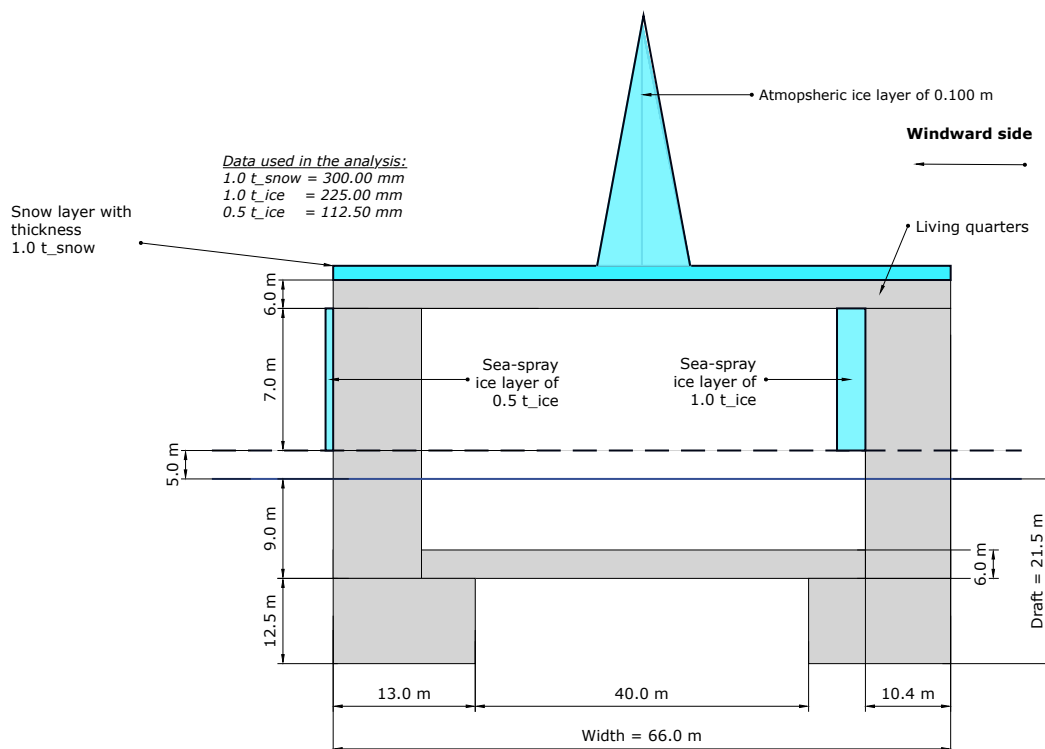


Figure 4.1-20 Front view of the West Alpha rig with the assumed ice and snow loads

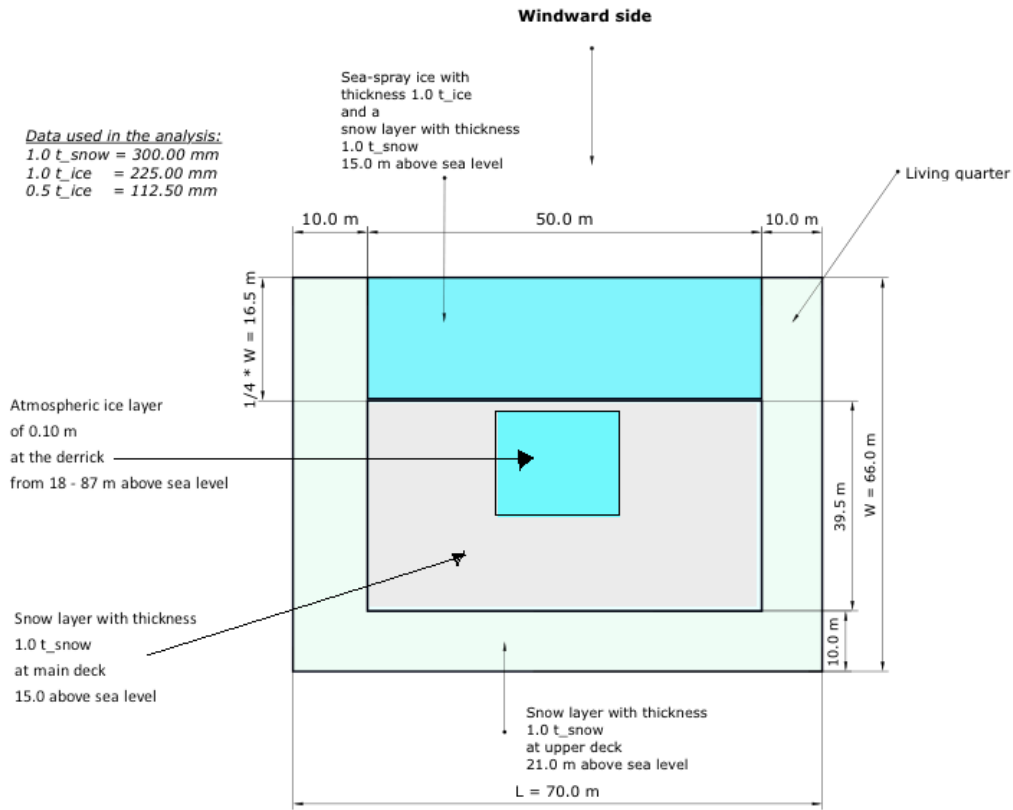


Figure 4.1-21 Top view of West Alpha

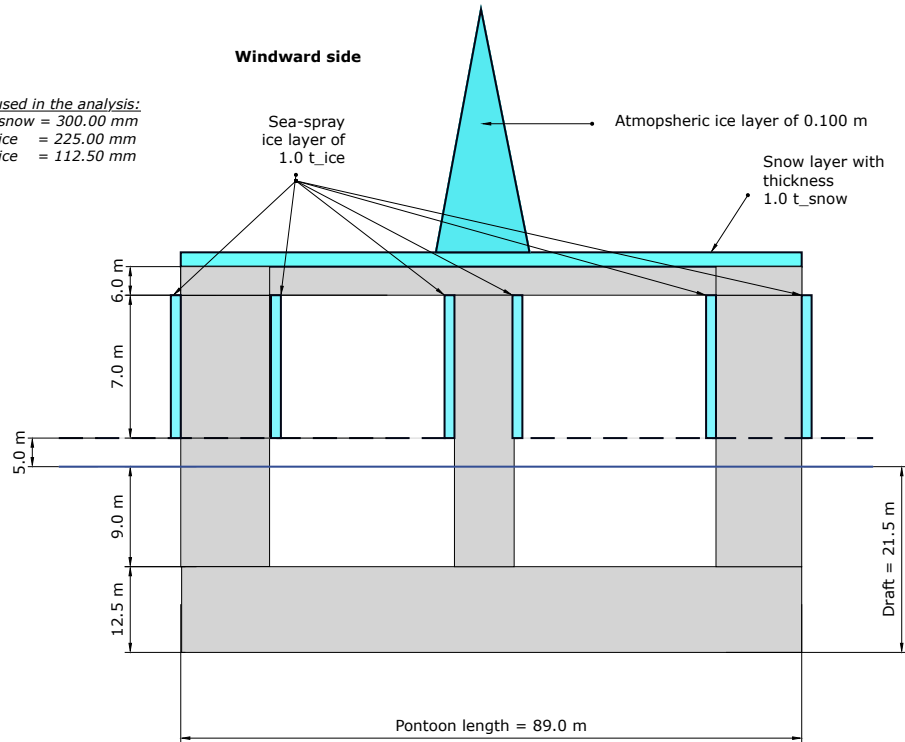


Figure 4.1-22 Side view from the windward side

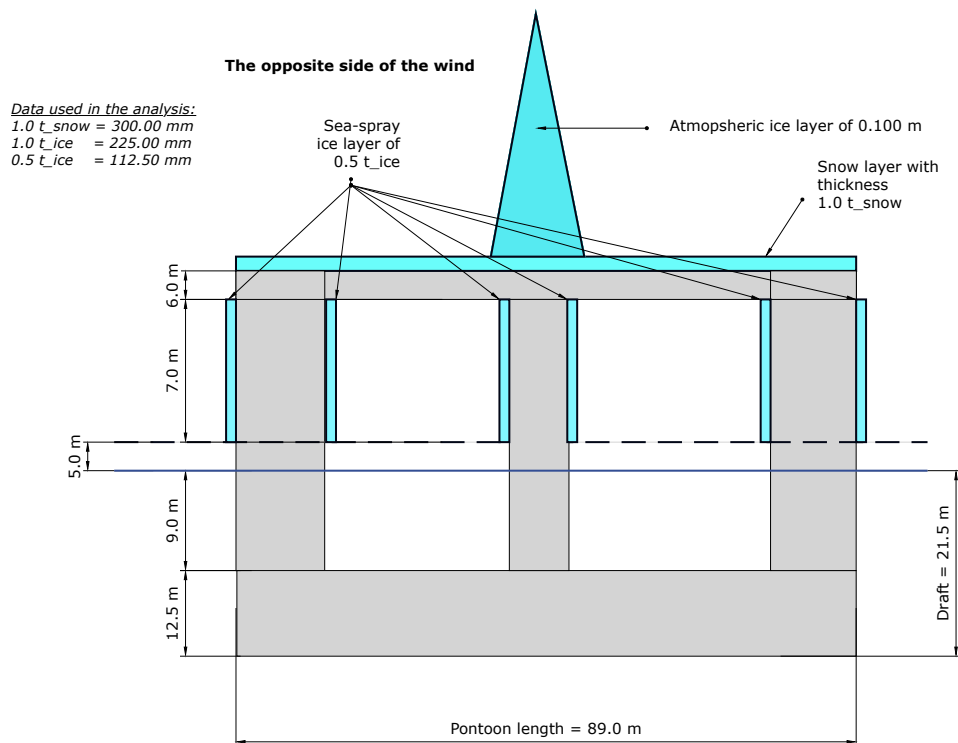


Figure 4.1-23 Side view from the opposite side of the wind

4.1.7. Ice Protection, Prevention and Detection Technologies

There are many different methods to be used on offshore vessels in order to avoid the ice, to detect the ice and to get rid of the ice. Some of the most common methods used will be mentioned briefly in this section.

4.1.7.1. Chemicals, Coatings and Design

Today there are many different chemicals used for anti-icing and de-icing, and a variety of methods on how to apply the liquid or solid chemicals. Usually before, under and after storms they are applied to reduce the adhesion strength of ice to pavements (Ryerson, 2009). Sometimes chemicals are applied with warm water to melt snow and ice, and to lower the temperature of the freezing point to allow it to run off before freezing. Sometimes anti-icers are used to decrease the freezing point to prevent icing, or to absorb the freezing precipitation. Vessels have many surfaces that can benefit from the use of chemical de-icing treatment. Some of these areas are the stairs, helicopter landing pads and the decks.

Some of the chemicals that have been commonly used for anti-icing on offshore vessels are the potassium acetate and propylene glycol. The potassium acetate can be good to use on vessels because of its utility on helicopter pads, low corrosivity and low-temperature capability. The propylene glycol is also considered usable for offshore structures as it can be used as a de-icer or anti-icer. However, there is a significant setback with using chemicals offshore, as there is a possibility for dilution and wash off by heavy spray and waves (Ryerson, 2011). The release of the toxic chemicals to the water can pollute the water that can affect the environment and poison the nearby wildlife.

Another method used to reduce or prevent icing is by the use of coatings, which lowers the adhesion strength of ice to substrates³. One of the most active researches within de-icing is the testing and development of coatings. Coatings have currently been used on aircraft de-icing boots, aircraft engine inlets and ship hulls, and researchers believe that there is a potential to apply this on drill rigs and ship superstructures. Some of the main advantages with coating is that is inexpensive, it can easily be applied over any substrate, it requires no power, and would require little or no maintenance. There are different types of coating technology with varieties in design, properties and chemistry. Single chemical compounds make up most of the coatings, and it is applied to surface by brushing or spraying (Ryerson, 2008).

The design of a vessel can have a significant impact in how much ice the vessel is accumulating. The amount of accumulated ice on the vessel can be significantly lower by optimizing the design of the vessel. This can be done by using techniques for preventing icing, avert water from freezing in the best possible way, the amount of accumulated ice on the superstructure can be significantly lower (Ryerson, 2011).

There are many suggestions on how to improve the design of vessels in cold waters in order to reduce the amount of ice accumulation. Ryerson (2011) mentions that there are many different types of rig design recommendations for the Northern Waters. The recommendations include adding heating capacity to the cellar deck, improving the derrick enclosure, use heat tracing on piping outdoors, and enclosing the cellar deck. Another recommendation is to minimize the vessel's surface imperfections, where ice forms and adheres most strongly and to add a payload to accommodate ice loads.

4.1.7.2. **Electrical Techniques, Mechanical De-icing and Ice Detection**

There have been developed different electrical techniques for de-icing structures. They can function in several ways; cause erosion of the ice in a way that it physically disconnects from the substrate, they can make the ice melt in a thin layer at the substrate's interface, or they can melt through the whole ice thickness. The three main methods for electrical techniques are pulse electro-thermal de-icing, application of DC bias voltage to the substrate's interface or ice dielectric heating (Ryerson, 2011). In order to not damage the equipment, application for the electrical de-icing methods must not be exposed conductors on a surface where is conductive, hence the lower part of the vessel may be the best location for this equipment.

Mechanical de-icing is one of the most common techniques used to remove ice from ships and other offshore structures. It involves hitting the ice on the vessel by use of tools as wooden hammers, mallets, crowbars, and even baseball bats to loosen the ice, which is then shovelled off the deck. It can be considered a dangerous job because of the slippery surfaces the crew works on, and also damaging to vessel and equipment. Sometimes the places where the ice lays can also be out of reach for the crew, and manual de-icing techniques are not possible. Mechanical de-icing is also affected by the properties of the ice, as fresh sea water ice is much softer than old sea water ice.

³ A substance on which an enzyme acts.



Figure 4.1-24 Manual de-icing on a crab fishing boat (Deadliest Catch. Man vs. Ice, 2006).

Ice detection technology may not be anti-icing or de-icing systems, but it is important to let operators know when their vessel is experiencing icing. Stated by Ryerson (2011), the ice detectors usually functions as information sources for other automated anti-icing systems. Ice detectors can be used to indicate that ice is present by mass or its thickness. Ice detectors can also be capable of deciding when a surface is clear of ice as a result of anti-icing or de-icing activity. Some of the most common ice detection methods used today are ice managing, ice mass sensing, ultrasonic, optical, di-electric property sensing and latent heat detection. However, most of the detectors are point devices that measure icing rate, most often at only one location. This is why it can be difficult to accurately represent the amount of ice accreting on a surface.

4.2. Freeboard of Vessels

In this section, the different equations on how to calculate the freeboard for vessels will be shown. As the ice and snow loads will reduce the freeboard of the vessels, it is important to calculate this parameter to determine whether this load makes the vessels unsafe or not.

This section has been divided into four sub-sections where the first section, section 4.2.1, describes the freeboard and buoyancy of a floating object. Section 4.2.2 explains how the freeboard of the ships is calculated. The method for calculating the freeboard of the semi-submersible is shown in section 4.2.3. In section 4.2.4, there will be presented a general formula on how to calculate the freeboard for any vessel that has accumulated ice loads.

4.2.1. Freeboard and Buoyancy of a Floating Object

Buoyancy can be described as the upward force that is exerted by a liquid that opposes the weight of a submerged body in a column of water. Stated by Ryerson (2011), a body that is submerged in fluid will experience greater pressure at the bottom than at the top. It is because of this pressure difference, that a force tends to accelerate the body upwards. It is a force that is proportional to the pressure difference between the bottom and the top of the column. It is also equal to the mass of the fluid that otherwise occupy the column, the displaced water, a phenomenon also called the “Archimedes principle”. This means that when the density of the body is greater than the fluid, the body will sink. If the body is shaped appropriately or if the object is less dense than the liquid, the buoyancy forces will keep the body floating. This means that a vessel made of steel can float because it is able to displace

more water than it weights. The different forces, gravitational and buoyancy forces on an element are shown in Figure 4.2-1.

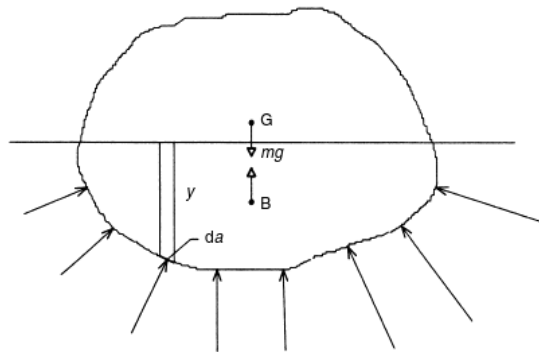


Figure 4.2-1 A submerged body in water (Tupper, 2004)

The freeboard can be described as the distance from the waterline to the deck of a ship or a semi-submersible. For semi-submersibles the freeboard is also called the air gap.

The formula for the freeboard of a vessel can be written as

$$f_v = h_v - d_v \quad (4.2-1)$$

Where

f_v	[m]	Freeboard of the vessel
h_v	[m]	Height of the vessel
d_v	[m]	Draft of the vessel

Figure 4.2-2 shows some parameters of a rectangular vessel that is needed in order to calculate the freeboard.

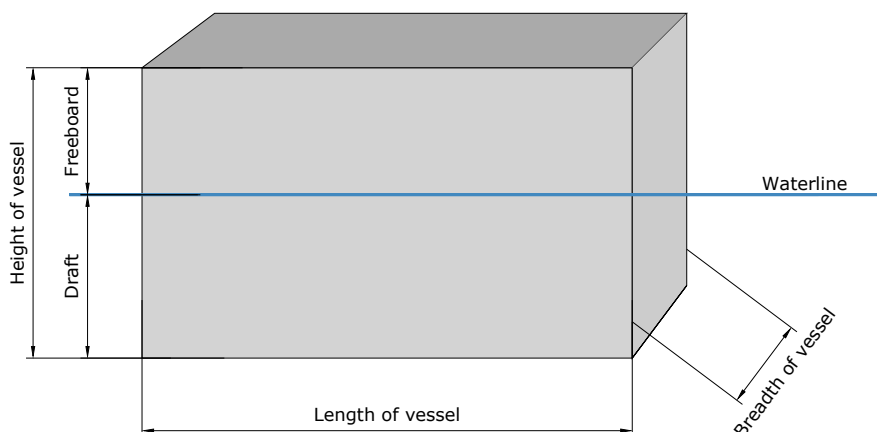


Figure 4.2-2 Draft and freeboard of a rectangular vessel

The Archimedes principle can be used to determine the draft of the vessel, see formula (4.2-2)

$$F_B = F_G \quad (4.2-2)$$

which becomes

$$\begin{aligned} \rho_w \cdot g \cdot \nabla &= m_v \cdot g \\ \nabla &= \frac{m_v}{\rho_w} \end{aligned} \quad (4.2-3)$$

where

F_B	[N]	Buoyancy force
F_G	[N]	Gravitational force
g	[m/s ²]	Gravitational acceleration
∇	[m ³]	Submerged volume of vessel
m_{total}	[kg]	Weight of the vessel
ρ_w	[kg/m ³]	Density of saltwater

4.2.2. Freeboard of the Ships

For a ship with a rectangular shaped hull, the equation for the submerged volume can be written as

$$\nabla = l_v \cdot b_v \cdot d_v \quad (4.2-4)$$

Where l_v and b_v are the length and breadth of the vessel respectively. Further, the draft of the ship can be calculated from inserting equation (4.2-4) into (4.2-3), see equation (4.2-5) below

$$d_v = \frac{m_v}{\rho_w \cdot l_v \cdot b_v} \quad (4.2-5)$$

The freeboard can be found when inserting (4.2-5) into (4.2-1), and can be written as formula (4.2-6)

$$f_v = h_v - \frac{m_v}{\rho_w \cdot l_v \cdot b_v} \quad (4.2-6)$$

The equation (4.2-6) can be used to determine the freeboard of the Lady of Grace, Viking Fighter vessel and the Drillmax Ice vessel by the reason that they have a rectangular shaped hull. The formula for the freeboard of the semi-submersible, West Alpha, will be different because it does not have a rectangular shaped hull structure.

4.2.3. Freeboard of the Semi-submersible

The hull structure of the semi-submersible is called a yatzy hull design. It consists of

four rectangular columns, two cylindrical columns, two pontoons and two cylindrical bracings. This can be seen in Figure 4.2-3.

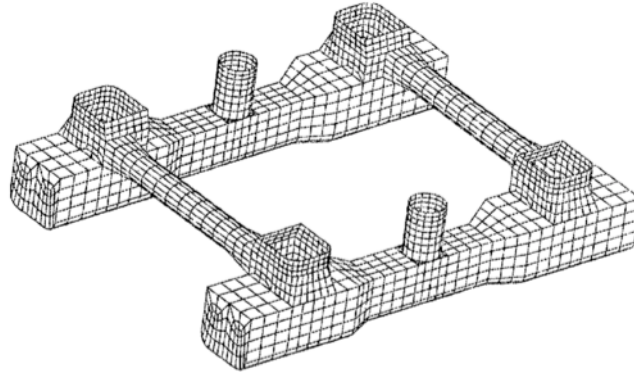


Figure 4.2-3 The submerged part of the hull structure of West Alpha under operating conditions (Erik Falkenberg, Xu and Odor, 2001)

In order to calculate the draft of this rig in operating condition, all six columns are considered together with the two pontoons, and the two braces.

The formula for the total submerged part of the rig ∇ can be written as

$$\nabla = \nabla_{\text{Pontoons}} + \nabla_{\text{Bracings}} + \nabla_{\text{R.Columns}} + \nabla_{\text{C.Columns}} \quad (4.2-7)$$

where

$$\nabla_{\text{Pontoons}} = 2 \cdot V_p = 2 \cdot b_p \cdot l_p \cdot h_p$$

$$\nabla_{\text{Bracings}} = 2 \cdot V_b = 2 \cdot r_b^2 \cdot \pi \cdot l_b$$

$$\nabla_{\text{R.Columns}} = 4 \cdot \nabla_{r.c} = 4 \cdot b_{r.c} \cdot l_{r.c} \cdot h_{c.wl}$$

$$\nabla_{\text{C.Columns}} = 2 \cdot \nabla_{c.c} = 2 \cdot \pi \cdot r_{c.c}^2 \cdot h_{c.wl}$$

Where the parameter $h_{c.wl}$, is the submerged height of the columns. It is the height from the top of the pontoons to the waterline. The submerged volume of the pontoons, bracings, rectangular columns and cylindrical columns are presented as ∇_{Pontoons} , ∇_{Bracings} , $\nabla_{\text{R.Columns}}$ and $\nabla_{\text{C.Columns}}$, respectively.

The formula for the top of the pontoons to the waterline $h_{c.wl}$, can be written as

$$h_{c.wl} = d_{\text{semi}} - h_p \quad (4.2-8)$$

The formula for the draft of this semi-submersible can be calculated when the equation (4.2-8) is inserted in equation (4.2-3), see equation (4.2-9)

$$2 \cdot (b_p \cdot l_p \cdot h_p + b_b \cdot l_b \cdot h_b + b_{c.c} \cdot l_{c.c} \cdot h_{c.wl}) + 4 \cdot b_{r.c} \cdot l_{r.c} \cdot h_{c.wl} = \frac{m_v}{\rho_w}$$

$$2 \cdot (b_p \cdot l_p \cdot h_p + b_b \cdot l_b \cdot h_b + b_{c.c} \cdot l_{c.c} \cdot (d_{semi} - h_p)) \quad (4.2-9)$$

$$+ 4 \cdot b_{r.c} \cdot l_{r.c} \cdot (d_{semi} - h_p) = \frac{m_v}{\rho_w}$$

When solving the d_{semi} out of equation (4.2-9), the freeboard of the semi-submersible can further be calculated by

$$f_{semi} = h_{maindeck} - d_{semi} \quad (4.2-10)$$

Where f_{semi} , $h_{maindeck}$ and d_{semi} is the freeboard, the height of the main deck above the bottom of the hull structure, and the draft of the semi-submersible.

4.2.4. Freeboard of a Vessel With Accumulated Ice

The freeboard of a vessel will change when there is an added load of ice and snow. The same principle can be applied for all three vessels when calculating the new freeboard and draft of the vessels. Each portion of ice and snow on the different areas on the vessels is described by x, where the difference in mass of ice and snow are termed $m_{x.ice}$ and $m_{x.snow}$. The formula for these parameters can be calculated by

$$m_{x.ice} = \rho_{ice} \cdot l_{x.ice} \cdot b_{x.ice} \cdot t_{ice} \quad (4.2-11)$$

$$m_{x.snow} = \rho_{snow} \cdot l_{x.snow} \cdot b_{x.snow} \cdot t_{snow} \quad (4.2-12)$$

Where the thickness of the ice is described by t_{ice} , and the thickness of the snow is described by t_{snow} . The length and breadth of the portion where the snow and ice have accumulated is termed $l_{x.snow} \cdot b_{x.snow}$ and $l_{x.ice} \cdot b_{x.ice}$ respectively.

The total mass of ice and snow on an offshore structure can be described as:

$$m_{ice} = \sum_{x=1}^n m_{x.ice} \quad (4.2-13)$$

$$m_{ice} = \sum_{x=1}^n m_{x.snow} \quad (4.2-14)$$

Where n is the number of portions of ice or snow on the vessel.

The equation of the new draft of the vessels can be written as

$$\nabla = \frac{m_v + m_{ice} + m_{snow}}{\rho_w} \quad (4.2-15)$$

4.3. Stability of Vessels

The added snow and sea-spray ice accumulations on a ship or a semi-submersible can have a significant impact on the vessel's stability, and it is therefore important to consider these in the stability calculations.

This section is further divided into three sections, where the first section 4.3.1, regards the intact stability at small angles of heel. Different formulas for calculating the intact stability for both the ships and the semi-submersible will be shown. In section 4.3.2, there will be a description of the intact stability at high angles of heel. Formulas for calculating the static heel angle for the semi-submersible because of the asymmetrical loads by the sea-spray ice accumulation will be presented in section 4.3.4.

4.3.1. Intact Stability at Small Angles of Heel

The stability of a vessel can be described as its ability to return to the upright condition from a disturbing moment or force. It can be described by a system of single degree of freedom, which rotates around the longitudinal axis.

Initial static stability regards the ability of a vessel to resist the initial heel from an upright equilibrium position. The primary measure of the initial static stability is the metacentric height, GM (Tupper, 2004). It is the length in meters from point G to point M in Figure 4.3-1. The metacenter, M , is the intersection of a vertical line through the centre of buoyancy of a floating vessel at equilibrium with a vertical line through the centre of gravity of the vessel when the vessel is tilted.

The static stability of a ship can be described by three different conditions; stable, neutral and unstable. It is stable when M is above B in Figure 4.3-1, and neutral when M is at G , and unstable when M is below G .

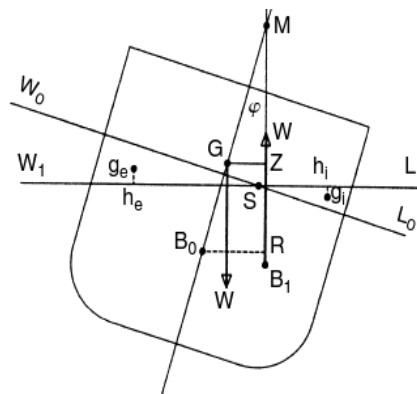


Figure 4.3-1 Front view of a ship with angles and stability parameters (Tupper, 2004)

The formula for the metacentric height \overline{GM} , can be written as

$$\overline{GM} = \overline{KB} + \overline{BM} - \overline{KG} \quad (4.3-1)$$

where

\overline{KB} [m] The vertical center of buoyancy

\overline{BM}	[m]	The metacentric radius
\overline{KG}	[m]	The center of gravity

4.3.1.1. Intact Stability of the Ships

The formulas for the vertical center of buoyancy, the metacentric radius and the center of gravity has been collected from the book of Tupper (2004).

It is assumed that all three ships, the Lady of Grace, the Viking Fighter and the Drillmax Ice, has a near rectangular hull, and therefore the formula for the \overline{KB} can be written as

$$\overline{KB} = \frac{d_v}{2} \quad (4.3-2)$$

The formula for the metacentric radius for these two ships \overline{BM} , can be calculated by

$$\overline{BM} = \frac{b_v^2}{12 \cdot d_v} \quad (4.3-3)$$

If the mass of the ship is evenly distributed, the equation for the centre of gravity for the ships \overline{KG} , can be described by

$$\overline{KG} = \frac{h_v}{2} \quad (4.3-4)$$

The equation of the metacentric height for the ships can therefore be calculated by

$$\overline{GM} = \frac{d_v}{2} + \frac{b_v^2}{12 \cdot d_v} - \frac{h_v}{2} \quad (4.3-5)$$

For later use, the metacentric radius \overline{BM} for pitch motion will be different. The formula for \overline{BM}_{pitch} can be written as:

$$\overline{BM} = \frac{l_v^2}{12 \cdot d_v} \quad (4.3-6)$$

The other parameters of the metacentric height formula, \overline{KB} and \overline{KG} will be the same, and therefore the formula for a rectangular vessel the \overline{GM}_{pitch} can be described by

$$\overline{GM}_{pitch} = \frac{d_v}{2} + \frac{l_v^2}{12 \cdot d_v} - \frac{h_v}{2} \quad (4.3-7)$$

4.3.1.2. Intact Stability of the Semi-submersible

The same principle of stability with the metacentre height \overline{GM} , regards also semi-submersibles, which is shown in equation (4.3-1). However the formulas for the \overline{KB} , \overline{BM} and \overline{KG} will be different from the formula for the ships by the reason that the hull

structure of the semi-submersible cannot be considered as rectangular.

The \overline{KB} for the semi-submersible can be calculated as

$$\overline{KB} = \left(\frac{1}{\nabla_{\text{Pontoons}} + \nabla_{\text{Bracings}} + \nabla_{\text{R.Column}} + \nabla_{\text{C.Column}}} \right) \quad (4.3-8)$$

$$\cdot (\nabla_{\text{Bracings}} \cdot y_p + \nabla_{\text{Bracings}} \cdot y_b + (\nabla_{\text{R.Column}} + \nabla_{\text{C.Column}}) \cdot y_{\text{subm}})$$

where

$$y_p = \frac{h_p}{2}$$

$$y_b = h_p + \frac{h_b}{2}$$

$$y_{\text{subm}} = h_p + \frac{h_{c.wl}}{2}$$

where

y_p	[m]	Vertical gravity height of the pontoons
y_b	[m]	Vertical gravity height of the braces
y_{subm}	[m]	Vertical gravity height of the submerged part

The vertical components; y_p , y_b , y_{subm} are shown in Figure 4.3-2 below.

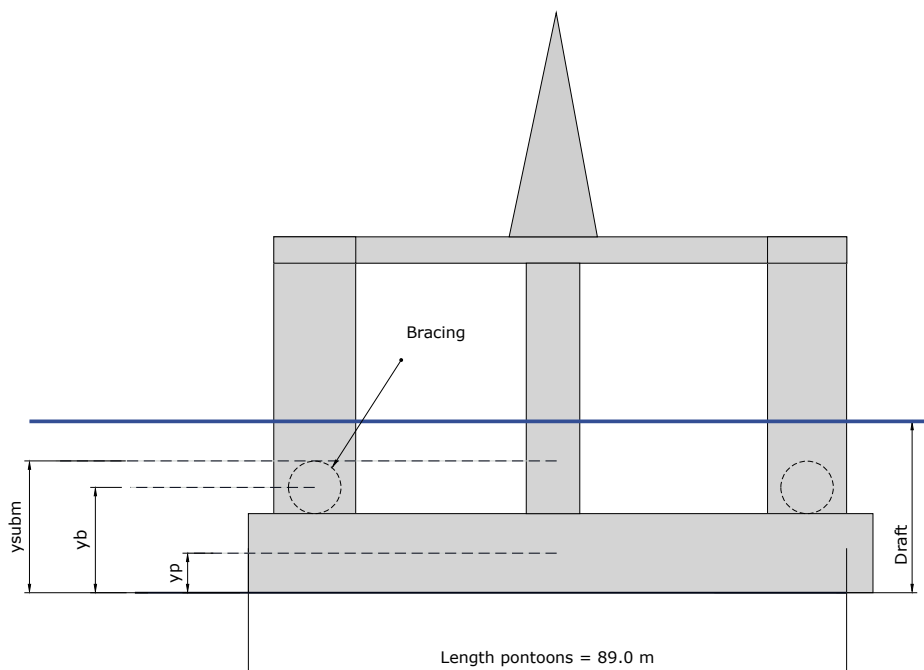


Figure 4.3-2 Showing the different vertical parameters

The formula for the metacentric radius \overline{BM} , can be calculated by

$$\overline{BM} = \frac{I_{semi}}{\nabla_{semi}} \quad (4.3-9)$$

Where I_{semi} is the second moment of inertia of the rig. It can be calculated by the Steiner's formula, see equation (4.3-10).

$$I_{semi} = 4 \cdot [I_{r.c} + x_{r.c}^2 \cdot A_{r.c}] + 2 \cdot [I_{c.c} + x_{c.c}^2 \cdot A_{c.c}] \quad (4.3-10)$$

$$I_{semi} = 4 \cdot \left[\frac{b_{r.c} \cdot l_{r.c}^3}{12} + x_{r.c}^2 \cdot b_{r.c} \cdot l_{r.c} \right] + 2 \cdot \left[\frac{\pi \cdot r_{c.c}^4}{4} + x_{c.c}^2 \cdot \pi \cdot r_{c.c}^2 \right]$$

$$\overline{BM} = \frac{\left(4 \cdot \left[\frac{b_{r.c} \cdot l_{r.c}^3}{12} + x_{r.c}^2 \cdot b_{r.c} \cdot l_{r.c} \right] + 2 \cdot \left[\frac{\pi \cdot r_{c.c}^4}{4} + x_{c.c}^2 \cdot \pi \cdot r_{c.c}^2 \right] \right)}{\nabla_{semi}} \quad (4.3-11)$$

Where the $x_{r.c}$ is the horizontal distance from the center of the rectangular column and the x-axis, and that $x_{c.c}$ is the horizontal distance from the center of the cylindrical column and the x-axis, see Figure 4.3-3.

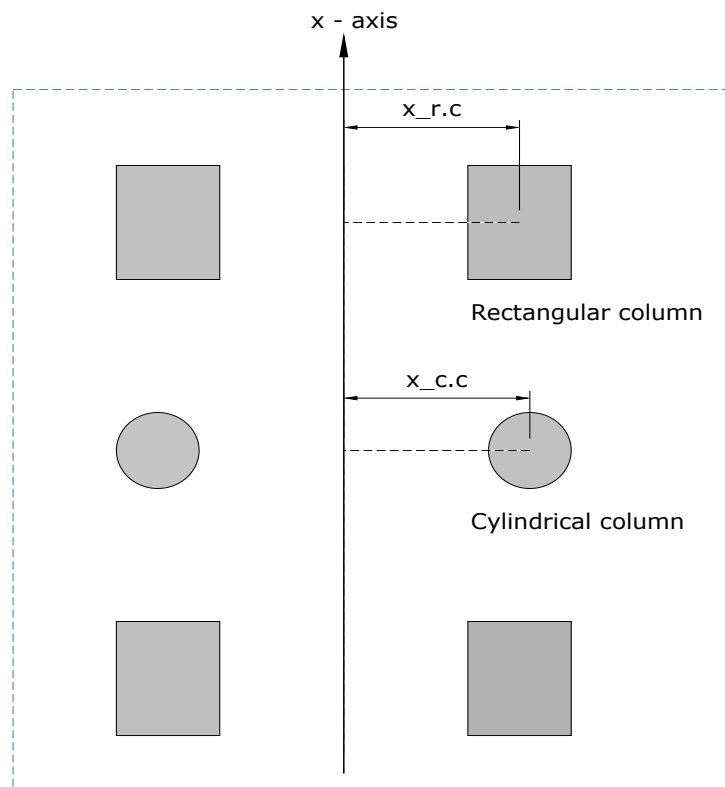


Figure 4.3-3 The waterline area of the semi-submersible

The center of gravity \overline{KG} , of the structure can be written as

$$\overline{KG} = \left(\frac{1}{2 \cdot V_{ponton} + 2 \cdot V_b + 4 \cdot V_{R.Column} + 2 \cdot V_{C.Column} + V_{deck}} \right) \cdot (2 \cdot V_{ponton} \cdot y_p + 2 \cdot V_b \cdot y_b + 4 \cdot V_{R.Column} \cdot y_{all} + 2 \cdot V_{C.Column} \cdot y_{all} + V_{deck} \cdot y_{deck}) \quad (4.3-12)$$

where

$$V_{R.Column} = l_{R.C} \cdot b_{R.C} \cdot h_{all}$$

$$V_{C.Column} = \pi \cdot r_{c.c}^2 \cdot h_{all}$$

$$V_{deck} = l_{deck} \cdot b_{deck} \cdot h_{deck}$$

By assuming that the derrick consists of four triangular plates with thickness of 0.4 m, the formula for the volume one of these plates can be written as

$$V_{derrick} = \left(\frac{l_{derrick} \cdot h_{derrick}}{2} \right) \cdot t_{derrick}$$

and

$$y_{all} = h_p + \frac{h_{all}}{2}$$

$$y_{deck} = h_p + h_{all} + \frac{h_{deck}}{2}$$

$$y_{derrick} = h_p + h_{all} + h_{deck} + \left(\frac{2}{3} \right) \cdot h_{derrick}$$

where

$V_{r.c}$	$[m^3]$	Volume of one rectangular column
$V_{c.c}$	$[m^3]$	Volume of one cylindrical column
V_{deck}	$[m^3]$	Volume of the deck
h_{all}	$[m]$	Length of all the columns (rectangular and cylindrical)
y_{all}	$[m]$	Distance from the top of the pontoons to the middle of the columns
y_{deck}	$[m]$	Distance from the middle of the deck and to the bottom

$y_{derrick}$ [m] Vertical distance from the gravity of the derrick to the bottom

The different parameters explained above are shown in Figure 4.3-4.

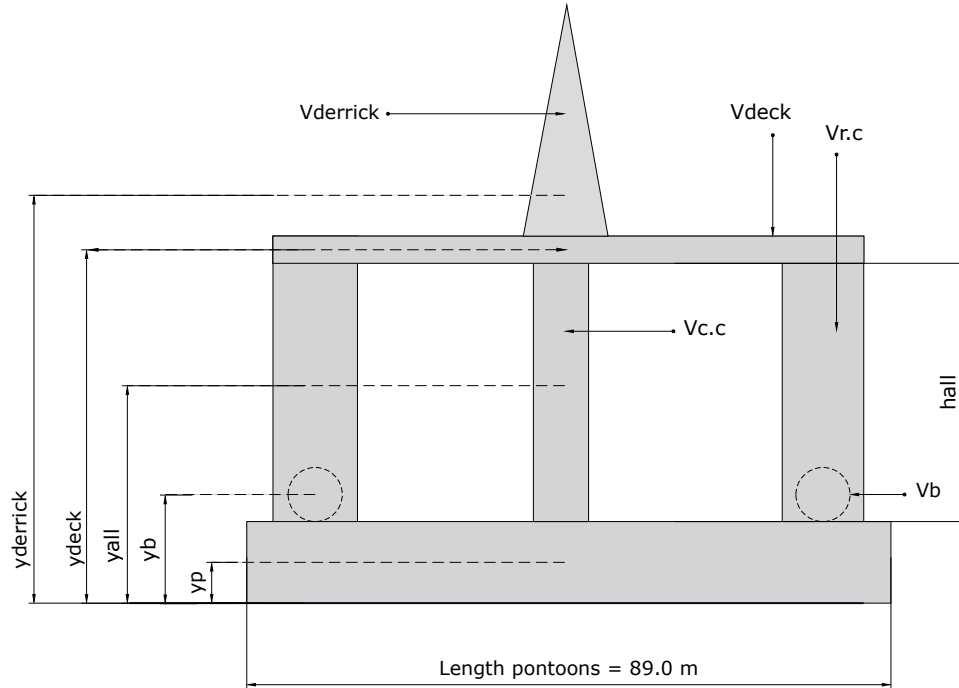


Figure 4.3-4 Parameters used in the formula for the centre of gravity, \overline{KG}

When inserting equation (4.3-8), (4.3-11) and (4.3-12) into equation (4.3-1). The formula for the intact stability of the semi-submersible can be written as

$$\overline{GM} = \frac{2 \cdot V_{pontoon} \cdot y_p + 2 \cdot V_b \cdot y_b + 4 \cdot V_{R.Column} \cdot y_{all} + 2 \cdot V_{C.Column} \cdot y_{all} + V_{deck} \cdot y_{deck}}{2 \cdot V_{pontoon} + 2 \cdot V_b + 4 \cdot V_{R.Column} + 2 \cdot V_{C.Column} + V_{deck}} + \frac{4 \cdot \left(\frac{b_{r.c} \cdot l_{r.c}^3}{12} + x_{r.c}^2 \cdot b_{r.c} \cdot l_{r.c} \right) + 2 \cdot \left(\frac{\pi \cdot r_{c.c}^4}{4} + x_{c.c}^2 \cdot \pi \cdot r_{c.c}^2 \right)}{V_{semi}} - \left(\frac{1}{2 \cdot V_{pontoon} + 2 \cdot V_b + 4 \cdot V_{R.Column} + 2 \cdot V_{C.Column} + V_{deck} + 4 \cdot V_{derrick}} \cdot 2 \cdot V_{pontoon} \cdot y_p + 2 \cdot V_b \cdot y_b + 4 \cdot V_{R.Column} \cdot y_{all} + 2 \cdot V_{C.Column} \cdot y_{all} + V_{deck} \cdot y_{deck} + 4 \cdot V_{derrick} \cdot y_{derrick} \right)$$

For later use, the metacentric radius \overline{BM} for pitch motion will be decided. The formula for \overline{BM}_{pitch} can be written as

$$\overline{BM}_{pitch} = \frac{I_{semi.pitch}}{\nabla_{semi}} \quad (4.3-13)$$

where

$$I_{semi} = 4 \cdot [I_{pitch.r.c} + y_{r.c}^2 \cdot A_{r.c}] + 4 \cdot [I_{pitch.c.c} + y_{c.c}^2 \cdot A_{c.c}(\frac{1}{2})] \quad (4.3-14)$$

$$I_{semi.pitch} =$$

$$4 \cdot \left[\frac{b_{r.c}^3 \cdot l_{r.c}^1}{12} + y_{r.c}^2 \cdot b_{r.c} \cdot l_{r.c} \right] + 4 \cdot \left[\frac{\pi \cdot r_{c.c}^4}{8} + y_{c.c}^2 \cdot \frac{\pi \cdot r_{c.c}^2}{2} \right]$$

$$\overline{BM} = \frac{4 \cdot \left[\frac{b_{r.c}^3 \cdot l_{r.c}^1}{12} + y_{r.c}^2 \cdot b_{r.c} \cdot l_{r.c} + \frac{\pi \cdot r_{c.c}^4}{8} + y_{c.c}^2 \cdot \frac{\pi \cdot r_{c.c}^2}{2} \right]}{\nabla_{semi}} \quad (4.3-15)$$

Where the $y_{r.c}$ is the vertical distance from the center of the rectangular column and the y-axis, and that $y_{c.c}$ is the vertical distance from the center of the cylindrical column and the y-axis, see Figure 4.3-3.

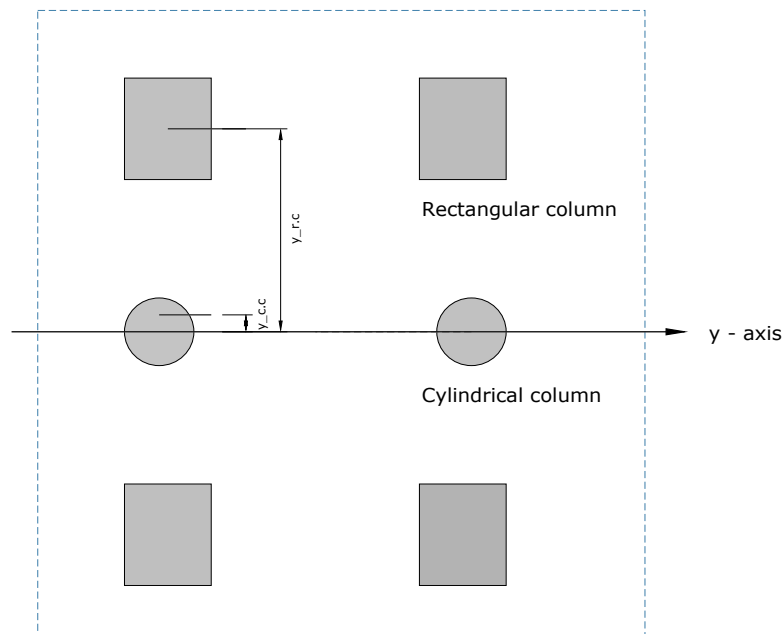


Figure 4.3-5 The waterline area of the semi-submersible

The other parameters of the metacentric height formula, \overline{KB} and \overline{KG} will be the same, and thus the formula for a rectangular vessel the \overline{GM}_{pitch} can be described by

$$\overline{GM}_{pitch} = \overline{KB} + \overline{BM}_{pitch} - \overline{KG} \quad (4.3-16)$$

Which gives the equation

$$\overline{GM}_{pitch} = \frac{2 \cdot V_{pontoon} \cdot y_p + 2 \cdot V_b \cdot y_b + 4 \cdot V_{R.Column} \cdot y_{all} + 2 \cdot V_{C.Column} \cdot y_{all} + V_{deck} \cdot y_{deck}}{2 \cdot V_{pontoon} + 2 \cdot V_b + 4 \cdot V_{R.Column} + 2 \cdot V_{C.Column} + V_{deck}} + \frac{4 \cdot \left[\frac{b_{r.c}^3 \cdot l_{r.c}^1}{12} + y_{r.c}^2 \cdot b_{r.c} \cdot l_{r.c} + \frac{\pi \cdot r_{c.c}^4}{8} + y_{c.c}^2 \cdot \frac{\pi \cdot r_{c.c}^2}{2} \right]}{\nabla_{semi}}$$

$$- \frac{2 \cdot V_{pontoon} \cdot y_p + 2 \cdot V_b \cdot y_b + 4 \cdot V_{R.Column} \cdot y_{all} + 2 \cdot V_{C.Column} \cdot y_{all} + V_{deck} \cdot y_{deck}}{2 \cdot V_{pontoon} + 2 \cdot V_b + 4 \cdot V_{R.Column} + 2 \cdot V_{C.Column} + V_{deck}}$$

4.3.1.3. Intact Stability of a Vessel With Accumulated Ice

When a vessel is experiencing different portions of ice and snow ($m_{x.ice}$ and $m_{x.snow}$) the \overline{KB} and \overline{BM} values change due to the changed freeboard, and the \overline{KG} will also change.

The changed \overline{KB} and \overline{BM} for a ship can be written as

$$\overline{KB}_{ice} = \frac{d_{ice}}{2} \quad (4.3-17)$$

$$\overline{BM}_{ice} = \frac{b_v^2}{d_{ice}} \quad (4.3-18)$$

The changed \overline{KB} and \overline{BM} for the semi-submersible can be written as

$$\overline{KB}_{ice} = \left(\frac{1}{\nabla_{Pontoons} + \nabla_{Bracings} + \nabla_{R.Column} + \nabla_{C.Column}} \right) \quad (4.3-19)$$

$$\cdot (\nabla_{Bracings} \cdot y_p + \nabla_{Bracings} \cdot y_b + (\nabla_{R.Column} + \nabla_{C.Column}) \cdot y_{subm})$$

$$\overline{BM}_{ice} = \frac{\left(4 \cdot \left[\frac{b_{r.c} \cdot l_{r.c}^3}{12} + x_{r.c}^2 \cdot b_{r.c} \cdot l_{r.c} \right] + 2 \cdot \left[\frac{\pi \cdot r_{c.c}^4}{4} + x_{c.c}^2 \cdot \pi \cdot r_{c.c}^2 \right] \right)}{\nabla_{semi}} \quad (4.3-20)$$

Where the values for the submerged parts ∇ , and the value for y_{subm} , are different in the formula since the value for $h_{c.wl}$ has increased with the additional ice and snow loads.

The principle of calculating the changed \overline{KG} with the accumulated ice is the same for ships and semi-submersibles. An example of a vessel with different portions of snow and ice is shown in Figure 4.3-6.

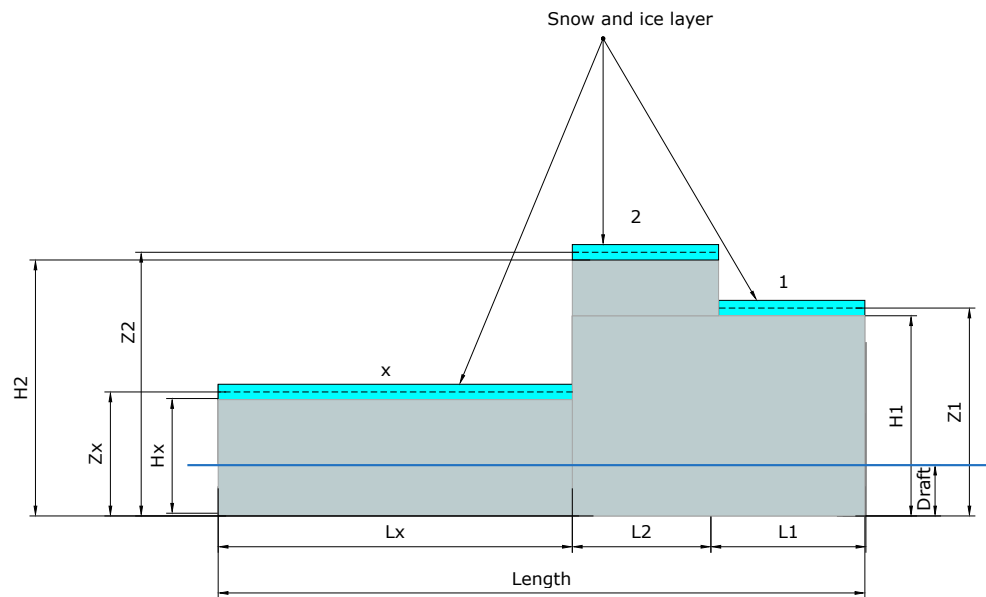


Figure 4.3-6 Figure of a vessel with masses of ice and snow

Seen from the figure, each portions of ice will each have a value for the height, z_x . The equation for the center of gravity for the vessels when ice loads are included, \overline{KG}_{ice} , can be described as

$$\overline{KG}_{ice} = \frac{m_v \cdot \frac{h_v}{2} + m_1 \cdot z_1 + m_2 \cdot z_2 + \dots}{m_{vessel} + m_{ice} + m_{snow}} \quad (4.3-21)$$

$$z_x = h_{level} + \frac{t_{ice}}{2}$$

$$\text{or } z_x = h_{level} + \frac{t_{snow}}{2}$$

The formula for the intact stability when ice and snow loads are included can be written as

$$\overline{GM}_{ice} = \overline{KB}_{ice} + \overline{BM}_{ice} - \overline{KG}_{ice} \quad (4.3-22)$$

By inserting equation (4.3-17), (4.3-18) and (4.3-21) into (4.3-22) the equations for the stability of the two ships can be done.

By inserting equation (4.3-19), (4.3-20) and (4.3-21) into (4.3-22), the equations for the stability of the semi-submersible can be done.

4.3.2. Intact Stability at High Angles of Heel

The metacentric height, \overline{GM} , is often used as a measure of the stability at small angles of heel, usually between $0 - 5^\circ$. When the heeling angle is higher than 5° , the stability of the ship is dominated by the righting moment and righting arm (Tupper, 2004).

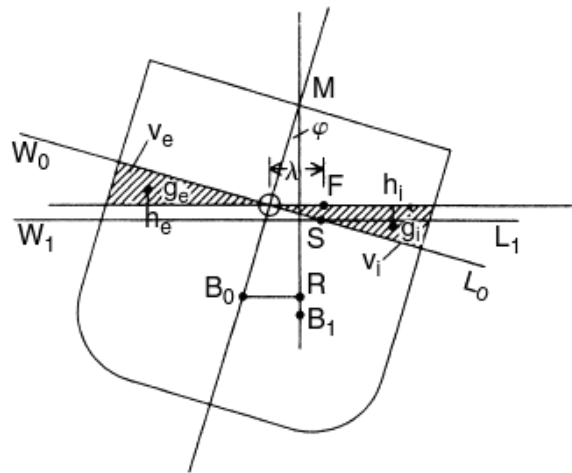


Figure 4.3-7 Stability of a vessel at large angles (Tupper, 2004)

The righting moment is a result from the ship being heeled by external forces such as waves, wind, and more, from of the initial horizontal equilibrium position. The heeling angle, φ , due to this force is shown in Figure 4.3-7. Ships usually have relatively constant displacement, which is why the righting arm that determines the righting moment.

The equation for the righting moment, M_r , of a vessel can be written as:

$$M_r = \overline{GZ} \cdot \rho_w \cdot g \cdot \nabla = \overline{GM} \cdot \Delta \cdot \sin(\varphi) \quad (4.3-23)$$

$$\Delta = m \cdot g \quad (4.3-24)$$

Where \overline{GZ} is the righting arm and Δ is the mass displacement. The righting arm, \overline{GZ} , is the horizontal distance between the vertical line through the center of buoyancy in upright position and the center of gravity. It is the distance between point G and Z in Figure 4.3-7.

According to Tupper (2004), the equation for the righting arm of a vessel can be written as

$$\overline{GZ} = \overline{GM} \cdot \sin\varphi + \frac{1}{2} \cdot \overline{BM} \cdot \tan^2 \varphi \cdot \sin\varphi \quad (4.3-25)$$

4.3.3. Static Heel Angle of a Vessel Due to Asymmetric Load of Ice

When a vessel experiences higher loading on one side, as the semi-submersible rig will in this case due to the asymmetric load of sea-spray ice on one side, it will experience a heeling angle, φ . This can be seen in Figure 4.3-8.

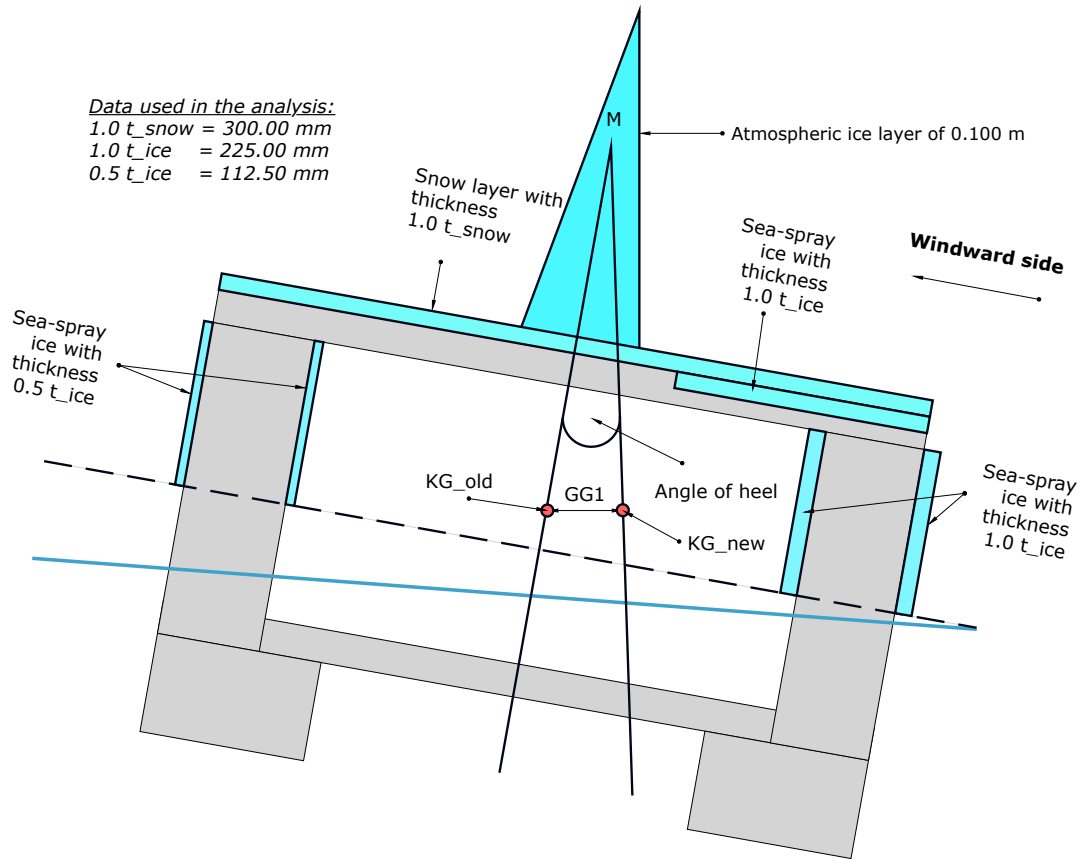


Figure 4.3-8 Static heeling angle due to the asymmetric load of sea-spray ice

By the equation for the GG_1 given by Tupper (2004), the heeling angle for this semi-submersible can be calculated:

$$\tan\varphi^{-1} = \frac{GG_1}{GM_{ice}} \quad (4.3-26)$$

$$GG_1 = KG_{H.old} - KG_{H.new}$$

Where GG_1 is the difference in KG horizontally due to the sea-spray ice. The sea-spray ice will cover up more on the windward side and those are the factors to consider:

$$KG_{H.old} = \left(\frac{1}{4 \cdot V_{r.c} + 2 \cdot V_{c.c} + V_{Deck} + 2 \cdot V_p + 2 \cdot V_b + V_{derrick}} \right) \cdot \quad (4.3-27)$$

$$(2 \cdot [V_{r.c}(x_{r.c.wind} + x_{r.c.nowind})]$$

$$+ [V_{c.c}(x_{c.c.wind} + x_{c.c.nowind})] + V_{Deck} \cdot x_{deck}$$

$$+ [V_p(x_{p.wind} + x_{p.nowind}) + [V_b(x_{b.wind} + x_{b.nowind})]])$$

The different parameters mentioned in equations (4.3-27) and (4.3-28) are shown in Figure 4.3-9.

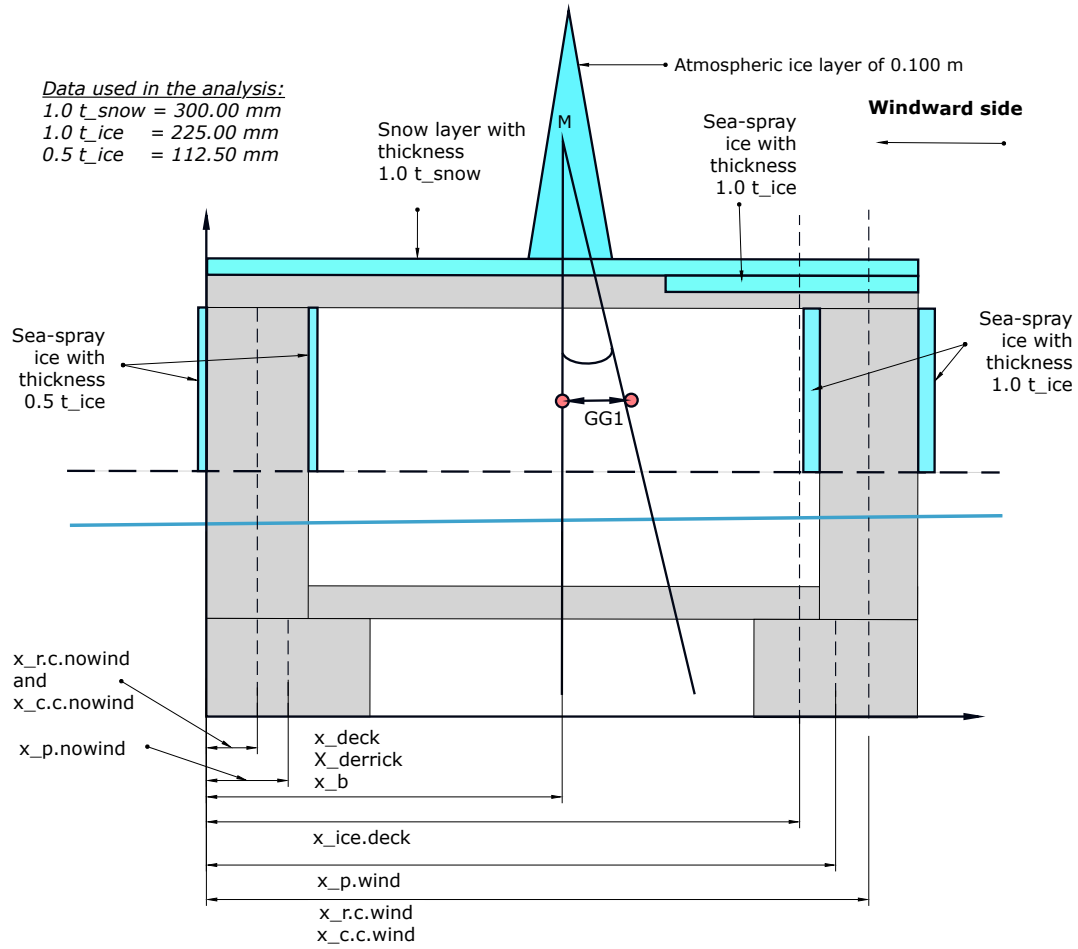


Figure 4.3-9 Parameters of the KG formula before the heeling moment

$$KG_{H.new} = \tag{4.3-28}$$

$$\left(\frac{1}{4 \cdot V_{r.c} + 2 \cdot V_{c.c} + V_{Deck} + 2 \cdot V_p + 2 \cdot V_b + 4 \cdot V_{derrick} + V_{ice} + V_{snow}} \right) \cdot [4 \cdot V_{r.c} (x_{r.c.wind} + x_{r.c.nowind})$$

$$+ 2 \cdot V_{c.c} (x_{c.c.wind} + x_{c.c.nowind}) + V_{Deck} \cdot x_{deck}$$

$$+ 4 \cdot V_{derrick} + 4 \cdot V_{derrickice}$$

$$+ 2 \cdot V_p (x_{p.wind} + x_{p.nowind}) + 2 \cdot V_b (x_{b.wind} + x_{b.nowind})$$

$$+ 2 \cdot V_{ice.r.c} (x_{r.c.wind} + x_{r.c.nowind})$$

$$+ V_{ice.c.c} (x_{c.c.wind} + x_{c.c.nowind}) + V_{ice.deck} \cdot x_{ice.deck}$$

$$+ V_{snow.maindeck} \cdot x_{snow.maindeck} + V_{snow.upperdeck} \cdot x_{snow.pperdeck}]$$

$$V_{ice} = \frac{m_{ice}}{\rho_{ice}}$$

$$V_{snow} = \frac{m_{snow}}{\rho_{snow}}$$

Where V_{ice} and V_{snow} is the total volume of ice and snow respectively, on the vessel.

4.4. Vessel Motion Characteristics

This section is divided into five parts. The first section regards the general vessel motions. In section 4.4.2, a description is given on the heave motion of the vessel, where a description on how it is calculated for ships and semi-submersibles is given. An explanation on how the pitch motion is calculated is given in section 4.4.3. The coupled heave and pitch motion is further explained in the next section. In section 4.4.5, the explanation on how to calculate the roll motion of the vessels is given.

4.4.1. The General Vessel Motions

The vessel motion characteristics are defined by six degrees of freedom that can be divided into translational motions and rotational motions. The amplitude of these motions will vary if there are ice and snow loads on the vessels. Both situations of where there are ice loads and where there is not, will be considered in the calculations.

The translational motions of a vessel are the heave, surge and sway motion. Where heave is the linear up-and-down (vertical) motion, surge is the linear front-to-back (longitudinal) motion, and sway is the side-to-side (lateral) motion. The rotational motions are the pitch, yaw and roll motions. The pitch motion is rotation of a ship about its transverse, the yaw motion is the rotation of a vessel around the vertical axis and the roll motion is the rotation about the vessels longitudinal axis (Tupper, 2004). An illustration of the motions is shown in Figure 4.4-1.

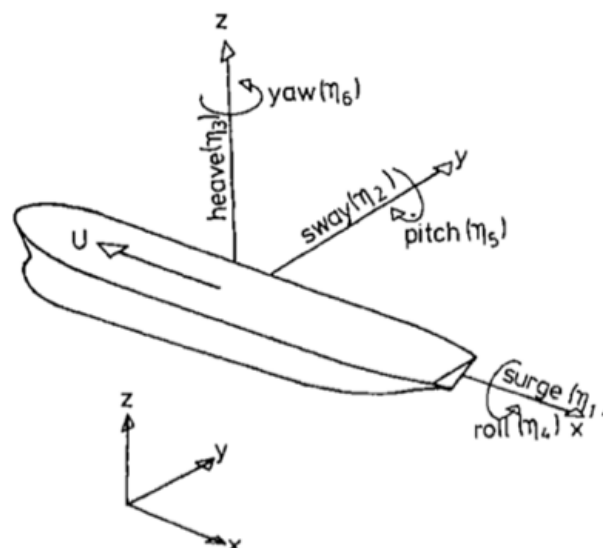


Figure 4.4-1 Vessel motion characteristics in a coordinate system (Faltinsen, 1993)

The greatest displacement of a vessel occurs in heave, pitch and roll motions, which is the reason why these motions will be calculated in the report. The centre of the effect of the vertical hydrostatic force is usually moving towards the ship stern when the

draft of the vessel is changed. The reason for this is that the frames in the stern are usually fuller than what it is in the bow region. A negative pitch angle will be caused when the displacement of the centre of effect is towards the stern, and therefore pitch oscillations cause heave oscillations and vice versa. This means that the heave and pitch motions are coupled.

4.4.2. Heave Motion

The formula for heave motion can be written as:

$$F(t) = m \cdot \ddot{z} + c \cdot \dot{z} + k \cdot z \quad (4.4-1)$$

where

$F(t)$	$[N]$	Force
m	$[kg]$	Mass
c		Damping
\ddot{z}	$[m/s^2]$	Acceleration of object
\dot{z}	$[m/s]$	Velocity of object
z	$[m]$	Displacement of object
k		Constant

The equation can be rewritten when there is an undamped free motion ($c = F(t) = 0$)

$$0 = m \cdot \ddot{z} + k \cdot z \quad (4.4-2)$$

The solution of this differential equation gives the equation for heave

$$u_{Heave}(t) = a \cdot RAO \cdot \sin(\omega_{0,h} \cdot t) \quad (4.4-3)$$

where

a	$[m]$	Amplitude in heave
$\omega_{0,h}$	$[s^{-1}]$	Natural frequency in heave
t	$[s]$	Time
RAO	$[-]$	Response Amplitude Operator

4.4.3. Pitch Motion

The angle of pitch is varying with time, and the expression can be written as

$$\varphi_p(t) = \varphi_{p.amplitude} \cdot \sin(\omega_{0,p} \cdot t) \quad (4.4-4)$$

Half of the total length of the vessel, $\frac{l_v}{2}$, is the distance from the middle of the ship and to each end sides. It is where the pitch displacement is at its greatest.

The translation of the angle to the pitch displacement can be written as

$$u_p(t) = \frac{l_v}{2} \cdot \varphi_{p.amplitude} \cdot \sin(\omega_{0,p} \cdot t) \quad (4.4-5)$$

where

$u_p(t)$	[m]	Pitch displacement
$\varphi_{p.amplitude}$	[rad]	Angle of pitch given in radians
$\omega_{0,p}$	[s ⁻¹]	Natural frequency of the pitch period
l_v	[m]	Length of the vessel (l.p.p)

4.4.4. Coupled Heave and Pitch Motion

It is also important to consider the coupled heave and pitch motion. This can be done by the superposition principle. The coupled heave and pitch motion can therefore be written as

$$u_{coupled}(t) = u_{Heave}(t) + u_p(t) \quad (4.4-6)$$

$$u_{coupled}(t) = \quad (4.4-7)$$

$$a \cdot RAO \cdot \sin(\omega_{0,h} \cdot t) + \frac{l_v}{2} \cdot \varphi_{p.amplitude} \cdot \sin(\omega_{0,p} \cdot t)$$

4.4.5. Roll Motion

The motion of roll seen from a front view on a ship is shown in Figure 4.4-2.

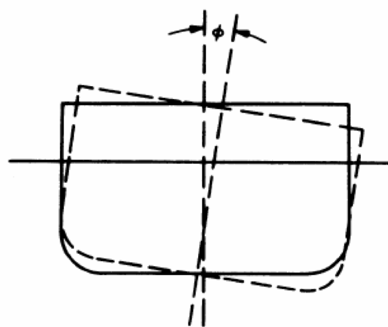


Figure 4.4-2 Roll motion of a ship (Tupper, 2004)

Stated by (Tupper and Rawson, 2001), the motion equation for an undamped rotational system can be written as

$$I_r \ddot{\varphi}_r(t) + c \dot{\varphi}_r(t) + k \varphi_r(t) = M(t) \quad (4.4-8)$$

Where the different parameters can be written as:

$$I_r = m \cdot r_r^2 \quad (4.4-9)$$

$$r_r = \sqrt{\frac{I_r}{m}} \quad (4.4-10)$$

$$k \varphi_r(t) = \overline{GM} \cdot \sin(\varphi_r) \cdot \Delta \quad (4.4-11)$$

where

I_T	$[m^4]$	The transverse mass moment of inertia
t	$[s]$	Time
m	$[kg]$	Mass of the vessel (without the added mass)
r_r	$[m]$	The mass radius of gyration
φ_r		Inclination of the vessel
c		The damping constant
$M(t)$	$[N \cdot m]$	The external moment
$k \varphi_r(t)$	$[N \cdot m]$	Up-righting moment

By assuming simple harmonic motions, the equation for roll motion can be developed from equation (4.3-23):

$$k \cdot \varphi_r(t) = \Delta \cdot \overline{GZ} = \Delta \cdot \overline{GM} \cdot \sin(\varphi_r) \quad (4.4-12)$$

At small angles (close to 0°), the sinusoidal function, $\sin(\approx 0^\circ) = 1$. This means that the equation can be rewritten for small angles as:

$$k = \Delta \cdot \overline{GM} \quad (4.4-13)$$

By the reason this is assumed to be an un-damped free system, the c value in equation (4.4-8) becomes zero, then the external moment ($M(t)$) also becomes zero.

This gives the equations:

$$0 = k \varphi_r(t) = \overline{GM} \cdot \varphi_r \cdot \Delta + \frac{\Delta}{g} \cdot r_r^2 \cdot \ddot{\varphi}_r \quad (4.4-14)$$

$$\ddot{\varphi}_r + \frac{\overline{GM} \cdot g}{r_r^2} \cdot \varphi_r = M(t) = 0 \quad (4.4-15)$$

These are differential equations with simple harmonic motions. The solution of equation (4.3-3) gives the equation (4.4-16), which is the equation of the angular displacement, φ_r :

$$\varphi_r(t) = \varphi_{r.amplitude} \cdot \sin(\omega_{0,r} \cdot t) \quad (4.4-16)$$

where

$\varphi_r(t)$	[degrees]	Roll angle
$\varphi_{r.amplitude}$	[m]	Corresponding amplitude in roll to the direction and natural period
$\omega_{0,r}$	[s ⁻¹]	Natural frequency of the roll period

4.5. Natural Periods

Section 4.5.1 provides some general information about the natural periods. The natural period in heave for the vessels will be explained in section 4.5.2. In section 4.5.3, the natural period in pitch will be described. The natural period in roll for the ships and the semi-submersible will be explained in section 4.5.4

4.5.1. General Information About Natural Periods

The natural periods together with the damping level and wave excitation level are three important factors when calculating the amplitudes of motion for ships or offshore platforms. The largest motions are usually occurring when the constructions are excited with the natural periods, when they are in resonance with the waves (Tupper and Rawson, 2001).

4.5.2. Natural Period in Heave

According to Faltinsen (1993), the uncoupled natural period in heave for a freely floating offshore vessel can be written as

$$T_{Heave} = 2\pi \cdot \sqrt{\frac{m_v + A_{33}}{k}} \quad (4.5-1)$$

$$k = \rho_w \cdot g \cdot A_w \quad (4.5-2)$$

where

T_{Heave}	[s]	Natural period in heave
-------------	-----	-------------------------

A_{33}	[kg]	Added mass
m_v	[kg]	Mass of the vessel
k	[N/m]	Stiffness
A_W	[m ²]	Water plane area of the structure

The heave equation for the two ships will be different from the heave equation for the semi-submersible because of the difference in the hull geometry.

4.5.2.1. Natural Period in Heave for the two Ships

The equation for a rectangular vessel, with water plane area, A_p , can be written as

$$A_p = l_v \cdot b_v \quad (4.5-3)$$

According to Faltinsen (1993), the value of added mass in heave for three-dimensional, non-perforated structures and with vertical sides can be written as

$$A_{33} \approx \left[1 + \sqrt{\frac{1 - \lambda^2}{2(1 + \lambda^2)}} \right] \cdot A_{33o} \quad (4.5-4)$$

$$\lambda = \frac{\sqrt{A_p}}{h + \sqrt{A_p}} \quad (4.5-5)$$

where

A_{33o}	[kg]	Added mass for a flat plate
λ		Factor between height of object and area of submerged part
h	[m]	Height of the structure
A_p	[m ²]	Area of submerged part of object that is projected on a horizontal plane

The added mass, m_{added} , is a phenomenon that occurs when water particles move due to movement of floating objects with amplitudes that declines away from the objects.

Further the value for the added mass for a three-dimensional flat plate in infinite fluid, A_{33o} , can be written as:

$$A_{33o} = \rho_w \cdot C_A \cdot V_R \quad (4.5-6)$$

$$V_R = \frac{\pi}{4} \cdot b_v^2 \cdot l_v \quad (4.5-7)$$

Where the parameter C_A is decided by the factor between length and breadth of the ship. The table for C_A is shown in Appendix B, and in order to get an accurate value for C_A from the table interpolation can be used. The formula for interpolation can be written as

$$y = y_a + (y_b - y_a) \cdot \left(\frac{x - x_a}{x_b - x_a} \right) \quad (4.5-8)$$

The natural frequency in heave for the ships can be written as

$$\omega_{0,h} = \frac{2\pi}{T_{Heave}} \quad (4.5-9)$$

When ice and snow are included on the ships the equation for the natural period and the frequency can be calculated by

$$T_{Heave.ice} = 2\pi \cdot \sqrt{\frac{m_v + m_{ice} + A_{33}}{k}} \quad (4.5-10)$$

$$\omega_{0,h.ice} = \frac{2\pi}{T_{Heave.ice}} \quad (4.5-11)$$

4.5.2.2. Natural Period in Heave for the Semi-submersible

When the ice and snow are included on the vessel the equation for the natural period in pitch and the frequency can be calculated by

$$T_{Heave.ice} = 2\pi \cdot \sqrt{\frac{m_{semi} + m_{ice} + A_{33}}{k}} \quad (4.5-12)$$

$$\omega_{0,h.ice} = \frac{2\pi}{T_{Heave.ice}} \quad (4.5-13)$$

Where the value for k can be calculated by equation (4.5-2), and where the waterline area for the pontoons can be written as

$$A_W = l_p \cdot b_p \quad (4.5-14)$$

By assuming that it is considered as a perforated vessel the formula (4.5-4) cannot be used.

The value for the added mass for the semi-submersible, A_{33} , can be calculated by

$$A_{33} = 2 \cdot l_p \cdot A_{330} \quad (4.5-15)$$

where

$$A_{330} = \rho_w \cdot C_{A.semi} \cdot A_R \quad (4.5-16)$$

The parameter $C_{A.semi}$ is decided by the factor between length and breadth of the pontoons, where this value can also be found in Appendix B.

$$A_R = \pi \cdot \left(\frac{b_p}{2}\right)^2 \quad (4.5-17)$$

4.5.3. Natural Period in Pitch

The natural period in pitch can be found in similar ways as in roll, where the main change is the axis, see Figure 4.5-1.

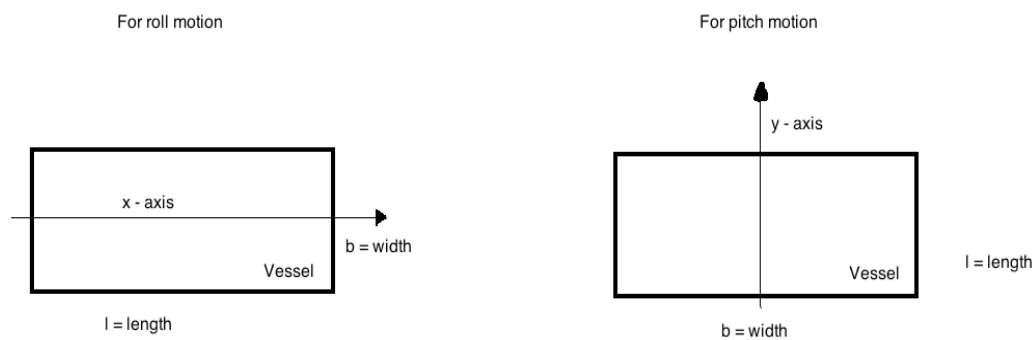


Figure 4.5-1 Different axes for roll and pitch motions

The pitch and roll equations for the two ships will differ from the heave equation for the semi-submersible due to the difference in the hull geometry.

The uncoupled natural period in pitch for a freely floating offshore vessel can be calculated by

$$T_{0,p} = 2 \cdot \pi \cdot \sqrt{\frac{I_p + A_{55}}{k_p}} \quad (4.5-18)$$

$$\omega_{0,p} = \frac{2 \cdot \pi}{T_{0,p}} \quad (4.5-19)$$

Where

A_{55}

Pitch added moment of inertia

I_p

Rigid body mass moment of inertia about the transverse axis (y-axis)

4.5.3.1. Natural Period in Pitch for Ships

The pitch mass moment of inertia for pitch, I_p , for the ships can be calculated from

$$I_p = \rho_w \cdot d \cdot \int_{-l_v/2}^{l_v/2} x^2 dx \cdot \int_0^b db_v$$

$$I_p = \frac{\rho_w \cdot d \cdot l_v^3 \cdot b_v}{12} \quad (4.5-20)$$

The formula for k_p can be written as

$$k_p = \overline{GM_{pitch}} \cdot \rho_w \cdot g \cdot \nabla \quad (4.5-21)$$

$$\nabla = l_v \cdot b_v \cdot d_v \quad (4.5-22)$$

Where, ∇ , is the submerged volume of the ship and the formula for $\overline{GM_{pitch}}$ is shown in equation (4.3-16) above.

The pitch added moment of inertia for ships are usually very small. According to Debabrata (2011), it is usually very small for ships, not more than 20% of the mass moment of inertia in pitch. It has been chosen to include the effect and it is assumed to be 20% of the mass moment of inertia in pitch.

$$A_{55} = I_p \cdot 1.2 \quad (4.5-23)$$

The natural period of the ships in pitch can therefore be written as

$$T_{0,p} = 2 \cdot \pi \cdot \sqrt{\frac{(\rho_w \cdot d \cdot l_v^3 \cdot b_v) \cdot 1.2}{\overline{GM_{pitch}} \cdot \rho_w \cdot g \cdot l_v \cdot b_v \cdot d_v \cdot 12}} \quad (4.5-24)$$

4.5.3.2. Natural Period in Pitch for the Semi-submersible

The pitch mass moment of inertia for pitch, I_p , for the rig can be calculated as

$$I_p = \rho_w \cdot h_p \cdot 2 \cdot I_{0p}$$

$$I_p = \rho_w \cdot h_p \cdot 2 \cdot \frac{b_p^3 \cdot l_p}{12}$$

$$I_p = \rho_w \cdot h_p \cdot \frac{b_p^3 \cdot l_p}{6} \quad (4.5-25)$$

This formula is based on Figure 4.5-2 below.

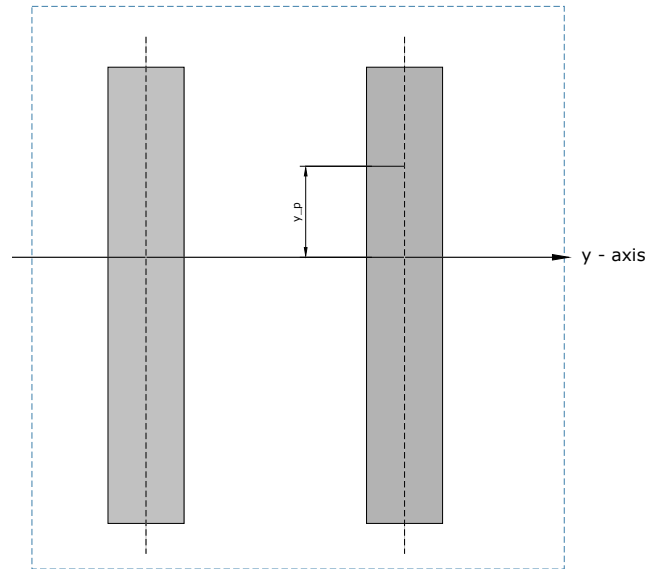


Figure 4.5-2 The plane area of the pontoons for the pitch motion

The pitch added moment of inertia of the semi-submersible can be much greater than for ships and can be written as

$$A_{55} = \frac{\rho_w \cdot \pi \cdot b_p^2}{8} \int_{-\frac{l_p}{2}}^{\frac{l_p}{2}} x^2 dx$$

$$A_{55} = \frac{\rho_w \cdot \pi \cdot b_p^2}{8} \cdot \frac{l_p^3}{12} \quad (4.5-26)$$

The formula for k_p for the rig can be written as in equation (4.5-21) but the equation for the submerged volume, ∇ , equation (4.5-22) will be different for the semi-submersible. The equation for the submerged volume for the rig can be written as in equation (4.5-27), where it is assumed that the pontoons are totally submerged.

$$\nabla = 2 \cdot (l_p \cdot b_p \cdot h_p) \quad (4.5-27)$$

From equation (4.5-18), equation (4.5-21) and equation (4.5-27) above, the natural period in pitch for the rig can be written as

$$T_{0,p} = 2 \cdot \pi \cdot \sqrt{\frac{h_p \cdot \frac{b_p^2}{6} + \frac{\pi}{8} \cdot \frac{1}{12}}{GM_{pitch} \cdot g \cdot 2 \cdot h_p}} \quad (4.5-28)$$

4.5.4. Natural Period in Roll

The uncoupled natural period in roll for a freely floating offshore vessel can be calculated by

$$T_{0,r} = 2 \cdot \pi \cdot \sqrt{\frac{I_r + A_{44}}{k_r}} \quad (4.5-29)$$

$$\omega_{0,r} = \frac{2 \cdot \pi}{T_{0,r}} \quad (4.5-30)$$

Where

A_{44} Roll added moment of inertia

I_r Rigid body mass moment of inertia about the longitudinal axis (x-axis)

The roll equation for the two ships will differ from the heave equation for the semi-submersible due to the difference in the hull geometry.

4.5.4.1. Natural Period in Roll for the Two Ships

The transverse mass moment of inertia, I_r , for rectangular ships can be written as:

$$I_r = \rho_w \cdot d \cdot \int_{-b/2}^{b/2} x^2 dx \cdot \int_0^L dl$$

$$I_r = \frac{\rho_w \cdot d_v \cdot b_v^3 \cdot l_v}{12} \quad (4.5-31)$$

The roll added moment of inertia, A_{44} , for ships are usually very small. According to Debabrata (2011), it is usually very small for ships, not more than 20% of the mass moment of inertia in roll. Assuming that in this case it is 20% of the mass moment inertia, it can be written as

$$A_{44} = I_r \cdot 1.2 \quad (4.5-32)$$

The formula for k_r can be calculated by

$$k_r = \overline{GM} \cdot \rho_w \cdot g \cdot \nabla \quad (4.5-33)$$

Where the submerged part of the ship, ∇ , can be calculated from formula (4.5-22) above.

The natural period in roll for the ships can therefore be written as

$$T_{0,r} = 2 \cdot \pi \cdot \sqrt{\frac{b_v^2 \cdot 1.2}{12 \cdot GM \cdot g}} \quad (4.5-34)$$

4.5.4.2. Natural Period in Roll for the Semi-submersible

The longitudinal mass moment of inertia for roll, I_r , can be written as

$$I_r = \rho_w \cdot h_p \cdot 2 \cdot (I_{0r} + x_{0r} \cdot A_p)$$

$$I_r = 2 \cdot \left(\frac{l_p \cdot b_p^3}{12} + x_{0r} \cdot l_p \cdot b_p \right)$$

$$I_r = \frac{l_p \cdot b_p^3}{6} + 2 \cdot x_{0r} \cdot l_p \cdot b_p \quad (4.5-35)$$

The formula for longitudinal mass moment of inertia is based on Figure 4.5-3 below.

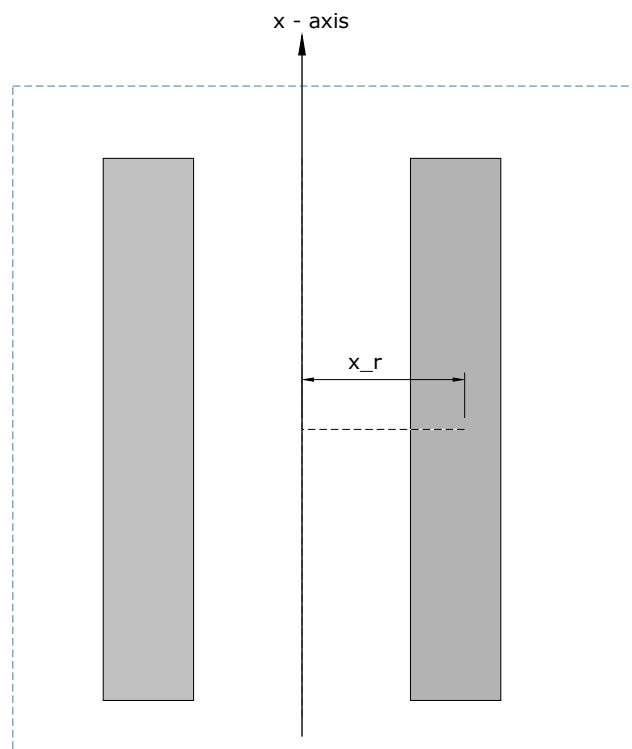


Figure 4.5-3 The plane area of the pontoons for the roll motion

The roll added moment of inertia of the semi-submersible can be written as

$$A_{44} = \frac{\rho_w \cdot \pi \cdot l_p^2}{8} \int_{-\frac{b_p}{2}}^{\frac{b_p}{2}} x^2 dx$$

$$A_{44} = \frac{\rho_w \cdot \pi \cdot l_p^2}{8} \cdot \frac{b_p^3}{12} \quad (4.5-36)$$

The formula for k_r for the semi-submersible can be calculated by

$$k_r = \overline{GM} \cdot \rho_w \cdot g \cdot \nabla$$

$$k_r = \overline{GM} \cdot \rho_w \cdot g \cdot (2 \cdot l_p \cdot b_p \cdot h_p) \quad (4.5-37)$$

By inserting equations (4.5-37) and (4.5-35) into equation (4.5-29), the natural period in roll for the semi-submersible can therefore be written as

$$T_{0,r} = 2 \cdot \pi \cdot \sqrt{\frac{\frac{b_p^2}{6} + 2 \cdot x_{0r} + \frac{\rho_w \cdot \pi \cdot l_p}{8} \cdot \frac{b_p^2}{12}}{\overline{GM} \cdot \rho_w \cdot g \cdot 2 \cdot h_p}} \quad (4.5-38)$$

4.6. Response Amplitude Operators

The response amplitude operator (RAO), also called the transfer function, is an important parameter for offshore vessels. It is an engineering statistic used to decide the probable behaviour of a vessel at sea; it gives an indication of how much the vessel moves with the waves. The most dangerous situation for a vessel is when the RAO period of the vessel is in resonance with the period of the waves. When it gets in resonance with the waves the vessel motions are much larger, which can cause a dangerous situation.

The value of the RAO depends on the structure of each vessel and the environment it will operate in. It is usually obtained from computational fluid dynamic (CFD) programs, or from models of ship designs tested in a model basin. Sometimes even both methods are used to determine the RAO of a vessel. The transfer function are usually calculated for all wave headings from 0° to 360° and all ship motions (heave, pitch, roll, surge, sway and yaw).

Two datasheets with different values of RAO has been used in the calculations, whereas one table is given for a ship, and the other for a semi-submersible. These two sheets are also given in Appendix C. They were produced by a fellow student who collected them from the computer program Orcflex.

5. Requirements

Requirements are important to consider when determining whether a vessel is safe to use or not. There are many types of criteria used for vessels around the world, where some of the most used are set by DNV, which will be used in this Thesis.

In section 5.1, provides information about the intact stability requirements for ships given by DNV. There will be a short description of the intact stability requirements for semi-submersible in section 5.2, also given by DNV.

5.1. Stability Requirements for Ships

The intact stability requirements mentioned in this section will regard large ships. There are three different criteria that are of particular concern regarding this; freeboard, minimum metacentric height and the minimum righting lever. The requirement for these has been given in Table 5.1-1.

Table 5.1-1 Stability requirements for a ship (DNV, 2005)

Freeboard	The freeboard must be at least 1.0 m.
Minimum metacentric height, GM	The initial metacentric height, GM, should not be less than 0.30 m.
Minimum righting lever, GZ	The righting lever, GZ, must be at least 0.20 m at an angle of heel equal to or greater than 30°.

5.2. Stability Requirements for Semi-submersibles

The intact stability requirements mentioned in this section will regard all column-stabilized units, such as semi-submersibles. Some of the main parameters of concern are the freeboard, metacentric height, and static angle of heel, see Table 5.2-1.

Table 5.2-1 Stability requirements for semi-submersible (DNV, 2013)

Freeboard	The freeboard must be at least 1.50 m.
Minimum metacentric height, GM	The initial metacentric height, GM, should not be less than 1.0 m.
Static angle of heel (damaged stability)	The static heeling angle can not be more than 17 °
Static angle of heel (intact stability)	The static heeling angle can not be more than 21 °

6. Conditions of the Barents Sea

As traditional fossil fuel supply is diminishing, the oil and gas industry seek for natural resources in new areas such as the Barents Sea. It has been shown that the Norwegian Barents Sea could contain billions barrels of oil, which could mean that some of the vessels used in this analysis could be used in this area in the future. Therefore it is important to be aware of the meteorological conditions at this site.

This section is divided into five parts, where the first section, section 6.1, gives a general description of the Barents Sea. Information about the changes in the ice cap over this area for a period of 45 years will be given in section 6.2. In section 6.3, the different physical environmental conditions of this area are described. In the last section, section 6.4, the dangerous phenomena of polar lows are enlightened.

6.1. General Description

There are many challenges associated with operating in this area. Not only can there be quite harsh weather, but there is also a great danger of sea ice, vessel icing, wind chill, and there are also possibilities that icebergs can be floating around. The weather forecasts in this area are also considered less reliable due to polar lows (DNV, 2005). In the north, the Barents Sea is bounded by Franz Josef Land and Svalbard. It is limited in the south by the Russian and Norwegian mainland. Further, the border is the Greenland Sea in the west, and Novaya Zemlya archipelago in the east. A map of a part of the Arctic has been shown in Figure 6.1-1, where the Barents Sea is shown on the east side in the map.



Figure 6.1-1 Map over the Arctic, showing where the Barents Sea is located (Stroeve et al., 2012)

The climate in the Barents Sea is subarctic, with summer air temperatures averaging from 0°C in the north to 10°C in the southwest; the winter air temperatures average in the same regions -25°C to -5°C .

The average depth of the Barents Sea has been estimated to be 230 m and the maximum depth has been estimated at 500 m (Loeng, 1991). In the north the annual precipitation is approximately 250 mm, and in the south it is approximately 500 mm. The overall estimated salinity of Barents Sea is high, as much as 34 parts per 1000, where the ice forms in the winter period and ice fields are thin. In the summer period the edge of ice goes far back to the north, whereas this ice cover has been reduced significantly each year during the last 40 years (Iden et al., 2012).

6.2. Changes in the Ice Cover

As mentioned above, there have been changes in the climate during last decades. Seen from the Figure 6.2-1 below, the ice cover in the Barents Sea has almost disappeared the last few years.

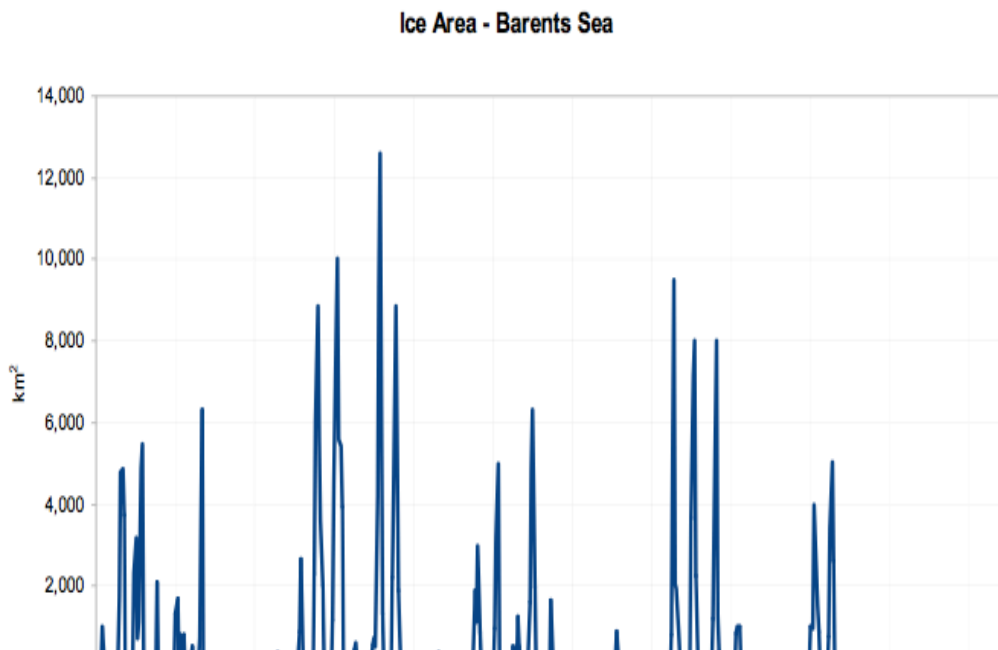


Figure 6.2-1 Time series of the ice area in the Barents Sea from January 1967 to June 2012 (Iden et al., 2012)

The maximum ice cover of the Barents Sea was in May 1981, with a total cover of $12\,609\text{ km}^2$, which corresponds to 28.6 % of the total area. By an analysis by the ACSYS database performed by Iden et al. (2012), it has been estimated that there might be a new top in the diagram of ice cover in the period from 2014 – 2016 with an area of about 6000 to 8000 km^2 .

6.3. Environmental Characteristics

The wind, current, wave height and air temperature that exists in this environment describes the ocean characteristics. They are all characteristics that are important for vessel icing to occur, as icing largely depends on the wave heights, wind speeds, air and water temperatures.

The environmental characteristics will be based on a measurement done by Iden et al. (2012) with different buoys placed in different areas of the Barents Sea, see Figure 6.3-1 below.

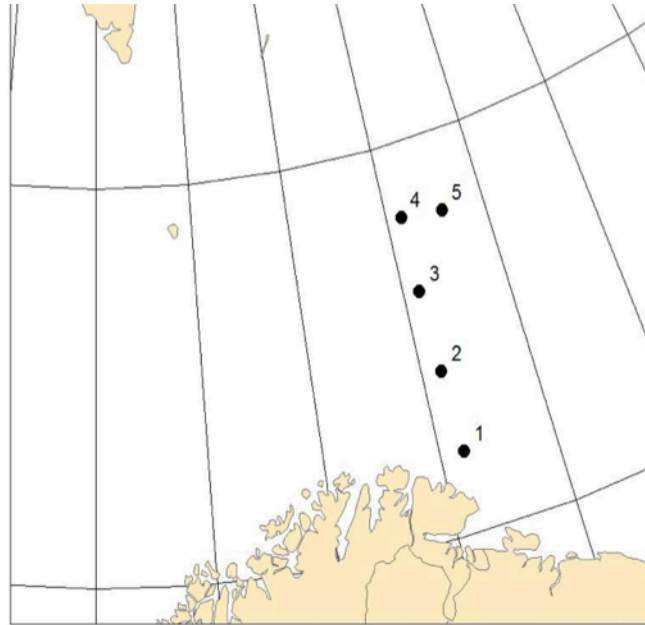


Figure 6.3-1 The position of the points from the NORA10 database in the Barents Sea which are used in the study (Iden et al., 2012)

Name of the buoys in the different points:

Point 1, NORA10_7103N_3104E

Point 2, NORA10_7207N_3090E

Point 3, NORA10_7311N_3077E

Point 4, NORA10_7407N_3079E

Point 5, NORA10_7400N_3288E

6.3.1. Waves

The significant wave height and the maximum peak period are some important parameters when calculating the motion responses. The significant wave height is defined as the average wave height, from trough to crest of the third highest waves in a wave set. The maximum period related to the significant wave height is the maximum time it takes for two wave crests to pass a specific point.

The frequency table for the worst conditions from the five points above are shown in Table 6.3-1. These measurements were taken from point 5 in Figure 6.3-1 above, in the time period from January 1958 to December 2011. The numbers are based on peak periods, T_p , and significant wave heights, H_s , which are measured every third hour during this period. The total numbers of wave occurrences have also been summarized.

Table 6.3-1 Wave height frequency with corresponding peak periods in the Barents Sea (Iden et al., 2012)

Norwegian Meteorological Institute
Climate Department

HINDCAST DATA Period: Position:
POINT: 7400N_3288E 1958 --> 74.0N,32.9E

Frequency table of significant wave height (HMO) m
and peak period (TP) s
Jan.-Dec. 1958 - 2011

TP	0.0	1.0	2.0	3.0	4.0	5.0	6.0	7.0	8.0	9.0	10.0	11.0	12.0	13.0	>=14.0	SUM	MARG. PROB.	CUM. PROB.	MEAN TP	STDEV. TP
HMO	0.0-0.9	0.9-1.9	1.9-2.9	2.9-3.9	3.9-4.9	4.9-5.9	5.9-6.9	6.9-7.9	7.9-8.9	8.9-9.9	9.9-10.9	10.9-11.9	11.9-12.9	12.9-13.9	13.9-14.9	14.9-15.9	15.9-16.9	16.9-17.9	17.9-18.9	18.9-19.9
	.	.	83	1252	3725	5900	4368	1136	1162	1125	1015	731	487	280	322	21586	13.84	13.84	6.72	2.52
	1.0-1.9	.	.	114	2765	10673	17246	7973	5592	4300	3405	3370	2632	1586	1683	61339	39.32	53.15	7.93	2.59
	2.0-2.9	.	.	.	14	877	8663	6990	5232	3984	2960	2455	2852	2255	2051	38333	24.57	77.72	9.21	2.67
	3.0-3.9	5	689	2398	4541	3301	2014	1504	1515	1450	1762	19179	12.29	90.02	10.18	2.59
	4.0-4.9	9	122	915	2388	1903	935	797	777	1130	8976	5.75	95.77	11.00	2.40
	5.0-5.9	4	47	431	1194	838	443	431	619	4007	2.57	98.34	11.74	2.22
	6.0-6.9	2	23	238	475	338	242	309	1627	1.04	99.38	12.45	1.94
	7.0-7.9	12	113	195	150	159	629	0.40	99.78	13.20	1.74	
	8.0-8.9	10	72	91	73	246	0.16	99.94	13.76	1.68	
	9.0-9.9	1	4	26	27	58	0.04	99.98	14.59	1.77
	10.0-10.9	2	4	16	22	0.01	99.99	15.74	2.01
	11.0-11.9	6	0.00	100.00	17.73	0.65
	12.0-12.9	4	0.00	100.00	16.83	1.49
	13.0-13.9	2	0.00	100.00	18.00	0.00
	>=14.0	1	0.00	100.00	18.00	0.00
SUM	0	0	83	1366	6504	17455	30975	18623	17491	15552	12741	10432	9337	7292	81641	56015				
MARG.PROB.	0.00	0.00	0.05	0.88	4.17	11.19	19.85	11.94	11.21	9.97	8.17	6.69	5.98	4.67	5.23					
CUM.PROB.	0.00	0.00	0.05	0.93	5.10	16.29	36.14	48.08	59.29	69.26	77.42	84.11	90.09	94.77	100.00					
MAX.HMO	.	.	0.70	1.50	2.40	3.10	4.20	5.10	6.10	6.60	7.50	9.40	10.20	10.60	14.00					
MEAN HMO	.	.	0.44	0.66	0.91	1.19	1.63	2.04	2.37	2.64	2.84	2.80	2.84	3.08	3.25					
STDV.HMO	.	.	0.13	0.22	0.31	0.44	0.61	0.78	0.99	1.24	1.50	1.63	1.61	1.65	1.72					
Statistics:																				
Minimum HMO	0.1																			
TP	11.2																			
Date	1998.06.04.00																			
Maximum HMO	14.0																			
Mean HMO	2.2																			
St.dev. HMO	1.3																			
Minimum TP	2.4																			
HMO	0.5																			
Date	2003.05.02.03																			
Maximum TP	21.8																			
Mean TP	8.7																			
St.dev. TP	2.9																			

The table shows that the most frequent waves in this area vary between 0.0 – 2.9 m with a peak period of 5.0 – 7.0 seconds. As the vessel movement increases when it goes into resonance with the period of the waves, it is not desirable to have a floating vessel with a natural period from 5.0 – 7.0 seconds in this area. However, the most dangerous situations are caused by the big waves and periods, as these have the highest energy impact on the vessel.

6.3.2. Wind

The wind plays a vital role for vessel icing to occur, as mentioned under section 4.1.3 above, the vessel icing usually starts at 9 m/s or higher. During the winter the dominating wind direction comes from the northeast, while for the summer the dominating wind direction comes from the west.

Different measurements on the wind speeds in this area have been conducted over the time period from January 1958 to December 2011, which are shown in Table 6.3-2 below. The worst conditions in the measurements for the wind were also taken from point 5 in Figure 6.3-1.

Table 6.3-2 Wind speed frequencies in the Barents Sea (Iden et al., 2012)

Norwegian Meteorological Institute
Climate Department

HINDCAST DATA Period: Position:
POINT: 7400N_3288E 1958 --> 74.0N,32.9E

Frequency table of wind speed (WSP) m/s
and wind direction (WDIR) degrees
Jan.-Dec. 1958 - 2011

WDIR	345.0	15.0	45.0	75.0	105.0	135.0	165.0	195.0	225.0	255.0	285.0	315.0	MARG.	CUM.	
WSP	15.0	45.0	75.0	105.0	135.0	165.0	195.0	225.0	255.0	285.0	315.0	345.0	SUM	PROB.	PROB.
m/s															
0.0- 1.9	420	394	357	406	392	364	404	385	341	382	395	393	4633	2.94	2.94
2.0- 3.9	1312	1393	1296	1213	1249	1172	1128	1098	1131	1209	1182	1255	14638	9.28	12.21
4.0- 5.9	2460	2585	2501	2383	2497	2157	2056	1922	1928	1997	1996	2086	26568	16.84	29.05
6.0- 7.9	3333	3307	2820	2874	3081	2973	2328	2250	1942	2198	2095	2525	31726	20.11	49.16
8.0- 9.9	2974	2825	2533	2734	3085	3038	2368	1873	1723	1882	1842	2216	29093	18.44	67.60
10.0-11.9	2297	2114	1907	2146	2511	2464	1780	1434	1363	1341	1324	1680	22361	14.17	81.77
12.0-13.9	1291	1311	1157	1301	1806	1621	1207	972	881	900	925	1034	14406	9.13	90.90
14.0-15.9	639	654	615	703	1039	907	782	518	562	586	578	581	8164	5.17	96.07
16.0-17.9	301	278	319	320	511	537	360	274	282	316	267	294	4059	2.57	98.65
18.0-19.9	93	102	138	108	197	230	181	80	97	122	138	97	1583	1.00	99.65
20.0-21.9	33	36	42	26	50	63	56	21	23	27	48	19	444	0.28	99.93
22.0-23.9	6	13	9	4	18	4	12	1	2	15	4	10	98	0.06	99.99
24.0-25.9	3	3	3	1	.	.	10	0.01	100.00
26.0-27.9	0	0.00	100.00
28.0-29.9	0	0.00	100.00
>=30.0	0	0.00	100.00
SUM	15162	15015	13697	14218	16436	15530	12662	10828	10275	10976	10794	12190157783			
MAR.PROB.	9.61	9.52	8.68	9.01	10.42	9.84	8.02	6.86	6.51	6.96	6.84	7.73			
CUM.PROB.	9.61	19.13	27.81	36.82	47.23	57.08	65.10	71.96	78.48	85.43	92.27	100.00			
MAX.WSP	24.70	24.50	24.70	23.40	23.60	22.70	23.40	22.80	23.90	25.00	23.00	23.60			
MEAN WSP	8.27	8.21	8.26	8.38	8.87	8.93	8.61	8.14	8.18	8.17	8.17	8.18			
STDV.WSP	3.66	3.70	3.82	3.76	3.95	3.95	4.06	3.87	3.98	4.04	4.05	3.83			

Statistics:
Minimum WSP 0.1 Maximum WSP 25.0 Mean WSP 8.4
WDIR 291.0 WDIR 267.0 St.dev. WSP 3.9
Date 2011.07.31.21 Date 1959.02.16.21

The north-western wind is from the direction of about 315°, whereas the north-eastern wind has a direction of about 45°, this can be seen in Figure 6.3-2.

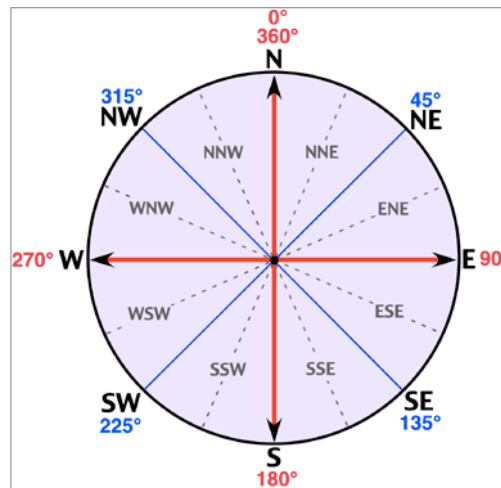


Figure 6.3-2 Wind directions and degrees (BP, 2007)

The maximum wind speed at this period of 53 years was measured 10 times in the intervals between 22.0 – 23.9 m/s. The maximum wind speed during this period of 53 years, were measured at 25.0 m/s from a direction of 267.0°, a wind coming from the west as shown in Figure 6.3-2. The most frequent wind situations in this area varied from 6.0 – 9.9 m/s from a direction of 345° – 165°.

6.3.3. Air Temperature

The air temperature must be $-1.7\text{ }^{\circ}\text{C}$ or colder in order for sea-spray icing to occur (Ryerson, 2011). The measured maximum average temperature in the Barents Sea is at $+4.4\text{ }^{\circ}\text{C}$ with an annual range from $+2.0\text{ }^{\circ}\text{C}$ to $+7.0\text{ }^{\circ}\text{C}$ (Jacobsen and Gudmestad, 2012). At the Snøhvit and Goliat fields, the temperature of the sea is usually at the maximum, where the value varies in the range from $+20\text{ }^{\circ}\text{C}$ to $+25\text{ }^{\circ}\text{C}$. The measured minimum average temperature for the Barents Sea is $-7.7\text{ }^{\circ}\text{C}$ with an annual range between $-6.0\text{ }^{\circ}\text{C}$ and down to $-9.0\text{ }^{\circ}\text{C}$. It is typically coldest in in the northeast part of the sea, where the temperatures ranges between $-20\text{ }^{\circ}\text{C}$ to $-30\text{ }^{\circ}\text{C}$. The different maximum and minimum temperatures for the different positions in Figure 6.3-1 above, during the period of 1958 – 2011 is shown in Table 6.3-3 below.

Table 6.3-3 The maximum and minimum temperatures in $^{\circ}\text{C}$ (Iden et al., 2012)

Posisjon	Maks.	Min.
71,03 N, 31,04 E	14,8	-14,6
72,07 N, 30,90 E	12,7	-16,6
73,11 N, 30,77 E	11,6	-19,6
74,07 N, 30,79 E	10,6	-24,9
74,00 N, 32,88 E	10,8	-25.1

The coldest measured temperature was at buoy NORA10_7407N_3079E, at point 4 in Figure 6.3-1. The varying temperatures measured at point 4 in the period from January 1958 – December 2011 are shown in Figure 6.3-3 below.

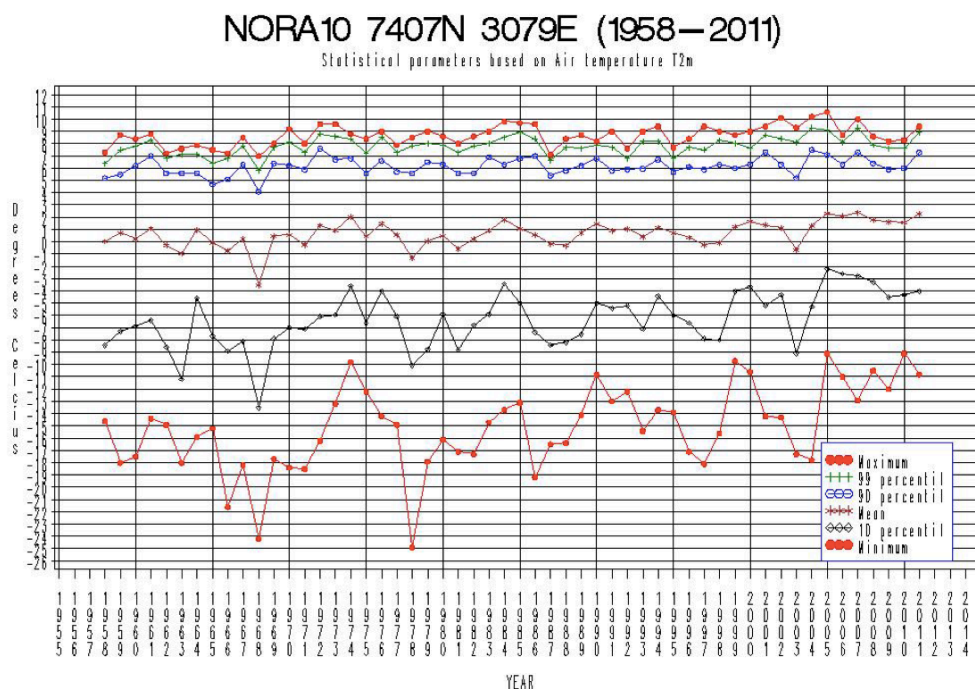


Figure 6.3-3 The maximum, middle and minimum, as well as 99, 90 and 10 per centile on yearly basis for the period of 1958 – 2011 (Iden et al., 2012)

The minimum temperature at this location varies from $-10\text{ }^{\circ}\text{C}$ to $-25\text{ }^{\circ}\text{C}$, and the mean varies between $-4\text{ }^{\circ}\text{C}$ to $+1.5\text{ }^{\circ}\text{C}$, with an increasing trend in the temperature over the years.

6.3.4. Sea Temperature

In order for sea spray icing to occur, the temperature of the water needs be $+ 7.0\text{ }^{\circ}\text{C}$ or colder. In the Barents Sea, the average maximum sea temperature is $+ 7.0\text{ }^{\circ}\text{C}$. The annual variation of the maximum ranges from $+ 5.0\text{ }^{\circ}\text{C}$ to $+ 9.0\text{ }^{\circ}\text{C}$ (Jacobsen and Gudmestad, 2012). The minimum temperature measured in the Barents Sea is measured in the northeast where the minimum sea temperature usually varies in the range of $+ 2.0\text{ }^{\circ}\text{C}$ to $- 2.0\text{ }^{\circ}\text{C}$. The different maximum and minimum temperatures for the different positions in Figure 6.3-1 above, during the period of 1958 – 2011 are shown in Table 6.3-4 below, for temperatures given in Celsius measured at the sea surface in the period 1958 – 2011.

Table 6.3-4 The maximum and minimum temperatures (Iden et al., 2012)

Posisjon	Maks.	Min.
71,03 N, 31,04 E	11,9	1,6
72,07 N, 30,90 E	11,3	1,8
73,11 N, 30,77 E	10,6	1,1
74,07 N, 30,79 E	9,9	-0,7
74,00 N, 32,88 E	11,3	1,8

The coldest measured sea temperature was at buoy NORA10_7407N_3079E, with a temperature at $- 0.7\text{ }^{\circ}\text{C}$, which is at point 4 in Figure 6.3-1 above. The varying sea temperatures measured at point 4 in the period from January 1958 – December 2011 are shown in below.

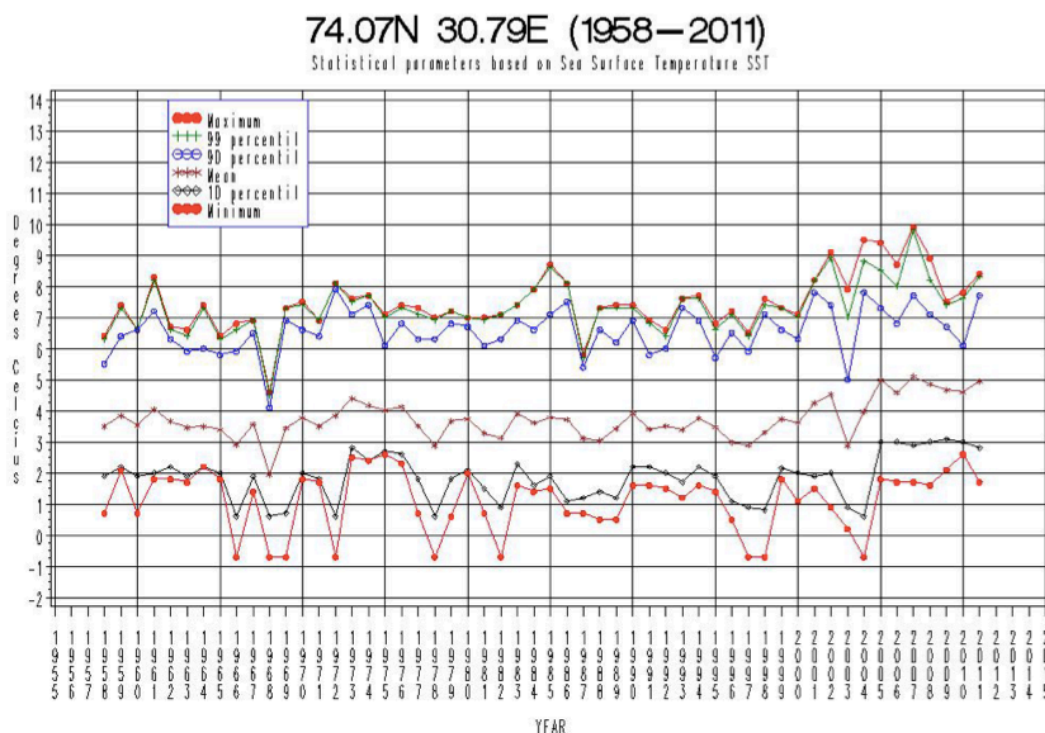


Figure 6.3-4 The maximum, middle and minimum, as well as 99, 90 and 10 per centile on yearly basis for the period of 1958 – 2011 (Iden et al., 2012)

The minimum temperature at this location varies from $+ 2.8\text{ }^{\circ}\text{C}$ to $- 0.7\text{ }^{\circ}\text{C}$, and the mean varies between $+ 2.0\text{ }^{\circ}\text{C}$ to $+ 5.1\text{ }^{\circ}\text{C}$.

6.4. Polar Lows

The polar low is a weather phenomenon that can be described as a short-lived atmospheric low-pressure system that is prevalent in the northern and southern hemisphere. They develop during cold air outbreaks over the ocean in both Southern and Northern Hemispheres. The Barents Sea and Norwegian Sea are among the regions where polar lows break out most often, while the secondary area of polar low formation is considered in the sea south and west of Iceland.

The danger of the polar lows is that they are difficult to predict and they often have a very rapid development. A polar low can cause storm force winds and sometimes even hurricanes. It causes icing, changing in wind direction and heavy snow showers. It is a phenomenon that can have a life span from six hours to two days (Iden et al., 2012). Polar lows usually occur in the period from October to May, with most frequent occurrences from December to March. They usually cause a small storm, and in 30% of the cases they cause a full storm around parts of the centre. One of the greatest dangers from this phenomenon is the rapid change in the weather. The wind can change from a small breeze to storm in minutes, and the corresponding wave height can increase by as much as five meters in less than one hour. Sea-spray icing and atmospheric icing such as snow also closely follow the low pressure and it can also give a poor visibility.

The frequency point of polar low formations in the Norwegian region during the period from 2000 - 2012 (166 cases in total) is given by the blue triangles. The sea temperatures are given with blue shading is shown in Figure 6.4-1.

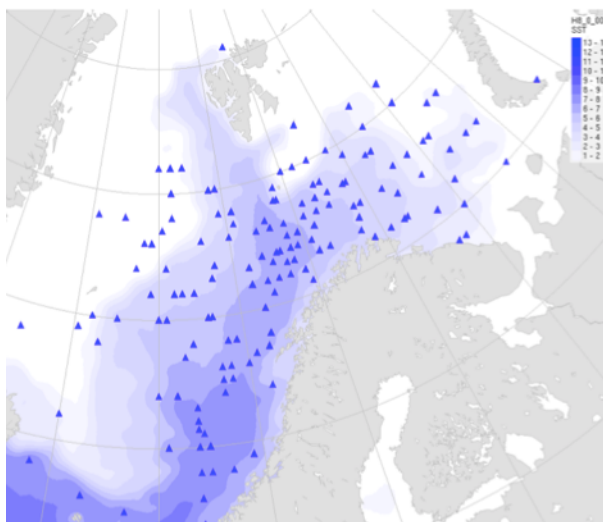


Figure 6.4-1 Frequency point of polar low formations in the Norwegian region (Iden et al., 2012)

The strongest measured wind due to a polar low was at 70 knots of wind (36 m/s) over a period of 12 hours, northeast off Varanger, Norway on 3rd April 2005 (Iden et al., 2012). An accident in February 1848 occurred when 500 fishing men drowned off the Lofoten Islands due to an outbreak of a polar low (Kolstad, 2007). A total of 56 vessels were lost in accidents in different Norwegian waters during the 20th century according to Kari Wilhemsen (interviewed by Grønås and Skeie, 1999). Many of these losses were related to the occurrence of polar low pressures. The total lives lost due to these 56 vessels were 342.

7. Results

The results from the case study and the parameter study of the four vessels will be presented in this chapter. In section 7.1, the results from the calculations of the freeboard, intact stability, righting arm and static heeling angle for all four vessels will be presented. In section 7.2, a table summarizing these calculated results are given. The motion response results calculated for the situations with and without the ice and snow loads will be showed in section 7.3. In the last section of this chapter, section 7.4, a table summarizing the motion response results will be given.

7.1. Freeboard, Stability, Righting arm and Heeling Angle Results

The results from the calculations are found by using the assumptions given in section 4.1.4, which regards where the ice accretes on the vessels and the different ice thicknesses on areas of the vessels.

7.1.1. Results from the Lady of Grace Boat

The calculated freeboard in the case study was changed from 1.83 m without the ice to 1.40 m with the ice, which is a noteworthy change in freeboard of 0.43 m. However, the DNV's requirement of having a freeboard of minimum 1.00 m is still fulfilled in this situation.

The parameter study revealed that if the maximum sea-spray ice thickness was more than 0.73 m, the requirement was no longer fulfilled. This is shown in Figure 7.1-1, where the red line shows the decreasing freeboard and the blue line shows the requirement of a minimum freeboard as given by DNV (2005).

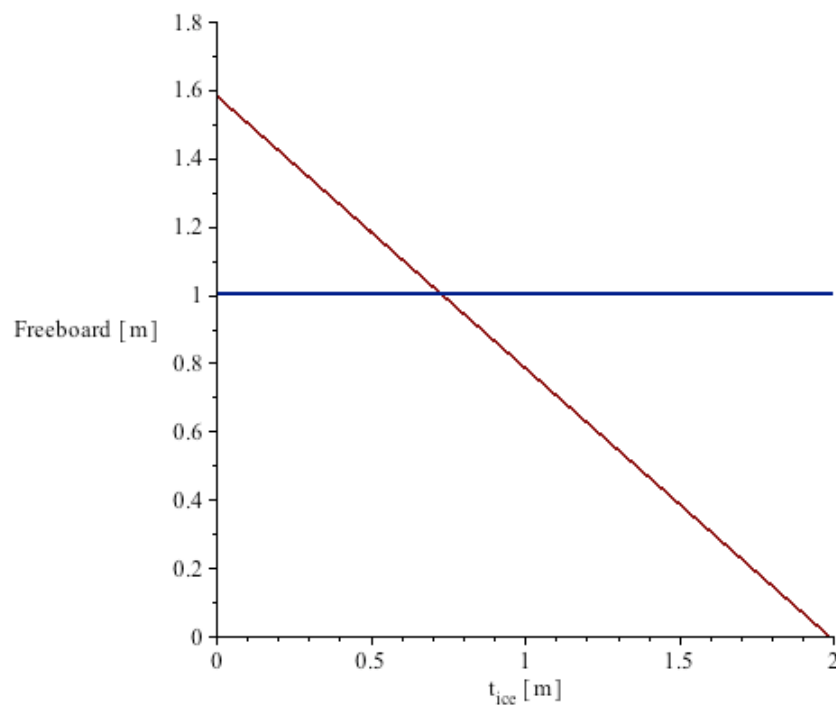


Figure 7.1-1 Varying freeboard for different thicknesses of sea-spray ice

The intact initial stability was changed from 1.46 m without the ice to 0.44 m with the ice, which is a significant change in intact stability of 1.02 m. The minimum acceptable height of stability given by the DNV (2005) is at 0.30 m, which means that the requirements are still fulfilled in this situation.

The parameter study showed that the Lady of Grace did need a maximum sea-spray ice thickness of 0.31 m in order to longer meet the requirement. This is shown in Figure 7.1-2, where the intact stability (the red line) is decreasing because of the icing loads.

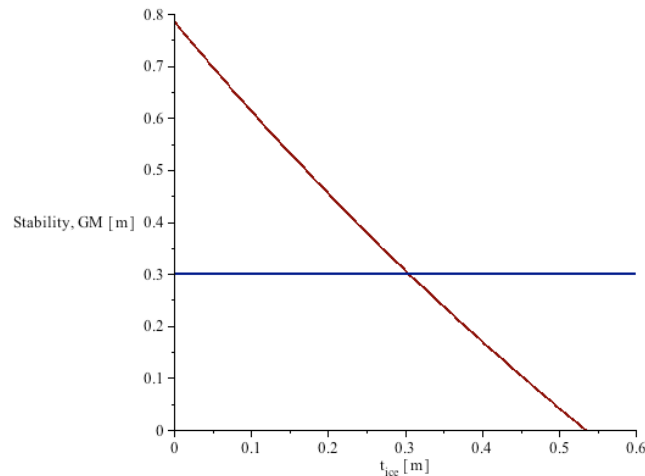


Figure 7.1-2 Varying stability for different thicknesses of sea-spray ice

The righting arm was changed from 0.93 m without the ice to 0.38 m with the ice, which is a change of 0.55 m. The minimum righting arm requirement given by DNV is 0.20 m, which means that the requirement is still fulfilled in this situation.

The parameter study revealed that the calculated maximum ice thickness for the Lady of Grace vessel must be 0.44 m in order to not meet the minimum righting arm criterion. This is shown in Figure 7.1-2, where the intact stability (the red line) is decreasing because of the icing loads.

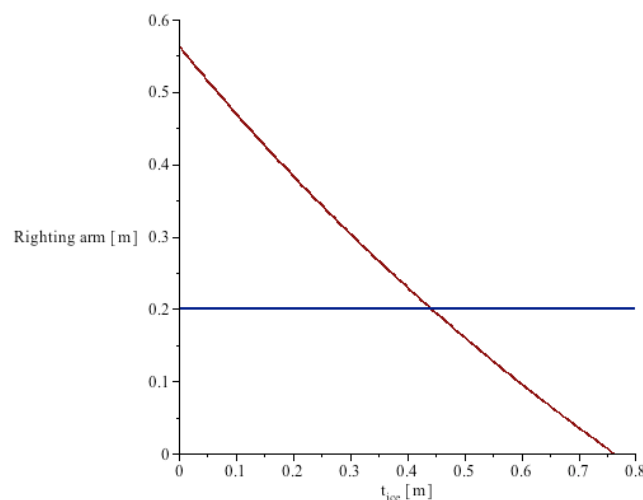


Figure 7.1-3 Varying righting arm for different thicknesses of sea-spray ice

7.1.2. Results from the Viking Fighter Vessel

In the case study the freeboard was changed from 2.31 m without the ice to 1.88 m with the ice, which is a reduction in freeboard of 0.43 m. When the vessel has a freeboard of 1.88 m, it still fulfils the minimum freeboard criterion from DNV (2005).

The parameter study revealed that the calculated maximum sea-spray ice thickness for the Viking Fighter vessel must be at least 1.63 m in order to no longer meet the minimum freeboard criterion. This is shown in Figure 7.1-4, where the freeboard (the red line) is decreasing due to the varying icing loads.

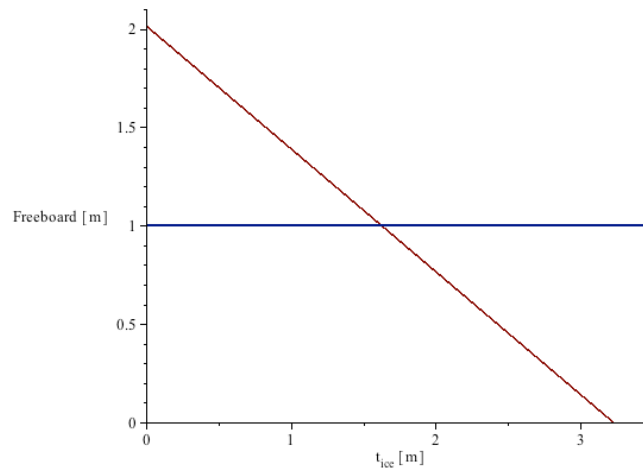


Figure 7.1-4 Varying freeboard for different thicknesses of sea-spray ice

The intact stability was changed from 3.76 m without the ice to 2.94 m when the ice was included. It is a significant reduction in intact stability of 0.82 m. However, it still fulfils the requirement given by DNV (2005).

It was found in the parameter study that if the maximum ice thickness was 2.95 m or more, the minimum intact stability criterion would no longer be met. This can be seen in Figure 7.1-5.

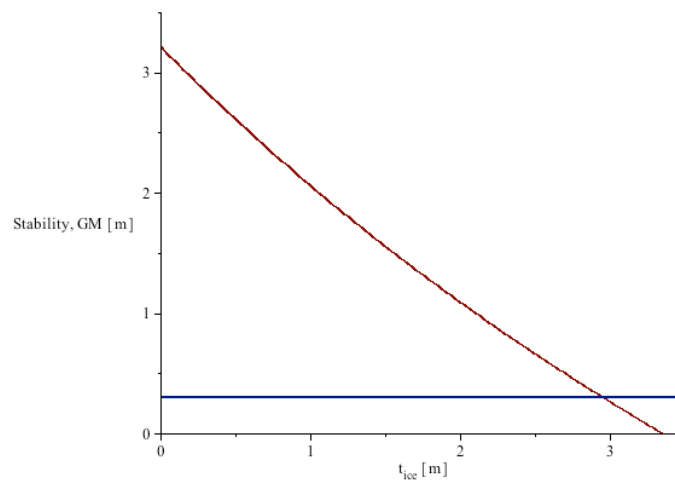


Figure 7.1-5 Varying stability for different thicknesses of sea-spray ice

The righting arm was changed from 2.29 m without the ice to 1.85 m with the ice, which is a decrease in righting arm of 0.44 m. The requirement of having a minimum 0.20 m righting arm is still fulfilled in this situation.

The parameter study revealed that the calculated maximum ice thickness for the Viking Fighter vessel must be 3.57 m in order to no longer meet the minimum righting arm criterion. This is shown in Figure 7.1-6.

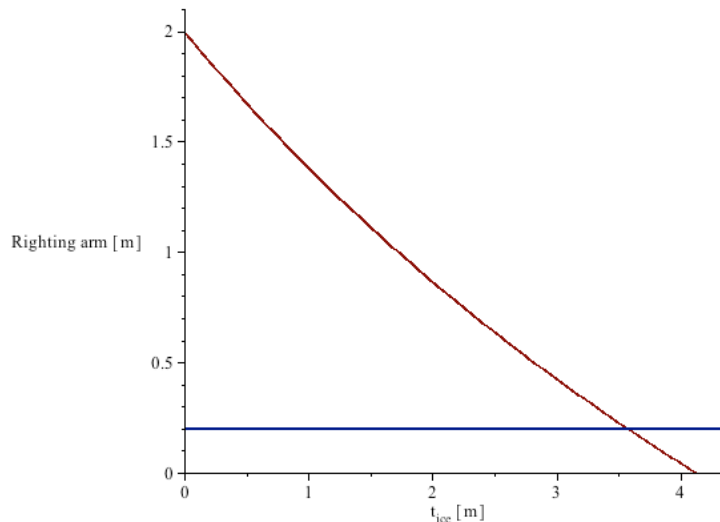


Figure 7.1-6 Varying stability for different thicknesses of sea-spray ice

7.1.3. Results from the DrillMax Ice Drillship

The freeboard was changed from 6.80 m without the ice to 6.47 m with the ice in the case study. It is a small change in freeboard of 0.33 m, and the vessel still fulfils the requirement of having at least 1.0 m of freeboard.

The parameter study revealed that the calculated maximum ice thickness for the DrillMax Ice ship must be 11.39 m in order to no longer meet the freeboard criterion. This is shown in Figure 7.1-7.

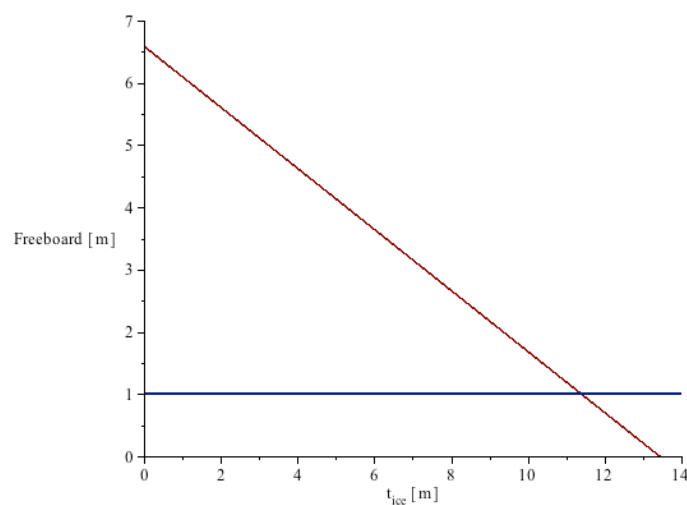


Figure 7.1-7 Varying freeboard for different thicknesses of sea-spray ice

The intact stability was changed from 9.50 m without the ice to 7.87 m with the ice, which is a huge change in the intact stability of 1.63 m. However, the vessel still fulfils the minimum intact stability requirement given by DNV (2005).

The parameter study revealed that the maximum ice thickness for the DrillMax Ice vessel must be at least 8.35 m in order to no longer meet the intact stability criterion of minimum 0.30 m given by DNV (2005). This is shown in Figure 7.1-8, where the intact stability (the red line) is decreasing because of the icing loads.

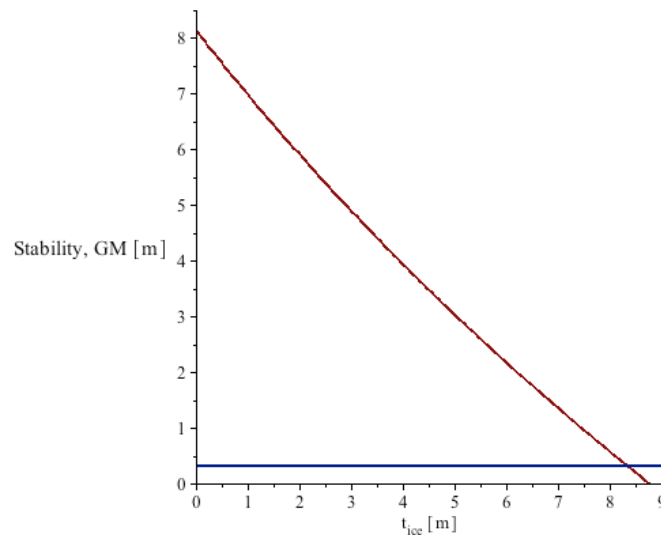


Figure 7.1-8 Varying stability for different thicknesses of sea-spray ice

The righting arm was changed from 5.33 m without the ice to 4.91 m with the ice, which is a reduction in righting arm of 0.42 m. This shows that the vessel have a righting arm that is far bigger than the minimum criterion of 0.20 m, and a that it would probably need a lot more ice in order to no longer fulfil that requirement.

The parameter study revealed that the maximum ice thickness for the DrillMax Ice vessel must be at least 10.17 m in order to no longer meet the minimum righting arm criterion. This is shown in Figure 7.1-9.

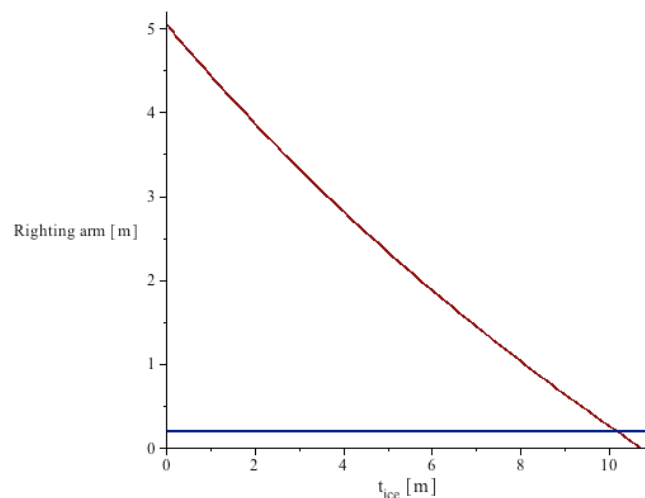


Figure 7.1-9 Varying righting arm for different thicknesses of sea-spray ice

7.1.4. Results from the West Alpha Semi-submersible Rig

In the case study the freeboard was changed from 12.00 m without the ice to 8.75 m with the ice, which is a significant reduction in freeboard of 3.25 m. The requirement for the minimum freeboard for a semi-submersible given from DNV (2005) is 1.50 m. This means that the freeboard criterion for the rig is still met in this situation.

The parameter study revealed that the calculated maximum sea-spray ice thickness for the West Alpha rig must be at least 4.18 m in order to not meet the minimum freeboard criterion. This is shown in Figure 7.1-10.

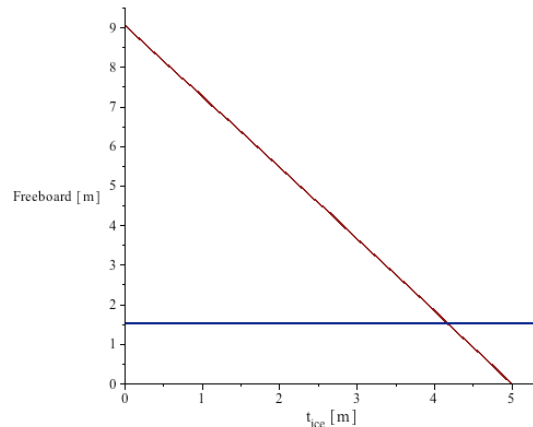


Figure 7.1-10 Varying freeboard for different thicknesses of sea-spray ice

The intact stability was changed from 3.06 m without the ice to 2.44 m with the ice, which is a reduction in intact stability of 0.62 m. The minimum allowable intact stability for the semi-submersible was 1.00, which was given by DNV (2013). This means that if the rig has an intact stability of 2.44 with the ice, the requirement is still fulfilled.

The parameter study revealed that the calculated maximum sea-spray ice thickness for the West Alpha rig must be at least 4.67 m in order to no longer meet the intact stability criterion. This is shown in Figure 7.1-11, where the intact stability (the red line) is decreasing because of the icing loads.

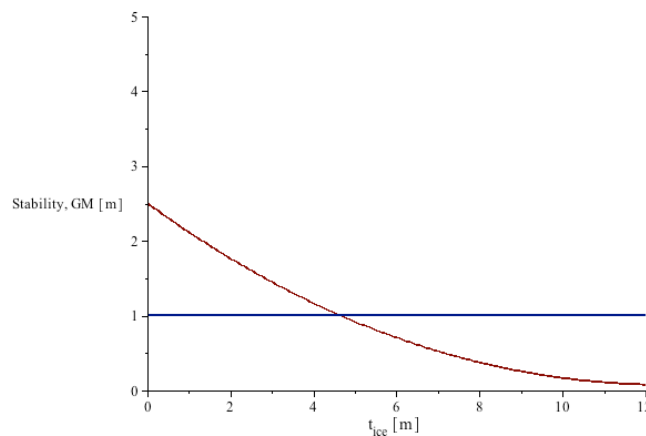


Figure 7.1-11 Varying stability for different thicknesses of sea-spray ice

As the rig will experience asymmetric loadings of sea-spray ice it will experience a static heeling angle. According to DNV (2013), the maximum allowable heeling angle is 17° for semi-submersibles. It was calculated in the analysis that the heeling angle changed from 0° to 2.67° when the ice loads were included. This shows that the requirement for the maximum allowable heeling angle is still fulfilled.

It was also calculated that the rig needed a thickness of sea-spray ice of 0.48 m in order to get a heeling angle of 8° . The parameter study revealed that the maximum sea-spray ice thickness for the rig must be at least 0.99 m and 1.21 m in order to no longer meet the requirement for the damaged stability and intact stability respectively. This can be seen in Figure 7.1-12.

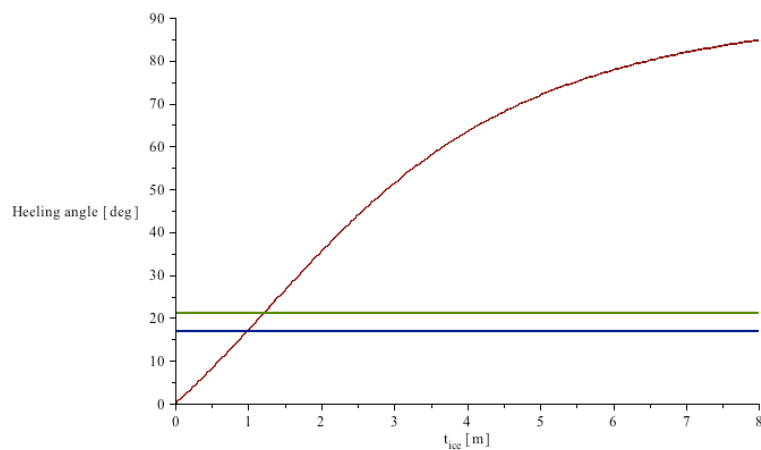


Figure 7.1-12 Varying heeling angle for different thicknesses of sea-spray ice

7.2. Summarization of the Stability Results

The results from the case study and the parameter study are shown in Table 7.2-1 and Table 7.2-2, respectively.

Table 7.2-1 Results from the case study

		Lady of Grace	Viking Fighter	DrillMax Ice	West Alpha
Freeboard [m]	Without ice	1.83	2.31	6.80	12.00
	With ice	1.40	1.88	6.47	8.75
	Change [%]	23.50	18.62	4.85	27.08
Stability [m]	Without ice	1.46	3.76	9.50	3.06
	With ice	0.44	2.94	7.87	2.44
	Change [%]	69.86	21.81	17.16	20.26
Righting arm [m]	Without ice	0.93	2.29	5.33	-
	With ice	0.38	1.85	4.91	-
	Change [%]	59.14	19.21	7.88	-
Heeling angle [degrees]	Without ice	-	-	-	0
	With ice	-	-	-	2.67

Table 7.2-2 Results from the parameter study showing the amount of ice (given in m) needed in order to make to no longer fulfil DNVs requirements

	Lady of Grace	Viking Fighter	DrillMax Ice	West Alpha
Freeboard	0.73	1.63	11.39	4.18
Intact stability	0.31	2.95	8.35	4.67
Righting arm	0.44	3.57	10.72	-
Heeling angle (damaged stability)	-	-	-	0.99
Heeling angle (intact stability)	-	-	-	1.21

7.3. Motion Response

The motion response in heave, pitch and roll have been calculated for all four vessels for the purpose of discovering the impact the ice will have on the vessels' motions. The pitch and heave motions have been calculated for three different situations; when the waves are in the directions of 0° , 45° and 90° of the vessels. Two situations have been checked for the roll motions, which are when the waves are in the directions of 45° and 90° of the vessels.

The calculated results for the heave and pitch translations will be at the point where the displacements are at the greatest. This means that these displacements will occur at the stern and the bow of the ships, and for the semi-submersible these displacements will occur at the two ends of the longest deck.

7.3.1. Motion Response for the Lady of Grace

The results of the calculated natural periods in heave, pitch and roll for this ship are shown in Table 7.3-1 below. These values have further been used to calculate the motion response of this vessel.

Table 7.3-1 Calculated natural periods for the Lady of Grace boat

	Without ice and snow loads	With ice and snow loads
Natural period in heave [s]	5.58	5.74
Natural period in pitch [s]	2.81	3.22
Natural period in roll [s]	3.52	6.41

The maximum coupled heave and pitch displacement for the Lady of Grace in waves with direction of 0° with the vessel (head sea) was calculated to be at 0.366 m at the time of 9.83 seconds when ice and snow loads were not included. When ice and snow loads were included, the maximum displacement was at 0.370 m at 10.00 seconds. This can be seen in Figure 7.3-1 below.

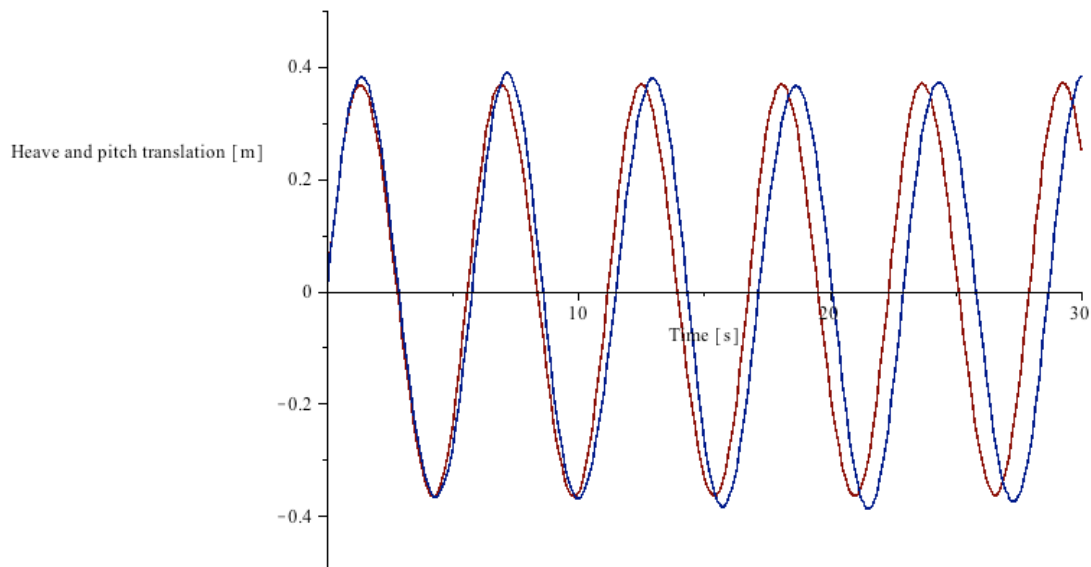


Figure 7.3-1 Coupled heave and pitch motion for the Lady of Grace in head sea (0°); blue line is when ice is included, red line when there is no ice

The maximum coupled heave and pitch displacement for the Lady of Grace in waves with direction of 45° with the vessel, was calculated to be at 0.63 m at the time of 9.83 seconds when ice and snow loads were not included. When ice and snow loads were included, the maximum displacement was at 0.75 m at the time of 10.01 seconds. This can be seen in Figure 7.3-2.

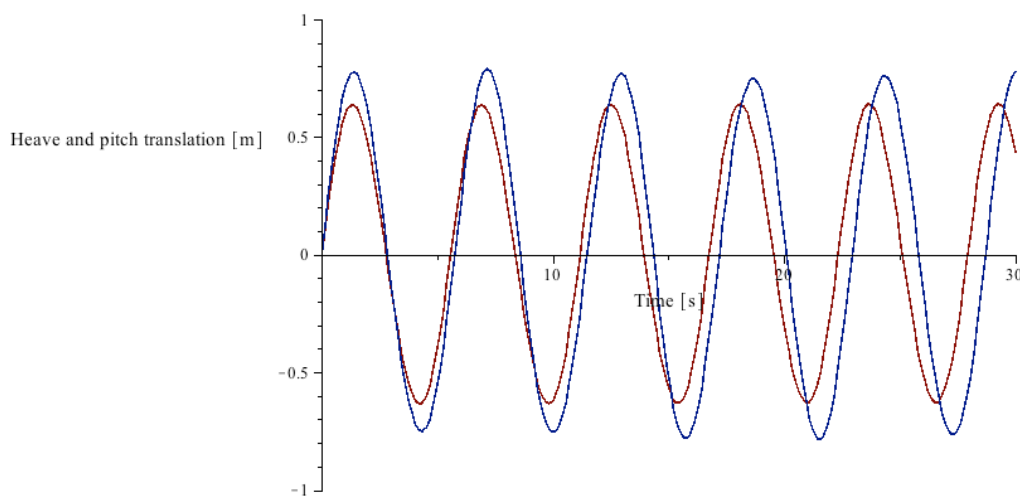


Figure 7.3-2 Coupled heave and pitch motion for the Lady of Grace in waves with direction of 45° with the vessel; blue line is when ice is included, red line when there is no ice

The maximum coupled heave and pitch displacement for the Lady of Grace in waves with direction of 90° with the vessel (beam sea) was calculated to be at 2.12 m at the time of 9.79 seconds when ice and snow loads were not included. When ice and snow loads were included, the maximum displacement was at 2.53 m at the time of 10.03 seconds, which can be seen in Figure 7.3-3.

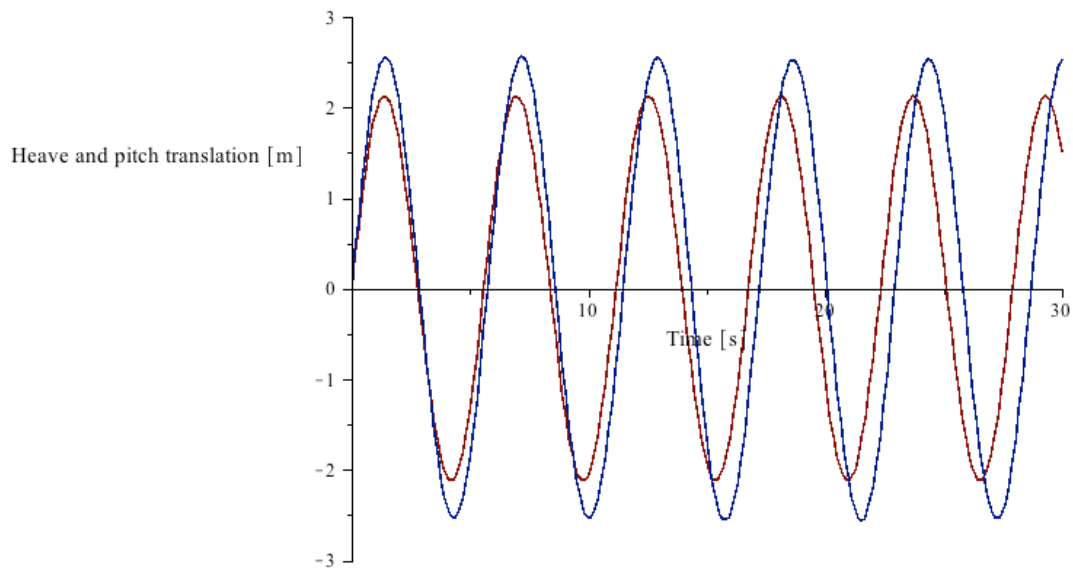


Figure 7.3-3 Coupled heave and pitch motion for the Lady of Grace in beam sea (90°); blue line is when ice is included, red line when there is no ice

The maximum roll displacement for the Lady of Grace in the direction of 45° with the vessel, was calculated to be at 0.13 m at 9.68 seconds when ice and snow loads were not included. When ice and snow loads were included, the maximum displacement was at 0.75 m at the time of 11.23 seconds. This can be seen in Figure 7.3-4.

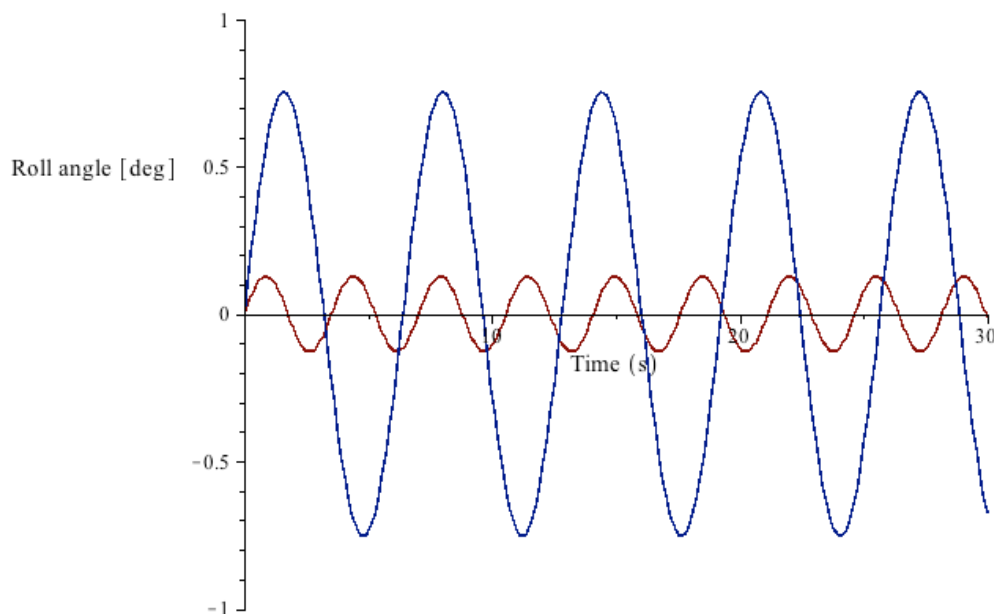


Figure 7.3-4 Roll motion for the Lady of Grace in waves with direction of 45° with the vessel; blue line is when ice is included, red line when there is no ice

The maximum roll displacement for the ship in beam sea was at 0.28 m at the time of 9.68 seconds when ice and snow loads were not included. When ice and snow loads were included, the maximum displacement was at 2.25 m at the time of 11.23 seconds, which can be seen in Figure 7.3-5.

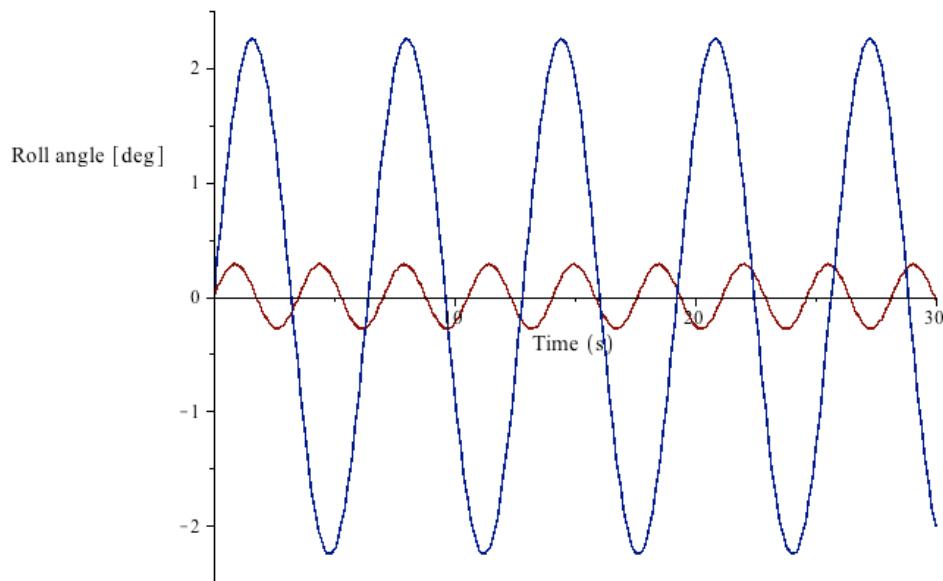


Figure 7.3-5 Roll motion for the Lady of Grace in beam sea (90°); blue line is when ice is included, red line when there is no ice

7.3.2. Motion Response for the Viking Fighter

The results of the calculated natural periods in heave, pitch and roll for this ship are shown in Table 7.3-2 below. These values have further been used to calculate the motion response of this vessel.

Table 7.3-2 Calculated natural periods for the Viking Fighter vessel

	Without ice and snow loads	With ice and snow loads
Natural period in heave [s]	9.33	9.43
Natural period in pitch [s]	5.19	5.41
Natural period in roll [s]	5.89	6.67

The maximum coupled heave and pitch displacement for the Viking Fighter in head sea, was calculated to be at 1.65 m at the time of 11.67 seconds when ice and snow loads were not included. When ice and snow loads were included, the maximum displacement was at 1.81 m at the time of 11.94 seconds. This can be seen in Figure 7.3-6 below.

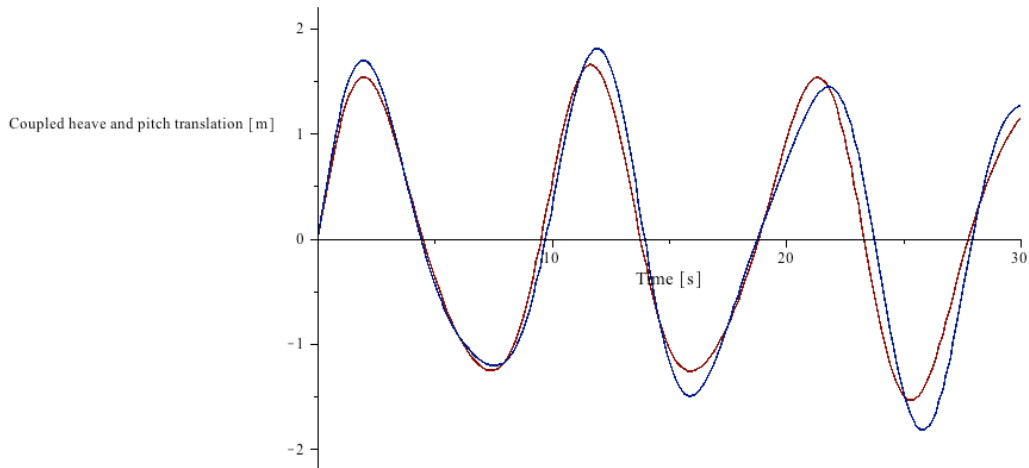


Figure 7.3-6 Coupled heave and pitch motion for the Viking Fighter in head sea (0°); blue line is when ice is included, red line when there is no ice

The maximum coupled heave and pitch displacement of the ship in waves with the direction of 45° with the vessel was calculated to be at 2.82 m at the time of 11.67 seconds when ice and snow loads were not included. When ice and snow loads were included, the maximum displacement was at 2.85 m at the time of 11.87 seconds, see Figure 7.3-7.

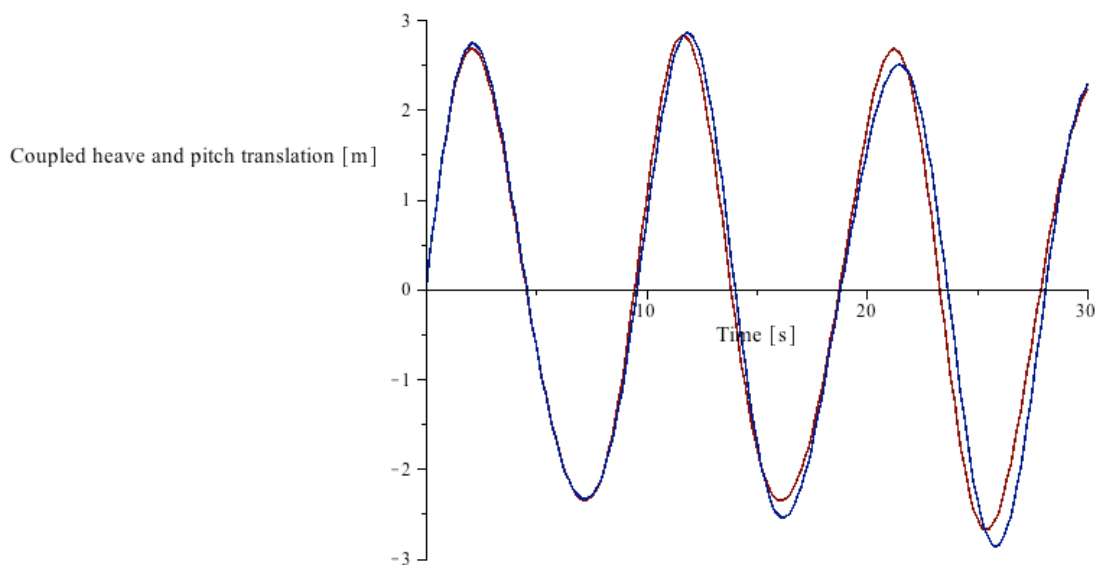


Figure 7.3-7 Coupled heave and pitch motion for the Viking Fighter in waves with direction of 45° with the vessel; blue line is when ice is included, red line when there is no ice

The maximum coupled heave and pitch displacement for the Viking Fighter in beam sea (90°) was calculated to be at 4.30 m at the time of 11.66 seconds when ice and snow loads were not included. When ice and snow loads were included, the maximum displacement was at 4.31 m at the time of 11.85 seconds. This can be seen in Figure 7.3-8.

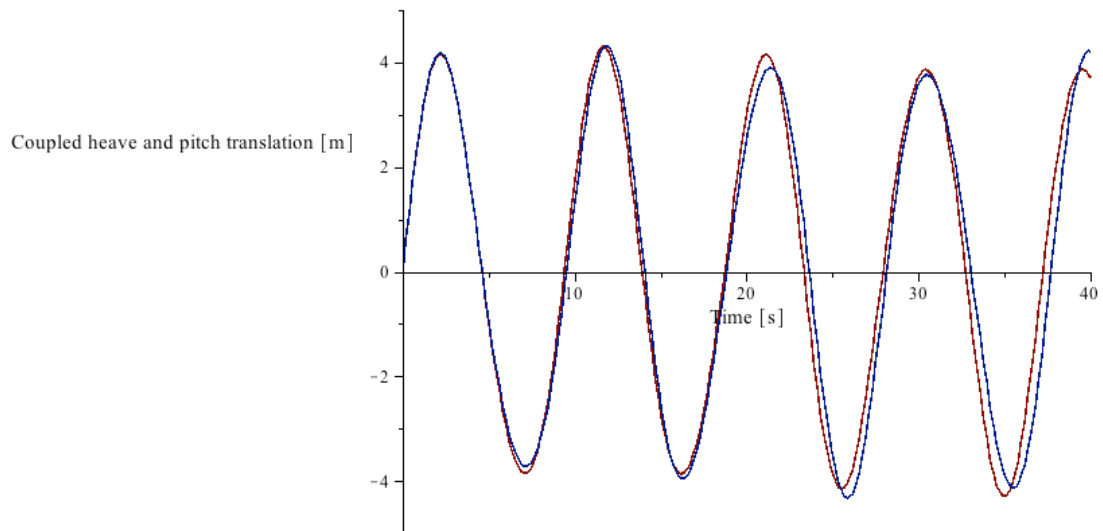


Figure 7.3-8 Coupled heave and pitch motion for the Viking Fighter in beam sea (90°); blue line is when ice is included, red line when there is no ice

The maximum roll displacement for the ship in the direction of 45° with the vessel, was calculated to be at 0.74 m at the time of 10.30 seconds when ice and snow loads were not included. When ice and snow loads were included, the maximum displacement was at 0.79 m at the time of 11.66 seconds, see Figure 7.3-9.

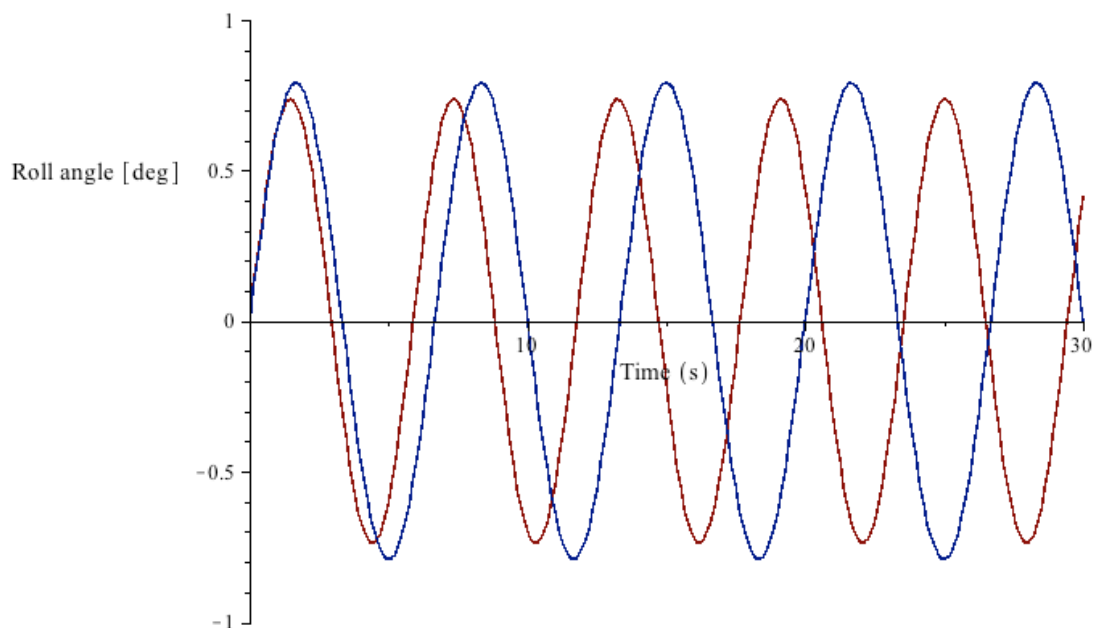


Figure 7.3-9 Roll motion for the Viking Fighter in waves with direction of 45° with the vessel; blue line is when ice is included, red line when there is no ice

The maximum roll displacement for the ship in beam sea was at 1.57 m at the time of 10.30 seconds when ice and snow loads were not included. When ice and snow loads were included, the maximum displacement was at 1.53 m at 11.66 seconds. This can be seen in Figure 7.3-10 below.

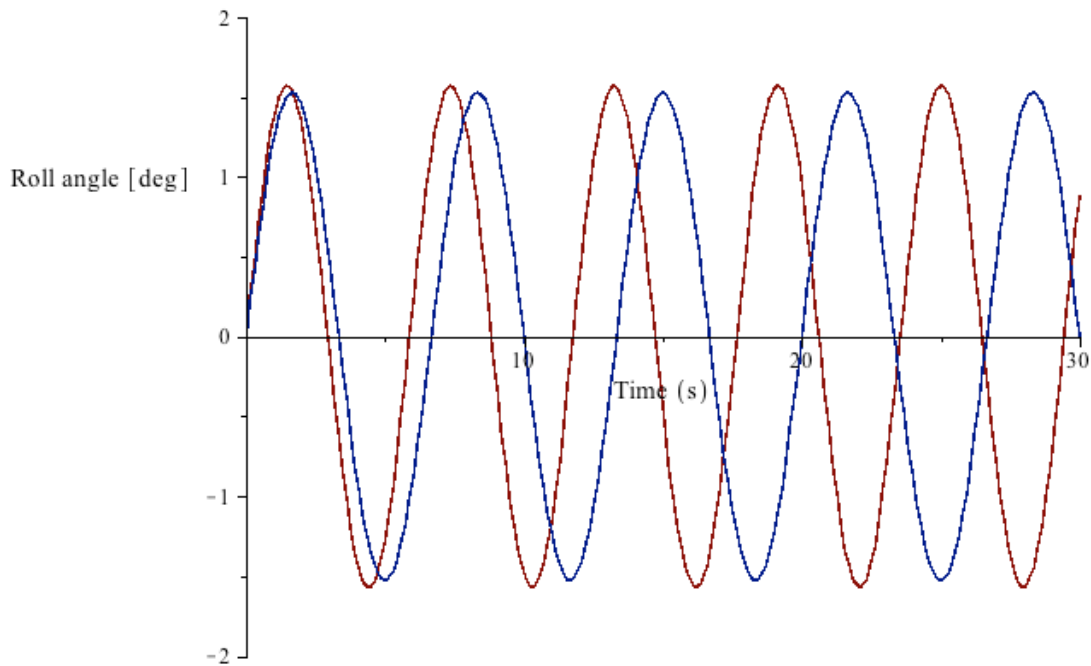


Figure 7.3-10 Roll motion of the motion for the Viking Fighter in beam sea (90°); blue line is when ice is included, red line when there is no ice

7.3.3. Motion Response for the DrillMax Ice

The results of the calculated natural periods in heave, pitch and roll for this ship are shown in Table 7.3-3 below. These values have further been used to calculate the motion response of this vessel.

Table 7.3-3 Calculated natural periods for the DrillMax Ice

	Without ice and snow loads	With ice and snow loads
Natural period in heave [s]	14.30	14.34
Natural period in pitch [s]	7.72	7.83
Natural period in roll [s]	9.06	9.50

The maximum coupled heave and pitch displacement for the DrillMax Ice ship in head sea was calculated to be at 5.67 m at the time of 17.35 seconds when ice and snow loads were not included. When ice and snow loads were included, the maximum displacement was at 5.86 m at the time of 17.85 seconds. This can be seen in Figure 7.3-11.

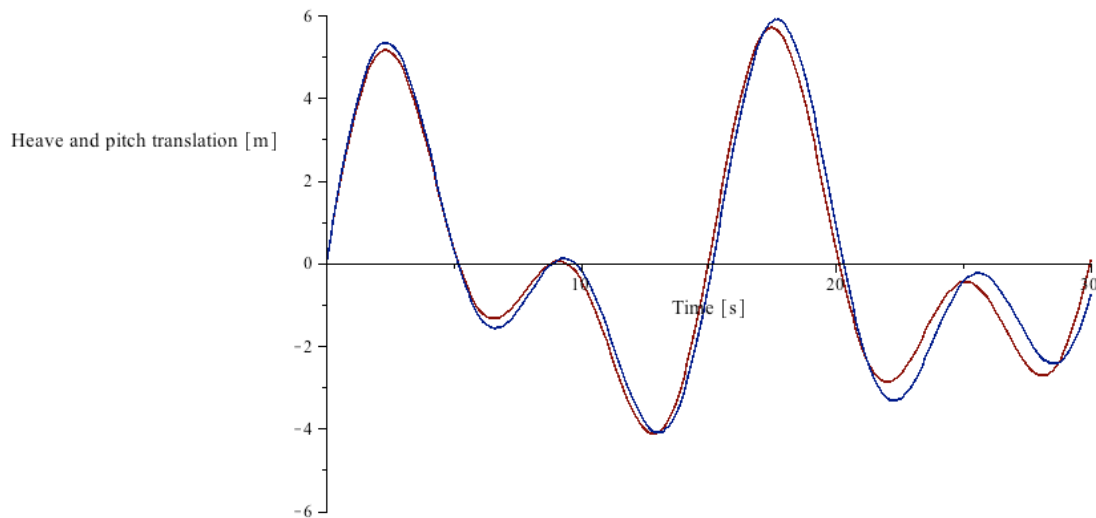


Figure 7.3-11 Coupled heave and pitch motion for the DrillMax Ice in head sea (0°); blue line is when ice is included, red line when there is no ice

The maximum coupled heave and pitch displacement for the DrillMax Ice in waves with direction of 45° with the vessel was calculated to be at 7.44 m at the time of 17.45 seconds when ice and snow loads were not included. When ice and snow loads were included, the maximum displacement was at 7.43 m at the time of 17.67 seconds. This can be seen in Figure 7.3-12.

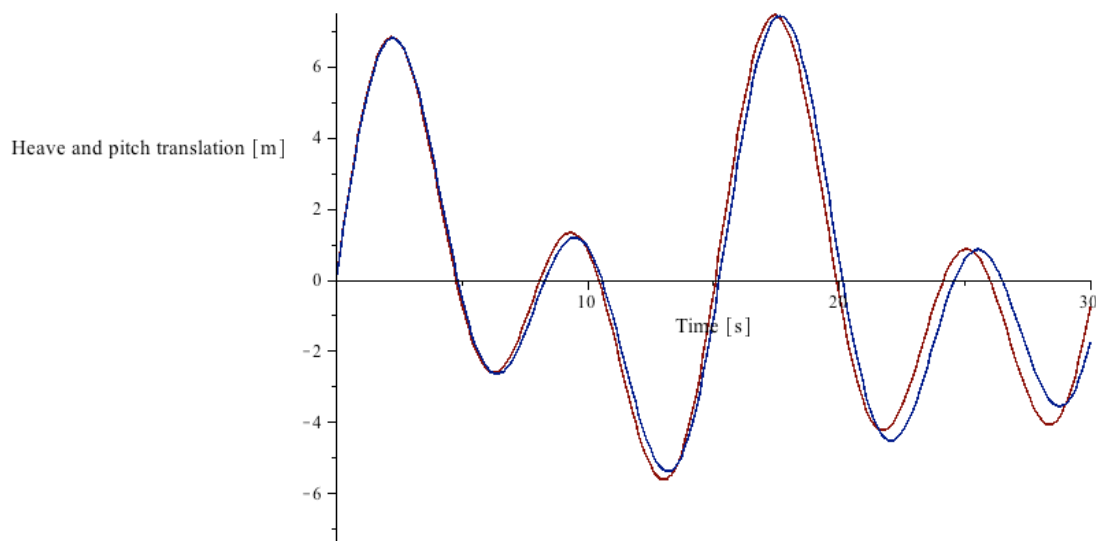


Figure 7.3-12 Coupled heave and pitch motion for the DrillMax Ice in waves with direction of 45° with the vessel; blue line is when ice is included, red line when there is no ice

The maximum coupled heave and pitch displacement for the ship in beam sea was calculated to be at 3.84 m at the time of 3.01 seconds when ice and snow loads were not included. When ice and snow loads were included, the maximum displacement was at 3.81 m at the time 3.08 seconds, see Figure 7.3-13.

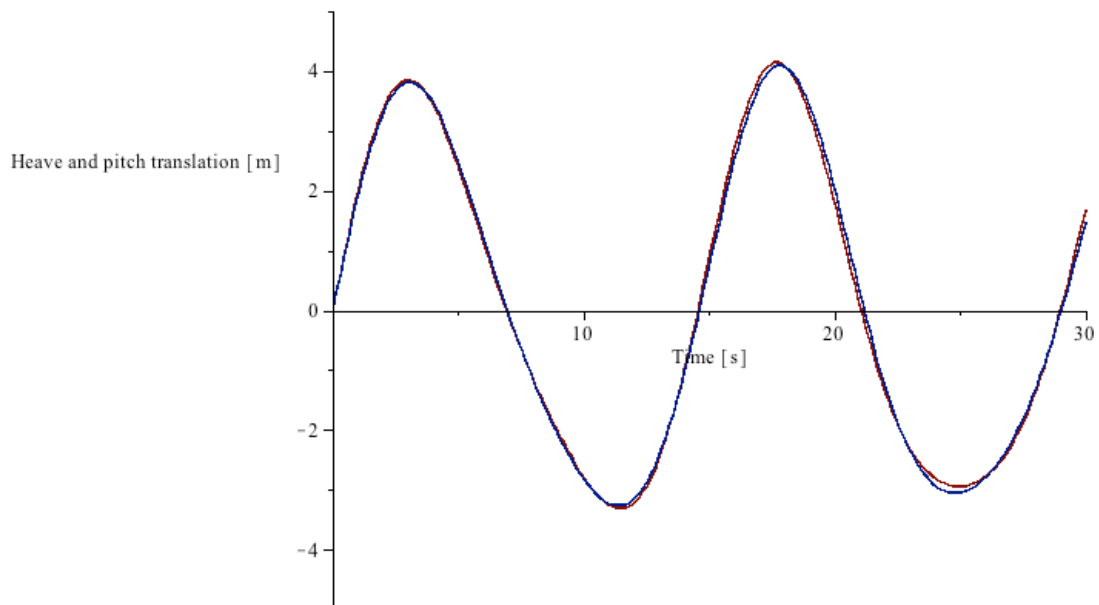


Figure 7.3-13 Coupled heave and pitch motion for the DrillMax Ice in beam sea (90°); blue line is when ice is included, red line when there is no ice

The maximum roll displacement for the ship in the direction of 45° with the vessel, was calculated to be at 3.85 m at the time of 11.32 seconds when ice and snow loads were not included. When ice and snow loads were included, the maximum displacement was at 3.32 m at the time of 11.82 seconds. This can be seen in Figure 7.3-14.

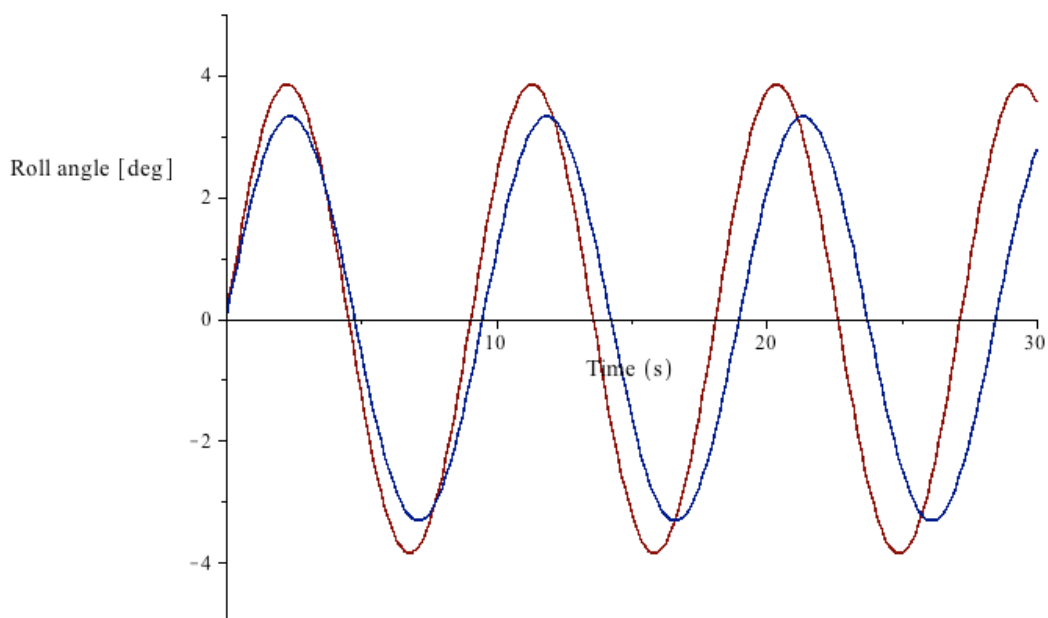


Figure 7.3-14 Roll motion for the DrillMax Ice in waves with direction of 45° with the vessel; blue line is when ice is included, red line when there is no ice

The maximum roll displacement for the ship in beam sea was at 9.17 m at 11.32 seconds when ice and snow loads were not included. When ice and snow loads were included, the maximum displacement was at 7.04 m at the time of 11.87 seconds, see Figure 7.3-15.

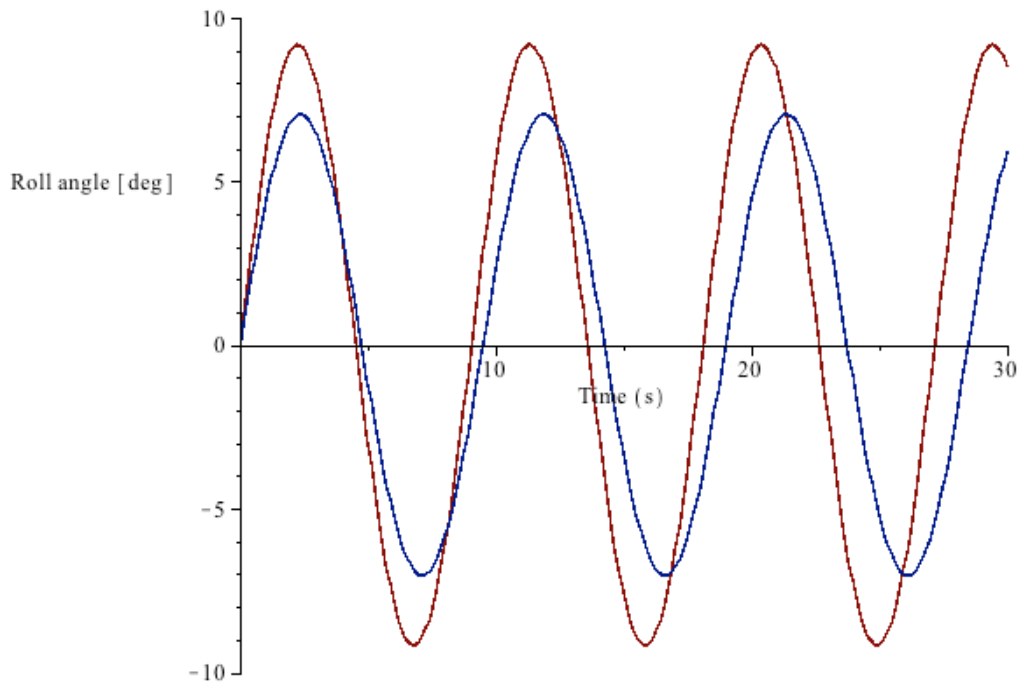


Figure 7.3-15 Roll motion for the DrillMax Ice in beam sea (90°); blue line is when ice is included, red line when there is no ice

7.3.4. Motion Response for the West Alpha

The results of the calculated natural periods in heave, pitch and roll for this semi-submersible are shown in Table 7.3-4 below. These values have further been used to calculate the motion response of this vessel.

Table 7.3-4 Calculated natural periods for West Alpha

	Without ice and snow loads	With ice and snow loads
Natural period in heave [s]	17.22	17.38
Natural period in pitch [s]	23.56	26.78
Natural period in roll [s]	29.73	33.26

The maximum coupled heave and pitch displacement for the rig in head sea was calculated to be at 0.80 m at the time of 13.12 seconds when ice and snow loads were not included. When ice and snow loads were included, the maximum displacement was at 0.70 m at the time of 13.25 seconds. This can be seen in Figure 7.3-16 below.

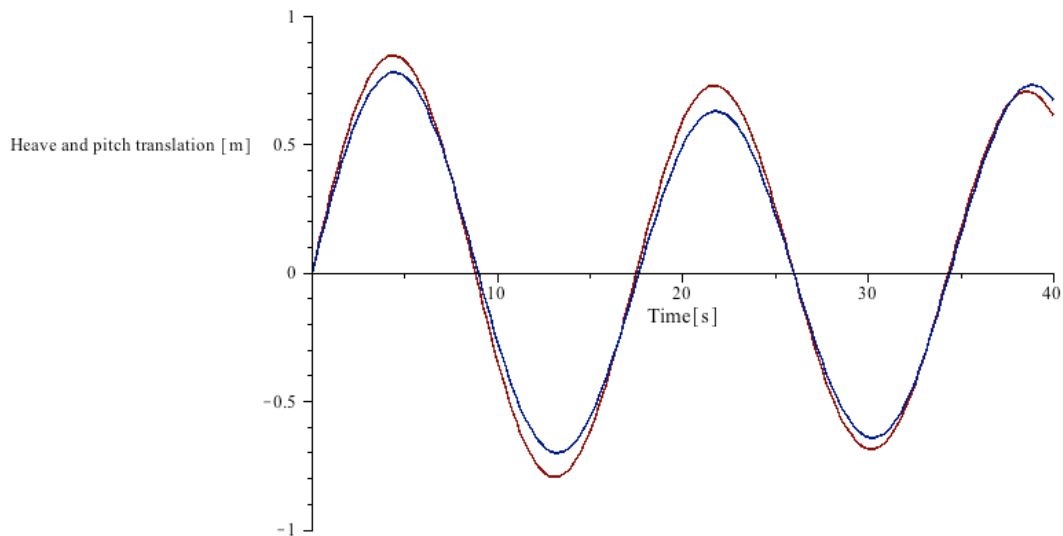


Figure 7.3-16 Coupled heave and pitch motion for West Alpha in head sea (0°); blue line is when ice is included, red line when there is no ice

The maximum coupled heave and pitch displacement for the rig in the direction of 45° with the vessel, was calculated to be at 0.79 m at the time of 13.14 seconds when ice and snow loads were not included. When ice and snow loads were included, the maximum displacement was at 0.69 m at the time of 13.27 seconds, see Figure 7.3-17.

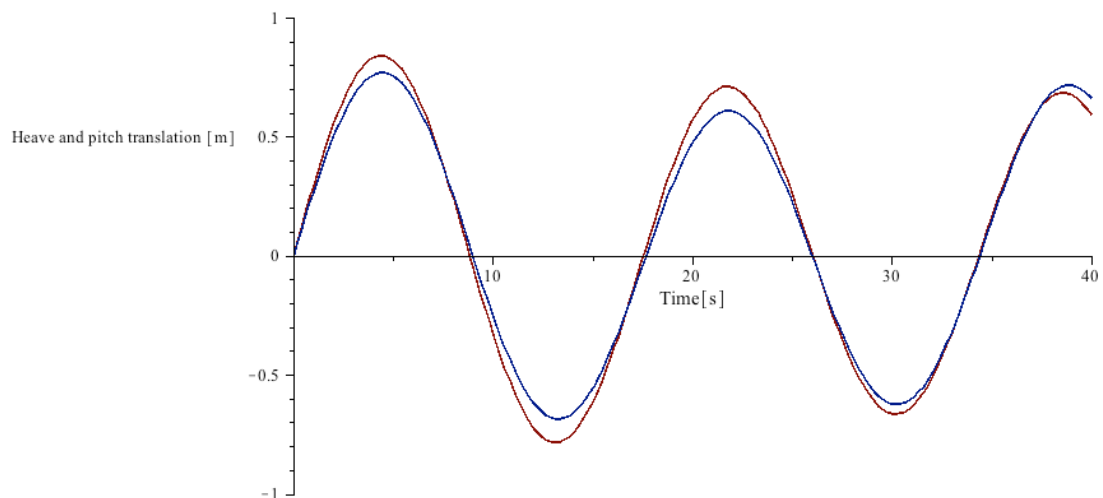


Figure 7.3-17 Coupled heave and pitch motion for West Alpha in waves with direction of 45° with the rig; blue line is when ice is included, red line when there is no ice

By the reason that the displacement in pitch will become zero when using the RAO tables (given in Appendix C), only the heave motion will be considered here. The maximum uncoupled heave displacement for West Alpha in beam sea was calculated to be at 0.57 m at the time of 12.92 seconds when ice and snow loads were not included. When ice and snow loads were included, the maximum displacement was at 0.64 m at the time of 13.03 seconds. This can be seen in Figure 7.3-18.

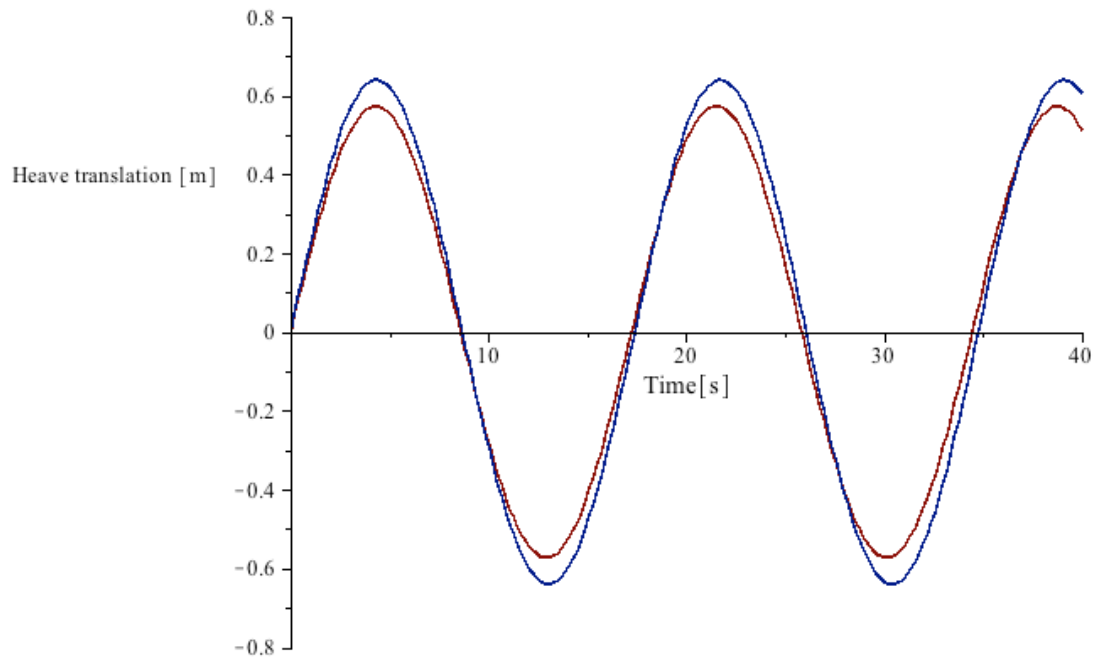


Figure 7.3-18 Heave motion for West Alpha in 90° sea; blue line is when ice is included, red line when there is no ice

The maximum roll displacement in the direction of 45° with the vessel, was calculated to be at 0.33 m at the time of 7.43 seconds when ice and snow loads were not included. When ice and snow loads were included, the maximum displacement was at 0.36 m at the time of 8.32 seconds. This can be seen in Figure 7.3-19.

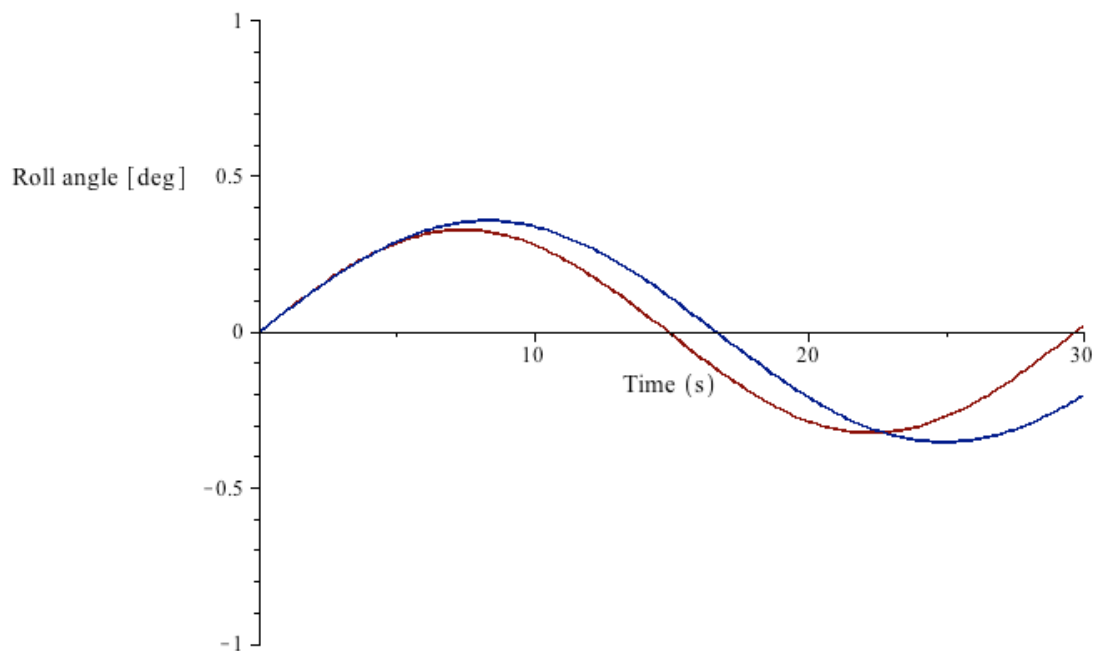


Figure 7.3-19 Roll motion for West Alpha in waves with direction of 45° with the rig; blue line is when ice is included, red line when there is no ice

The maximum roll displacement for the rig in beam sea was calculated to be at 0.18 m at the time of 7.43 seconds when ice and snow loads were not included. When ice and snow loads were included, the maximum displacement was at 0.22 m at the time of 8.32 seconds, see Figure 7.3-20.

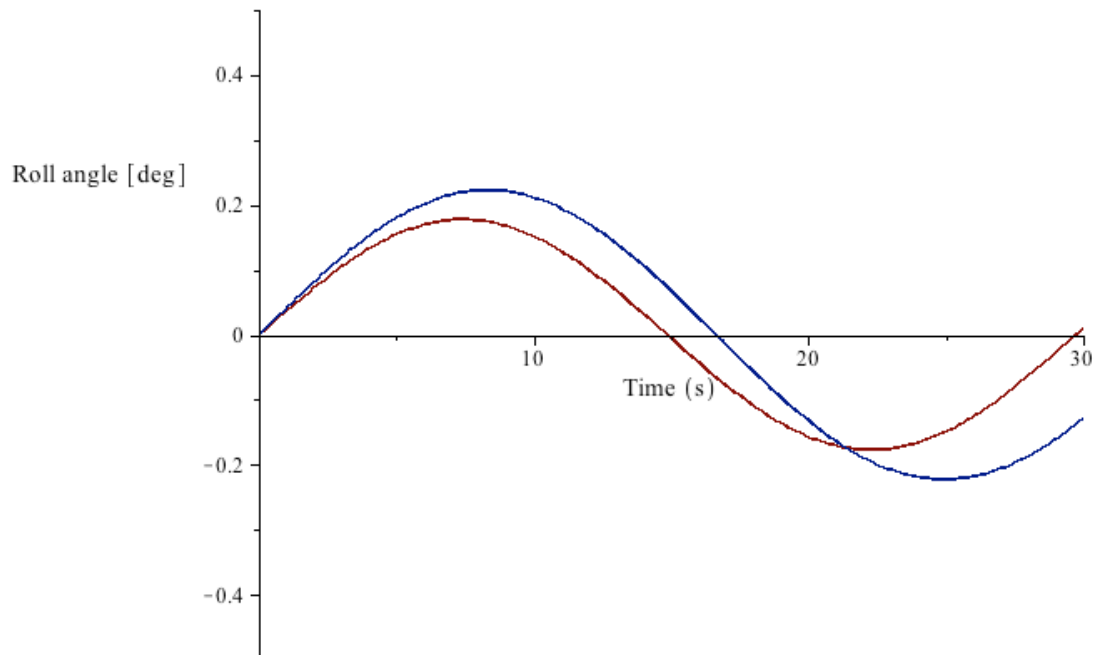


Figure 7.3-20 Roll motion for the West Alpha rig in beam sea (90°); blue line is when ice is included, red line when there is no ice

7.4. Summarization of the Motion Response Results for the Vessels

The calculated displacements for each vessel in each of the situations are presented in Table 7.4-1 below.

Table 7.4-1 Maximum displacement and angle results for the vessels

		Lady of Grace	Viking Fighter	DrillMax Ice	West Alpha
Coupled heave and pitch translation in direction 0° [m]	Without ice and snow loads	0.366	1.65	5.67	0.80
	With ice and snow loads	0.370	1.81	5.86	0.70
Coupled heave and pitch translation in direction 45° [m]	Without ice and snow loads	0.63	2.82	7.44	0.79
	With ice and snow loads	0.75	2.85	7.43	0.69
Coupled heave and pitch translation in direction 90° [m]	Without ice and snow loads	2.12	4.30	3.84	(only heave motion) 0.57
	With ice and snow loads	2.53	4.31	3.81	(only heave motion) 0.64
Roll angle in direction 45° [deg]	Without ice and snow loads	0.13	0.74	3.85	0.33
	With ice and snow loads	0.75	0.79	3.32	0.36
Roll angle in direction 90° [deg]	Without ice and snow loads	0.28	1.57	9.17	0.18
	With ice and snow loads	2.25	1.53	7.04	0.22

8. Discussion

In this section the calculated results of the freeboard, stability, righting arm, heeling angle and motion response of the vessels will be interpreted and discussed. Some of the most important assumptions made in the calculations will also be discussed here.

This section has been divided into six sub-sections. In the first section, section 8.1, some of the most important assumptions made in order to perform the calculations have been highlighted and discussed. In section 8.2, the most important findings from the calculated results for the freeboard and stability will be discussed for all four vessels. The results for the calculated righting arms for the three ships are discussed under section 8.3. The result for the static heeling angle for semi-submersible is discussed in section 8.4. In the next section, section 8.5, a comparison between the vessels' results will be conducted. In the last section of this chapter, section 8.6, the calculated results for the motion response in heave, pitch and roll for all the vessels will be discussed.

8.1. Assumptions

Several important assumptions have been made in order to perform the calculations for these vessels. The assumptions which are considered as the most important in this report regard where the sea-spray ice and snow would accrete on the vessels, where the maximum ice thickness would occur, how much ice the maximum accretion of ice would be, the dimensions of the vessels read or measured from the general arrangement drawings, and the different densities of the sea-spray ice, snow and sea water.

For the three ships considered in this report; Lady of Grace, Viking Fighter and DrillMax Ice, the area of where the maximum ice accretion would occur was mostly based on Figure 4.1-7, Figure 4.1-8 and Figure 4.1-9. These figures were based on previous observations of where ice has accreted on ships. There is, however, a possibility that the maximum accretion icing zone could occur differently than assumed, due to different sizes of the vessels, the way the vessel was designed and constructed, or if the environment was different; higher wind speeds, lower sea temperature, etc.

Documentation on how big portion of a semi-submersibles sea-spray ice actually has covered in the past was pretty much non-existent. Therefore it was assumed that the sea-spray ice could cover as much as 25 % of the width of the deck, which is considered as a conservative value where it in reality could be much less. In order to make a more accurate assumption, it is necessary to have more observations and documentations.

There have also been observations of icing accretion on different equipment or other elements of the vessels. For example, it was mentioned under section 4.1.4 that a ship had accumulated up to 350 mm of ice on the wire from the bow and to a point above the pilothouse of the ship and ice thicknesses up to 300 mm on handrails on vessels. However, when the mass of the ice on these smaller elements was calculated, they were small compared to the ice loads on the deck, bridge and columns. Therefore it was also assumed that the icing on these elements would have little contribution to a

reduction in freeboard, stability, etc. that it could be neglected.

The maximum ice accretion rate used in the analysis was taken to be 15 mm/hr. This was based on previous data taken over the period from 1957 – 2009 in the eastern part of the Barents Sea, where this rate was the maximum rate that has occurred a few times during this period. There will be uncertainties on what effect the decrease in the polar ice cap will have on the maximum ice accretion rate in this area in the future (waves and winds may increase in intensity), but as this value of ice accretion rate has occurred several times in the past, it did seem all right to use as a probable situation in the analysis.

The different dimensions used in the calculations were either measured or read from some of the general arrangement drawings given in Appendix A. As there was limited information about some of the parameters that were needed in the stability calculations of the vessels, alternative calculations using variations of these parameters was sometimes done.

The sea-spray ice density may decrease with the level of height above the water. As most of the sea-spray ice would accrete on the vessels at a height between 10 m to 25 m, a mean value of 700 kg/m^3 was chosen from a table in NORSOK N-003 (2007) and used in the calculations. It was also given in a table in NORSOK N-003 (2007) that the density of atmospheric icing or snow is 900 kg/m^3 regardless of the height above the water. Therefore this value was chosen as the density of the atmospheric icing and (frozen) snow in the calculations. The density of the seawater the vessels would operate in was assumed to be 1025 kg/m^3 . This parameter could vary depending on the different areas of where the vessels would work. However, this difference in density for the Barents Sea is assumed to be so small that it can be neglected.

8.2. Freeboard and Stability Results

All four vessels were calculated to have an acceptable freeboard and stability for the case analysed with the maximum sea-spray ice thickness of 225 mm and a snow thickness of 300 mm. This amount of sea-spray ice and snow was assumed to be the result of the average storm duration in the North Sea of 15 hours with an ice accretion rate that has occurred several times earlier in the Barents Sea. However, the freeboard and the stability were significantly reduced for all the vessels. This indicates that if the ice accretion rate was higher or if the duration of the storm was much longer, the possibility of losing freeboard or having an unstable vessel is possible.

In the parameter study, it was proven that the smallest ship, Lady of Grace, was most likely to lose its freeboard and stability. The boat needed a sea-spray ice thickness of 730 mm to lose its freeboard, and only a sea-spray thickness of 310 mm to lose its stability.

Icing on equipment located above the pilothouse have not been accounted for, which will decrease the stability further. It is assumed that this boat had a ballast of 100 ton, and if it would have more ballast than this, the stability would be better. However, if the boat had more ballast, the freeboard would, however, be less, and could then become the critical factor.

In order to have a sea-spray thickness of 310 mm for the situation with the maximum ice accretion rate of 15 mm/hour will require a storm with a minimum duration of 21 hours. There has also been mentioned earlier that storm durations can last up to seven days. There have also been recorded incidents where the total ice thickness on deck has reached as much as 1000 mm. This is the reason why the value of 310 mm of sea-spray ice can be considered as a probable situation that can realistically occur in the Barents Sea.

The Viking Fighter vessel needed as much as 1.63 m of sea-spray ice and 2.95 m of sea-spray ice in order to no longer fulfil the minimum freeboard and stability requirements from DNV. These vast amounts of sea-spray ice are considered as highly unlikely to occur in the Barents Sea, or somewhere else in the Arctic.

The DrillMax Ice ship, which is much larger than the Viking Fighter ship, needs an amount of 11.39 m and 8.35 m of sea-spray ice in order to no longer satisfy the freeboard and stability requirements given by DNV. These amounts of ice are so great that they also are considered highly unlikely to occur.

The parameter study also revealed that the semi-submersible rig, West Alpha, needed the amounts of 4.18 m and 4.67 m of sea-spray ice in order to no longer fulfil the freeboard and stability criteria, respectively. These amounts of sea-spray ice are also considered as highly unlikely to occur. However, it was found from the analysis that there would be a significant change in the freeboard and stability for the rig.

In the analysis a snow thickness of 30 cm was assumed to be on the deck, a thickness of 10 cm of ice on the derrick due to atmospheric icing, and a thickness of sea-spray ice of 22.5 cm on the columns and a portion of the deck. The stability (GM) was changed from 3.06 m without the ice to 2.44 m when the ice was included, which is a reduction in stability of 0.62 m. The freeboard changed from 12.0 m without the ice to 8.75 m with ice, which is a reduction in freeboard of 3.25 m, which shows a significant change in freeboard.

8.3. Righting Arm Results

When the ships experience higher angles of heel (more than 5°) due to vessel motions, it is important that the righting arm is big enough so that the vessel can stay upright in the motions.

In the situation with the thickness of 225 mm of sea-spray ice and thickness of 300 mm snow, the righting arm for all four vessels still fulfilled the requirements given by DNV (2005) and DNV (2013).

The parameter study revealed that the smallest ship, the Lady of Grace, was most likely to have too short righting arm. At a sea-spray ice thickness of 440 mm, the requirement for this ship was no longer fulfilled. This is an amount of sea-spray ice that is assumed to be possible in the Barents Sea. For the other two ships, the Viking Fighter and the DrillMax Ice, they needed a vast amount of sea-spray ice, 3.57 m and 10.72 m respectively to lose the righting arm, which is considered as not likely to occur.

8.4. Static Heeling Angle

As the semi-submersible probably will experience asymmetric loading, with more ice on the windward side, it will also experience a static heeling angle. In the analysis the heeling angle was calculated to be 2.67° , which is much less than the criteria of 17° . It was calculated that a heeling angle of 8° would occur with an amount of 0.49 m of sea-spray ice including a thickness of 0.30 m of snow on the deck.

The parameter study revealed that the semi-submersible needed an ice thickness of 0.99 m to have a heeling angle of more than 17° which was the minimum damaged stability criteria for the rig. It was also calculated that it needed an ice thickness of more than 1.21 m to have a heeling angle of more than 21° which was the minimum intact stability criteria for the rig.

In order to have a sea-spray thickness of 0.99 m for the situation with the maximum ice accretion rate of 15 mm/hour will require a storm with a minimum duration of 2 days and 18 hours (66 hours). As the average storm duration in the Barents Sea is approximately 15 hours only, viewed together with the small probability of having an ice accretion of 15 mm/hour, it is assumed unlikely that this will occur on the rig in the Barents Sea. It is also considered unrealistic to have a thickness of 0.99 m on the vertical elements of the semi-submersible like on the columns, trusses, etc. as the ice will be so heavy and probably break off before it gets to that ice thickness.

By the reason that the parameter study revealed that the rig needed an amount of 4.18 m and 4.67 m of sea-spray ice thickness to lose its freeboard and stability, respectively, the static heeling angle will become the critical element for this rig. This is because it only needs a thickness of 0.99 m of ice in order to no longer be safe.

8.5. Comparison of the Vessels

The percentage of change in the different parameters shown in Table 7.2-1 reveals that the larger the ship is, the smaller the change will be in reduction of any of freeboard, stability and righting arm. Therefore it seems that at some size of a ship, it will be so big that the amount of ice needed to make it unsafe will be highly unlikely to occur.

This is probably the reason why most reported accidents with vessel icing where the ships have capsized due to heavy icing has mostly involved small fishing boats and not large ships. However, even though the freeboard, stability or righting arm are not critical for a vessel's safety, the icing could still create other dangerous situations. As mentioned under section 4.1.2, the icing could make different components or equipment on vessels to fail or deteriorate.

Component malfunction or dangerous situations could be caused by immense loads of ice and snow, or just a small layer of 1 mm of glaze ice, which could make the surfaces very slippery and present a slipping hazard for the crew. Therefore it is very important for vessels that shall operate in cold areas to have ice protection and to take preventive actions.

If some of the elements of the vessels were iced up, the most critical situation would be if the vessels integrity were lost, as it could lead to a loss of the vessel. Another critical element is if the fire and rescue equipment become unreachable or unusable

due to vessel icing, which could lead to loss of lives. This underlines how important it is to use vessels that are winterized or made to operate in cold areas where vessel icing might occur.

For the semi-submersible, the most critical requirement was the static heeling angle, and the second-most critical element was the freeboard. The semi proved to be very stable compared to the ships, and the probability of getting the amount of ice needed for it to be unstable is considered as unlikely. However, it did experience great reduction in freeboard.

8.6. Motion Response Results

The motion response results were found from the analysis where the maximum sea-spray ice thickness was 225 mm and where the snow thickness was 300 mm on the ships. Those loads were included in the calculation of the semi-submersible, with an extra load of 100 mm ice thickness on the derrick.

The calculated natural period in heave, pitch and roll increased for all four vessels when the ice was included. The change in the natural period in heave and pitch was not much, but the natural period in roll changed more significantly. The greatest change in roll period due to vessel icing was for the Lady of Grace boat, where the roll period was almost doubled with the ice load.

For some situations the vessels experienced greater displacements when the ice was included, and for other situations, the vessels experienced smaller displacements when the ice was included. In some situations the difference in displacement due to ice was so small that it could be considered negligible.

The smallest difference in the motion for the vessels was the coupled heave and pitch motion for the Lady of Grace vessel in the direction of 0° with the ship. The difference in the maximum displacement was changed from 0.366 m to 0.370 m when the ice loads was included, which is a difference of 0.04 m (4.0 cm).

The largest difference in the motion for the vessels was the difference in roll angle for the DrillMax Ice vessel in the direction of 90° with the ship. The maximum roll angle changed from 9.17° without the ice loads to 7.04° with the ice loads, which is a reduction in angle of 2.13° .

Seen from the summarization table above Table 7.4-1, the DrillMax Ice vessel experiences larger displacements and roll angles compared to the other three vessels. The reason for this is because the natural period in heave, pitch and roll are more or less the same as the natural period for the waves. This means that this vessel almost goes into resonance with the waves for these situations, which causes larger displacements and angles compared to the other three vessels. The Lady of Grace vessel and the Viking Fighter vessel have initially so short natural periods in heave, pitch and roll that for all the situations the motions and angles got larger with the added ice mass on the vessel as the natural period increased and got closer to the waves natural period.

The semi-submersible on the other hand, had so long natural periods in heave, pitch and roll, that the displacements and angles were initially quite small. For the

situations with the coupled heave and pitch motions, the motions decreased a little with the ice loads. The displacement in heave in the direction of 90° with the vessel as well as the two roll angles in the direction of 45° and 90° with the vessel, increased a little when the ice load was included.

The reason why all the displacements did not just increase (or decrease) is because of the values used in the RAO tables, which are given in Appendix C. As these tables are based on the natural periods of the vessels, and since the natural periods of the vessels had sometimes peaked at/before the ships own natural period in the RAO tables without the ice, the increased natural period by the icing loads corresponded to lower values in the RAO tables.

It was also shown in the results that all the four vessels in the different wave directions had a slower motion when the ice loads were included. This especially applies to the roll motion, which got far slower than the heave and pitch motion when the ice was included.

9. Conclusion

The parameter study revealed that the smallest ship, the fishing boat, was much more likely to lose its freeboard and stability due to vessel icing, and that the calculated amount of ice needed in order to make the two larger ships and the semi-submersible unsafe was so much that such a situation is considered as highly unlikely to occur. For the fishing vessel, the amount of ice needed to make it unsafe is much less which is much more likely to occur.

Results from the case study revealed that the freeboard and stability requirements from Det Norske Veritas were still fulfilled for all vessels. Results from calculations also showed that the most critical element for the Viking Fighter ship was the freeboard, while the stability was the most critical feature for the drillship and the fishing boat. For the semi-submersible, the heeling angle due to asymmetric sea-spray ice accumulation on the rig was the most critical feature.

If there would occur some problems with the ballast tanks of the rig, and/or if wind forces were extremely high, this together with the icing accumulations could contribute to a dangerous heeling angle. However, it is assumed that the icing would probably not be the sole reason for an unstable semi-submersible due to the vast amount of ice needed. A large heel angle will, however, make operations on the semi-submersible dangerous.

Results from the motion responses revealed that when the ice load was included, displacements were sometimes increased and sometimes decreased. All the vessels got an increased period in heave, pitch and roll with the ice accumulation, and therefore all the motions acted slower (longer roll period) when the ice load was included, especially the roll motion.

However, other hazards could occur due to icing on any vessel as the ice can have other impacts on the vessel. Different important functions could deteriorate or be destroyed by the ice. This could also lead to a loss of the vessel, loss of lives onboard, personal injuries or loss of assets. This is the reason why it is important to use vessels that have been winterized or made to operate in cold areas where vessel icing might occur.

There are also some suggestions on further work in this area. For example model testing of vessels in a basin can be done to study the impact of icing on the different sizes of the vessels. Different simulation program can also be taken into use to determine the effect of icing on a vessel, and then it may also be possible to study the effect under different environmental conditions. For example by using different input parameters such as wind speed, air temperature etc. Several semi-submersibles and ships can be analysed and compared. The impact of ice accumulations on other vessels can also be studied, for example on jack-ups, deep draft floaters, jackets and more.

List of References

- ABRAHAMSEN, E. & JOHANSEN, T. (2000). *Fishing and fishing boats*, Brevik, Norway, Brevik historielag.
- ANDREAS, E. L. & JONES, K. F. (2009). *Technology assessment and research program, safety and engineering research: sea spray icing of drilling and production platforms*. Hanover, NH 03755-1290: Cold Regions Research and Engineering Laboratory.
- Deadliest catch, Man vs. Ice*, (2006). Directed by BEERS, T. <http://www.netflix.com>, 13 February 2014.
- BOWDITCH, N. (2002). *The American Practical Navigator, U.S.*, Washington, U.S. Hydrographic Office, Pub. 9, 1995.
- BP. (2007). *Wind Compass* [Online]. Available: http://1.bp.blogspot.com/_c8EartLqdVs/TM1a1BbGD4I/AAAAAAAAA1c/7uWR_1f0gF4/s1600/wind_compass.gif.
- BROWN, R. D. & ROEBBER, P. (1985). *The Ice Accretion Problem in Canadian Waters Related to Offshore Energy and Transportation*, Canadian Climate Centre Report, No. 85-13, pp. 295.
- CAMMAERT, G. (2013). *Marine Icing on Arctic Offshore Operations - Pilot Project. Arctic Marine Operations Challenges & Recommendations* Delft University of Technology, Vol. 5, Report MAR11908-E/1133-RP05, pp. 49.
- CROWLEY, J. D. *Cold water effects upon marine operations*. OCEANS '88., Oct. 31 1988-Nov. 2 1988 1988 Baltimore, MD, USA. pp. 543 - 548.
- DEBABRATA, S. (2011). *Uncoupled Heave, Pitch and Roll* Department of Ocean Engineering and Naval Architecture, Indian Institute of Technology, Kharagpur, pp.23.
- DNV (2005). *Hull Equipment and Safety*. Part 3. Det Norske Veritas, Høvik, Oslo, Norway.
- DNV (2011). *Modelling and Analysis of Marine Operations*. Technical report DNV-RP-H103. Det Norske Veritas, Høvik, Oslo, Norway.
- DNV (2013). *Stability and Watertight Integrity*. Technical report DNV-OS-C301. Det Norske Veritas, Høvik, Oslo, Norway.
- EFIMOV, Y. O. (2012). *Vessel Icing on the Shtokman FPSO*. M.Sc. Thesis, University of Stavanger.
- EIDESVIK (2012). *Viking Fighter*.

- EKEBERG, O. C. (2010). *State-of-the-art: On marine icing models and observations*. Technical Report Det Norske Veritas, No 2010-0745, pp. 87.
- ERIK FALKENBERG, XU, J. & ODOR, G. *Mooring a Drilling Semi Over a Pre-Installed Riser System - West Alpha at Snorre B*. Proceedings of the Eleventh (2001) International Offshore and Polar Engineering Conference, 2001 Stavanger, Norway. The International Society of Offshore and Polar Engineers, Vol. 2, ISSN 1098-6189, pp 299 - 305.
- ERNST & YOUNG (2013). *Arctic oil and gas*. <http://www.ey.com>.
- FALTINSEN, O. M. (1993). *Sea loads on ships and offshore structures*, Cambridge Ocean Technology Series, Cambridge university press, Cambridge, pp. 328.
- FETT, R. W., ENGLEBRETSON, R. & PERRYMAN, D. (1993). *Forecasters Handbook for the Bering Sea, Aleutian Islands, and Gulf of Alaska*, Naval Research Laboratory, Monterey CA.
- FUNK, C. (2012). *Freezing Spray & Ice Accretion on Vessels: A Comprehensive Study*. Proceedings of the National Conference On Undergraduate Research (NCUR) Weber State University, Ogden UT.
- GALLALA, J. R. (2013). *Hull Dimensions of a Semi-Submersible Rig: A Parametric Optimization Approach*. Master's Thesis, Norwegian University of Science and Technology, Trondheim. pp. 123.
- GOULD, R. A. (2011). *Archaeology and the Social History of Ships*, New York, U.S.A., Cambridge University Press.
- GRØNÅS, S. & SKEIE, P. (1999). *A case study of strong winds at an Arctic front*. Tellus A, 51 (5), pp. 865 - 879.
- HAMILTON, W. (2006). *Polar travelling* [Online]. Available: http://www.rosssea.info/polar_travel.html [Accessed 27th February 2014].
- HANSEN, E. S. (2012). *Numerical modelling of marine icing on offshore structures and vessels*. M.Sc Thesis. Norwegian University of Science and Technology, Trondheim.
- HOVLAND, K. M. (2012). *Norway Agency to Investigate Barents Sea Oil Rig Incident* [Online]. Euroinvestor. Available: <http://www.euroinvestor.no/nyheter/2012/09/12/norway-agency-to-investigate-barents-sea-oil-rig-incident/12088041> [Accessed 29th May 2014].
- IDEN, K. A., REISTAD, M., AARNES, O. J., GANGSTØ, R., NOER, G. & HUGHES, N. E. (2012). *Knowledge about wind, waves, temperature, ice extent, visibility and more - Barents Sea SE*. pp. 82.

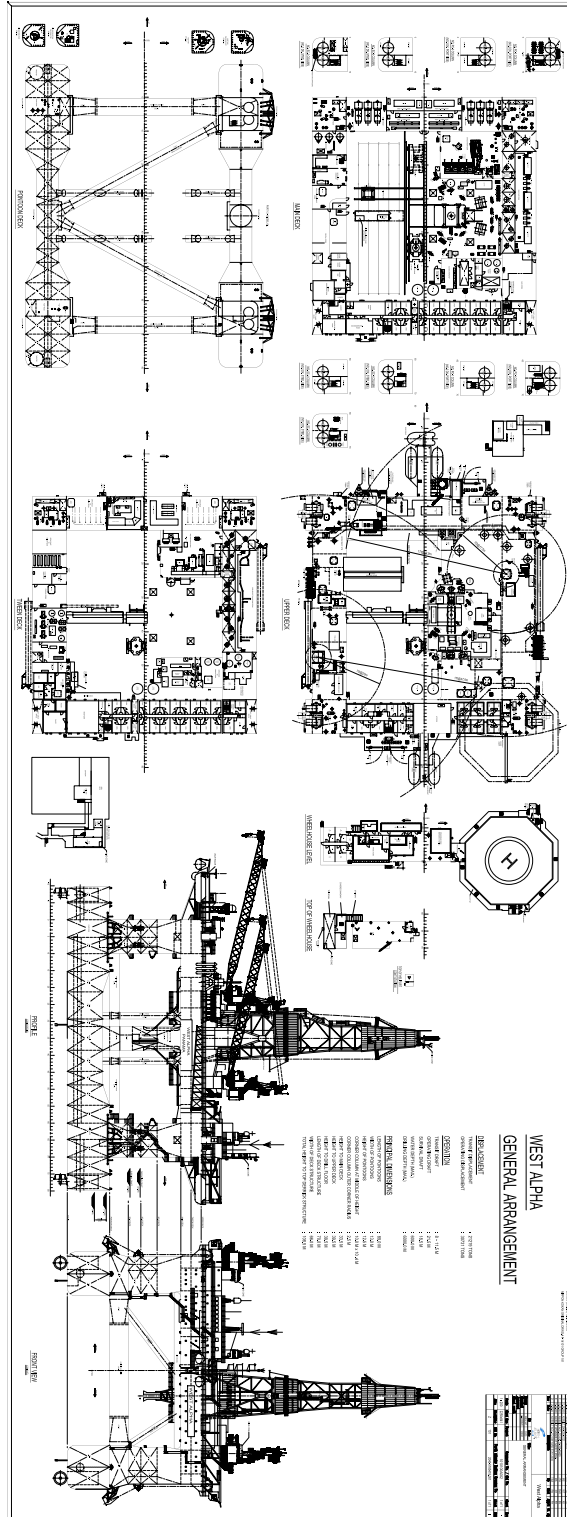
- ISMAIL, Z., KUAN, K. K., OTHMAN, S. Z., HING, L. K., YEE, K. S., CHAO, O. Z. & SHIRAZI, S. (2014). *Evaluating accidents in the offshore drilling of petroleum: regional picture and reducing impact. Measurement*, vol. 51, p.18-33.
- ISO (2010). *Arctic offshore structures. Petroleum and natural gas industries*. Geneva, FDIS version: International Standardization Organization.
- JACOBSEN, S. R. & GUDMESTAD, O. T. *Evacuation from Petroleum Facilities Operating in the Barents Sea*. ASME 2012 31st International Conference on Ocean, Offshore and Arctic Engineering, 2012. American Society of Mechanical Engineers, pp. 457-466.
- KOLSTAD, E. W. (2007). *Extreme winds in the Nordic seas: polar lows and Arctic fronts in a changing climate*. Bergen.
- LANGE, M. D. (2011). *Morphodynamic Analysis Ecobeach Project*. Delft University of Technology, Faculty of Civil Engineering, pp. 229.
- LOENG, H. (1991). *Features of the physical oceanographic conditions of the Barents Sea. Polar research*, Vol. 10, pp. 5-18.
- MAINWARING, J. (2013). *Arctic Oil, Gas Vessels: The Next Generation* [Online]. Available: http://www.rigzone.com/news/oil_gas/a/127372/Arctic_Oil_Gas_Vessels_The_Next_Generation [Accessed 10th February 2014].
- MAKKONEN, L. (1984). *Atmospheric icing on sea structures*, US Army Cold Regions Research and Engineering Laboratory, Hanover, New Hampshire, CRREL Monograph 84-2, pp. 102.
- MAUNG, K. (1974). *The design of semi-submersibles for minimum vertical motion*. PhD Thesis, University of Glasgow.
- MINSK, L. D. (1980). *Icing in structures*. New Hampshire, U.S.A: United States Army Corps of Engineers Cold Regions Research and Engineerin. Report no. 80-31, pp. 26.
- MINSK, L. D. (1984). *Ice Observation Program on the Semisubmersible Drilling Vessel SEDCO 708*. Hanover, New Hampshire 03755: U.S. Army Cold Regions Research and Engineering Laboratory, Special Report 84-2, 20 p.
- NAUMAN, J. W. (1984). *Superstructure Icing Observations on the Semisubmersible Ocean Bounty in Lower Cook Inlet, Alaska. Proceedings of the Second International Workshop on Atmospheric Icing of Structures*. Trondheim, Norway. pp. 71 - 79.
- NORSOK, N. (2007). *Actions and action effects*. Rev. 4. Standards Norway Strandveien 18, P.O. Box 242 N-1326, Lysaker, Norway: Norwegian Technology Standards Institution.

- OFFSHORE-TECHNOLOGY.COM. (2013). *Gygrid Prospect* [Online]. Available: <http://www.offshore-technology.com/projects/gygrid-prospect/> [Accessed 22th May 2014].
- OFFSHORE.NO. (2014). *West Alpha* [Online]. <http://www.offshore.no>. Available: <http://www.offshore.no/Projekter/rigg-informasjon.aspx?navn=West+Alpha> [Accessed 17th March 2014].
- OVERLAND, J. E. (1990). *Prediction of Vessel Icing for Near-Freezing Sea Temperatures. Weather and Forecasting. Pacific Marine Environmental Laboratory*, Seattle, Washington. Vol. 5, pp. 62-77.
- PEREZ-ROJAS, L. (2008). *Review of the ship accidents investigations. Proceedings of the 10th International Ship Stability Workshop*. Madrid, Spain: University of Madrid.
- PEROVICH, D. K. & RICHTER-MENGE, J. A. (2009). *Loss of sea ice in the arctic. Annual Review of Marine Science*, Vol. 1, pp. 417-441.
- RYERSON, C. C. (2008). *Assessment of Superstructure Ice Protection as Applied to Offshore Oil Operations Safety: Problems, Hazards, Needs, and Potential Transfer Technologies*. Hanover NH: Engineer, Research and Development Center Hanover Nh Cold Regions, Report ERDC-CRREL-TR-08-14.
- RYERSON, C. C. (2009). *Assessment of Superstructure Ice Protection as Applied to Offshore Oil Operations Safety: Ice Protection Technologies, Safety Enhancements, and Development Needs, Report ERDC/CRREL TR-09-4*, Hanover, U.S., US Army Engineer Research and Development Center.
- RYERSON, C. C. (2011). *Ice protection of offshore platforms. Cold Regions Science and Technology*, pp. 97-110, Report nr. 65.
- RYERSON, C. C. (2013). *Icing Management for Coast Guard Assets*. Hanover, U.S.: Cold Regions Research and Engineering Laboratory U.S. Army Engineer Research and Development Center. Report ERDC/CRREL TR-13-7, pp. 529.
- RYERSON, C. C. (2014). *Question about vessel icing for a Master`s thesis*. [Charles.C.Ryerson@erdc.dren.mil]: Sent to Charles Ryerson, 6th March 2014.
- SEADRILL (2009). *West Alpha*.
- SHIP-TECHNOLOGY. (2012). *Viking Fighter Offshore Supply Vessel, Norway* [Online]. <http://www.ship-technology.com>. Available: <http://www.ship-technology.com/projects/viking-fighter-offshore-supply-vessel/> [Accessed 17th March 2014].

- SHIPILOVA, O., KULYAKHTIN, A., TSARAU, A., LIBBY, B., MOSLET, P. & LOSET, S. *Mechanism and Dynamics of Marine Ice Accretion on Vessel Archetypes*. OTC Arctic Technology Conference, 2012. Offshore Technology Conference, Paper nr. 23762.
- STEEL, D. (2004). *Report of the Re-opened Formal Investigation Into the Loss of the FV Gaul*. UK, Norwich: The UK Stationary Office, N174460-C6, 176 p.
- STENA, D. (2011). *Stena DrillMAX ICE*.
- STROEVE, J. C., SERREZE, M. C., HOLLAND, M. M., KAY, J. E., MALANIK, J. & BARRETT, A. P. (2012). *The Arctic's rapidly shrinking sea ice cover: a research synthesis*. *Climatic Change*, Vol. 110, pp. 1005-1027.
- TARALDSEN, L. (2013). *Inocean - The engineers goodie bag* [Online]. Teknisk Ukeblad. Available: <http://www.tu.no/petroleum/2013/11/29/-dette-er-ingeniorennes-godtepose> [Accessed 10th February 2014].
- TUPPER, E. C. (2004). *Introduction to naval architecture: Naval architecture*, Jordan Hill, GBR, Butterworth-Heinemann, 464 p.
- TUPPER, E. C. & RAWSON, K. (2001). *Basic Ship Theory, Combined Volume*, Vol. 2, Butterworth-Heinemann, 368 p.
- USCG (2008). *Investigation into the sinking and loss of life of four crew members aboard the commercial fishing vessel, Lady of Grace*. 2100 Second Street, S.W. Washington: U.S. Department of Homeland Security, Report nr. 16732.
- WRIGHT, B. (2000). *Full Scale Experience with Kulluk Stationkeeping Operations in Pack Ice (With Reference to Grand Banks Developments)*. Canada: The National Research Council of Canada.
- YOUNG, I. R., ZIEGER, S. & BABANIN, A. V. (2011). *Global trends in wind speed and wave height*. *Science*, vol. 332 (6028), pp. 451-455.
- ØKLAND, J. (2012). *Ice cold mission for West Alpha* [Online]. offshore.no. Available: http://www.offshore.no/sak/36401_iskaldt_oppdrag_for_west_alpha [Accessed 10th February 2014].

A – 2 General Arrangement Drawing of the West Alpha

Some of the dimensions used in the calculations are taken from this general arrangement drawing of the West Alpha semi-submersible platform. The PDF file for this drawing has also been given on the CD in the back.



Appendix B - Added Mass Coefficients

B - 1 The Added Mass Coefficients

The tables in this appendix are taken from DNV (2011) has been taken into use in order to calculate the added mass for the vessels; see Table 8.6-1, Table 8.6-1 and Table 8.6-2 below.

Table 8.6-1 Analytical added mass coefficients

Table A-2 Analytical added mass coefficient for three-dimensional bodies in infinite fluid (far from boundaries). Added mass is $A_{ij} = \rho C_A V_R$ [kg] where V_R [m³] is reference volume


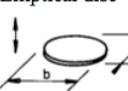
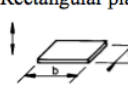
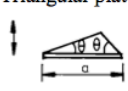
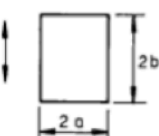
Body shape		Direction of motion	C_A				V_R
Flat plates	Circular disc 	Vertical	$2/\pi$				$\frac{4}{3} \pi a^3$
	Elliptical disc 	Vertical	b/a	C_A	b/a	C_A	$\frac{\pi}{6} a^2 b$
			∞	1.000	5.0	0.952	
			14.3	0.991	4.0	0.933	
			12.8	0.989	3.0	0.900	
10.0			0.984	2.0	0.826		
7.0			0.972	1.5	0.758		
6.0	0.964	1.0	0.637				
Rectangular plates 	Vertical	b/a	C_A	b/a	C_A	$\frac{\pi}{4} a^2 b$	
		1.00	0.579	3.17	0.840		
		1.25	0.642	4.00	0.872		
		1.50	0.690	5.00	0.897		
		1.59	0.704	6.25	0.917		
		2.00	0.757	8.00	0.934		
		2.50	0.801	10.00	0.947		
		3.00	0.830	∞	1.000		
Triangular plates 	Vertical	$\frac{1}{\pi} (\tan \theta)^{3/2}$				$\frac{a^3}{3}$	

Table 8.6-1 Determining the C_A coefficient

l/b	C_A	l/b	C_A
1.00	0.579	3.17	0.840
1.25	0.642	4.00	0.872
1.50	0.690	5.00	0.897
1.59	0.704	6.25	0.917
2.00	0.757	8.00	0.934
2.50	0.801	10.00	0.947
3.00	0.830	∞	1.000

Table 8.6-2 The added mass coefficient and formula for A_R

Table A-1 Analytical added mass coefficient for two-dimensional bodies, i.e. long cylinders in infinite fluid (far from boundaries). Added mass (per unit length) is $A_{ij} = \rho C_A A_R$ [kg/m] where A_R [m²] is the reference area

Section through body		Direction of motion	C_A	A_R	Added mass moment of inertia [(kg/m)*m ²]		
	$a/b = \infty$ $a/b = 10$ $a/b = 5$ $a/b = 2$ $a/b = 1$ $a/b = 0.5$ $a/b = 0.2$ $a/b = 0.1$	Vertical	1.0	πa^2	$\beta_1 \rho m^2$ or $\beta_2 \rho m b^2$		
			1.14		a/b	β_1	β_2
			1.21		0.1	-	0.147
			1.36		0.2	-	0.15
			1.51		0.5	-	0.15
			1.70		1.0	0.234	0.234
			1.98		2.0	0.15	-
			2.23		5.0	0.15	-
					∞	0.125	-

Appendix C - RAO Tables for the Vessels

C - 1 RAO Tables for a Ship

Three tables for are given where the RAO, heave amplitudes and roll amplitudes has been calculated for a ship that is 103m x 16m x 13.32 m. From the data program Orcaflex.

It is assumed in the calculations that it is vessels follows this table even though they are not the exact same size, see Table 8.6-1, Table 8.6-2 and Table 8.6-3.

Table 8.6-1 The displacement RAOs at 0° for a standard flat-bottom ship

Period (s)	Surge		Sway		Heave		Roll		Pitch		Yaw	
	Ampl. (m/m)	Phase (deg)	Ampl. (m/m)	Phase (deg)	Ampl. (m/m)	Phase (deg)	Ampl. (m/m)	Phase (deg)	Ampl. (m/m)	Phase (deg)	Ampl. (m/m)	Phase (deg)
0	0	360	0	0	0	360	0	0	0	0	0	0
4	0,0062	227	0	0	0,0088	226	0	0	0,0601	-140	0	0
5	0,0222	84	0	0	0,0588	116	0	0	0,235	-263,3	0	0
5,5	0,0009	-5	0	0	0,103	160	0	0	0,59	-191	0	0
6	0,0381	-54	0	0	0,113	207	0	0	1,05	-180	0	0
6,5	0,0616	-58	0	0	0,257	243	0	0	0,777	-177	0	0
7	0,028	-67	0	0	0,306	220	0	0	0,662	-112	0	0
7,5	0,0517	111	0	0	0,145	201	0	0	1,22	-92	0	0
8	0,152	106	0	0	0,0352	35,9	0	0	1,6	-90	0	0
8,5	0,254	102	0	0	0,192	17,7	0	0	1,79	-91	0	0
9	0,349	100	0	0	0,328	13,9	0	0	1,84	-91	0	0
9,5	0,433	98,4	0	0	0,443	11,6	0	0	1,82	-92	0	0
10	0,505	97,2	0	0	0,538	9,77	0	0	1,76	-92	0	0
11	0,621	95,7	0	0	0,68	7,16	0	0	1,59	-92	0	0
12	0,706	94,7	0	0	0,773	5,43	0	0	1,41	-91	0	0
13	0,768	93,9	0	0	0,835	4,27	0	0	1,25	-91	0	0
14	0,814	93,4	0	0	0,877	3,48	0	0	1,1	-91	0	0
15	0,849	93	0	0	0,906	2,91	0	0	0,975	-91	0	0
16	0,876	92,6	0	0	0,927	2,48	0	0	0,867	-91	0	0
17	0,896	92,3	0	0	0,943	2,15	0	0	0,775	-90	0	0
18	0,912	92,1	0	0	0,954	1,89	0	0	0,696	-90	0	0
19	0,925	91,8	0	0	0,963	1,68	0	0	0,628	-90	0	0
20	0,936	91,7	0	0	0,97	1,51	0	0	0,569	-90	0	0
21	0,945	91,5	0	0	0,975	1,36	0	0	0,518	-90	0	0
22	0,953	91,4	0	0	0,979	1,23	0	0	0,473	-90	0	0
Infinity	1	90	0	0	1	0	0	0	0	0	0	0

Table 8.6-2 The displacement RAOs at 45° for a standard flat-bottom ship

Period (s)	Surge		Sway		Heave		Roll		Pitch		Yaw	
	Ampl. (m/m)	Phase (deg)	Ampl. (m/m)	Phase (deg)	Ampl. (m/m)	Phase (deg)	Ampl. (m/m)	Phase (deg)	Ampl. (m/m)	Phase (deg)	Ampl. (m/m)	Phase (deg)
0	0	360	0	360	0	0	0	0	0	-360	0	0
4	0,0159	399,4	0,0106	386,1	0,0179	58,8	0,128	-102	0,102	-324,3	0,0563	-145
5	0,0351	231	0,0265	268	0,0632	228	0,228	53,1	0,41	-158	0,144	6,96
5,5	0,0482	231	0,0643	268	0,16	268	0,574	88,6	0,437	-114	0,0468	-55
6	0,0486	193	0,0551	245	0,285	264	0,783	93,8	0,995	-65	0,275	-153
6,5	0,0881	137	0,0491	165	0,238	218	0,747	95,1	1,88	-69	0,543	-165
7	0,16	116	0,115	120	0,185	79	0,401	105	2,27	-80	0,717	-171
7,5	0,233	107	0,188	107	0,392	31	0,5	210	2,24	-86	0,814	-173
8	0,299	102	0,249	102	0,525	17,8	1,7	212	2,11	-89	0,854	-175
8,5	0,356	99	0,309	103	0,619	12,3	3,36	186	1,96	-91	0,855	-175
9	0,405	97,1	0,382	101	0,691	9,48	3,92	151	1,8	-92	0,843	-175
9,5	0,444	95,9	0,433	97,8	0,749	7,72	3,32	128	1,65	-92	0,826	-175
10	0,478	95	0,469	95,9	0,794	6,47	2,7	117	1,51	-92	0,796	-176
11	0,53	94	0,523	94,1	0,86	4,75	1,93	107	1,28	-92	0,721	-177
12	0,568	93,3	0,561	93,2	0,901	3,64	1,49	102	1,09	-91	0,642	-177
13	0,595	92,8	0,59	92,6	0,929	2,9	1,2	99,9	0,937	-91	0,57	-178
14	0,616	92,4	0,611	92,2	0,947	2,38	0,995	98,4	0,814	-91	0,506	-178
15	0,632	92,1	0,628	91,9	0,96	2,01	0,843	97,3	0,713	-91	0,451	-178
16	0,644	91,9	0,64	91,7	0,969	1,72	0,725	96,5	0,629	-91	0,403	-179
17	0,653	91,6	0,65	91,5	0,975	1,5	0,631	95,9	0,559	-90	0,361	-179
18	0,661	91,5	0,658	91,3	0,98	1,32	0,555	95,4	0,5	-90	0,326	-179
19	0,667	91,3	0,665	91,2	0,984	1,18	0,493	95	0,45	-90	0,295	-179
20	0,672	91,2	0,67	91,1	0,987	1,06	0,44	94,7	0,406	-90	0,268	-179
21	0,677	91,1	0,675	91	0,989	0,96	0,396	94,4	0,369	-90	0,245	-179
22	0,681	91	0,679	90,9	0,991	0,87	0,359	94,1	0,337	-90	0,225	-179
Infinity	0,707106781	90	0,707106781	90	1	0	0	0	0	0	0	0

Table 8.6-3 The displacement RAOs at 90° for a standard flat-bottom ship

Period (s)	Surge		Sway		Heave		Roll		Pitch		Yaw	
	Ampl. (m/m)	Phase (deg)	Ampl. (m/m)	Phase (deg)	Ampl. (m/m)	Phase (deg)	Ampl. (m/m)	Phase (deg)	Ampl. (m/m)	Phase (deg)	Ampl. (m/m)	Phase (deg)
0	0	360	0	360	0	0	0	360	0	360	0	0
4	0,0087	361,02	0,221	50,2	0,0703	61,3	0,281	229	0,0897	438,8	0,0205	148
5	0,0203	343	0,387	71,7	0,284	95,3	0,788	247	0,284	438,3	0,0196	117
5,5	0,035	321	0,457	77	0,54	94,8	1,18	248	0,541	419,9	0,0216	105
6	0,0547	276	0,518	80,8	0,933	84,2	1,68	250	0,969	377,4	0,0221	95,4
6,5	0,053	219	0,571	83,4	1,49	65,4	2,37	249	1,09	317	0,0244	91,6
7	0,0345	173	0,611	85,2	1,75	35,5	3,35	245	0,718	264	0,0297	85,1
7,5	0,0194	144	0,638	87	1,56	17	4,85	237	0,391	233	0,0376	74
8	0,0112	126	0,656	89,9	1,37	8,85	7,19	222	0,228	217	0,0492	55,8
8,5	0,0065	115	0,7	94,7	1,26	5,01	9,89	192	0,143	206	0,0601	24,1
9	0,0039	110	0,79	95,3	1,19	3,05	9,45	155	0,0954	199	0,0515	-14
9,5	0,0023	110	0,837	93	1,14	1,93	7,03	132	0,0662	193	0,0348	-39
10	0,0015	119	0,857	91,6	1,1	1,27	5,24	120	0,0476	190	0,0238	-52
11	0,0009	148	0,88	90,6	1,06	0,59	3,34	109	0,0267	185	0,0132	-63
12	0,0008	166	0,897	90,3	1,04	0,29	2,42	104	0,0164	183	0,0085	-69
13	0,0008	174	0,912	90,2	1,03	0,15	1,87	101	0,0108	182	0,006	-72
14	0,0007	177	0,924	90,1	1,02	0,08	1,51	99,2	0,0074	181	0,0045	-74
15	0,0007	178	0,933	90,1	1,01	0,05	1,26	98	0,0053	181	0,0035	-75
16	0,0007	179	0,941	90,1	1,01	0,03	1,07	97	0,0039	180	0,0028	-76
17	0,0006	179	0,948	90	1,01	0,02	0,922	96,3	0,0029	180	0,0023	-77
18	0,0006	180	0,954	90	1,01	0,01	0,805	95,8	0,0023	180	0,0019	-78
19	0,0006	180	0,958	90	1,01	0,01	0,711	95,3	0,0018	180	0,0016	-78
20	0,0005	180	0,963	90	1	0,01	0,633	94,9	0,0014	180	0,0014	-79
21	0,0005	180	0,967	90	1	0	0,568	94,6	0,0011	180	0,0012	-79
22	0,0005	180	0,971	90	1	0	0,513	94,3	0,0009	180	0,0011	-80
Infinity	6,12E-17	90	1	90	1	0	0	0	0	0	0	0

C – 2 RAO Tables for a Semi-submersible

Three tables for are given where the RAO, heave amplitudes and roll amplitudes has been calculated from the program Orcaflex for a semi-submersible rig with a pontoon with the given dimensions below:

Semi-Submersible Dimensions for the calculated RAO

- Length of work deck: 109.73m
- Breadth of deck: 88.392m
- Height of deck: 19.812m
- Length of pontoons: 85.344m
- Breadth of Pontoons: 76.2m
- Height of pontoons: 7.925mm
- Length of column: 15.24m
- Breadth of column: 15.24m
- Height of column: 53.04m

The values for the RAO for that semi-submersible are shown in for 0°, 45° and 90° respectively, see Table 8.6-2, Table 8.6-1 and Table 8.6-2.

Table 8.6-4 Displacement RAO at 0° for a standard semi-submersible

Period (s)	Surge		Sway		Heave		Roll		Pitch		Yaw	
	Ampl. (m/m)	Phase (deg)	Ampl. (m/m)	Phase (deg)	Ampl. (m/m)	Phase (deg)	Ampl. (m/m)	Phase (deg)	Ampl. (m/m)	Phase (deg)	Ampl. (m/m)	Phase (deg)
0	0	0	0	0	0	0	0	0	0	0	0	0
4	0,063	267,751	0	0	0,006	12,79	0	0	0,025	-97,22	0	0
4,5	0,071	246,3289	0	0	0,001	-8,12	0	0	0,023	-117,34	0	0
5	0,079	66,4782	0	0	0,007	164,45	0	0	0,015	13,25	0	0
5,5	0,089	71,1242	0	0	0,018	-170,4	0	0	0,044	69,28	0	0
6	0,1	75,8611	0	0	0,014	-148,64	0	0	0,065	75,48	0	0
6,5	0,114	83,8805	0	0	0,01	-155,97	0	0	0,085	82,85	0	0
7	0,129	90,6374	0	0	0,011	0,81	0	0	0,116	90,69	0	0
7,5	0,145	94,0613	0	0	0,025	-18,48	0	0	0,141	95,52	0	0
8	0,164	92,3039	0	0	0,042	-25,41	0	0	0,154	101,16	0	0
9	0,207	279,8508	0	0	0,124	-22,24	0	0	0,377	96,12	0	0
10	0,257	276,134	0	0	0,213	-12,52	0	0	0,207	95,88	0	0
11	0,314	274,4574	0	0	0,278	-5,69	0	0	0,218	90,95	0	0
12	0,376	273,6696	0	0	0,317	-2,17	0	0	0,216	91,97	0	0
13	0,441	273,2858	0	0	0,337	-0,87	0	0	0,213	91,97	0	0
14	0,508	273,0838	0	0	0,35	-0,65	0	0	0,202	88,78	0	0
15	0,575	272,9828	0	0	0,335	-1,2	0	0	0,176	90,44	0	0
16	0,641	272,9323	0	0	0,304	-2,85	0	0	0,155	88,7	0	0
17	0,703	272,9121	0	0	0,245	-7,85	0	0	0,135	87	0	0
18	0,76	272,9323	0	0	0,131	-34,33	0	0	0,108	83,28	0	0
19	0,809	272,9727	0	0	0,253	-133,61	0	0	0,078	80,03	0	0
20	0,851	273,0939	0	0	1,119	-139,27	0	0	0,056	57,99	0	0
21	0,883	273,4777	0	0	3,612	-74,17	0	0	0,061	17,07	0	0
22	0,905	273,336	0	0	2,258	-20,200	0	0	0,054	-31,54	0	0
23	0,918	273,569	0	0	1,648	-9,500	0	0	0,120	-59,35	0	0
24	0,921	274,225	0	0	1,405	-5,670	0	0	0,098	-63,50	0	0
25	0,931	274,599	0	0	0,917	-2,740	0	0	0,107	-83,42	0	0
26	0,939	275,043	0	0	0,491	4,525	0	0	0,115	-99,40	0	0
27	0,945	275,558	0	0	0,125	7,905	0	0	0,108	-111,44	0	0

Table 8.6-1 Displacement RAO at 45° for a standard semi-submersible

Period (s)	Surge		Sway		Heave		Roll		Pitch		Yaw	
	Ampl. (m/m)	Phase (deg)	Ampl. (m/m)	Phase (deg)	Ampl. (m/m)	Phase (deg)	Ampl. (m/m)	Phase (deg)	Ampl. (m/m)	Phase (deg)	Ampl. (m/m)	Phase (deg)
0	0	0	0	0	0	0	0	0	0	0	0	0
4	0,063	34,239	0,063	34,2188	0,008	-44,08	0,008	36,47	0,008	36,47	0	0
4,5	0,071	266,3067	0,071	-97,2933	0,005	170,55	0,019	-100,81	0,019	-100,81	0	0
5	0,079	255,4795	0,079	-108,1306	0,003	107,27	0,036	-109,38	0,036	-109,38	0	0
5,5	0,089	250,6214	0,089	-112,9887	0,017	136,53	0,027	-115,67	0,027	-115,67	0	0
6	0,1	258,0954	0,1	-105,5046	0,0185	164,64	0,01	-112,22	0,01	-112,22	0	0
6,5	0,114	317,2713	0,114	-46,5913	0,021	178,62	0,028	48,25	0,028	48,25	0	0
7	0,129	23,836	0,129	23,4825	0,016	9,53	0,065	56,12	0,065	56,12	0	0
7,5	0,145	46,8943	0,145	46,4802	0,018	-10,08	0,115	63,62	0,115	63,62	0	0
8	0,164	19,7253	0,164	11,9382	0,046	-15,99	0,157	75,07	0,157	75,07	0	0
9	0,207	270,5285	0,207	-93,1321	0,113	-17,72	0,196	86,35	0,196	86,35	0	0
10	0,257	273,0636	0,257	-90,5667	0,203	-10,55	0,199	91,1	0,199	91,1	0	0
11	0,314	273,4171	0,314	-90,2031	0,261	-4,91	0,199	92,55	0,199	92,55	0	0
12	0,376	273,2858	0,376	-90,3243	0,306	-1,87	0,195	90,84	0,195	90,84	0	0
13	0,441	273,1141	0,441	-90,4859	0,335	-0,74	0,184	91,24	0,184	91,24	0	0
14	0,508	272,9929	0,508	-90,6071	0,338	-0,56	0,164	92,13	0,164	92,13	0	0
15	0,575	272,9222	0,575	-90,6879	0,329	-1,09	0,151	91,19	0,151	91,19	0	0
16	0,641	272,8818	0,641	-90,7283	0,306	-2,68	0,135	88,94	0,135	88,94	0	0
17	0,703	272,8717	0,703	-90,7384	0,241	-7,39	0,114	88,84	0,114	88,84	0	0
18	0,76	272,8818	0,76	-90,7283	0,126	-33,16	0,1	85,84	0,100	85,84	0	0
19	0,809	272,9121	0,809	-90,698	0,251	-134,85	0,076	81,44	0,076	81,44	0	0
20	0,851	273,0333	0,851	-90,597	1,134	-143,45	0,051	70,5	0,051	70,5	0	0
22	0,905	273,2454	0,905	-90,4253	2,282	-19,18	0,033	-7,88	0,033	-7,88	0	0
23	0,918	273,4474	0,918	-90,3041	1,658	-8,84	0,073	-57,17	0,073	-57,17	0	0
24	0,921	274,0231	0,921	-89,9708	1,410	-5,35	0,152	-63,94	0,152	-63,94	0	0
25	0,916	275,8815	0,916	-89,1527	1,272	-3,84	0,163	-59,93	0,104	-59,93	0	0
26	0,977	275,2943	0,977	-89,3432	2,059	18,99	0,197	-115,27	0,111	-115,27	0	0
27	1,000	275,7098	1,000	-89,1119	2,283	36,18	0,232	-145,83	0,117	-145,83	0	0
28	1,000	276,1253	1,000	-88,8807	2,508	53,38	0,266	-176,39	0,124	-176,39	0	0
29	1,000	276,5409	1,000	-88,6495	2,732	70,58	0,300	-206,95	0,131	-206,95	0	0
30	1,036	276,9694	1,036	-88,4194	3,098	85,18	0,335	-237,56	0,137	-237,56	0	0
31	1,055	277,3619	1,055	-88,2008	3,399	101,42	0,302	-268,84	0,144	-268,84	0	0
32	1,074	277,7543	1,074	-87,9821	3,700	117,67	0,336	-300,13	0,151	-300,13	0	0
33	1,102	278,1648	1,102	-87,7577	4,034	133,08	0,351	-331,07	0,157	-331,07	0	0
34	1,126	278,5681	1,126	-87,5356	4,355	148,83	0,365	-362,15	0,164	-362,15	0	0

Table 8.6-2 Displacement RAO at 90° for a standard semi-submersible

Period (s)	Surge		Sway		Heave		Roll		Pitch		Yaw	
	Ampl. (m/m)	Phase (deg)	Ampl. (m/m)	Phase (deg)	Ampl. (m/m)	Phase (deg)	Ampl. (m/m)	Phase (deg)	Ampl. (m/m)	Phase (deg)	Ampl. (m/m)	Phase (deg)
0	0	0	0	0	0	0	0	0	0	0	0	0
4	0	0	0,063	-95,8692	0,008	-8,27	0,024	84,83	0	0	0	0
4,5	0	0	0,071	-117,2812	0,007	165,19	0,02	65,69	0	0	0	0
5	0	0	0,079	66,5489	0,016	-172,9	0,016	195,06	0	0	0	0
5,5	0	0	0,089	71,1242	0,008	-148,18	0,044	250,22	0	0	0	0
6	0	0	0,1	75,851	0,008	-154,82	0,061	260,89	0	0	0	0
6,5	0	0	0,114	83,8704	0,01	0,84	0,088	260,61	0	0	0	0
7	0	0	0,129	90,6172	0,021	-17,98	0,11	270,94	0	0	0	0
7,5	0	0	0,145	94,0209	0,042	-25,26	0,14	282,85	0	0	0	0
8	0	0	0,164	92,1322	0,123	-22,18	0,151	278,23	0	0	0	0
9	0	0	0,207	-83,7896	0,218	-12,65	0,173	286,34	0	0	0	0
10	0	0	0,257	-87,4963	0,274	-5,61	0,201	282,57	0	0	0	0
11	0	0	0,314	-89,1527	0,315	-2,2	0,213	278,1	0	0	0	0
12	0	0	0,376	-89,9405	0,339	-0,86	0,214	270,22	0	0	0	0
13	0	0	0,441	-90,3243	0,342	-0,67	0,206	279,17	0	0	0	0
14	0	0	0,508	-90,5263	0,331	-1,23	0,193	274,77	0	0	0	0
15	0	0	0,575	-90,6273	0,302	-2,88	0,174	275,14	0	0	0	0
16	0	0	0,641	-90,6778	0,244	-7,99	0,146	272,08	0	0	0	0
17	0	0	0,703	-90,6879	0,137	-34,61	0,126	265,32	0	0	0	0
18	0	0	0,76	-90,69	0,26	-133,55	0,11	266,87	0	0	0	0
19	0	0	0,81	-90,65	1,12	-139,42	0,08	261,82	0	0	0	0
20	0	0	0,85	-90,55	3,60	-72,31	0,04	236,14	0	0	0	0
21	0	0	0,883	-90,2132	2,261	-20,18	0,049	202,04	0	0	0	0
22	0	0	0,905	-90,3546	1,653	-9,27	0,046	152,2	0	0	0	0
23	0	0	0,918	-90,2132	1,408	-5,69	0,096	122,4	0	0	0	0
24	0	0	0,921	-89,8496	1,275	-3,98	0,18	116,6	0	0	0	0
25	0	0	0,97	-89,85	1,89	47,83	0,12	77,78	0	0	0	0
26	0	0	1,00	-89,72	1,95	73,52	0,13	48,73	0	0	0	0
27	0	0	1,03	-89,59	2,01	99,20	0,14	19,67	0	0	0	0
28	0	0	1,05	-89,47	2,07	124,89	0,15	-9,39	0	0	0	0
29	0	0	1,08	-89,34	2,13	150,57	0,17	-38,44	0	0	0	0
30	0	0	1,11	-89,21	2,19	176,26	0,18	-67,50	0	0	0	0
31	0	0	1,13	-89,08	2,25	201,95	0,19	-96,56	0	0	0	0
32	0	0	1,16	-88,95	2,31	227,63	0,20	-125,61	0	0	0	0
33	0	0	1,19	-88,83	2,37	253,32	0,22	-154,67	0	0	0	0
34	0	0	1,21	-88,70	2,43	279,00	0,23	-183,73	0	0	0	0

Appendix D – Conference in Narvik

This Master's Thesis was presented at the International Conference on Cold Climate Technology 2014 in Narvik, Norway from 26 – 28 May 2014.

D - 1 The Program of the Conference

Monday, 26 May 2014			Room: Ofofbanen
19:00	21:00	Icebreaker, poster set-up	
Tuesday, 27 May 2014			Room: Ofofbanen
08:15	08:45	Late registration, poster set-up	
08:45	09:00	Welcome	
09:00	09:40	Keynote presentation <i>Considering regionally specific challenges in the Barents Sea</i> Knut Aaneland, North Energy, Norway	
09:40	09:55	BREAK	
09:55	11:35	Wind <i>Smart gas detection and ventilation system for enclosed offshore structures</i> Qusai Al-Hamdan, Mohamad Y. Mustafa, Mohammad Awad, Bjørn Reidar Sørensen <i>Assessment of wind induced hazards on winterized offshore structures</i> Albara Mustafa, Wei Solvang, Eric Dykes, Mohamad Y. Mustafa <i>Design of a field experimental set-up for the investigation of wind shielding performance of porous panel geometries</i> Mohamad Y. Mustafa, Per-Arne Sundsbø, Yizhong Xu, Geanette Polanco <i>Analysis of air flow through porous panels and its application to weather shielding structures</i> Taoying Huang, Per-Arne Sundsbø, Mohamad Y. Mustafa, Yizhong Xu, Geanette Polanco <i>Wind Turbine's Operation in High North</i> Geanette Polanco, Muhammad Virk, Matthew Homola	
11:35	12:20	LUNCH	
12:20	13:20	Energy supply <i>Renewable Energy Integration in Remote Islanded Microgrids: Strategies and Limits</i> Marc Mueller-Stoffels, Philip Maker <i>Evaluation of Grid-Interactive Electric Thermal Storage (GETS) Heaters for Islanded Renewable Energy-Diesel Microgrids in Cold Regions</i> Richard Wies, Nicholas Janssen, Rorik Peterson <i>PV system in cold climates</i> Øystein Kleven, Hanna Persson, Dilip Chithambaranadhan	
13:20	14:00	Ice loads and forces <i>Preliminary results from 2 years of ice stress measurements in a small reservoir</i> Bård Arntsen, Irina Sæther, Chris Petrich, Ronald Andersen, Bjørnar Sand, Lennart Fransson <i>Energy efficient operations in cold climate</i> Joachim Amland, Knut Espen Solberg, Arnaud Le Breton	
14:00	14:15	BREAK	
14:15	15:55	<i>First-year ice ridge loads at Norströmsgrund lighthouse</i> Denise Sudom, Louis Poirier, Robert Frederking <i>Numerical simulation of level ice loads on Norströmsgrund lighthouse</i> Bjørnar Sand, Lennart Fransson <i>Structure and internal properties of brash ice covered ship channels</i> Victoria Bonath <i>Numerical simulations of punch shear test on ice rubble using a continuous surface cap model</i> Aniket Patil, Bjørnar Sand, Lennart Fransson <i>Properties of broken ice obtained from collision tests</i> Lennart Fransson	

10:20	10:40	Construction <i>Energy Performance of Highly Insulated Canadian Wood-Frame Wall Systems Using VIP</i> Michael Swinton, Wahid Maref, Phalguni Mukhopadhyaya, Rock Glazer, Anil Parekh	Oil Spills <i>Biofilter Plantation Technology for Oil Spill Clean-up in the Arctic Coastal Waters</i> Masoud Naseri, Abbas Barabadi, Javad Barabady, Grigorii Voskoboynikov
10:40	10:50	BREAK	
10:50	11:30	Construction <i>Performance of a low energy concrete house</i> Bård Arntsen, Ove Lorentzen <i>Low Energy Concrete Building - a case study</i> Kim Dahl, Bård Arntsen	Challenges <i>Operational challenges and experiences in the Sub-Arctic regions</i> Stig Karlstad, Trond Nilsen, Ingvild Nylund <i>Enhancing competitive competence and sustainability of manufacturers in remote high-north regions of Norway through holistic supply chain network design</i> Hao Yu, Wei Deng Solvang, Mohamad Y. Mustafa
11:30	11:50	Replacing spacers and lattice girders with CFRP Gabriel Sas, Bård Arntsen, Cosmin Daescu	
11:50	12:00	Closing session	
12:00	13:00	LUNCH	
15:55	16:10	BREAK	
16:10	16:40	Poster introduction	
16:40	17:30	Poster session with snacks (see separate program)	
17:30	18:30	ColdTech session	
19:30	22:00	DINNER	

Wednesday, 28 May 2014			Room: Ofotbanen
08:30	09:10	Keynote presentation <i>Challenges caused by cold climate when designing, constructing and operating overhead lines</i> Sonja Berlijn, Bergit Svenning, Statnett, Norway	
09:10	09:20	BREAK	
		Room: Ofotbanen	Room: Narvik
09:20	10:20	Construction <i>Innovative heating solutions for Arctic climate</i> Steinar Os <i>Artificial Thawing of Seasonally Frozen ground</i> Svein-Erik Sveen, Thanh Nguyen Hung <i>Winter Casting of Power mast Rock Foundations</i> Chris Petrich, Bård Arntsen, Irina Sæther	Icing <i>Icing and performability of Arctic offshore production facilities</i> Abbas Barabadi <i>Study of Atmospheric Ice Accretion on Structures Using CFD based Multiphase Numerical Approach</i> Muhammad Virk, Umair Mughal, Mohamad Y. Mustafa <i>Physical Techniques for Robust Measurement of Icing Parameters</i> Umair Mughal, Muhammad Virk

D - 2 The Poster Presented in the Conference

The Thesis was presented in the conference for about two minutes. After the presentation there was a poster session and for that purpose this poster was made. The poster dimensions are 200 cm x 85 cm. The PDF file for this poster has also been given on the CD in the back.

A study of the changes in freeboard, stability and motion response of ships and semi-submersible platforms due to vessel icing

Lise Eide Wold and Ove T. Gudmestad
University of Stavanger,
Norway

General information about the University of Stavanger

The University of Stavanger has been welcoming students from all over the world since it was established in 2005. It has about 2000 students and 1300 employees. The UoS is also privileged to have a number of research institutions in the University's immediate vicinity.

The University of Stavanger has established a research and educational basis in oil and gas technology that has attracted students not only from Norway, but from many other parts of the world. The two-year Master of Science Programme in Offshore Technology is designed to meet the growing demand for skilled professionals in the offshore industry.

In the MSc Marine and Subsea Technology programme, the students gain advanced knowledge about systems and operations related to marine and subsea technology. The students gain specialised insight in systems and operations by combining basic mechanical engineering subjects and marine technology.

These students also have the opportunity to learn more about the Arctic and the cold climate. There is also an opportunity for students to participate in course work at UNIS in Trondheim, or to take an elective course about Arctic technology.

Introduction

There are essentially two main categories of vessel icing: atmospheric icing and sea-spray icing. The atmospheric icing consists of freshwater and is a result from precipitation and lay upon the vessel in the shape of snow, ice-storm, snow or freezing rain. The sea-spray icing is produced by the breaking waves against the vessels hull, which is the main source of ice accumulations on offshore vessels.

It can reduce the freeboard, raise the centre of gravity and increase the rolling moment that can lead to a decrease in the vessel's stability. The vessel can capsize if there is too much ice on the deck.


Vessel icing can also cause other hazardous situations such as slippery surfaces, ice damage or deterioration of the fire and rescue equipment, communication equipment, and more.

When does it occur?
It is generated under environmental conditions with strong winds (usually 9 m/s or more), cold air temperature (generally lower than -2 °C) and low sea temperature (7°C or colder).

Where does the ice accumulate?
On ships, usually most of the ice accumulates on the bow and on the midship, which can be seen on the figure to the right. On semi-submersible platforms, the sea spray ice will typically lay upon the bracing, legs, mooring chains, mooring steel, ball and choker lines, in the splash zone from five to seven metres above the water. Under extreme conditions sea spray icing could also probably coat portions of the deck. The sea-spray icing event also often occurs together with snow, which accumulates on the horizontal surfaces of the rig casing even more problems.

Objectives

The purpose of this thesis was to reveal whether or not the realistic amount of ice accumulation on vessels could result in hazardous situations due to the decrease in freeboard and stability, with a special focus on the Barneis Sea.




Another aim of the thesis was to discover and compare the differing results from several types of vessels. Therefore four different vessels were analysed: a fishing boat, a platform supply vessel, an offshore supply vessel and a semi-submersible drilling platform.

Methods

Assumptions were made regarding where the ice probably would accumulate on the vessels, and where the maximum ice accretion would be, which is shown in the figures below. These assumptions were made by previous observations of vessel icing.

There were two types of calculations performed: (1) an analysis of a case where the maximum ice thickness of 225 mm, and a constant ice thickness of 100 mm to study the change due to icing, and (2) a parameter study to investigate the required thickness of sea-spray ice for the vessels to no longer meet the DNV's stability requirements.

The amount of ice used in the analysis was assumed to be a possible situation for the Barneis Sea, given by previous data on ice accretion on this area.



Requirements given by DNV

Parameter	The International Code of Safety for High-Speed Craft (HSC)	Default	The minimum ice thickness for ice class 1A1
Minimum freeboard height	0.100 m	0.100 m	0.100 m
Minimum freeboard height	0.100 m	0.100 m	0.100 m
Minimum freeboard height	0.100 m	0.100 m	0.100 m

The results from the freeboard, intact stability, righting arm and heeling angle from the calculations are shown in the table below.

	Lady of Grace	Viking Fighter	DrillMax Ice	West Alpha
Freeboard	0.100 m	0.100 m	0.100 m	0.100 m
Righting arm	0.010 m	0.010 m	0.010 m	0.010 m
Heeling angle	0.010 m	0.010 m	0.010 m	0.010 m

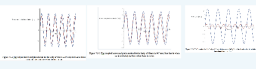
The motion response in heave, pitch and roll have been calculated for all four vessels for the purpose of discovering the impact the ice will have on the vessels motion. The roll and pitch motions were calculated for three different situations, where the waves are in the direction of 45°, 67° and 90° of the vessel. The heave motion was calculated for the roll motions, which are when the waves are in the direction of 45° and 90° of the vessel.

The calculated results of the heave and pitch translation will be at the point where the displacement is at the greatest. This means that these displacements will occur at the same time when the bow of the ship, and for the semi-submersible these displacements will occur at the two ends of the longest deck.

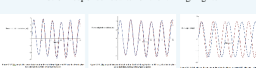
A summarization of the calculated results for the vessel motion response are shown in the table below.

	Lady of Grace	Viking Fighter	DrillMax Ice	West Alpha
Heave	0.010 m	0.010 m	0.010 m	0.010 m
Pitch	0.010 m	0.010 m	0.010 m	0.010 m
Roll	0.010 m	0.010 m	0.010 m	0.010 m

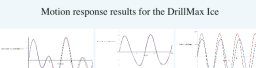
Motion response results for the Lady of Grace



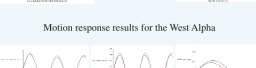
Motion response results for the Viking Fighter



Motion response results for the DrillMax Ice



Motion response results for the West Alpha



Discussion

In the parameter study, it was proven that the smallest ship, Lady of Grace, was most likely to lose its freeboard and stability. The boat needed a sea-spray ice thickness of 720 mm to lose its freeboard, and a sea-spray thickness of 100 mm to lose its stability. Note that the ice here was accounted for icing on equipment located above the platform, which will decrease the stability further. It is assumed that the boat had a ballast of 200 tons, and if it would have more than this, the stability would be better. However, if the boat had more ballast, the freeboard would be less, and could thus become the critical factor. A value of 100 mm of sea-spray ice can be considered as a possible situation that can occur in the Barneis Sea. The reason for this opinion is that there have been incidents where the total ice thickness on deck has reached as much as 100 mm.

The Viking Fighter vessel needed as much as 1.63 m of sea-spray ice and 2.95 m of sea-spray ice in order to no longer fulfil the minimum freeboard and stability requirements. These vast amounts of sea-spray ice are considered as highly unlikely to occur in the Barneis Sea, or in the Arctic.

The DrillMax Ice vessel, which is much larger than the Viking Fighter vessel, needs an amount of 11.90 m and 15 m of sea-spray ice to no longer fulfil the freeboard and stability requirements, respectively. These amounts of ice are so large that they also are considered as highly unlikely to occur.

The parameter study also revealed that the semi-submersible rig, West Alpha, needed amounts of 4.18 m and 4.47 m of sea-spray ice in order to no longer fulfil the freeboard and stability criteria, respectively. These amounts of sea-spray ice are also considered as highly unlikely to occur. However, it was calculated in the analysis that there would be a significant change in the freeboard and stability for the rig. In the analysis it was used a thickness of 90 cm on the deck, a thickness of 10 cm of ice on the deck due to atmospheric icing, and a thickness of sea-spray ice of 22.5 m on the columns and portions of the deck. The freeboard changed from 12.5 m without ice to 1.75 m with ice, which is a reduction in freeboard of 10.75 m. The stability was changed from 1.06 m with ice to 0.24 m when the ice was included, which is a reduction in stability of 0.82 m.

Conclusion

The parameter study revealed that the smallest ship, the fishing boat, was most likely to lose its freeboard and stability due to vessel icing, and that the calculated amount of ice needed in order to make the two larger ships and the semi-submersible platform was so much that such a situation is considered as highly unlikely to occur. For the fishing vessel, the amount of ice needed to make it unsafe is much less which is much more likely to occur.

If there would occur severe problems with the ballast tanks of the rig, and/or if the wind forces were extremely high, this together with the icing accumulations could contribute to a dangerous heeling angle. However, it is assumed that the icing would probably not be the sole reason for an unstable semi-submersible due to the vast amount of ice needed. A large heeling angle will, however, make operations on the semi-submersible.

The results from the motion responses revealed that when the ice load was included, the displacements were sometimes increased and sometimes decreased. All the vessels got an increased period in heave, pitch and roll with the ice accumulation, and therefore all the motions acted slower (longer roll period) when the ice load was included, especially the roll motion. Based on the results from the calculations, it was concluded as unlikely that large vessels will be lost due to a reduction in freeboard or stability from vessel icing. For small vessels, the amount of ice needed to make them unstable is much less, and therefore it is more likely to lose a small vessel because of icing.

However, other hazards could occur due to icing on any vessel as the ice can have other impacts on the vessel. Different important functions could deteriorate or be destroyed by the ice. This could also lead to a loss of the vessel, loss of lives onboard, personal injuries or loss of assets. This is the reason why it is important to use vessels that have been winterized or made to operate in cold areas when vessel icing might occur.

There are also some suggestions on further work in this area. For example, model testing of vessels in a basin can be done to study the impact of icing on the different sizes of the vessels. Different simulation programs can also be taken into use to determine the effect of icing on a vessel, and there may also be possible to study the effect under different environmental conditions. Several semi-submersible and ship can be analysed and compared. The impact of ice accumulation on other vessels can also be modelled, for example on jack-up, deep draft, hulkers, jockers, and more.

References

ANDREAS, E. L. & JONES, K. F. (2009). Technology investment and research program, safety and engineering research: sea spray icing of drilling and production platforms. Houston, NH 07755-1290: Cold Region Research and Engineering Laboratory.

DNV (2013). Ship rules – Hull Equipment and Safety, Part 3. Det Norske Veritas, Hovik, Oslo, Norway.

DNV (2013). Stability and Watertight Integrity. Technical report DNV-OS-C501. Det Norske Veritas, Hovik, Oslo, Norway.

WORLD, I. E. (2014). A study of the changes in freeboard, stability and motion response of ships and semi-submersible platforms due to vessel icing. M.Sc. Thesis, University of Stavanger.

RYBERGEN, C. C. (2009). Assessment of Superstructure Ice Protection as Applied to Offshore Oil Operations. Ice Protection Technologies, Safety Enhancements, and Development Needs, Report FRDC/CRREL/TR-09-4, Hannover, U.S.A., US Army Engineer Research and Development Center.

D-1

Appendix E – Calculations

The calculations that were conducted in Maplesoft, is given in this section. Most of the values for the parameters have been taken from the General Arrangement drawings given in Appendix A. Further the parameters used here are also shown in the figures of each vessel given in section 4.1.5.

First the case study will be shown, thereafter the calculations for the parameter study will be shown.

The first calculations presented in this section will be for the Viking Fighter vessel, which was calculated first. Thereafter the calculations for the Lady of Grace will be shown, and after that, the DrillMax Ice. Lastly, the calculations of the West Alpha will be presented.

The numbers given to the right in the grey colour are the calculated result from Maplesoft.

E - 1 Calculations of the Viking Fighter Vessel

The Case Study

The case study regards the situation when there is a storm of 15 hours with a maximum accretion of 15 mm/hr.

The assumed accumulated ice on this vessel with the different ice thicknesses is shown in Figure 4.1-16 and Figure 4.1-17. The vessels dimensions are that have been used in the calculations are also shown in those figures.

Parameters

Thickness of ice and snow:

$$t[\text{ice}] := .225 \qquad t[\text{snow}] := .300$$

Densities:

$$\rho[\text{w}] := 1025: \qquad \rho[\text{ice}] := 700 \qquad \rho[\text{snow}] := 900$$

Vessel dimensions:

$$l[\text{v}] := 74 \qquad b[\text{v}] := 18 \qquad h[\text{v}] := 7.8$$

Where $l[\text{v}]$ is the length w.l.

$$\begin{aligned} h[\text{vhouse}] &:= 23.8-19 & h[\text{topofhouse}] &:= 23.8 \\ h[\text{maindeck}] &:= 7.8 & h[\text{adeck}] &:= 10.8 & h[\text{upperdeck}] &:= 19.0 \end{aligned}$$

Lengths:

$$l[1] := 10.5 \quad l[2] := 15.4 \quad l[3] := 32.8 \quad l[4] := 23.0$$

Determining mass of vessel

In the technical drawing of the Viking Fighter, the draft is at 5.50 m. In order to do the calculation the displacement weight of the vessel will be decided by this.

$$5.50 = m[v]/(\rho[w]*l[v]*b[v]):$$

$$\text{solve}(\%, m[v]) \quad 7509150.000$$

$$m[v] := 7500*10^3$$

Freeboard

Without ice:

$$\text{draft} := m[v]/(\rho[w]*l[v]*b[v]):$$

$$f := h[v]-\text{draft} \quad 2.306701824$$

With ice:

Masses of ice and snow:

$$m[\text{upperdeck}] := \rho[\text{ice}]*t[\text{ice}]*b[v]*l[1]+\rho[\text{snow}]*t[\text{snow}]*b[v]*l[1]:$$

$$m[\text{topofhouse}] := \rho[\text{ice}]*t[\text{ice}]*b[v]*l[2]+\rho[\text{snow}]*t[\text{snow}]*b[v]*l[2]:$$

$$m[\text{vhouse}] := .5*h[\text{vhouse}]*\rho[\text{ice}]*b[v]*t[\text{ice}]:$$

$$m[\text{maindeck3}] := (1/2)*l[3]*\rho[\text{ice}]*t[\text{ice}]*(b[v]-$$

$$1.6*2)+l[3]*\rho[\text{snow}]*t[\text{snow}]*(b[v]-1.6*2)$$

$$m[\text{maindeck4}] := l[4]*\rho[\text{ice}]*t[\text{ice}]*(b[v]-1.6*2)+l[4]*\rho[\text{snow}]*t[\text{snow}]*(b[v]-$$

$$1.6*2):$$

$$m[\text{adeck3}] := (1/2)*l[3]*\rho[\text{ice}]*t[\text{ice}]*(1.6*2)+l[3]*\rho[\text{snow}]*t[\text{snow}]*(1.6*2):$$

$$m[\text{adeck4}] := l[4]*\rho[\text{ice}]*t[\text{ice}]*(1.6*2)+l[4]*\rho[\text{snow}]*t[\text{snow}]*(1.6*2):$$

$$m[\text{ice}] :=$$

$$m[\text{upperdeck}]+m[\text{topofhouse}]+m[\text{vhouse}]+m[\text{maindeck3}]+m[\text{maindeck4}]+m[\text{adeck3}]$$

$$+m[\text{adeck4}] \quad 5.889915000 \cdot 10^5$$

$$d[\text{ice}] := (m[v]+m[\text{ice}])/(\rho[w]*l[v]*b[v]) \quad 5.924698967$$

$$f[\text{ice}] := h[v]-d[\text{ice}] \quad 1.875301033$$

Initial stability, GM

Without ice:

$$\text{KB} := (1/2)*\text{draft} \quad \text{BM} := b[v]^2/(12*\text{draft}) \quad \text{KG} := (1/2)*m[v]*h[v]*(1/m[v]):$$

$$\text{GM} := \text{KB}+\text{BM}-\text{KG} \quad 3.761729088$$

With ice:

$$\text{KBice} := (1/2)*d[\text{ice}]: \quad \text{BMice} := b[v]^2/(12*d[\text{ice}]):$$

$$\text{KGice} :=$$

$$((1/2)*m[v]*h[v]+m[\text{upperdeck}]*(h[\text{upperdeck}]+(t[\text{ice}]+t[\text{snow}]))*(1/2))+m[\text{topofhou}$$

$$\text{se}]*(h[\text{topofhouse}]+(t[\text{ice}]+t[\text{snow}]))*(1/2))+m[\text{vhouse}]*(h[\text{upperdeck}]+(1/2)*h[\text{vhou}$$

$$\text{se}))+m[\text{maindeck3}]*(h[\text{maindeck}]+(.5*t[\text{ice}]+t[\text{snow}]))*(1/2))+m[\text{maindeck4}]*(h[\text{main}$$

$$\text{deck}]+(t[\text{ice}]+t[\text{snow}]))*(1/2))+m[\text{adeck3}]*(h[\text{adeck}]+(.5*t[\text{ice}]+t[\text{snow}]))*(1/2))+m[\text{a}$$

$$\text{deck4}*(h[\text{adeck}]+(t[\text{ice}]+t[\text{snow}]))*(1/2)))/(m[v]+m[\text{ice}]):$$

$$\text{GMice} := \text{KBice}+\text{BMice}-\text{KGice} \quad 2.935152431$$

Minimum righting arm

$$\phi[\text{max}] := \text{evalf}((1/180)*(30*3.1416))$$

Without ice:

$$GZ[\max] := GM*\sin(\phi[\max])+(1/2)*BM*\tan(\phi[\max])^2*\sin(\phi[\max])$$

2.290461718

With ice:

$$GZ[\maxice] := GMice*\sin(\phi[\max])+(1/2)*BMice*\tan(\phi[\max])^2*\sin(\phi[\max])$$

1.847348411

Motion response

The resulting motion response from the case study is shown here.

Heave added mass and period

$$g := 9.81 \quad H[s] := 7 \quad a := (1/2)*H[s] \quad k := \rho[w]*g*l[v]*b[v] \quad A[p] := l[v]*b[v]$$

The value for C_A is collected from a table from DNV for this factor of l/b value

$$\text{evalf}(l[v]/b[v]) \quad 4.111111111$$

The value for C_A for heave from the tables is then:

$$C[Aheave] := .872$$

$$V[R] := (3.1416*(1/4))*b[v]^2*l[v] \quad A[330] := \rho[w]*C[Aheave]*V[R]:$$

$$\lambda := \text{evalf}(\sqrt{A[p]}/(h[v]+\sqrt{A[p]})):$$

$$m[\text{added}] := (1+\sqrt{(1-\lambda^2)/(2*(1+\lambda^2))}))*A[330]$$

2.203631689 10⁷

Without ice:

$$T[\text{heave}] := \text{evalf}(2*\text{Pi}*\sqrt{(m[v]+m[\text{added}])/k}) \quad 9.330598223$$

With ice:

$$T[\text{heaveice}] := \text{evalf}(2*\text{Pi}*\sqrt{(m[v]+m[\text{added}]+m[\text{ice}])/k}) \quad 9.423170962$$

From table of RAOs for heave motion a ship (see Appendix C):

At $T = 9.0$ s; 0 degrees = 0.328 , 45 degrees = 0.691, 90 degrees = 1.19

At $T = 9.5$ s; 0 degrees = 0.443 , 45 degrees = 0.749, 90 degrees = 1.14

By assuming that the RAO is linearly dependent, the exact RAO value for these situations can be found by interpolating.

Heave motion for 0 degrees

$$\text{RAO}[\text{heave}0] := .328+(.443-.328)*(T[\text{heave}]-9)/(9.5-9) \quad 0.404037591$$

$$\text{RAO}[\text{heaveice}0] := .328+(.443-.328)*(T[\text{heaveice}]-9)/(9.5-9) \quad 0.425329321$$

$$\omega[\text{heave}] := (2*3.1416)/T[\text{heave}] \quad 0.6733973374$$

$$\omega[\text{heaveice}] := (2*3.1416)/T[\text{heaveice}] \quad 0.6667819170$$

Heave motion for 45 degrees

$$\text{RAO}[\text{heave}45] := .691+(.749-.691)*(T[\text{heave}]-9)/(9.5-9) \quad 0.729349394$$

$$\text{RAO}[\text{heaveice}45] := .691+(.749-.691)*(T[\text{heaveice}]-9)/(9.5-9) \quad 0.740087832$$

$$\omega[\text{heave}] := (2*3.1416)/T[\text{heave}] \quad 0.6733973374$$

$$\omega[\text{heaveice}] := (2*3.1416)/T[\text{heaveice}] \quad 0.6667819170$$

Heave motion for 90 degrees

$$\text{RAO}[\text{heave}90] := 1.19+(1.14-1.19)*(T[\text{heave}]-9)/(9.5-9) \quad 1.156940178$$

$$\text{RAO}[\text{heaveice90}] := 1.19 + (1.14 - 1.19) * (T[\text{heaveice}] - 9) / (9.5 - 9) \quad 1.147682904$$

Pitch added mass and period

Without ice:

$$\begin{aligned} \text{BMpitch} &:= I[v]^2 / (12 * \text{draft}); & \text{GMpitch} &:= \text{KB} + \text{BMpitch} - \text{KG}; \\ \text{submerged} &:= b[v] * I[v] * \text{draft}; & \text{K[rpitch]} &:= \text{GMpitch} * \rho[w] * g * \text{submerged}; \\ \text{Inertia[rpitch]} &:= (1/12) * \rho[w] * \text{draft} * I[v]^3 * b[v]; \\ \text{omega[pitch]} &:= \sqrt{\text{K[rpitch]} / (\text{Inertia[rpitch]} + .2 * \text{Inertia[rpitch]})}; \end{aligned}$$

$$T[\text{pitch}] := (2 * 3.1416) / \text{omega[pitch]} \quad 5.186681402$$

With ice:

$$\begin{aligned} \text{BMpitchice} &:= I[v]^2 / (12 * d[\text{ice}]); & \text{GMpitchice} &:= \text{KBice} + \text{BMpitchice} - \text{KGice}; \\ \text{submergedice} &:= b[v] * I[v] * d[\text{ice}]; \\ \text{K[rpitchice]} &:= \text{GMpitchice} * \rho[w] * g * \text{submergedice}; \\ \text{Inertia[rpitchice]} &:= (1/12) * \rho[w] * d[\text{ice}] * I[v]^3 * b[v]; \\ \text{omega[pitchice]} &:= \sqrt{\text{K[rpitchice]} / (\text{Inertia[rpitchice]} + .2 * \text{Inertia[rpitchice]})}; \end{aligned}$$

$$T[\text{pitchice}] := (2 * 3.1416) / \text{omega[pitchice]} \quad 5.406198365$$

From the RAO table of pitch angles for a ship (Appendix C):

$$\begin{aligned} \text{At } T = 5.0 \text{ s:} & \quad 0 \text{ degrees} = 0.235, \quad 45 \text{ degrees} = 0.41, \quad 90 \text{ degrees} = 0.284 \\ \text{At } T = 5.5 \text{ s:} & \quad 0 \text{ degrees} = 0.59, \quad 45 \text{ degrees} = 0.437, \quad 90 \text{ degrees} = 0.541 \end{aligned}$$

Pitch motion at 0 degrees

$$\begin{aligned} \text{pitchangle0} &:= .235 + (.59 - .235) * (T[\text{pitch}] - 5) / (5.5 - 5); \\ \text{phi[pitch0]} &:= \text{evalf}(3.1416 * \text{pitchangle0} * (1/180)); \end{aligned}$$

$$\begin{aligned} \text{pitchangleice0} &:= .235 + (.59 - .235) * (T[\text{pitchice}] - 5) / (5.5 - 5); \\ \text{phi[pitchice0]} &:= \text{evalf}(3.1416 * \text{pitchangleice0} * (1/180)); \end{aligned}$$

Pitch motion for 45 degrees

$$\begin{aligned} \text{pitchangle45} &:= .41 + (.437 - .41) * (T[\text{pitch}] - 5) / (5.5 - 5); \\ \text{phi[pitch45]} &:= \text{evalf}(3.1416 * \text{pitchangle45} * (1/180)); \end{aligned}$$

$$\begin{aligned} \text{pitchangleice45} &:= .41 + (.437 - .41) * (T[\text{pitchice}] - 5) / (5.5 - 5); \\ \text{phi[pitchice45]} &:= \text{evalf}(3.1416 * \text{pitchangleice45} * (1/180)); \end{aligned}$$

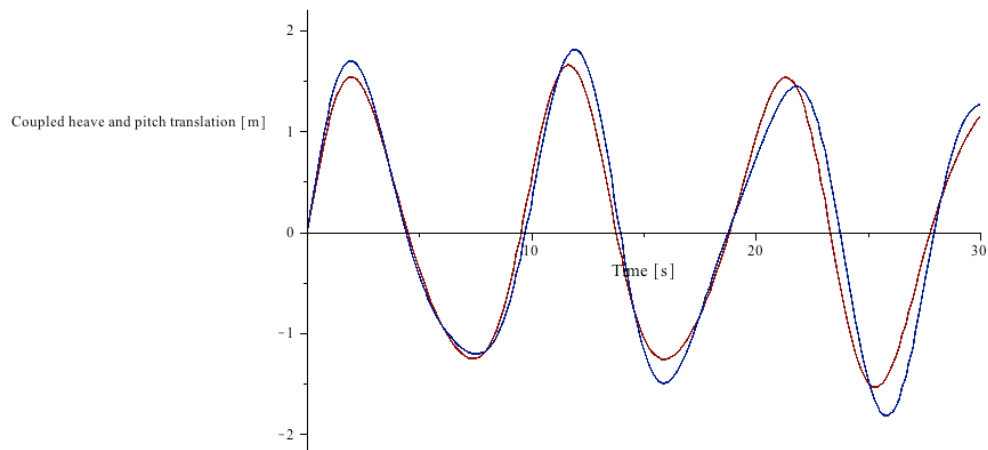
Pitch motion at 90 degrees

$$\begin{aligned} \text{pitchangle90} &:= .284 + (.541 - .284) * (T[\text{pitch}] - 5) / (5.5 - 5); \\ \text{phi[pitch90]} &:= \text{evalf}(3.1416 * \text{pitchangle90} * (1/180)); \end{aligned}$$

$$\begin{aligned} \text{pitchangleice90} &:= .284 + (.541 - .284) * (T[\text{pitchice}] - 5) / (5.5 - 5); \\ \text{phi[pitchice90]} &:= \text{evalf}(3.1416 * \text{pitchangleice90} * (1/180)); \end{aligned}$$

Coupled heave and pitch motion for 0 degrees

$$\text{plot}([a * \text{RAO}[\text{heave0}] * \sin(\text{omega}[\text{heave}] * t) + (1/2) * I[v] * \text{phi}[\text{pitch0}] * \sin(\text{omega}[\text{pitch}] * t), a * \text{RAO}[\text{heaveice0}] * \sin(\text{omega}[\text{heaveice}] * t) + (1/2) * I[v] * \text{phi}[\text{pitchice0}] * \sin(\text{omega}[\text{pitchice}] * t)], t = 0 .. 50, y = -2.2 .. 2.2);$$



Finding the maximum heave and pitch displacement without the ice:

```
diff(a*RAO[heave0]*sin(omega[heave]*t) +
(1/2)*l[v]*phi[pitch0]*sin(omega[pitch]*t), t):
```

```
fsolve(%, t = 0 .. infinity)
```

11.66560884

```
a*RAO[heave0]*sin(omega[heave]*%) + (1/2)*l[v]*phi[pitch0]*sin(omega[pitch]*%)
1.651476354
```

Finding the maximum heave and pitch displacement with the ice:

```
diff(a*RAO[heaveice0]*sin(omega[heaveice]*t) +
(1/2)*l[v]*phi[pitchice0]*sin(omega[pitchice]*t), t):
```

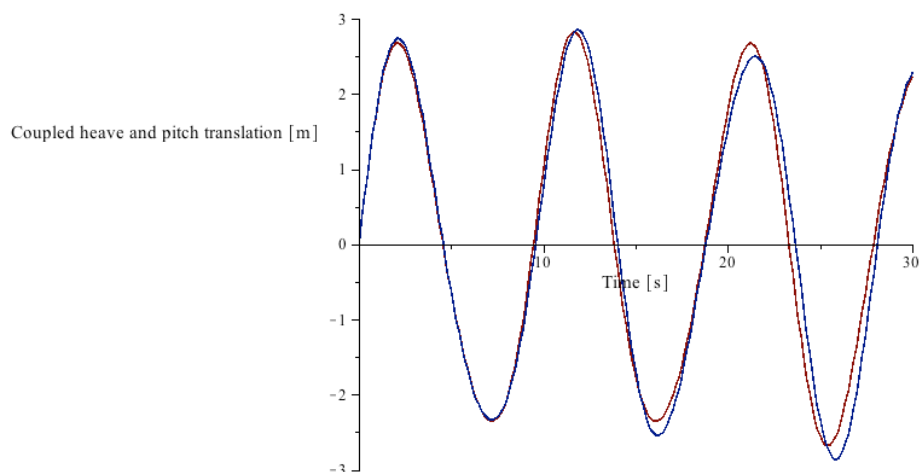
```
fsolve(%, t = 0 .. infinity)
```

11.93516374

```
a*RAO[heaveice0]*sin(omega[heaveice]*%) + (1/2)*l[v]*phi[pitchice0]*sin(omega[pitchice]*%)
1.806706106
```

Coupled heave and pitch motion for 45 degrees

```
plot([a*RAO[heave45]*sin(omega[heave]*t) + (1/2)*l[v]*phi[pitch45]*sin(omega[pitch]*t),
a*RAO[heaveice45]*sin(omega[heaveice]*t) + (1/2)*l[v]*phi[pitchice45]*sin(omega[pitchice]*t)],
t = 0 .. 50, y = -3 .. 3);
```



Finding the maximum heave and pitch displacement without the ice:

$\text{diff}(a \cdot \text{RAO}[\text{heave}45] \cdot \sin(\omega[\text{heave}] \cdot t) + (1/2) \cdot l[v] \cdot \phi[\text{pitch}45] \cdot \sin(\omega[\text{pitch}] \cdot t), t):$

$\text{fsolve}(\%, t = 0 \dots \infty)$ 11.66495690

$a \cdot \text{RAO}[\text{heave}45] \cdot \sin(\omega[\text{heave}] \cdot \%) + (1/2) \cdot l[v] \cdot \phi[\text{pitch}45] \cdot \sin(\omega[\text{pitch}] \cdot \%)$ 2.823993035

Finding the maximum heave and pitch displacement with the ice:

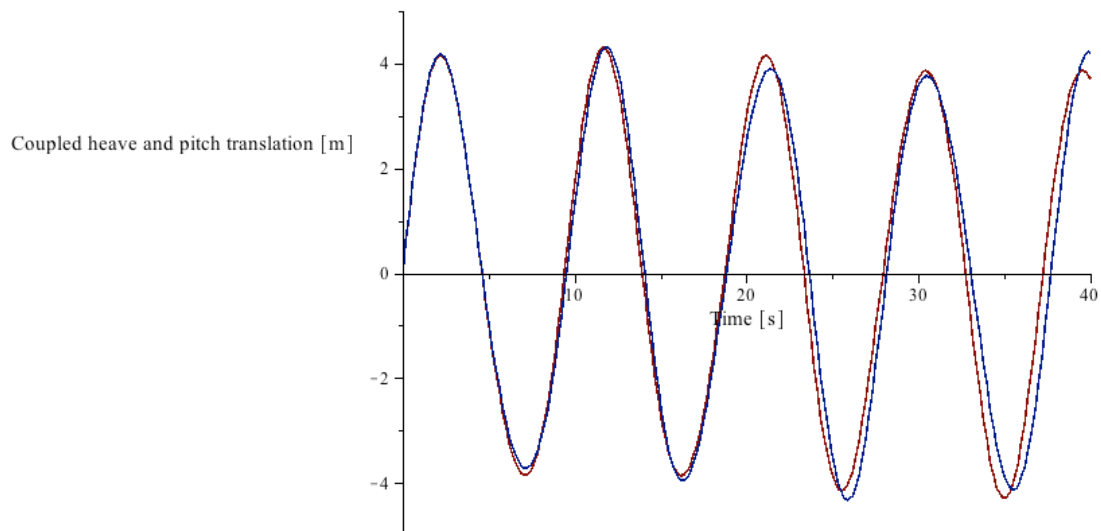
$\text{diff}(a \cdot \text{RAO}[\text{heaveice}45] \cdot \sin(\omega[\text{heaveice}] \cdot t) + (1/2) \cdot l[v] \cdot \phi[\text{pitchice}45] \cdot \sin(\omega[\text{pitchice}] \cdot t), t):$

$\text{fsolve}(\%, t = 0 \dots \infty)$ 11.87251844

$a \cdot \text{RAO}[\text{heaveice}45] \cdot \sin(\omega[\text{heaveice}] \cdot \%) + (1/2) \cdot l[v] \cdot \phi[\text{pitchice}45] \cdot \sin(\omega[\text{pitchice}] \cdot \%)$ 2.848353985

Coupled heave and pitch motion for 90 degrees

$\text{plot}([a \cdot \text{RAO}[\text{heave}90] \cdot \sin(\omega[\text{heave}] \cdot t) + (1/2) \cdot l[v] \cdot \phi[\text{pitch}90] \cdot \sin(\omega[\text{pitch}] \cdot t), a \cdot \text{RAO}[\text{heaveice}90] \cdot \sin(\omega[\text{heaveice}] \cdot t) + (1/2) \cdot l[v] \cdot \phi[\text{pitchice}90] \cdot \sin(\omega[\text{pitchice}] \cdot t)], t = 0 \dots 50, y = -5 \dots 5);$



Finding the maximum heave and pitch displacement without the ice:

$\text{diff}(a \cdot \text{RAO}[\text{heave}90] \cdot \sin(\omega[\text{heave}] \cdot t) + (1/2) \cdot l[v] \cdot \phi[\text{pitch}90] \cdot \sin(\omega[\text{pitch}] \cdot t), t):$

$\text{fsolve}(\%, t = 0 \dots \infty)$ 11.66433294

$a \cdot \text{RAO}[\text{heave}90] \cdot \sin(\omega[\text{heave}] \cdot \%) + (1/2) \cdot l[v] \cdot \phi[\text{pitch}90] \cdot \sin(\omega[\text{pitch}] \cdot \%)$ 4.294648010

Finding the maximum heave and pitch displacement with the ice:

$\text{diff}(a \cdot \text{RAO}[\text{heaveice}90] \cdot \sin(\omega[\text{heaveice}] \cdot t) + (1/2) \cdot l[v] \cdot \phi[\text{pitchice}90] \cdot \sin(\omega[\text{pitchice}] \cdot t), t):$

fsolve(%, t = 0 .. infinity) 11.85233260

a*RAO[heaveice90]*sin(omega[heaveice]*%) +
(1/2)*l[v]*phi[pitchice90]*sin(omega[pitchice]*%) 4.309669787

Roll added mass and period

Without ice:

submerged := b[v]*l[v]*draft: K[rroll] := GM*rho[w]*g*submerged:
Inertia[rroll] := (1/12)*rho[w]*draft*l[v]*b[v]^3:
omega[roll] := sqrt(K[rroll]/(Inertia[rroll]+.2*Inertia[rroll]))

T[roll] := (2*3.1416)/omega[roll] 5.887421476

With ice:

submergedice := b[v]*l[v]*d[ice]: K[rrollice] := GMice*rho[w]*g*submergedice:
Inertia[rrollice] := (1/12)*rho[w]*d[ice]*l[v]*b[v]^3:
omega[rollice] := sqrt(K[rrollice]/(Inertia[rrollice]+.2*Inertia[rrollice]]):
T[rollice] := (2*3.1416)/omega[rollice] 6.665052200

From the RAO tables for ships

At T= 5.5 s roll 45 degrees = 0.574, roll at 90 degrees = 1.18

At T= 6.0s roll 45 degrees = 0.783, roll at 90 degrees = 1.68

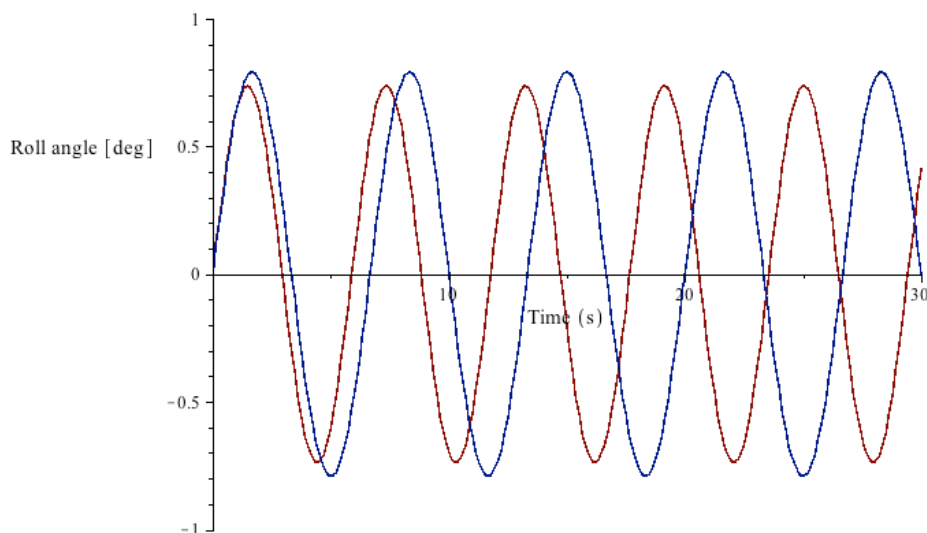
At T= 6.5s roll 45 degrees = 0.747, roll at 90 degrees = 2.37

Roll motion for 45 degrees

rollangle45 := .574+(.783-.574)*(T[roll]-5.5)/(6-5.5) 0.735942177

rollangleice45 := .783+(.747-.783)*(T[roll]-6)/(6.5-6) 0.7911056537

plot([rollangle45*sin(omega[roll]*t), rollangleice45*sin(omega[rollice]*t)], t=0 .. 30,
y = -1 .. 1)



Finding the maximum roll angle without the ice:

diff(rollangle45*sin(omega[roll]*t), t) 10.30296349

fsolve(%, t = 0 .. infinity):

rollangle45*sin(omega[roll]*%) -0.735942177

Finding the maximum roll angle without the ice:

diff(rollangleice45*sin(omega[rollice]*t), t) 11.66381408

fsolve(%, t = 0 .. infinity):

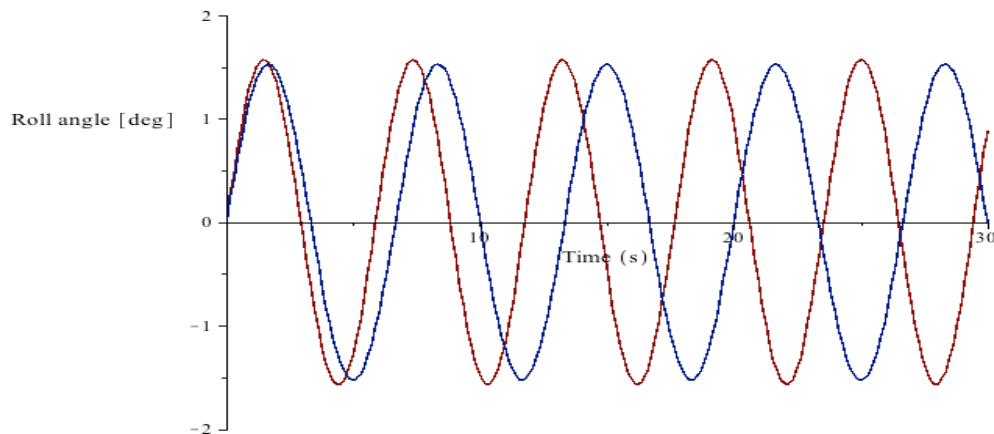
rollangleice45*sin(omega[rollice]*%) -0.7911056537

Roll motion for 90 degrees

rollangle90 := 1.18+(1.68-1.18)*(T[roll]-5.5)/(6-5.5) 1.567421476

rollangleice90 := 1.68+(2.37-1.68)*(T[roll]-6)/(6.5-6) 1.524641637

plot([rollangle90*sin(omega[roll]*t), rollangleice90*sin(omega[rollice]*t)], t=0 .. 30,
y = -2 .. 2)



Finding the maximum roll angle without the ice:

diff(rollangle90*sin(omega[roll]*t), t) 10.30296349

fsolve(%, t = 0 .. infinity):

rollangle90*sin(omega[roll]*%) -1.567421476

Finding the maximum roll angle without the ice:

diff(rollangleice90*sin(omega[rollice]*t), t) 11.66381408

fsolve(%, t = 0 .. infinity):

rollangleice90*sin(omega[rollice]*%) -1.524641637

The Parameter Study

In the parameter study the snow accumulation has been set constant at all horizontal surfaces with a value of 300 mm. The thickness of sea-spray ice is the parameter that changes.

Parametres

Thickness of snow only:

t[snow] := .300

Densities:

rho[w] := 1025: rho[ice] := 700

rho[snow] := 900

Vessel dimensions:

$$l[v] := 74 \quad b[v] := 18 \quad h[v] := 7.8$$

Where $l[v]$ is the length w.l.

$$h[vhouse] := 23.8-19 \quad h[topofhouse] := 23.8$$

$$h[maindeck] := 7.8 \quad h[adeck] := 10.8 \quad h[upperdeck] := 19.0$$

Lengths:

$$l[1] := 10.5 \quad l[2] := 15.4 \quad l[3] := 32.8 \quad l[4] := 23.0$$

Masses:

$$m[v] := 7500 \cdot 10^3$$

$$m[upperdeck] := \rho[ice] \cdot t[ice] \cdot b[v] \cdot l[1] + \rho[snow] \cdot t[snow] \cdot b[v] \cdot l[1]:$$

$$m[topofhouse] := \rho[ice] \cdot t[ice] \cdot b[v] \cdot l[2] + \rho[snow] \cdot t[snow] \cdot b[v] \cdot l[2]:$$

$$m[vhouse] := .5 \cdot h[vhouse] \cdot \rho[ice] \cdot b[v] \cdot t[ice]:$$

$$m[maindeck3] := .5 \cdot l[3] \cdot \rho[ice] \cdot t[ice] \cdot (b[v] - 1.6 \cdot 2) + l[3] \cdot \rho[snow] \cdot t[snow] \cdot (b[v] - 1.6 \cdot 2):$$

$$m[maindeck4] := l[4] \cdot \rho[ice] \cdot t[ice] \cdot (b[v] - 1.6 \cdot 2) + l[4] \cdot \rho[snow] \cdot t[snow] \cdot (b[v] - 1.6 \cdot 2):$$

$$m[adeck3] := (1/2) \cdot l[3] \cdot \rho[ice] \cdot t[ice] \cdot (1.6 \cdot 2) + l[3] \cdot \rho[snow] \cdot t[snow] \cdot (1.6 \cdot 2):$$

$$m[adeck4] := l[4] \cdot \rho[ice] \cdot t[ice] \cdot (1.6 \cdot 2) + l[4] \cdot \rho[snow] \cdot t[snow] \cdot (1.6 \cdot 2):$$

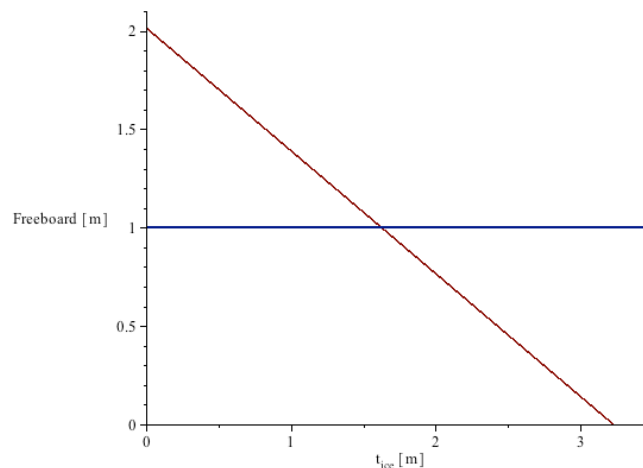
$$m[ice] := m[upperdeck] + m[topofhouse] + m[vhouse] + m[maindeck3] + m[maindeck4] + m[adeck3] + m[adeck4]:$$

Freeboard

$$d[ice] := (m[v] + m[ice]) / (\rho[w] \cdot l[v] \cdot b[v]):$$

$$f[ice] := h[v] - d[ice] \quad 2.015877829 - 0.6247857614 \cdot t[ice]$$

$$\text{plot}([f[ice], 1], t[ice] = 0 \dots 4, y = 0 \dots 2.5)$$



$$f[\text{limit}] = \text{fsolve}(2.015877829 - 0.6247857614 \cdot t[ice] = 1, t[ice] = 0 \dots 4)$$

$$1.625961876$$

Initial stability

No ice:

$$KB := (1/2) \cdot \text{draft} \quad BM := b[v]^2 / (12 \cdot \text{draft}) \quad KG := (1/2) \cdot m[v] \cdot h[v] \cdot (1/m[v]):$$

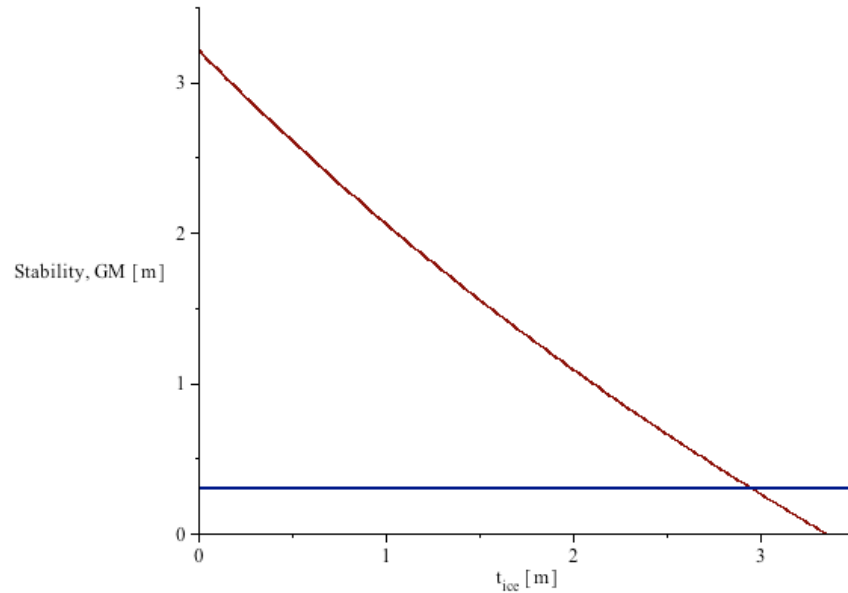
$$GM := KB + BM - KG \quad 3.761729088$$

With ice:

$$KB_{ice} := (1/2) \cdot d[ice] \quad BM_{ice} := b[v]^2 / (12 \cdot d[ice]):$$

$$KGice := ((1/2) * m[v] * h[v] + m[upperdeck] * (h[upperdeck] + (t[ice] + t[snow]) * (1/2)) + m[topofhouse] * (h[topofhouse] + (t[ice] + t[snow]) * (1/2)) + m[vhouse] * (h[upperdeck] + (1/2) * h[vhouse]) + m[maindeck3] * (h[maindeck] + (.5 * t[ice] + t[snow]) * (1/2)) + m[maindeck4] * (h[maindeck] + (t[ice] + t[snow]) * (1/2)) + m[adeck3] * (h[adeck] + (.5 * t[ice] + t[snow]) * (1/2)) + m[adeck4] * (h[adeck] + (t[ice] + t[snow]) * (1/2))) / (m[v] + m[ice]):$$

GMice := KBice + BMice - KGice: plot([GMice, .3], t[ice] = 0 .. 4, y = 0 .. 4);



GMlimit = fsolve(GMice = .3, t[ice] = 0 .. 4)

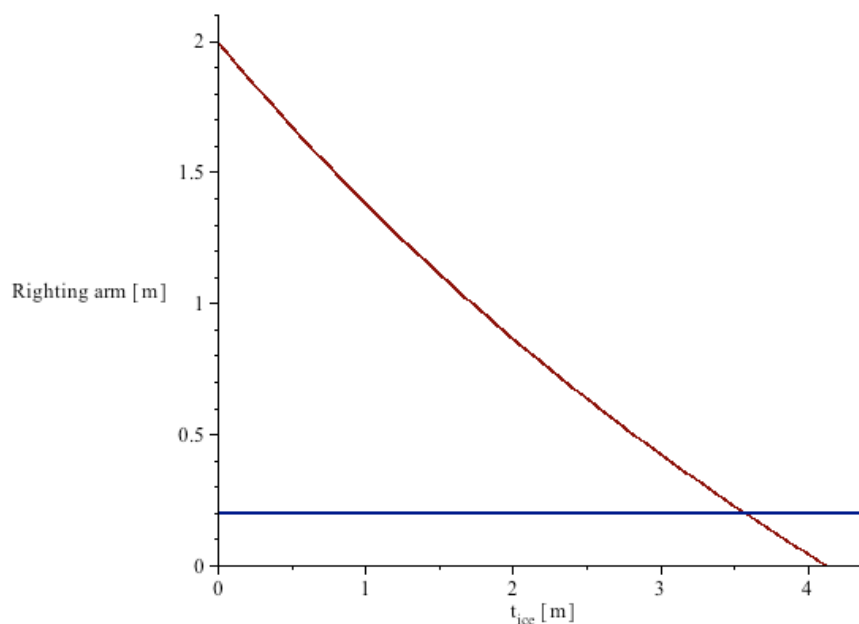
2.952089886

Minimum righting arm

phi[max] := evalf((1/180)*(30*3.1416))

GZ[maxice] := GMice * sin(phi[max]) + (1/2) * BMice * tan(phi[max])^2 * sin(phi[max]):

plot([GZ[maxice], .2], t[ice] = 0 .. 5, y = 0 .. 3);



GZ[limit] = fsolve(GZ[maxice] = .2, t[ice] = 0 .. 5)

3.573282410

E - 2 Calculations of the Lady of Grace Boat

The Case Study

The case study regards the situation when there is a storm of 15 hours with a maximum accretion of 15 mm/hour.

Parameters

Thickness of ice and snow:

$$t[\text{ice}] := .225 \quad t[\text{snow}] := .300$$

Densities:

$$\rho[\text{w}] := 1025 \quad \rho[\text{ice}] := 700 \quad \rho[\text{snow}] := 900$$

Vessel dimensions:

$$\begin{aligned} l[\text{v}] &:= 23.1 & b[\text{v}] &:= 6.70 & m[\text{v}] &:= 250 \cdot 10^3 & h[\text{v}] &:= 3.41 \\ h[1] &:= 5; & h[2] &:= 8 & h[3] &:= h[\text{v}] & h[\text{vhouse}] &:= h[2] - h[1] \\ l[1] &:= 9 & l[2] &:= 4.5 & l[3] &:= 12 \end{aligned}$$

Freeboard

No ice

$$\begin{aligned} \text{draft} &:= m[\text{v}] / (\rho[\text{w}] \cdot l[\text{v}] \cdot b[\text{v}]) && 1.575902558 \\ f &:= h[\text{v}] - \text{draft} && 1.834097442 \end{aligned}$$

With ice

$$\begin{aligned} m[1] &:= (\rho[\text{ice}] \cdot t[\text{ice}] + \rho[\text{snow}] \cdot t[\text{snow}]) \cdot l[1] \cdot b[\text{v}] && 22160.25000 \\ m[2] &:= (\rho[\text{ice}] \cdot t[\text{ice}] + \rho[\text{snow}] \cdot t[\text{snow}]) \cdot l[2] \cdot b[\text{v}] && 11080.12500 \\ m[3] &:= (\rho[\text{ice}] \cdot t[\text{ice}] + \rho[\text{snow}] \cdot t[\text{snow}]) \cdot l[3] \cdot b[\text{v}] && 29547.00000 \\ m[\text{vhouse}] &:= (\rho[\text{ice}] \cdot 0.5 \cdot t[\text{ice}]) \cdot h[\text{vhouse}] \cdot b[\text{v}] && 5803.875000 \\ m[\text{ice}] &:= \text{evalf}(m[1] + m[2] + m[3] + m[\text{vhouse}]) && 68591.25000 \end{aligned}$$

$$\begin{aligned} d[\text{ice}] &:= (m[\text{v}] + m[\text{ice}]) / (\rho[\text{w}] \cdot l[\text{v}] \cdot b[\text{v}]); && 2.008275064 \\ f[\text{ice}] &:= h[\text{v}] - d[\text{ice}]; && 1.401724936 \end{aligned}$$

Initial stability, GM

No ice

$$\begin{aligned} \text{KB} &:= (1/2) \cdot \text{draft}; & \text{BM} &:= b[\text{v}]^2 / (12 \cdot \text{draft}); & \text{KG} &:= (1/2) \cdot m[\text{v}] \cdot h[\text{v}] \cdot (1/m[\text{v}]); \\ \text{GM} &:= \text{KB} + \text{BM} - \text{KG} && 1.456723257 \end{aligned}$$

With ice

$$\text{KBice} := (1/2) \cdot d[\text{ice}]; \quad \text{BMice} := b[\text{v}]^2 / (12 \cdot d[\text{ice}]);$$

KGice :=

$$\begin{aligned} &((1/2) \cdot m[\text{v}] \cdot h[\text{v}] + m[1] \cdot (h[1] + (t[\text{ice}] + t[\text{snow}]) \cdot (1/2)) + m[2] \cdot (h[2] + (t[\text{ice}] + t[\text{snow}]) \cdot (1/2)) + m[3] \cdot (h[3] + (t[\text{ice}] + t[\text{snow}]) \cdot (1/2)) + m[\text{vhouse}] \cdot (h[1] + (h[\text{vhouse}]) \cdot (1/2))) \\ &/ (m[\text{v}] + m[\text{ice}]); \end{aligned}$$

$$\text{GMice} := \text{KBice} + \text{BMice} - \text{KGice} \quad 0.439058913$$

Minimum righting arm*No ice*

The angle of 30 degrees into radians:

$$\text{phi}[\text{max}] := \text{evalf}((1/180)*(30*3.1416));$$

$$\text{GZ}[\text{max}] := \text{GM}*\sin(\text{phi}[\text{max}])+(1/2)*\text{BM}*\tan(\text{phi}[\text{max}])^2*\sin(\text{phi}[\text{max}]);$$

0.9261790429

With ice

$$\text{GZ}[\text{maxice}] := \text{GMice}*\sin(\text{phi}[\text{max}])+(1/2)*\text{BMice}*\tan(\text{phi}[\text{max}])^2*\sin(\text{phi}[\text{max}]);$$

0.3747569330

Motion response

The resulting motion response from the case study is represented here.

Heave added mass and period

$$\begin{aligned} g &:= 9.81; & H[s] &:= 7; & a &:= (1/2)*H[s]; \\ k &:= \rho[w]*g*l[v]*b[v]; & & & A[p] &:= l[v]*b[v]; \end{aligned}$$

The value for C_A is collected from a table from DNV for this factor of l/b value:

$$\text{evalf}(l[v]/b[v]) \quad 3.447761194$$
The C_A for from the table heave will be:

$$C[\text{Aheave}] := .872;$$

$$\begin{aligned} V[R] &:= (3.1416*(1/4))*b[v]^2*l[v]; & A[330] &:= \rho[w]*C[\text{Aheave}]*V[R]; \\ \lambda &:= \text{evalf}(\sqrt{A[p]} / (h[v] + \sqrt{A[p]})); \\ m[\text{added}] &:= (1 + \sqrt{(1 - \lambda^2) / (2*(1 + \lambda^2))}) * A[330] \quad 9.78841 \cdot 10^5 \end{aligned}$$

Without ice

$$T[\text{heave}] := \text{evalf}(2*\text{Pi}*\sqrt{(m[v]+m[\text{added}])/k}) \quad 5.583261838$$

With ice

$$T[\text{heaveice}] := \text{evalf}(2*\text{Pi}*\sqrt{(m[v]+m[\text{added}]+m[\text{ice}])/k}) \quad 5.736968795$$

From table of RAOs for heave motion a ship (see Appendix C):

At $T = 5.5$ s: 0 degrees = 0.103, 45 degrees = 0.16, 90 degrees = 0.54At $T = 6.0$ s: 0 degrees = 0.113, 45 degrees = 0.285, 90 degrees = 0.933**Heave motion for 0 degrees**

$$\text{RAO}[\text{heave0}] := .103 + (.113 - .103) * (T[\text{heave}] - 5.5) / (6.0 - 5.5) \quad 0.1046652368$$

$$\text{RAO}[\text{heaveice0}] := .103 + (.113 - .103) * (T[\text{heaveice}] - 5.5) / (6.0 - 5.5) \quad 0.1077393759$$

$$\omega[\text{heave}] := (2*3.1416)/T[\text{heave}] \quad 1.125363664$$

$$\omega[\text{heaveice}] := (2*3.1416)/T[\text{heaveice}] \quad 1.095212511$$

Heave motion for 45 degrees

$$\text{RAO}[\text{heave45}] := .16 + (.285 - .16) * (T[\text{heave}] - 5.5) / (6.0 - 5.5) \quad 0.180815460$$

$$\text{RAO}[\text{heaveice45}] := .16 + (.285 - .16) * (T[\text{heaveice}] - 5.5) / (6.0 - 5.5) \quad 0.219242199$$

$$\omega[\text{heave}] := (2*3.1416)/T[\text{heave}] \quad 1.125363664$$

$$\text{omega}[\text{heaveice}] := (2*3.1416)/T[\text{heaveice}] \quad 1.095212511$$

Heave motion for 90 degrees

$$\text{RAO}[\text{heave90}] := .54+(.933-.54)*(T[\text{heave}]-5.5)/(6-5.5) \quad 0.605443805$$

$$\text{RAO}[\text{heaveice90}] := .54+(.933-.54)*(T[\text{heaveice}]-5.5)/(6-5.5) \quad 0.726257473$$

Pitch added mass and period*Without ice*

$$\begin{aligned} \text{BMpitch} &:= I[v]^2/(12*\text{draft}); & \text{GMpitch} &:= \text{KB}+\text{BMpitch}-\text{KG}; \\ \text{submerged} &:= b[v]*l[v]*\text{draft} & \text{K}[\text{rpitch}] &:= \text{GMpitch}*\rho[w]*g*\text{submerged} \\ \text{Inertia}[\text{rpitch}] &:= (1/12)*\rho[w]*\text{draft}*l[v]^3*b[v] \\ \text{omega}[\text{pitch}] &:= \text{sqrt}(\text{K}[\text{rpitch}]/(\text{Inertia}[\text{rpitch}]+.2*\text{Inertia}[\text{rpitch}])) \end{aligned}$$

$$T[\text{pitch}] := (2*3.1416)/\text{omega}[\text{pitch}] \quad 2.804633547$$

With ice

$$\begin{aligned} \text{BMpitchice} &:= I[v]^2/(12*d[\text{ice}]); & \text{GMpitchice} &:= \text{KBice}+\text{BMpitchice}-\text{KGice}; \\ \text{submergedice} &:= b[v]*l[v]*d[\text{ice}]; \\ \text{K}[\text{rpitchice}] &:= \text{GMpitchice}*\rho[w]*g*\text{submergedice}; & -1; & \text{Inertia}[\text{rpitchice}] := \\ & (1/12)*\rho[w]*d[\text{ice}]*l[v]^3*b[v]; \end{aligned}$$

$$\text{omega}[\text{pitchice}] := \text{sqrt}(\text{K}[\text{rpitchice}]/(\text{Inertia}[\text{rpitchice}]+.2*\text{Inertia}[\text{rpitchice}]))$$

$$T[\text{pitchice}] := (2*3.1416)/\text{omega}[\text{pitchice}] \quad 3.219432750$$

*From table of pitch angles for a ship (Appendix C):**At T = 4.0 s: 0 degrees = 0.0601 , 45 degrees = 0.102, 90 degrees = 0.0897.***Pitch motion at 0 degrees**

$$\text{pitchangle0} := 0.601e-1$$

$$\text{phi}[\text{pitch0}] := \text{evalf}(3.1416*\text{pitchangle0}*(1/180)) \quad 0.001048945333$$

$$\text{pitchangleice0} := 0.601e-1:$$

$$\text{phi}[\text{pitchice0}] := \text{evalf}(3.1416*\text{pitchangleice0}*(1/180)); \quad 0.001048945333$$

Pitch motion for 45 degrees

$$\text{pitchangle45} := .102$$

$$\text{phi}[\text{pitch45}] := \text{evalf}(3.1416*\text{pitchangle45}*(1/180)) \quad 0.001780240000$$

$$\text{pitchangleice45} := .102$$

$$\text{phi}[\text{pitchice45}] := \text{evalf}(3.1416*\text{pitchangleice45}*(1/180)) \quad 0.001780240000$$

Pitch motion at 90 degrees

$$\text{pitchangle90} := 0.897e-1$$

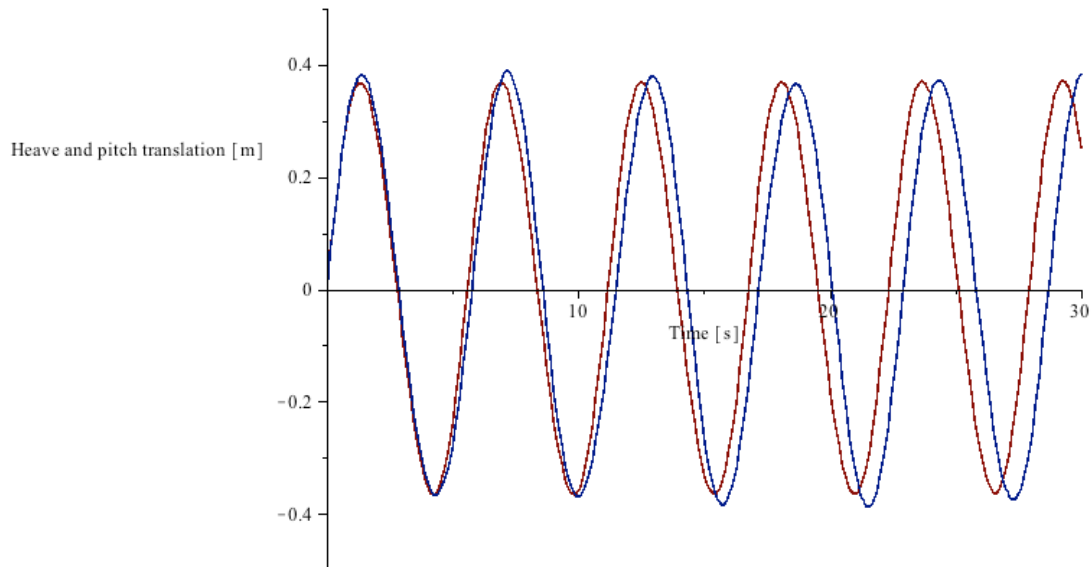
$$\text{phi}[\text{pitch90}] := \text{evalf}(3.1416*\text{pitchangle90}*(1/180)) \quad 0.001565564000$$

$$\text{pitchangleice90} := 0.897e-1$$

$$\text{phi}[\text{pitchice90}] := \text{evalf}(3.1416*\text{pitchangleice90}*(1/180)) \quad 0.001565564000$$

Coupled heave and pitch motion for 0 degrees

```
plot([a*RAO[heave0]*sin(omega[heave]*t)+(1/2)*l[v]*phi[pitch0]*sin(omega[pitch]*t),
a*RAO[heaveice0]*sin(omega[heaveice]*t)+(1/2)*l[v]*phi[pitchice0]*sin(omega[pitchice]*t)], t = 0 .. 30, y = -.5 .. .5);
```



Finding the maximum heave and pitch displacement without the ice:

```
diff(a*RAO[heave0]*sin(omega[heave]*t)+(1/2)*l[v]*phi[pitch0]*sin(omega[pitch]*t), t)
9.829206506
```

```
fsolve(%, t = 0 .. infinity):
```

```
a*RAO[heave0]*sin(omega[heave]*%)+(1/2)*l[v]*phi[pitch0]*sin(omega[pitch]*%)
-0.3658873141
```

Finding the maximum heave and pitch displacement with the ice:

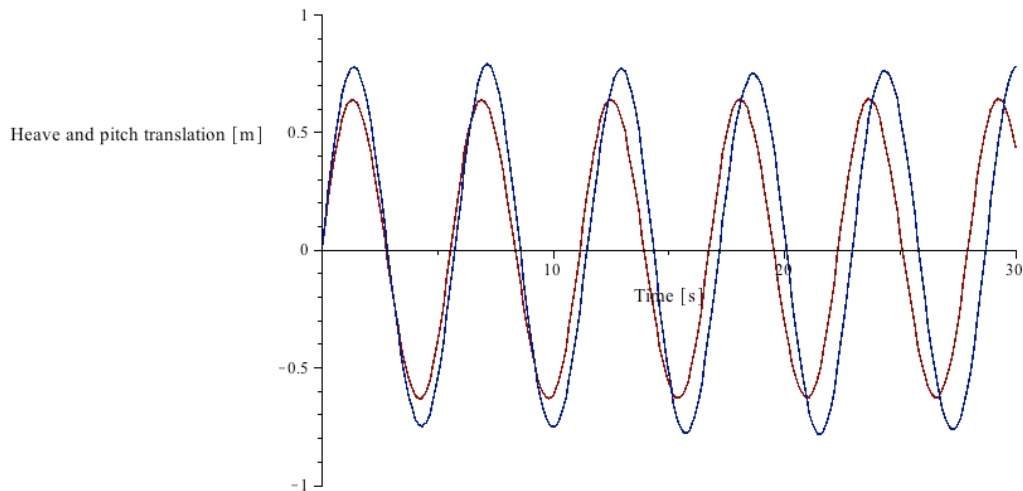
```
diff(a*RAO[heaveice0]*sin(omega[heaveice]*t)+(1/2)*l[v]*phi[pitchice0]*sin(omega[pitchice]*t), t):
```

```
fsolve(%, t = 0 .. infinity) 9.998488578
```

```
a*RAO[heaveice0]*sin(omega[heaveice]*%)+(1/2)*l[v]*phi[pitchice0]*sin(omega[pitchice]*%)
-0.3692382032
```

Coupled heave and pitch motion for 45 degrees

```
plot([a*RAO[heave45]*sin(omega[heave]*t)+(1/2)*l[v]*phi[pitch45]*sin(omega[pitch]*t),
a*RAO[heaveice45]*sin(omega[heaveice]*t)+(1/2)*l[v]*phi[pitchice45]*sin(omega[pitchice]*t)], t = 0 .. 30, y = -1 .. 1);
```



Finding the maximum heave and pitch displacement without the ice:

$\text{diff}(a*\text{RAO}[\text{heave}45]*\sin(\omega[\text{heave}]*t)+(1/2)*l[v]*\phi[\text{pitch}45]*\sin(\omega[\text{pitch}]*t), t):$

$\text{fsolve}(\%, t = 0 \dots \text{infinity})$

9.828179355

$a*\text{RAO}[\text{heave}45]*\sin(\omega[\text{heave}]*\%) + (1/2)*l[v]*\phi[\text{pitch}45]*\sin(\omega[\text{pitch}]*\%)$
 $\%$

-0.6320819232

Finding the maximum heave and pitch displacement with the ice:

$\text{diff}(a*\text{RAO}[\text{heaveice}45]*\sin(\omega[\text{heaveice}]*t)+(1/2)*l[v]*\phi[\text{pitchice}45]*\sin(\omega[\text{pitchice}]*t), t):$

$\text{fsolve}(\%, t = 0 \dots \text{infinity})$

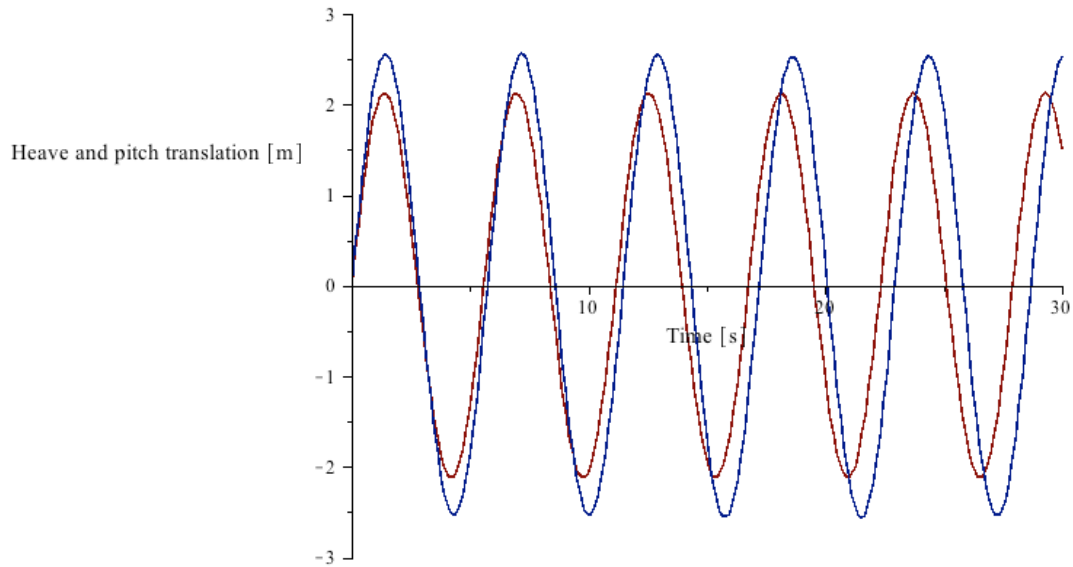
10.00571011

$a*\text{RAO}[\text{heaveice}45]*\sin(\omega[\text{heaveice}]*\%) + (1/2)*l[v]*\phi[\text{pitchice}45]*\sin(\omega[\text{pitchice}]*\%)$
 $\%$

-0.7539187317

Coupled heave and pitch motion for 90 degrees

$\text{plot}([a*\text{RAO}[\text{heave}90]*\sin(\omega[\text{heave}]*t)+(1/2)*l[v]*\phi[\text{pitch}90]*\sin(\omega[\text{pitch}]*t), a*\text{RAO}[\text{heaveice}90]*\sin(\omega[\text{heaveice}]*t)+(1/2)*l[v]*\phi[\text{pitchice}90]*\sin(\omega[\text{pitchice}]*t)], t = 0 \dots 30, y = -3 \dots 3);$



Finding the maximum heave and pitch displacement without the ice:

```
diff(a*RAO[heave90]*sin(omega[heave]*t)+(1/2)*I[v]*phi[pitch90]*sin(omega[pitch]*t), t):
```

```
fsolve(%, t = 0 .. infinity) 9.785745874
```

```
a*RAO[heave90]*sin(omega[heave]*%)+(1/2)*I[v]*phi[pitch90]*sin(omega[pitch]*%) -2.117516470
```

Finding the maximum heave and pitch displacement with the ice:

```
diff(a*RAO[heaveice90]*sin(omega[heaveice]*t)+(1/2)*I[v]*phi[pitchice90]*sin(omega[pitchice]*t), t):
```

```
fsolve(%, t = 0 .. infinity) 10.03102741
```

```
a*RAO[heaveice90]*sin(omega[heaveice]*%)+(1/2)*I[v]*phi[pitchice90]*sin(omega[pitchice]*%) -2.529762712
```

Roll added mass and period

Without ice

```
submerged := b[v]*I[v]*draft: K[rroll] := GM*rho[w]*g*submerged
```

```
Inertia[rroll] := (1/12)*rho[w]*draft*I[v]*b[v]^3:
```

```
omega[roll] := sqrt(K[rroll]/(Inertia[rroll]+.2*Inertia[rroll])):
```

```
T[roll] := (2*3.1416)/omega[roll] 3.521540246
```

With ice

```
submergedice := b[v]*I[v]*d[ice]: K[rrollice] := GMice*rho[w]*g*submergedice:
```

```
Inertia[rrollice] := (1/12)*rho[w]*d[ice]*I[v]*b[v]^3:
```

```
omega[rollice] := sqrt(K[rrollice]/(Inertia[rrollice]+.2*Inertia[rrollice])):
```

```
T[rollice] := (2*3.1416)/omega[rollice] 6.414455313
```

From RAO table

Finding the maximum roll angle without the ice:

```
diff(rollangle90*sin(omega[roll]*t), t)           9.684213033
fsolve(%, t = 0 .. infinity):
rollangle90*sin(omega[roll]*%)                   -0.281
```

Finding the maximum roll angle without the ice:

```
diff(rollangleice90*sin(omega[rollice]*t), t)     11.22527055
fsolve(%, t = 0 .. infinity):
rollangleice90*sin(omega[rollice]*%)              -2.251948332
```

The Parameter Study

In the parameter study the snow accumulation has been set constant at all horizontal surfaces with a value of 300 mm. The thickness of sea-spray ice is the parameter that changes.

Parameters

Thickness of snow only:

```
t[snow] := .300:
```

Densities:

```
rho[w] := 1025:      rho[ice] := 700:      rho[snow] := 900:
```

Vessel dimensions:

```
l[v] := 23.1:      b[v] := 6.70      m[v] := 250*10^3      h[v] := 3.41
h[1] := 5:      h[2] := 8      h[3] := h[v]
h[vhouse] := h[2]-h[1]
l[1] := 9      l[2] := 4.5      l[3] := 12
```

Freeboard

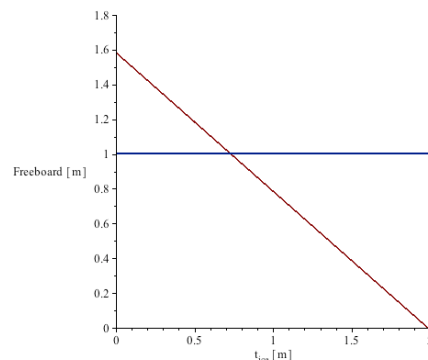
Masses of ice and snow:

```
m[1] := (rho[ice]*t[ice]+ rho[snow]*t[snow])*l[1]*b[v]:
m[2] := (rho[ice]*t[ice]+ rho[snow]*t[snow])*l[2]*b[v]:
m[3] := (rho[ice]*t[ice]+ rho[snow]*t[snow])*l[3]*b[v]:
m[vhouse] := (rho[ice]*0.5*t[ice])*h[vhouse]*b[v]:
m[ice] := evalf(m[1]+m[2]+m[3]+m[vhouse]):
```

```
d[ice] := (m[v]+m[ice])/(rho[w]*l[v]*b[v]):
```

```
f[ice] := h[v]-d[ice]:
```

```
plot([f[ice], 1], t[ice] = 0 .. 2.2, y = 0 .. 1.8);
```

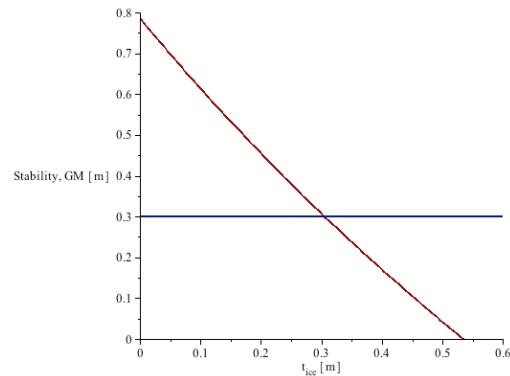


f[limit] = fsolve(f[ice] = 1, t[ice] = 0 .. 4)

0.7282720713

Initial stability, GM

```
KBice := (1/2)*d[ice]:
BMice := b[v]^2/(12*d[ice]):
KGice:=((1/2)*m[v]*h[v]+m[1]*(h[1]+(t[ice]+t[snow])*(1/2))+m[2]*(h[2]+(t[ice]+t[
snow])*(1/2))+m[3]*(h[3]+(t[ice]+t[snow])*(1/2))+m[vhouse]*(h[1]+(1/2)*h[vhouse
]))/(m[v]+m[ice]):
GMice := KBice+BMice-KGice:
plot([GMice, .3], t[ice] = 0 .. .6, y = 0 .. .8)
```



GMlimit = fsolve(GMice = .3, t[ice] = 0 .. 4)

0.3048739864

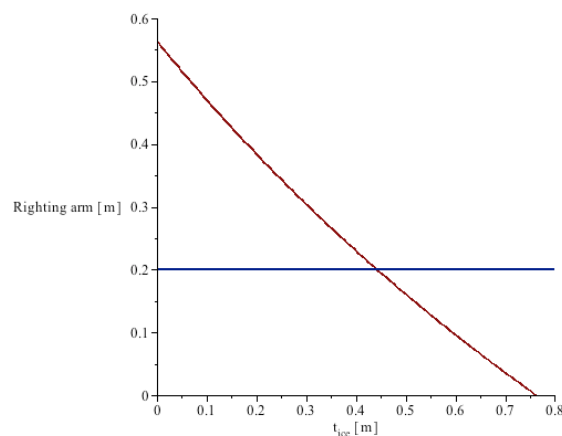
Minimum righting arm

The angle of 30 degrees into radians:

```
phi[max] := evalf((1/180)*(30*3.1416))
```

```
GZ[maxice] := GMice*sin(phi[max])+(1/2)*BMice*tan(phi[max])^2*sin(phi[max]):
```

```
plot([GZ[maxice], .2], t[ice] = 0 .. .8, y = 0 .. .6);
```



GZ[limit] = fsolve(GZ[maxice] = .2, t[ice] = 0 .. 5)

0.4426190395

E – 3 Calculations of the Drillmax Ice Vessel

The Case study

The case study regards the situation when there is a storm of 15 hours with a maximum accretion of 15 mm/hr.

Parameters

Thickness of ice and snow:

$$t[\text{ice}] := .225 \quad t[\text{snow}] := .300$$

Densities:

$$\rho[\text{w}] := 1025 \quad \rho[\text{ice}] := 700 \quad \rho[\text{snow}] := 900$$

Heights:

$$\begin{aligned} h[\text{vhouse}] &:= 24.2 & h[\text{frontdeck}] &:= 27.6 & h[\text{topofhouse}] &:= 51.8 \\ h[\text{upperdeck}] &:= 44.7 & h[\text{maindeck}] &:= 19.7 \end{aligned}$$

$$b[\text{top}] := 27.2$$

Dimensions of the vessel:

$$\begin{aligned} l[1] &:= 25.4 & l[2] &:= 23.6 & l[3] &:= 9.7 & l[4] &:= 48.4 & l[5] &:= 60.2 \\ l[6] &:= 61.0 & b[v] &:= 42.0 & h[v] &:= 19.0 & l[v] &:= 219.4 \end{aligned}$$

l[v] is the length w.l.

Determining mass of the vessel:

In the technical drawing of DrillMax Ice, the draft is at 12.00 m. In order to do the calculation the displacement weight of the vessel will be decided by this.

$$\begin{aligned} 12.0 &= m[v]/(\rho[\text{w}] * l[v] * b[v]): \\ \text{solve}(\%, m[v]) & & & 113.3420400 \cdot 10^6 \\ m[v] &:= 115 * 10^6 \end{aligned}$$

Freeboard

No ice

$$\begin{aligned} \text{draft} &:= m[v]/(\rho[\text{w}] * l[v] * b[v]) & & 12.19671006 \\ f &:= h[v] - \text{draft} & & 6.80328994 \end{aligned}$$

With ice

Masses:

$$\begin{aligned} m[\text{frontdeck}] &:= \rho[\text{ice}] * t[\text{ice}] * b[v] * l[1] + \rho[\text{snow}] * t[\text{snow}] * b[v] * l[1]: \\ m[\text{topofhouse}] &:= \rho[\text{ice}] * t[\text{ice}] * b[v] * l[2] + \rho[\text{snow}] * t[\text{snow}] * b[v] * l[2]: \\ m[\text{vhouse}] &:= .5 * h[\text{vhouse}] * \rho[\text{ice}] * b[v] * t[\text{ice}]: \\ m[\text{maindeck3}] &:= .5 * l[3] * \rho[\text{ice}] * t[\text{ice}] * b[v] + 1.0 * l[3] * \rho[\text{snow}] * t[\text{snow}] * b[v]: \\ m[\text{maindeck4}] &:= .5 * l[4] * \rho[\text{ice}] * t[\text{ice}] * (b[v] - \\ & b[\text{top}] + 1.0 * l[4] * \rho[\text{snow}] * t[\text{snow}] * (b[v] - b[\text{top}])): \\ m[\text{maindeck5}] &:= 1.0 * l[5] * (b[v] - b[\text{top}]) * \rho[\text{ice}] * t[\text{ice}] + l[5] * (b[v] - \\ & b[\text{top}]) * \rho[\text{snow}] * t[\text{snow}]: \\ m[\text{maindeck6}] &:= .5 * l[6] * \rho[\text{ice}] * t[\text{ice}] * (b[v] - b[\text{top}]) + l[6] * (b[v] - \end{aligned}$$

$$b[\text{top}] * \rho[\text{snow}] * t[\text{snow}]:$$

$$m[\text{upperdeck4}] := 1.0 * l[4] * b[\text{top}] * \rho[\text{ice}] * t[\text{ice}] + l[4] * \rho[\text{snow}] * t[\text{snow}] * b[\text{top}]:$$

$$m[\text{upperdeck5}] := .5 * l[5] * \rho[\text{ice}] * t[\text{ice}] * b[\text{top}] + l[5] * \rho[\text{snow}] * t[\text{snow}] * b[\text{top}]:$$

$$m[\text{ice}] := m[\text{frontdeck}] + m[\text{topofhouse}] + m[\text{vhouse}] + m[\text{maindeck3}] + m[\text{maindeck4}] + m[\text{maindeck5}] + m[\text{maindeck6}] + m[\text{upperdeck4}] + m[\text{upperdeck5}] \quad 3.181323150 \cdot 10^6$$

$$d[\text{ice}] := (m[\text{v}] + m[\text{ice}]) / (\rho[\text{w}] * l[\text{v}] * b[\text{v}]) \quad 12.53353018$$

$$f[\text{ice}] := h[\text{v}] - d[\text{ice}] \quad 6.46646982$$

Initial stability

No ice

$$\text{KB} := (1/2) * \text{draft} \quad \text{BM} := b[\text{v}]^2 / (12 * \text{draft}) \quad \text{KG} := (1/2) * h[\text{v}]$$

$$\text{GM} := \text{KB} + \text{BM} - \text{KG} \quad 3.762$$

With ice

$$\text{KBice} := (1/2) * d[\text{ice}]: \quad \text{BMice} := b[\text{v}]^2 / (12 * d[\text{ice}]):$$

$$\text{KGice} :=$$

$$((1/2) * m[\text{v}] * h[\text{v}] + m[\text{frontdeck}] * (h[\text{frontdeck}] + (t[\text{ice}] + t[\text{snow}]) * (1/2)) + m[\text{topofhouse}] * (h[\text{topofhouse}] + (t[\text{ice}] + t[\text{snow}]) * (1/2)) + m[\text{vhouse}] * (h[\text{frontdeck}] + (1/2) * h[\text{vhouse}]) + m[\text{maindeck3}] * (h[\text{maindeck}] + (t[\text{ice}] + t[\text{snow}]) * (1/2)) + m[\text{maindeck4}] * (h[\text{maindeck}] + (t[\text{ice}] + t[\text{snow}]) * (1/2)) + m[\text{maindeck5}] * (h[\text{maindeck}] + (t[\text{ice}] + t[\text{snow}]) * (1/2)) + m[\text{upperdeck4}] * (h[\text{upperdeck}] + (t[\text{ice}] + t[\text{snow}]) * (1/2)) + m[\text{upperdeck5}] * (h[\text{upperdeck}] + (t[\text{ice}] + t[\text{snow}]) * (1/2))) / (m[\text{v}] + m[\text{ice}]):$$

$$\text{GMice} := \text{KBice} + \text{BMice} - \text{KGice} \quad 7.86910467$$

Minimum righting arm

No ice

$$\phi[\text{max}] := \text{evalf}((1/180) * (30 * 3.1416)):$$

$$\text{GZ}[\text{max}] := \text{GM} * \sin(\phi[\text{max}]) + (1/2) * \text{BM} * \tan(\phi[\text{max}])^2 * \sin(\phi[\text{max}]) \quad 5.329778944$$

With ice

$$\text{GZ}[\text{maxice}] := \text{GMice} * \sin(\phi[\text{max}]) + (1/2) * \text{BMice} * \tan(\phi[\text{max}])^2 * \sin(\phi[\text{max}]) \quad 1.847348411$$

Motion response

The resulting motion response from the case study is shown here.

Calculating the added mass

$$g := 9.81 \quad H[\text{s}] := 7 \quad a := (1/2) * H[\text{s}] \quad k := \rho[\text{w}] * g * l[\text{v}] * b[\text{v}]$$

$$A[\text{p}] := l[\text{v}] * b[\text{v}]$$

The value for C_{A} is collected from a table from DNV for this factor of l/b value:

$$\text{evalf}(l[\text{v}]/b[\text{v}]) \quad 5.223809524$$

Interpolating between tables, the C_{A} for heave will be:

$$C[\text{Aheave}] := .897 + (.917 - .897) * (\% - 5) / (6.25 - 5) \quad 0.9005809524$$

$$V[R] := (3.1416*(1/4))*b[v]^2*l[v]; \quad A[330] := \rho[w]*C[Aheave]*V[R];$$

$$\lambda := \text{evalf}(\text{sqrt}(A[p])/(h[v]+\text{sqrt}(A[p]))):$$

$$m[\text{added}] := (1+\text{sqrt}((1-\lambda^2)/(2*(1+\lambda^2))))*A[330] \quad 3.644527494 \cdot 10^8$$

Without ice:

$$T[\text{heave}] := \text{evalf}(2*\text{Pi}*\text{sqrt}((m[v]+m[\text{added}])/k)) \quad 14.29565123$$

With ice:

$$T[\text{heaveice}] := \text{evalf}(2*\text{Pi}*\text{sqrt}((m[v]+m[\text{added}]+m[\text{ice}])/k)) \quad 14.34298123$$

From table of RAOs for heave motion of a ship:

$$\text{At } T = 14.0 \text{ s:} \quad 0 \text{ degrees} = 0.877, \quad 45 \text{ degrees} = 0.947, \quad 90 \text{ degrees} = 1.02$$

$$\text{At } T = 15.0 \text{ s:} \quad 0 \text{ degrees} = 0.906, \quad 45 \text{ degrees} = 0.96, \quad 90 \text{ degrees} = 1.01$$

Heave motion for 0 degrees

$$\text{RAO}[\text{heave}0] := .877+(.906-.877)*(T[\text{heave}]-14)/(15-14) \quad 0.8855738857$$

$$\text{RAO}[\text{heaveice}0] := .877+(.906-.877)*(T[\text{heaveice}]-14)/(15-14) \quad 0.8869464557$$

$$\omega[\text{heave}] := (2*3.1416)/T[\text{heave}] \quad 0.4395182772$$

$$\omega[\text{heaveice}] := (2*3.1416)/T[\text{heaveice}] \quad 0.4380679232$$

Heave motion for 45 degrees

$$\text{RAO}[\text{heave}45] := .947+(.96-.947)*(T[\text{heave}]-14)/(15-14) \quad 0.9508434660$$

$$\text{RAO}[\text{heaveice}45] := .947+(.96-.947)*(T[\text{heaveice}]-14)/(15-14) \quad 0.9514587560$$

$$\omega[\text{heave}] := (2*3.1416)/T[\text{heave}] \quad 0.4395182772$$

$$\omega[\text{heaveice}] := (2*3.1416)/T[\text{heaveice}] \quad 0.4380679232$$

Heave motion for 90 degrees

$$\text{RAO}[\text{heave}90] := 1.02+(1.01-1.02)*(T[\text{heave}]-14)/(15-14) \quad 1.017043488$$

$$\text{RAO}[\text{heaveice}90] := 1.02+(1.01-1.02)*(T[\text{heaveice}]-14)/(15-14) \quad 1.016570188$$

Pitch added mass and period

Without ice:

$$\text{BMpitch} := I[v]^2/(12*\text{draft}); \quad \text{GMpitch} := \text{KB}+\text{BMpitch}-\text{KG};$$

$$\text{submerged} := b[v]*l[v]*\text{draft}; \quad \text{K[rpitch]} := \text{GMpitch}*\rho[w]*g*\text{submerged};$$

$$\text{Inertia[rpitch]} := (1/12)*\rho[w]*\text{draft}*l[v]^3*b[v];$$

$$\omega[\text{pitch}] := \text{sqrt}(K[\text{rpitch}]/(\text{Inertia}[\text{rpitch}]+.2*\text{Inertia}[\text{rpitch}]));$$

$$T[\text{pitch}] := (2*3.1416)/\omega[\text{pitch}] \quad 7.714645366$$

With ice:

$$\text{BMpitchice} := I[v]^2/(12*d[\text{ice}]); \quad \text{GMpitchice} := \text{KBice}+\text{BMpitchice}-\text{KGice};$$

$$\text{submergedice} := b[v]*l[v]*d[\text{ice}]; \quad -1;$$

$$\text{K[rpitchice]} := \text{GMpitchice}*\rho[w]*g*\text{submergedice};$$

$$\text{Inertia[rpitchice]} := (1/12)*\rho[w]*d[\text{ice}]*l[v]^3*b[v];$$

$$\omega[\text{pitchice}] := \text{sqrt}(K[\text{rpitchice}]/(\text{Inertia}[\text{rpitchice}]+.2*\text{Inertia}[\text{rpitchice}]));$$

$$T[\text{pitchice}] := (2*3.1416)/\omega[\text{pitchice}] \quad 7.827231275$$

$$a*RAO[heave0]*\sin(17.35*\omega[heave])+(1/2)*l[v]*\phi[pitch0]*\sin(17.35*\omega[pitch])$$

5.667185580

Finding the maximum heave and pitch displacement with the ice:

$$\text{diff}(a*RAO[heaveice0]*\sin(\omega[heaveice]*t)+(1/2)*l[v]*\phi[pitchice0]*\sin(\omega[pitchice]*t), t):$$

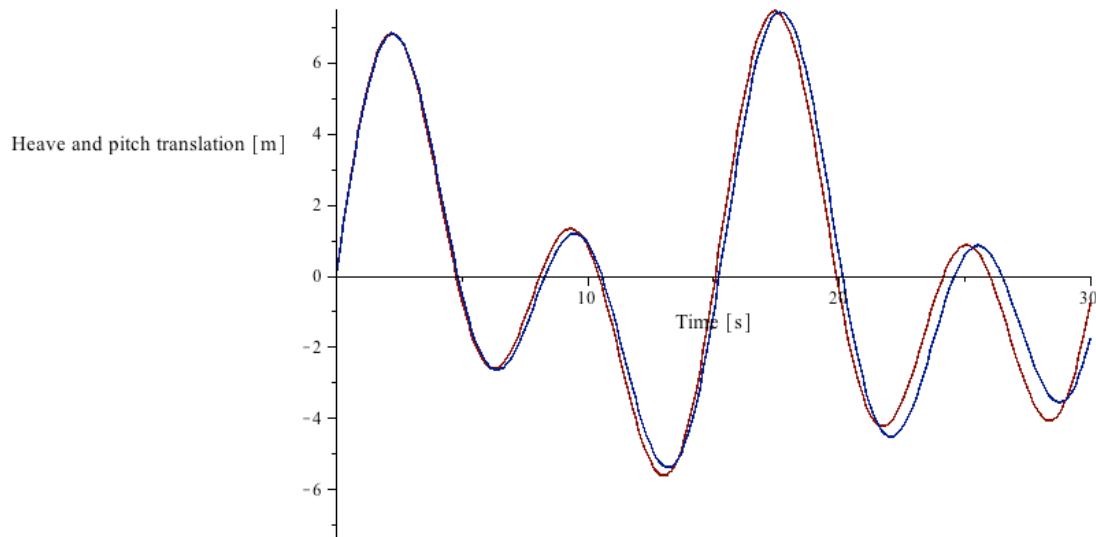
fsolve(17.85):

$$a*RAO[heaveice0]*\sin(17.85*\omega[heaveice])+(1/2)*l[v]*\phi[pitchice0]*\sin(17.85*\omega[pitchice])$$

5.862983610

Coupled heave and pitch motion for 45 degrees

plot([a*RAO[heave45]*sin(omega[heave]*t)+(1/2)*l[v]*phi[pitch45]*sin(omega[pitch]*t), a*RAO[heaveice45]*sin(omega[heaveice]*t)+(1/2)*l[v]*phi[pitchice45]*sin(omega[pitchice]*t)], t = 0 .. 50, y = -7.5 .. 7.5);



Finding the maximum heave and pitch displacement without the ice:

$$\text{diff}(a*RAO[heave45]*\sin(\omega[heave]*t)+(1/2)*l[v]*\phi[pitch45]*\sin(\omega[pitch]*t), t):$$

fsolve(%, t = 17 .. 18)

17.45381517

$$a*RAO[heave45]*\sin(\omega[heave]*t)+(1/2)*l[v]*\phi[pitch45]*\sin(\omega[pitch]*t)$$

7.441728476

Finding the maximum heave and pitch displacement with the ice:

$$\text{diff}(a*RAO[heaveice45]*\sin(\omega[heaveice]*t)+(1/2)*l[v]*\phi[pitchice45]*\sin(\omega[pitchice]*t), t):$$

fsolve(%, t = 17 .. 18)

17.67266456

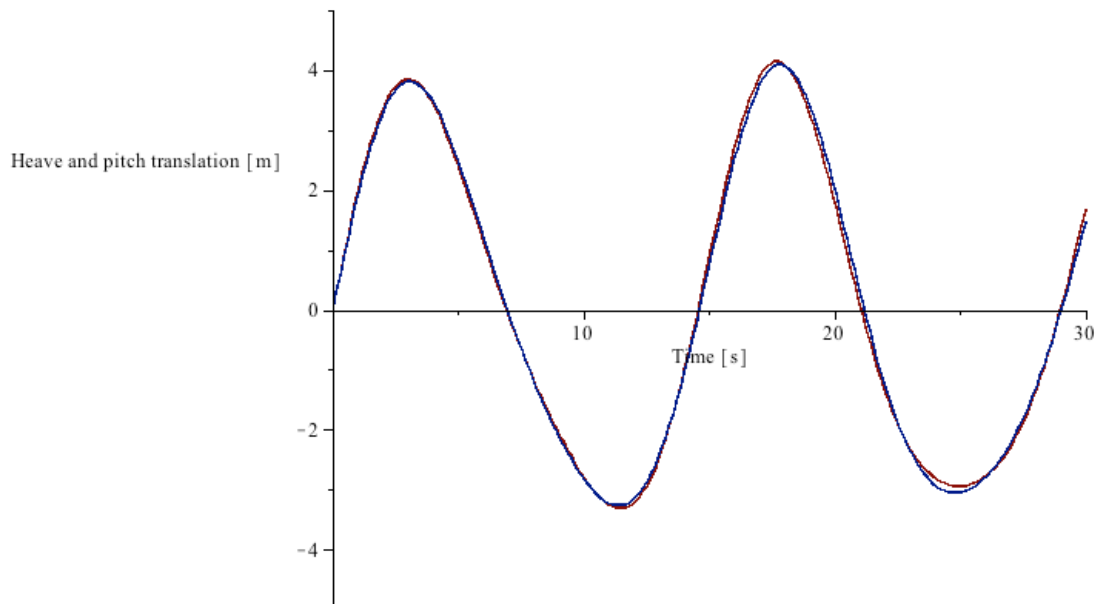
$$a*RAO[heaveice45]*\sin(\omega[heaveice]*t)+(1/2)*l[v]*\phi[pitchice45]*\sin(\omega[pitchice]*t)$$


```
[pitchice]*%)
```

7.430043022

Coupled heave and pitch motion for 90 degrees

```
plot([a*RAO[heave90]*sin(omega[heave]*t)+(1/2)*I[v]*phi[pitch90]*sin(omega[pitch]
h)*t),
a*RAO[heaveice90]*sin(omega[heaveice]*t)+(1/2)*I[v]*phi[pitchice90]*sin(omega[
pitchice]*t)], t = 0 .. 50, y = -5 .. 5);
```



Finding the maximum heave and pitch displacement without the ice:

```
diff(a*RAO[heave90]*sin(omega[heave]*t)+(1/2)*I[v]*phi[pitch90]*sin(omega[pitch]
]*t), t)
3.007572920
```

```
fsolve(%):
```

```
a*RAO[heave90]*sin(omega[heave]*%)+(1/2)*I[v]*phi[pitch90]*sin(omega[pitch]*
%)
3.842172581
```

Finding the maximum heave and pitch displacement with the ice:

```
diff(a*RAO[heaveice90]*sin(omega[heaveice]*t)+(1/2)*I[v]*phi[pitchice90]*sin(om
ega[pitchice]*t), t):
```

```
fsolve(%)
```

3.079715469

```
a*RAO[heaveice90]*sin(omega[heaveice]*%)+(1/2)*I[v]*phi[pitchice90]*sin(omega
[pitchice]*%)
3.808725335
```

Roll added mass and period

Without ice:

```
submerged := b[v]*l[v]*draft:      K[roll] := GM*rho[w]*g*submerged
```

```
Inertia[roll] := (1/12)*rho[w]*draft*l[v]*b[v]^3:
```

```
omega[roll] := sqrt(K[roll]/(Inertia[roll]+.2*Inertia[roll])):
```

$$T[\text{roll}] := (2*3.1416)/\omega[\text{roll}] \quad 9.058742163$$

With ice:

$$\text{submergedice} := b[v]*I[v]*d[\text{ice}]; \quad K[\text{rollice}] := GM_{ice}*\rho[w]*g*\text{submergedice};$$

$$\text{Inertia}[\text{rollice}] := (1/12)*\rho[w]*d[\text{ice}]*I[v]*b[v]^3;$$

$$\omega[\text{rollice}] := \sqrt{(K[\text{rollice}]/(\text{Inertia}[\text{rollice}]+.2*\text{Inertia}[\text{rollice}]))};$$

$$T[\text{rollice}] := (2*3.1416)/\omega[\text{rollice}] \quad 9.498018469$$

From RAO tables

$$\text{At } T = 9 \text{ s:} \quad \text{roll } 45 \text{ degrees} = 3.92, \text{ roll at } 90 \text{ degrees} = 9.45$$

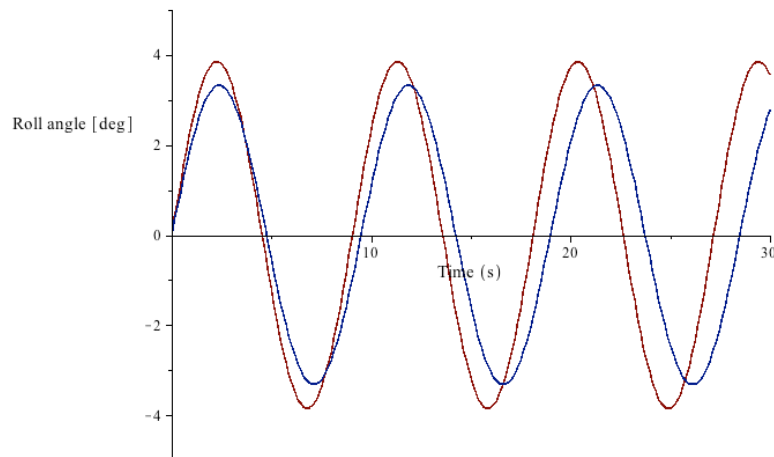
$$\text{At } T = 9.5: \quad \text{roll } 45 \text{ degrees} = 3.32, \text{ roll at } 90 \text{ degrees} = 7.03$$

Roll motion for 45 degrees

$$\text{rollangle45} := 3.92 + (3.32 - 3.92) * (T[\text{roll}] - 9) / (9.5 - 9) \quad 3.84950940$$

$$\text{rollangleice45} := 3.92 + (3.32 - 3.92) * (T[\text{rollice}] - 9) / (9.5 - 9) \quad 3.32237784$$

$$\text{plot}([\text{rollangle45}*\sin(\omega[\text{roll}]*t), \text{rollangleice45}*\sin(\omega[\text{rollice}]*t)], t = 0 \dots 30, y = -5 \dots 5)$$



Finding the maximum roll angle without the ice:

$$\text{diff}(\text{rollangle45}*\sin(\omega[\text{roll}]*t), t) \quad 11.32340122$$

$$\text{fsolve}(\%, t = 0 \dots \text{infinity}):$$

$$\text{rollangle45}*\sin(\omega[\text{roll}]*\%) \quad 3.84950940$$

Finding the maximum roll angle with the ice:

$$\text{diff}(\text{rollangleice45}*\sin(\omega[\text{rollice}]*t), t) \quad 11.87249532$$

$$\text{fsolve}(\%, t = 0 \dots \text{infinity}):$$

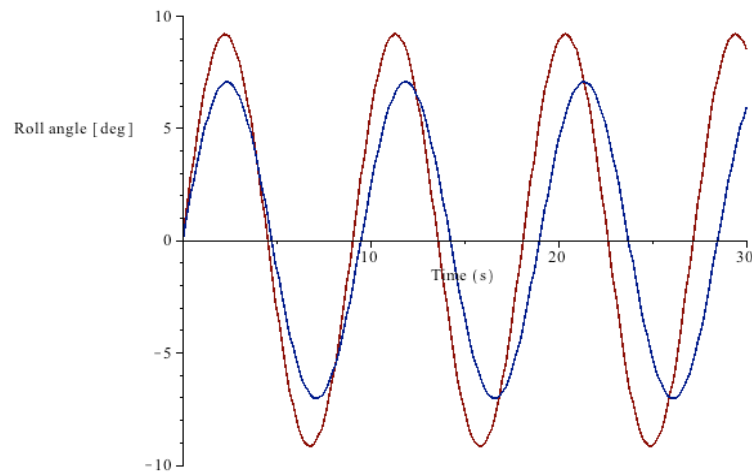
$$\text{rollangleice45}*\sin(\omega[\text{rollice}]*\%) \quad 3.32237784$$

Roll motion for 90 degrees

$$\text{rollangle90} := 9.45 + (7.03 - 9.45) * (T[\text{roll}] - 9) / (9.5 - 9) \quad 9.16568793$$

$$\text{rollangleice90} := 9.45 + (7.03 - 9.45) * (T[\text{rollice}] - 9) / (9.5 - 9) \quad 7.03959061$$

$$\text{plot}([\text{rollangle90}*\sin(\omega[\text{roll}]*t), \text{rollangleice90}*\sin(\omega[\text{rollice}]*t)], t = 0 \dots 30, y = -10 \dots 10)$$



Finding the maximum roll angle without the ice:

`diff(rollangle90*sin(omega[roll]*t), t)` 11.32340122

`fsolve(%, t = 0 .. infinity):`

`rollangle90*sin(omega[roll]*%)` 9.16568793

Finding the maximum roll angle without the ice:

`diff(rollangleice90*sin(omega[rollice]*t), t)` 11.87249532

`fsolve(%, t = 0 .. infinity)`

`rollangleice90*sin(omega[rollice]*%)` 7.03959061

The Parameter Study

In the parameter study the snow accumulation has been set constant at all horizontal surfaces with a value of 300 mm. The thickness of sea-spray ice is the parameter that changes.

Parameters

Thickness of snow only:

`t[snow] := .300`

Densities:

`rho[w] := 1025` `rho[ice] := 700` `rho[snow] := 900`

Heights:

`h[vhouse] := 24.2` `h[frontdeck] := 27.6` `h[topofhouse] := 51.8`

`h[upperdeck] := 44.7` `h[maindeck] := 19.7`

`b[top] := 27.2`

Dimensions of the vessel:

`l[1] := 25.4` `l[2] := 23.6` `l[3] := 9.7` `l[4] := 48.4` `l[5] := 60.2`

`l[6] := 61.0` `b[v] := 42.0` `h[v] := 19.0` `l[v] := 219.4`

`m[v] := 115*10^6`

Freeboard, f

Masses:

```

m[frontdeck] := rho[ice]*t[ice]*b[v]*l[1]+rho[snow]*t[snow]*b[v]*l[1]:
m[topofhouse] := rho[ice]*t[ice]*b[v]*l[2]+rho[snow]*t[snow]*b[v]*l[2]:
m[vhouse] := .5*h[vhouse]*rho[ice]*b[v]*t[ice]:
m[maindeck3] := .5*l[3]*rho[ice]*t[ice]*b[v]+1.0*l[3]*rho[snow]*t[snow]*b[v]:
m[maindeck4] := .5*l[4]*rho[ice]*t[ice]*(b[v]-
b[top])+1.0*l[4]*rho[snow]*t[snow]*(b[v]-b[top]):
m[maindeck5] := 1.0*l[5]*(b[v]-b[top])*rho[ice]*t[ice]+l[5]*(b[v]-
b[top])*rho[snow]*t[snow]:
m[maindeck6] := .5*l[6]*rho[ice]*t[ice]*(b[v]-b[top])+l[6]*(b[v]-
b[top])*rho[snow]*t[snow]:
m[upperdeck4] := 1.0*l[4]*b[top]*rho[ice]*t[ice]+l[4]*rho[snow]*t[snow]*b[top]:
m[upperdeck5] := .5*l[5]*rho[ice]*t[ice]*b[top]+l[5]*rho[snow]*t[snow]*b[top]:

m[ice] :=
m[frontdeck]+m[topofhouse]+m[vhouse]+m[maindeck3]+m[maindeck4]+m[maindeck5]+m[maindeck6]+m[upperdeck4]+m[upperdeck5];
4.623934000 10^6 t[ice] + 2.140938000 10^6

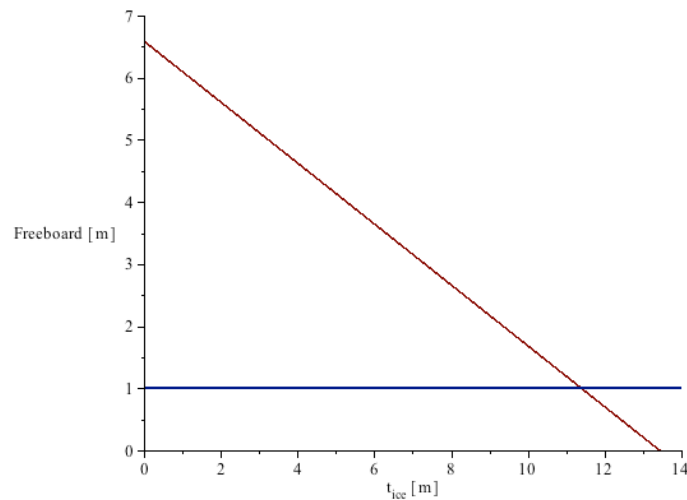
```

```

d[ice] := (m[v]+m[ice])/(rho[w]*l[v]*b[v]):
f[ice] := h[v]-d[ice]
6.57661980 - 0.4895554023 t[ice]

```

```
plot([h[v]-d[ice], 1], t[ice] = 0 .. 15, y = 0 .. 7);
```



```
f[limit] = fsolve(h[v]-d[ice] = 1, t[ice] = 0 .. 15)
11.39119244
```

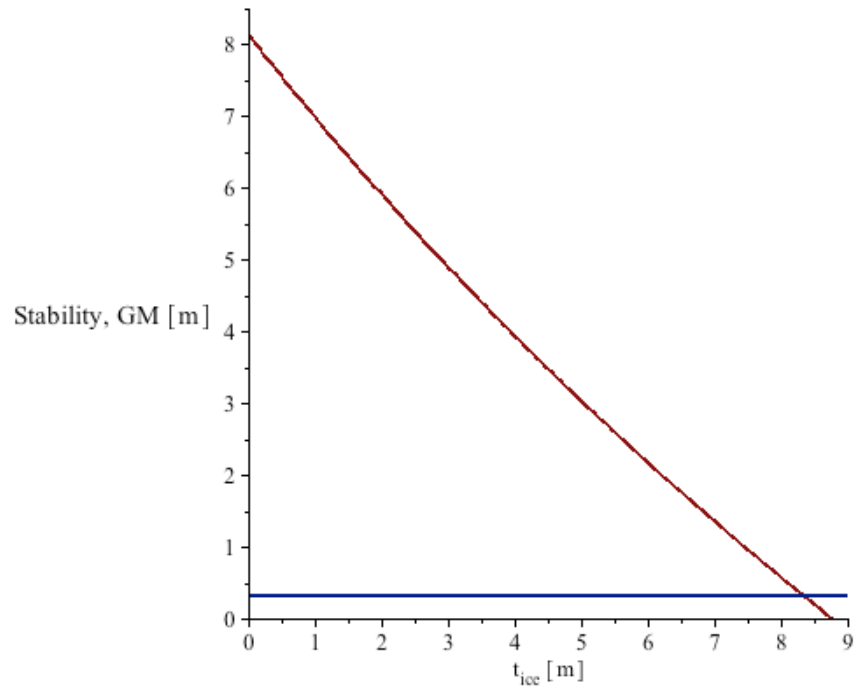
Initial stability

```

KBice := (1/2)*d[ice]:          BMice := b[v]^2/(12*d[ice]):
KGice :=
((1/2)*m[v]*h[v]+m[frontdeck]*(h[frontdeck]+(t[ice]+t[snow])*(1/2))+m[topofhouse]
*(h[topofhouse]+(t[ice]+t[snow])*(1/2))+m[vhouse]*(h[frontdeck]+(1/2)*h[vhouse])
+m[maindeck3]*(h[maindeck]+(t[ice]+t[snow])*(1/2))+m[maindeck4]*(h[maindeck]
+(t[ice]+t[snow])*(1/2))+m[maindeck5]*(h[maindeck]+(t[ice]+t[snow])*(1/2))+m[up
perdeck4]*(h[upperdeck]+(t[ice]+t[snow])*(1/2))+m[upperdeck5]*(h[upperdeck]+(t[ic
e]+t[snow])*(1/2)))/(m[v]+m[ice]):

```

GMice := KBice+BMice-KGice: plot([GMice, .3], t[ice] = 0 .. 10, y = 0 .. 8.5);



GM[limit] = fsolve(GMice = .3, t[ice] = 0 .. 14)

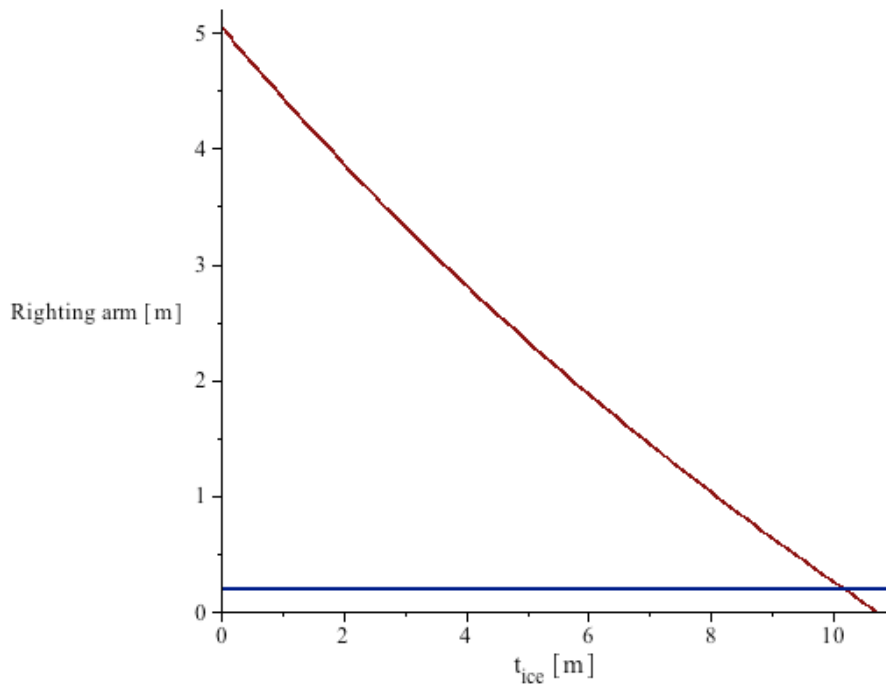
8.352735325

Minimum righting arm

phi[max] := evalf((1/180)*(30*3.1416));

GZ[maxice] := GMice*sin(phi[max])+(1/2)*BMice*tan(phi[max])^2*sin(phi[max]);

plot([GZ[maxice], .2], t[ice] = 0 .. 11, y = 0 .. 5.2)



GZ[limit] = fsolve(GZ[maxice] = .2, t[ice] = 0 .. 14)

10.16477115

E – 4 Calculations of the West Alpha Rig

The Case Study

The case study regards the situation when there is a storm of 15 hours with a maximum accretion of 15 mm/hr.

Parameters

t[snow] := .3; t[ice] := .225;
rho[w] := 1025; rho[ice] := 700; rho[snow] := 900
l[deck] := 70; b[deck] := 66

Pontoons and bracings:

l[p] := 89; b[p] := 13; h[p] := 12.5
l[b] := 44; d[b] := 6; r[b] := (1/2)*d[b]

Columns:

l[c] := 10; b[c] := 10.4

Cylindrical columns:

d[cc] := 6.5; r[cc] := (1/2)*d[cc]

Deck:

l[deck] := 70; b[deck] := 66

Heights:

h[all] := 21; h[upperdeck] := 39.5; h[derrick] := 69; b[derrick] := 14.3; t[derrick] := .4

Determining the operating mass:

By the reason that there is limited information available regarding the total displacement weight of the rig, the operating mass with the draft given on the general arrangement drawings will be calculated for further use. The drawing shows that Hc is 9 m and the draft is 21.50 m.

submb := 3.1416*l[b]*r[b]^2*2; submp := 2*l[p]*b[p]*h[p];
submwl := 9*(4*l[c]*b[c]+3.1416*r[cc]^2*2)
subm.vol := submp+submb+submwl
subm.vol = evalf(m[operating]/rho[w])
solve(%, m[operating]) 3.664830500 10^7

m[operating] := 3.665*10^7:

Masses:

Sea-spray ice:

m[cwind] := rho[ice]*((l[c]+t[ice])*(b[c]+t[ice])-l[c]*b[c]) 3248.437500
m[cnowind] := rho[ice]*((l[c]+.5*t[ice])*(b[c]+.5*t[ice])-l[c]*b[c]) 1615.359340
m[ccwind] := rho[ice]*(3.1416*(r[cc]+t[ice])^2-(3.1416*(1/4))*r[cc]^2)
20748.69720

m[ccnowind] := rho[ice]*(3.1416*(r[cc]+.5*t[ice])^2-(3.1416*(1/4))*r[cc]^2)
19057.09287

$$m[\text{deckice}] := (1/4)*b[\text{deck}]*l[\text{deck}]-2*10*t[\text{ice}]*\rho[\text{ice}] \quad 1.299375000 \cdot 10^5$$

Snow

$$m[\text{snowupperdeck}] := t[\text{snow}]*\rho[\text{snow}]*l[\text{deck}]*b[\text{deck}] \quad 1.2474000 \cdot 10^6$$

$$m[\text{icederrick}] := 1*(900*((1/2)*(14.3*69))) \quad 44401.50000$$

Total mass

$$m[\text{ice}] := 2*m[\text{cwind}]+2*m[\text{cnwind}]+m[\text{ccwind}]+m[\text{ccnowind}]+m[\text{deckice}]$$

$$1.794708838 \cdot 10^5$$

$$m[\text{snow}] := m[\text{snowupperdeck}]+4*m[\text{icederrick}]$$

$$1.425006000 \cdot 10^6$$

$$m[\text{total}] := m[\text{operating}]+m[\text{ice}]+m[\text{snow}]:$$

Freeboard

No ice

$$\text{submwl2} := h[\text{c}]*(4*l[\text{c}]*b[\text{c}]+3.1416*r[\text{cc}]^2*2)$$

$$\text{submp}+\text{submb}+\text{submwl2} = \text{evalf}(m[\text{operating}]/\rho[\text{w}])$$

$$31413.1472 + 482.3663000 h[\text{c}] = 35756.09756$$

$$\text{solve}(\%, h[\text{c}]): \quad h[\text{c}] := \%$$

$$\text{draft} := h[\text{c}]+h[\text{p}] \quad 21.50342822$$

$$\text{Freeboard} = h[\text{all}]-h[\text{c}] \quad 11.99657178$$

With ice

$$\text{submwl3} := h[\text{cice}]*(4*l[\text{c}]*b[\text{c}]+3.1416*r[\text{cc}]^2*2):$$

$$\text{subm.vol} := \text{submp}+\text{submb}+\text{submwl3} \quad 31413.1472 + 482.3663000 h[\text{cice}]$$

$$\text{submergedice} := 31413.1472+482.3663000*h[\text{cice}]:$$

$$\text{subm.vol} = m[\text{total}]/\rho[\text{w}];$$

$$\text{solve}(\%, h[\text{cice}]);$$

$$h[\text{cice}] := \% \quad 12.24856226$$

$$d[\text{ice}] := h[\text{cice}]+h[\text{p}] \quad 24.74856226$$

$$\text{Freeboard.ice} = h[\text{all}]-h[\text{cice}] \quad 8.75143774$$

Initial stability, GM

No ice

KB:

$$y[\text{p}] := (1/2)*h[\text{p}]: \quad y[\text{bracing}] := h[\text{p}]+(1/2)*d[\text{b}]: \quad y[\text{c}] := h[\text{p}]+(1/2)*h[\text{c}]:$$

$$y[\text{cc}] := y[\text{c}]: \quad V[\text{p}] := l[\text{p}]*b[\text{p}]*h[\text{p}]: \quad V[\text{bracing}] := 3.1416*l[\text{b}]*r[\text{b}]^2$$

$$V[\text{c}] := b[\text{c}]*h[\text{c}]*l[\text{c}]: \quad V[\text{cc}] := 3.1416*r[\text{cc}]^2*h[\text{c}]$$

KB :=

$$(2*V[\text{p}]*y[\text{p}]+2*V[\text{bracing}]*y[\text{bracing}]+4*V[\text{c}]*y[\text{c}]+2*V[\text{cc}]*y[\text{cc}])/(2*V[\text{p}]+2*V[\text{bracing}]+4*V[\text{c}]+2*V[\text{cc}]) \quad 8.199584183$$

BM:

$$I[\text{column}] := (1/12)*b[\text{c}]*l[\text{c}]^3+(22+(1/2)*l[\text{c}]^2*b[\text{c}]*l[\text{c}]:$$

$$I_{\text{cylindric}} := 3.1416 * r[\text{cc}]^4 * (1/4) + 3.1416 * (25.25 + (1/2) * r[\text{cc}])^2 * r[\text{cc}]^2:$$

$$I_{\text{semi}} := 4 * I_{\text{column}} + 2 * I_{\text{cylindric}}:$$

$$BM := I_{\text{semi}} / (\text{submp} + \text{submb} + \text{submwl}) \quad 9.924361106$$

KG:

$$y[\text{all}] := h[\text{p}] + (1/2) * h[\text{all}]: \quad y[\text{deck}] := h[\text{p}] + h[\text{all}] + (1/2) * h[\text{deck}]:$$

$$y[\text{derrick}] := (2/3) * h[\text{derrick}]$$

$$V[\text{call}] := l[\text{c}] * b[\text{c}] * h[\text{all}]: \quad V[\text{ccall}] := 3.1416 * r[\text{cc}]^2 * h[\text{all}]:$$

$$V[\text{derrick}] := (1/2) * t[\text{derrick}] * h[\text{derrick}] * b[\text{derrick}]:$$

$$V[\text{deck}] := h[\text{deck}] * l[\text{deck}] * b[\text{deck}]$$

KG :=

$$(2 * V[\text{p}] * y[\text{p}] + 2 * V[\text{bracing}] * y[\text{bracing}] + 4 * V[\text{call}] * y[\text{all}] + 2 * V[\text{ccall}] * y[\text{all}] + V[\text{deck}] * y[\text{deck}] + 4 * V[\text{derrick}] * y[\text{derrick}]) / (2 * V[\text{p}] + 2 * V[\text{bracing}] + 4 * V[\text{call}] + 2 * V[\text{ccall}] + V[\text{deck}] + 4 * V[\text{derrick}]) \quad 15.06690758$$

GM:

$$GM := KB + BM - KG \quad 3.05703771$$

With ice

KBice:

$$y[\text{cice}] := h[\text{p}] + (1/2) * h[\text{cice}]:$$

$$y[\text{ccice}] := y[\text{cice}]$$

$$V[\text{cice}] := b[\text{c}] * h[\text{cice}] * l[\text{c}]:$$

$$V[\text{ccice}] := 3.1416 * r[\text{cc}]^2 * h[\text{cice}]$$

KBice :=

$$(2 * V[\text{p}] * y[\text{p}] + 2 * V[\text{bracing}] * y[\text{bracing}] + 4 * V[\text{cice}] * y[\text{cice}] + 2 * V[\text{ccice}] * y[\text{ccice}]) / (2 * V[\text{p}] + 2 * V[\text{bracing}] + 4 * V[\text{cice}] + 2 * V[\text{ccice}]) \quad 8.825630683$$

BMice:

$$I_{\text{column}} := (1/12) * b[\text{c}] * l[\text{c}]^3 + (22 + (1/2) * l[\text{c}])^2 * b[\text{c}] * l[\text{c}]:$$

$$I_{\text{cylindric}} := 3.1416 * r[\text{cc}]^4 * (1/4) + 3.1416 * (25.25 + (1/2) * r[\text{cc}])^2 * r[\text{cc}]^2$$

$$I_{\text{semi}} := 4 * I_{\text{column}} + 2 * I_{\text{cylindric}}$$

$$BM_{\text{ice}} := I_{\text{semi}} / (\text{submp} + \text{submb} + \text{submwl}3) \quad 9.507671843$$

KGice:

New volumes for ice and snow:

$$V[\text{ice}] := m[\text{ice}] / \rho[\text{ice}]: \quad V[\text{snow}] := m[\text{snow}] / \rho[\text{snow}]:$$

$$V[\text{cwind}] := m[\text{cwind}] / \rho[\text{ice}]: \quad V[\text{cnowind}] := m[\text{cnowind}] / \rho[\text{ice}]:$$

$$V[\text{ccwind}] := m[\text{ccwind}] / \rho[\text{ice}]: \quad V[\text{ccnowind}] := m[\text{ccnowind}] / \rho[\text{ice}]:$$

$$V[\text{deckice}] := m[\text{deckice}] / \rho[\text{ice}]:$$

$$V[\text{snowupperdeck}] := m[\text{snowupperdeck}] / \rho[\text{snow}]:$$

$$V[\text{icederrick}] := m[\text{icederrick}] / \rho[\text{snow}]: \quad y[\text{derrick}] := (2/3) * h[\text{derrick}]:$$

Heights:

$$y[\text{cwind}] := h[\text{p}] + (1/2) * h[\text{all}]: \quad y[\text{cnowind}] := y[\text{cwind}]:$$

$$y[\text{ccwind}] := y[\text{cwind}]: \quad y[\text{ccnowind}] := y[\text{cwind}]$$

$$y[\text{deckice}] := h[\text{upperdeck}] + (1/2) * t[\text{ice}]:$$

$$y[\text{snowupperdeck}] := h[\text{upperdeck}] + (1/2) * t[\text{snow}]:$$

$$\text{KGice} := (2 * V[p] * y[p] + 2 * V[\text{bracing}] * y[\text{bracing}] + 4 * V[\text{call}] * y[\text{all}] + 2 * V[\text{ccall}] * y[\text{all}] + V[\text{deck}] * y[\text{deck}] + 4 * V[\text{derrick}] * y[\text{derrick}] + 2 * V[\text{cwind}] * y[\text{cwind}] + 2 * V[\text{cnowind}] * y[\text{cnowind}] + V[\text{ccwind}] * y[\text{ccwind}] + V[\text{ccnowind}] * y[\text{ccnowind}] + V[\text{deckice}] * y[\text{deckice}] + V[\text{snowupperdeck}] * y[\text{snowupperdeck}] + 4 * V[\text{icederrick}] * y[\text{derrick}]) / (2 * V[p] + 4 * V[\text{call}] + 2 * V[\text{ccall}] + V[\text{deck}] + 2 * V[\text{bracing}] + V[\text{ice}] + V[\text{snow}] + 4 * V[\text{icederrick}] + 4 * V[\text{derrick}])$$

15.89140477

GMice:

$$\text{GMice} := \text{KBice} + \text{BMice} - \text{KGice} \quad 2.44189776$$

Static heeling angle

No ice

Horizontal distance from the y-axis to KG

$$\begin{aligned} x[\text{cwind}] &:= 6.5 & x[\text{ccwind}] &:= x[\text{cwind}] & x[\text{pwind}] &:= x[\text{cwind}] \\ x[\text{cnowind}] &:= 63.5 & x[\text{ccnowind}] &:= x[\text{cnowind}] & x[\text{pnowind}] &:= x[\text{cnowind}]; \\ x[\text{bwind}] &:= 2.5 & x[\text{bnowind}] &:= 67.5 & x[\text{deck}] &:= 70 * (1/2) \end{aligned}$$

$$\text{KGtest} := (2 * V[c] * (x[\text{cwind}] + x[\text{cnowind}]) + V[\text{cc}] * (x[\text{ccwind}] + x[\text{ccnowind}]) + V[p] * (x[\text{pwind}] + x[\text{pnowind}]) + V[\text{deck}] * x[\text{deck}] + V[\text{bracing}] * (x[\text{bwind}] + x[\text{bnowind}]) + 4 * V[\text{derrick}] * x[\text{deck}]) / (4 * V[c] + 2 * V[\text{cc}] + 2 * V[p] + V[\text{deck}] + 2 * V[\text{bracing}] + 4 * V[\text{derrick}])$$

35.00000001

$$\arctan((35 - \text{KGtest}) / \text{GM}) * \text{evalf}(180 / (3.1416)) \quad -1.874221091 \cdot 10^{-7}$$

This means that the original heeling angle without the ice is ≈ 0 .

With ice

$$\begin{aligned} x[\text{deckice}] &:= (1/4) * b[\text{deck}] * (1/2): & x[\text{snowmaindeck}] &:= 70 * (1/2): \\ x[\text{snowupperdeck}] &:= 70 * (1/2): \end{aligned}$$

$$\text{KGtop} := 2 * V[c] * (x[\text{cwind}] + x[\text{cnowind}]) + V[\text{cc}] * (x[\text{ccwind}] + x[\text{ccnowind}]) + V[p] * (x[\text{pwind}] + x[\text{pnowind}]) + V[\text{deck}] * x[\text{deck}] + V[\text{bracing}] * (x[\text{bwind}] + x[\text{bnowind}]) + 2 * V[\text{cwind}] * x[\text{cwind}] + 2 * V[\text{cnowind}] * x[\text{cnowind}] + V[\text{ccwind}] * x[\text{ccwind}] + V[\text{ccnowind}] * x[\text{ccnowind}] + V[\text{deckice}] * x[\text{deckice}] + V[\text{snowupperdeck}] * x[\text{snowupperdeck}] + 4 * V[\text{derrick}] * x[\text{deck}] + 4 * V[\text{icederrick}] * x[\text{deck}]$$

KGbelow :=

$$4 * V[c] + 2 * V[\text{cc}] + 2 * V[p] + V[\text{deck}] + 2 * V[\text{bracing}] + V[\text{snow}] + V[\text{ice}] + 4 * V[\text{derrick}]$$

$$\text{KGnewice} := \text{KGtop} / \text{KGbelow} \quad 34.88604477$$

$$\text{KGnewice2} := 35 - \text{KGnewice} \quad 0.11395523$$

$$\arctan(\text{KGnewice2} / \text{GMice}) * \text{evalf}(180 / (3.1416)) \quad 2.671858373$$

Motion response

$$A[w] := l[p] * b[p]: \quad k := \rho[w] * g * A[w]$$

Calculating the heave added mass

g := 9.81: H[s] := 7: a := (1/2)*H[s]:
a1 := (1/2)*b[p]: b2 := (1/2)*I[p]
evalf(a1/b2) 0.1460674157

From the table from DNV, interpolation must be done between 0.1 and 0.2 (0.146)

C[A] := 1.98+(2.23-1.98)*(%-1)/(.-1) 2.095168539
A[R] := 3.1416*a1^2: A[33] := rho[w]*C[A]*A[R]:
m[added] := 2*A[33]*I[p] 5.073882822 10^7

Without ice:

T[heave] := evalf(2*Pi*sqrt((m[operating]+m[added])/k)) 17.22045850
omega[heave] := (2*3.1416)/T[heave]

With ice:

T[heaveice] := evalf(2*Pi*sqrt((m[total]+m[added])/k)) 17.37782505
omega[heaveice] := (2*3.1416)/T[heaveice]

From table of RAOs for heave motion a semi-submersible (Appendix C):

At T = 17.0 s: 0 degrees = 0.245 , 45 degrees = 0.241, 90 degrees = 0.137
At T = 18.0 s: 0 degrees = 0.131 , 45 degrees = 0.126, 90 degrees = 0.258

Heave motion at 0 degrees

RAO[heave0] := .245+(.131-.245)*(T[heave]-17)/(18-17) 0.219867731
RAO[heaveice0] := .245+(.131-.245)*(T[heaveice]-17)/(18-17) 0.201927944
u[heave0] := a*RAO[heave0]*sin(omega[heave]*t):
u[heaveice0] := a*RAO[heaveice0]*sin(omega[heaveice]*t)

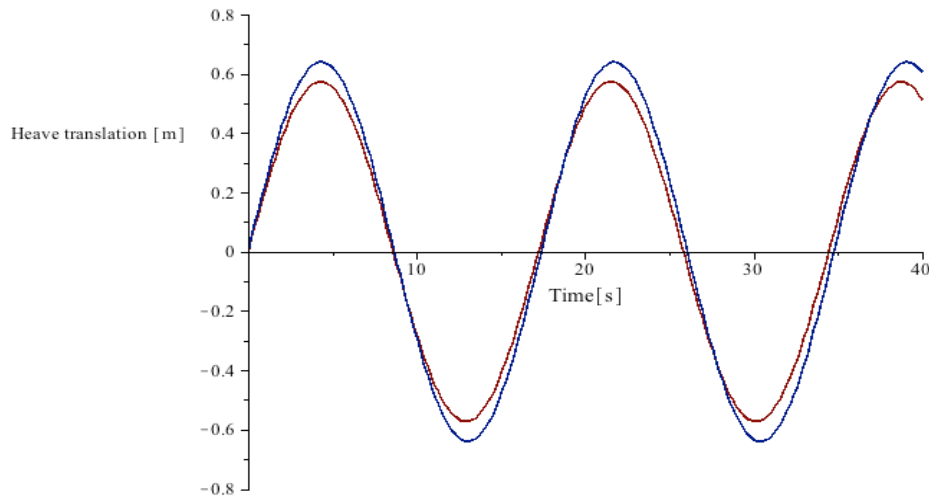
Heave motion at 45 degrees

RAO[heave45] := .241+(.126-.241)*(T[heave]-17)/(18-17) 0.215647272
RAO[heaveice45] := .241+(.126-.241)*(T[heaveice]-17)/(18-17) 0.197550119
u[heave45] := a*RAO[heave45]*sin(omega[heave]*t):
u[heaveice45] := a*RAO[heaveice45]*sin(omega[heaveice]*t):

Heave motion at 90 degrees

RAO[heave90] := .137+(.258-.137)*(T[heave]-17)/(18-17) 0.163675478
RAO[heaveice90] := .137+(.258-.137)*(T[heaveice]-17)/(18-17) 0.182716831

plot([a*RAO[heave90]*sin(omega[heave]*t),
a*RAO[heaveice90]*sin(omega[heaveice]*t)], t = 0 .. 40, y = -.8 .. .8)



Finding the maximum heave displacement without the ice:

```
diff(a*RAO[heave90]*sin(omega[heave]*t), t):
fsolve(%, t = 0 .. infinity)
heave.max = a*RAO[heave90]*sin(omega[heave]*%)
```

12.91531367
-0.5728641730

Finding the maximum heave displacement without the ice:

```
diff(a*RAO[heaveice90]*sin(omega[heaveice]*t), t):
fsolve(%, t = 0 .. infinity)
heave.max = a*RAO[heaveice90]*sin(omega[heaveice]*%)
```

13.03333831
-0.6395089085

Pitch added mass and period

Pitch added moment of inertia for a semi-submersible, A55:

```
A[55] := (1/12)*(3.1416*rho[w]*b[p]^2*(1/8))*l[p]^3
```

3.996319895 10⁹

GMpitch:

Due to the volume formulas for GM, the BM is the only one that changes, thus:

```
Icolumnpitch := (1/12)*b[c]^3*I[c]+32^2*b[c]*I[c]:
Icylindricpitch := 3.1416*r[cc]^4*(1/8)+3.1416*(4*r[cc]/(3*3.1416))^2*r[cc]^2
Isemipitch := 4*Icolumnpitch+4*Icylindricpitch:
BMpitch :=
Isemipitch/(2*l[p]*h[p]*b[p]+2*r[b]^2*I[b]+2*h[c]*(2*I[c]*b[c]+3.1416*r[cc]^2))
```

```
GMpitch := KB+BMpitch-KG
```

5.76221143

With ice

GMpitchice

```
BMpitchice := Isemipitch/submergedice
GMpitchice := KBice+BMpitchice-KGice
```

11.52585001
4.46007592

```
k[rpitch] := 9.81*GMpitch*rho[w]*(2*l[p]*h[p]*b[p]):
Inertia[pitchcolumns] := 2*rho[w]*h[p]*((1/12)*b[p]*I[p]^3):
omega[pitch] := sqrt(k[rpitch]/(Inertia[pitchcolumns]+A[55])):
```

```
T[pitch] := (2*3.1416)/omega[pitch]                                23.56140594
k[rpitchce] := 9.81*GMpitchce*rho[w]*(2*I[p]*h[p]*b[p]):
Inertia[pitchcolumnsize] := 2*rho[w]*h[p]*((1/12)*b[p]*I[p]^3)
omega[pitchce] := sqrt(k[rpitchce]/(Inertia[pitchcolumnsize]+A[55]));
```

```
T[pitchce] := (2*3.1416)/omega[pitchce]                            26.78086937
```

From table of RAOs for pitch motion a semi-submersible (Appendix C):

```
At T = 23.0 s:           0 degrees = 0.12 , 45 degrees = 0.073, 90 degrees = 0
At T = 24 s:           0 degrees = 0.098 , 45 degrees = 0.152, 90 degrees = 0
At T = 26 s:           0 degrees = 0.115 , 45 degrees = 0.111, 90 degrees = 0
At T = 27 s:           0 degrees = 0.108 , 45 degrees = 0.117, 90 degrees = 0
```

Pitch motion at 0 degrees

```
pitchangle0 := .12+(0.98e-1-.12)*(T[pitch]-23)/(24-23)           0.1076490693
pitchceangle0 := .115+(.108-.115)*(T[pitchce]-26)/(27-26)       0.1095339144
```

```
phi[pitchmax0] := evalf(3.1416*pitchangle0*(1/180)):
phi[pitchicemax0] := evalf(3.1416*pitchceangle0*(1/180))
```

```
phi[pitch0] := phi[pitchmax0]*sin(omega[pitch]*t):
phi[pitchce0] := phi[pitchicemax0]*sin(omega[pitchce]*t):
```

Pitch motion for 45 degrees

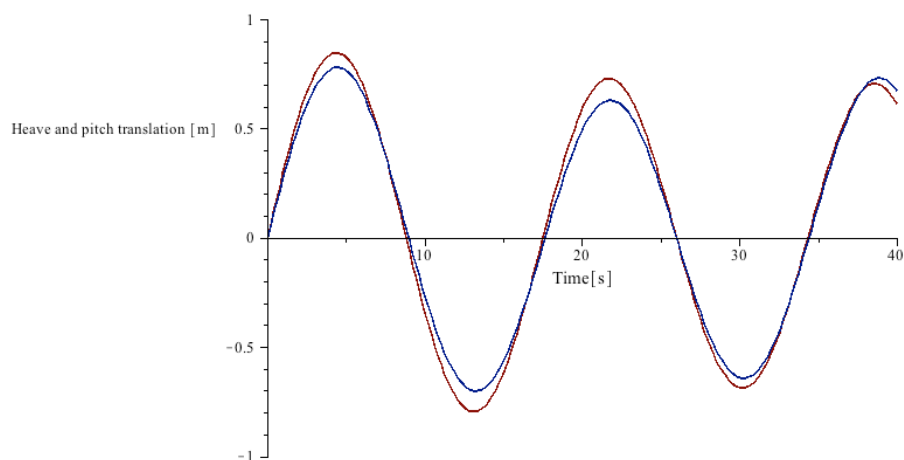
```
pitchangle45 := 0.73e-1+(.152-0.73e-1)*(T[pitch]-23)/(24-23)   0.117351069
pitchceangle45 := .111+(.117-.111)*(T[pitchce]-26)/(27-26)    0.1156852162
```

```
phi[pitchmax45] := evalf(3.1416*pitchangle45*(1/180)):
phi[pitchicemax45] := evalf(3.1416*pitchceangle45*(1/180))
```

```
phi[pitch45] := phi[pitchmax45]*sin(omega[pitch]*t):
phi[pitchce45] := phi[pitchicemax45]*sin(omega[pitchce]*t):
```

Coupled heave and pitch motion at 0 degrees

```
plot([u[pitch0]+u[heave0], u[pitchce0]+u[heaveice0]], t = 0 .. 40, y = -1 .. 1)
```



```
u[pitch0]+u[heave0]
0.08360816145 sin(0.2666733902 t) + 0.7695370585 sin(0.3648683338 t)
```

$$u[\text{pitchice0}] + u[\text{heaveice0}] \\ 0.08507207040 \sin(0.2346152365 t) + 0.7067478040 \sin(0.3615642339 t)$$

Finding the maximum pitch displacement without the ice:

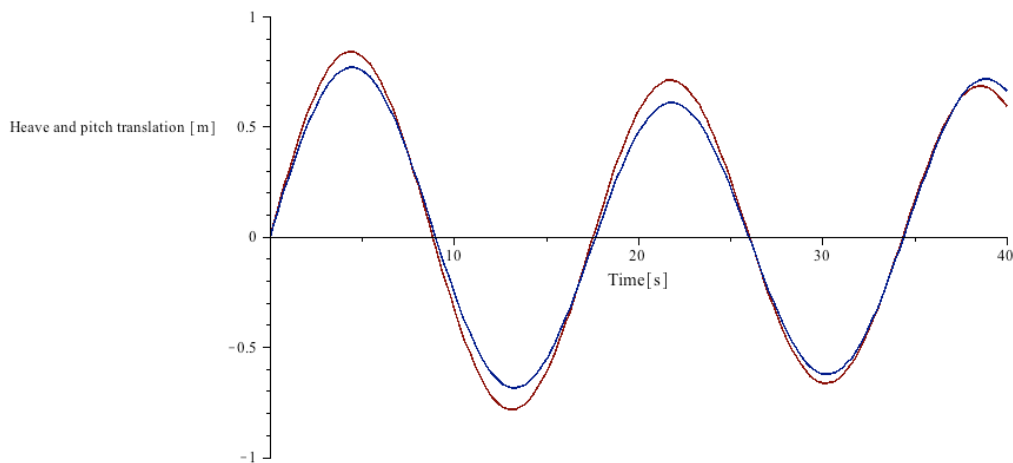
$$\begin{aligned} \text{diff}(u[\text{pitch0}] + u[\text{heave0}], t): \\ \text{fsolve}(\%, t = 0 \dots \text{infinity}) & 13.11941374 \\ 0.8360816145e-1 * \sin(.2666733902 * \%) + .7695370585 * \sin(.3648683338 * \%) & \\ & -0.7966228064 \end{aligned}$$

Finding the maximum pitch displacement with the ice:

$$\begin{aligned} \text{diff}(u[\text{pitchice0}] + u[\text{heaveice0}], t): \\ \text{fsolve}(\%, t = 0 \dots \text{infinity}) & 13.24946702 \\ 0.8507207040e-1 * \sin(.2346152365 * \%) + .7067478040 * \sin(.3615642339 * \%) & \\ & -0.7017785419 \end{aligned}$$

Coupled heave and pitch motion at 45 degrees

$$\text{plot}([u[\text{pitch45}] + u[\text{heave45}], u[\text{pitchice45}] + u[\text{heaveice45}]], t = 0 \dots 40, y = -1..1)$$



$$u[\text{pitch45}] + u[\text{heave45}] \\ 0.09114344590 \sin(0.2666733902 t) + 0.7547654520 \sin(0.3648683338 t)$$

$$u[\text{pitchice45}] + u[\text{heaveice45}] \\ 0.08984962250 \sin(0.2346152365 t) + 0.6914254165 \sin(0.3615642339 t)$$

Finding the maximum pitch displacement without the ice:

$$\begin{aligned} \text{diff}(u[\text{pitch45}] + u[\text{heave45}], t): \\ \text{fsolve}(\%, t = 0 \dots \text{infinity}) & 13.14170423 \\ \text{pitch.max} = \\ 0.9114344590e1 * \sin(.2666733902 * \%) + .7547654520 * \sin(.3648683338 * \%) & \\ & -0.7845509520 \end{aligned}$$

Finding the maximum pitch displacement without the ice:

$$\begin{aligned} \text{diff}(u[\text{pitchice45}] + u[\text{heaveice45}], t): \\ \text{fsolve}(\%, t = 0 \dots \text{infinity}) & 13.26673190 \\ \text{pitch.max} = \\ 0.8984962250e-1 * \sin(.2346152365 * \%) + .6914254165 * \sin(.3615642339 * \%) & \\ & -0.6863583727 \end{aligned}$$

Roll added mass and period

Roll added moment of inertia for a semi-submersible, A44:

$$A[44] := (1/12)*(3.1416*\rho[w]*l[p]^2*(1/8))*b[p]^3 \quad 5.837321194 \cdot 10^8$$

$$k[roll] := 9.81*GM*\rho[w]*(2*l[p]*h[p]*b[p]):$$

$$Inertia[rollcolumns] := 2*\rho[w]*h[p]*((1/12)*l[p]*b[p]^3+25.25^2*l[p]*b[p]):$$

$$\omega[roll] := \sqrt{k[roll]/(Inertia[rollcolumns]+A[44])}:$$

$$T[roll] := (2*3.1416)/\omega[roll] \quad 29.72798451$$

$$k[rollice] := 9.81*GM_{ice}*\rho[w]*(2*l[p]*h[p]*b[p]):$$

$$Inertia[rollcolumnsice] := 2*\rho[w]*h[p]*((1/12)*l[p]*b[p]^3+25.25^2*l[p]*b[p]):$$

$$\omega[rollice] := \sqrt{k[rollice]/(Inertia[rollcolumnsice]+A[44])}:$$

$$T[rollice] := (2*3.1416)/\omega[rollice] \quad 33.26228848$$

From table RAO tables for semi-submersible (Appendix C)

At T= 29 s : roll 0 degrees = 0, roll 45 degrees = 0.300, roll at 90 degrees = 0.17

At T= 30 s : roll 0 degrees = 0, roll 45 degrees = 0.335, roll at 90 degrees = 0.18

At T= 33 s : roll 0 degrees = 0, roll 45 degrees = 0.351, roll at 90 degrees = 0.22

At T= 34 s : roll 0 degrees = 0, roll 45 degrees = 0.365, roll at 90 degrees = 0.23

Roll motion for 45 degrees

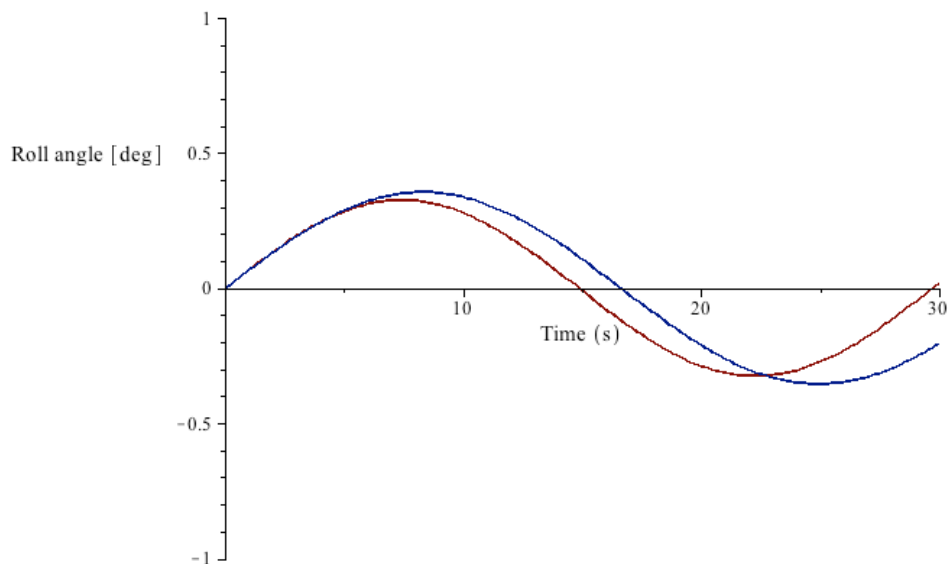
$$\text{rollangle45} := .300+(.335-.300)*(T[roll]-29)/(30-29) \quad 0.325479458$$

$$\text{rolliceangle45} := .351+(.365-.351)*(T[rollice]-33)/(34-33) \quad 0.3546720387$$

$$u[\text{roll45}] := \text{rollangle45}*\sin(\omega[\text{roll}]*t) \quad 0.325479458\sin(0.2113564072 t)$$

$$u[\text{rollice45}] := \text{rolliceangle45}*\sin(\omega[\text{rollice}]*t) \quad 0.3546720387\sin(0.1888986082t)$$

plot([u[roll45], u[rollice45]], t = 0 .. 30, y = -1 .. 1)



Finding the maximum roll angle without the ice:

$$\text{diff}(u[\text{roll45}], t) \quad 7.431978749$$

fsolve(%, t = 0 .. infinity):

$$\text{rollangle45}*\sin(\omega[\text{roll}]*) \quad 0.325479458$$

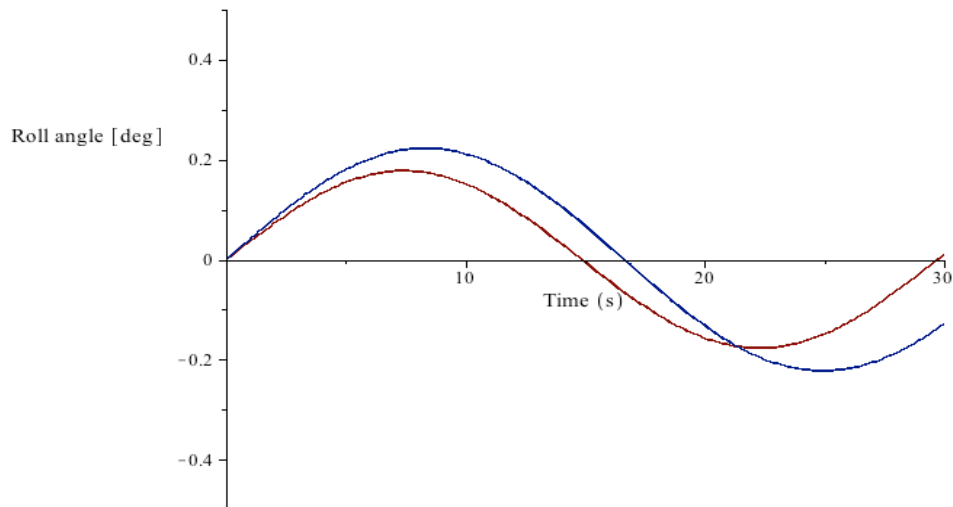
Finding the maximum roll angle without the ice:

```
diff(u[rollice45], t) 8.315552675
fsolve(% , t = 0 .. infinity):
rolliceangle45*sin(omega[rollice]*%) 0.3546720387
```

Roll motion at 90 degrees

```
rollangle90 := .17+(.18-.17)*(T[roll]-29)/(30-29) 0.1772798451
rolliceangle90 := .22+(.23-.22)*(T[rollice]-33)/(34-33) 0.2226228848

u[roll90] := rollangle90*sin(omega[roll]*t) 0.1772798451 sin(0.2113564072 t)
u[rollice90] := rolliceangle90*sin(omega[rollice]*t)
0.2226228848 sin(0.1888986082 t)
plot([u[roll90], u[rollice90]], t = 0 .. 30, y = -.5 .. .5)
```



Finding the maximum roll angle without the ice:

```
diff(u[roll90], t) 7.431978749
fsolve(% , t = 0 .. infinity):
pitch.max =rollangle90*sin(omega[roll]*%) 0.1772798451
```

Finding the maximum roll angle without the ice:

```
diff(u[rollice90], t) 8.315552675
fsolve(% , t = 0 .. infinity):
rolliceangle90*sin(omega[rollice]*%) 0.2226228848
```

The Parameter Study

In the parameter study the snow accumulation has been set constant at all horizontal surfaces with a value of 300 mm. The semi-submersible also has an extra loads of 100 mm of ice on the derrick. The thickness of sea-spray ice is the parameter that changes.

Parameters

```
t[snow] := .3
rho[w] := 1025:    rho[ice] := 700:    rho[snow] := 900:

b[deck] := 66:    l[deck] := 70:
```

Pontoon and bracings:

$$\begin{aligned} l[p] &:= 89: & b[p] &:= 13 & h[p] &:= 12.5: \\ l[b] &:= 44: & d[b] &:= 6 & r[b] &:= (1/2)*d[b] \end{aligned}$$

Columns:

$$l[c] := 10: \quad b[c] := 10.4:$$

Cylindrical columns:

$$d[cc] := 6.5: \quad r[cc] := (1/2)*d[cc]:$$

Deck:

$$l[deck] := 70: \quad b[deck] := 66:$$

Heights:

$$h[all] := 21: \quad h[maindeck] := 33.5: \quad h[upperdeck] := h[p]+h[all]+6:$$

$$h[derrick] := 69: \quad b[derrick] := 14.3: \quad t[derrick] := 0.4:$$

Masses:

$$m[operating] := 3.665*10^7:$$

Sea-spray ice

$$\begin{aligned} m[cwind] &:= \rho[ice]*((l[c]+t[ice])*(b[c]+t[ice])-l[c]*b[c]): \\ m[cnowind] &:= \rho[ice]*((l[c]+.5*t[ice])*(b[c]+.5*t[ice])-l[c]*b[c]): \\ m[ccwind] &:= \rho[ice]*(3.1416*(r[cc]+t[ice])^2-(3.1416*(1/4))*r[cc]^2): \\ m[ccnowind] &:= \rho[ice]*(3.1416*(r[cc]+.5*t[ice])^2-(3.1416*(1/4))*r[cc]^2): \\ m[deckice] &:= (1/4)*b[deck]*l[deck]*t[ice]*\rho[ice]: \end{aligned}$$

Snow

$$\begin{aligned} m[snowupperdeck] &:= t[snow]*\rho[snow]*b[deck]*l[deck]: \\ m[icederrick] &:= (1/2)*\rho[snow]*(14.3*69)*.1 \end{aligned}$$

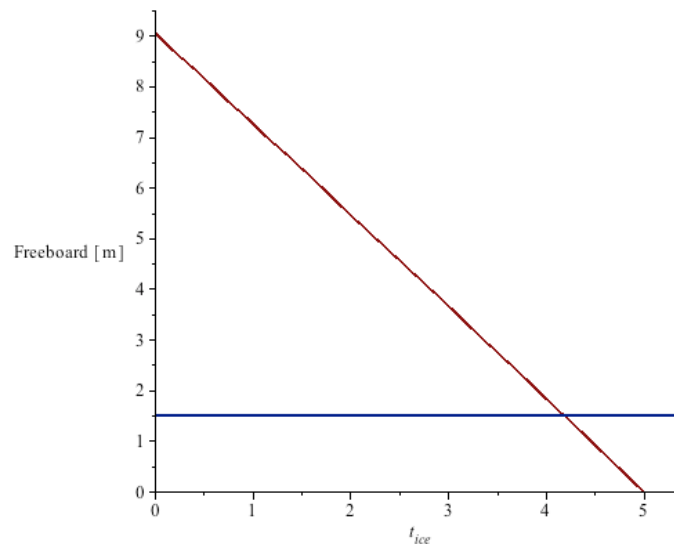
Total mass

$$\begin{aligned} m[ice] &:= 2*m[cwind]+2*m[cnowind]+m[ccwind]+m[ccnowind]+m[deckice]: \\ m[snow] &:= m[snowupperdeck]+4*m[icederrick]: \\ m[total] &:= m[operating]+m[ice]+m[snow]: \end{aligned}$$

Freeboard

$$\begin{aligned} \text{submb} &:= 3.1416*l[b]*r[b]^2*2: & \text{submp} &:= 2*l[p]*b[p]*h[p] \\ \text{submwl} &:= h[cice]*(4*l[c]*b[c]+2*r[cc]^2*3.1416) \\ \text{subm.vol} &:= \text{submp}+\text{submb}+\text{submwl} \\ \text{subm.vol} &= m[total]/\rho[w]: \\ \text{solve}(\%, h[cice]): \\ h[cice] &:= \% \\ d[ice] &:= h[cice]+h[p] \\ \text{freeboard} &:= h[maindeck]-d[ice] \end{aligned}$$

$$\text{plot}([\text{freeboard}, 1.5], t[ice] = 0 .. 5.4, y = 0 .. 9.5)$$



$$f[\text{limit}] = \text{fsolve}(\text{freeboard} = 1.5, t[\text{ice}] = 0 \dots 15)$$

4.183395259

Initial stability, GM

KB

$$\begin{aligned} y[p] &:= (1/2) * h[p]: & y[\text{bracing}] &:= h[p] + (1/2) * d[b] \\ y[c] &:= h[p] + (1/2) * h[\text{cice}]: & y[\text{cc}] &:= y[c]: \\ y[\text{cice}] &:= h[p] + (1/2) * h[\text{cice}]: & y[\text{ccice}] &:= y[\text{cice}]: \end{aligned}$$

$$\begin{aligned} V[p] &:= l[p] * b[p] * h[p]: & V[\text{bracing}] &:= 3.1416 * l[b] * r[b]^2 \\ V[c] &:= b[c] * h[\text{cice}] * l[c]: & V[\text{cc}] &:= 3.1416 * r[\text{cc}]^2 * h[\text{cice}]: \\ V[\text{cice}] &:= b[c] * h[\text{cice}] * l[c]: & V[\text{ccice}] &:= 3.1416 * r[\text{cc}]^2 * h[\text{cice}]: \end{aligned}$$

KB :=

$$(2 * V[p] * y[p] + 2 * V[\text{bracing}] * y[\text{bracing}] + 4 * V[\text{cice}] * y[\text{cice}] + 2 * V[\text{ccice}] * y[\text{ccice}]) / (2 * V[p] + 2 * V[\text{bracing}] + 4 * V[\text{cice}] + 2 * V[\text{ccice}]):$$

BM:

$$\begin{aligned} I_{\text{column}} &:= (1/12) * b[c] * l[c]^3 + (22 + (1/2) * l[c])^2 * b[c] * l[c]: \\ I_{\text{cylindric}} &:= 3.1416 * r[\text{cc}]^4 * (1/4) + 3.1416 * (25.25 + (1/2) * r[\text{cc}])^2 * r[\text{cc}]^2: \\ I_{\text{semi}} &:= 4 * I_{\text{column}} + 2 * I_{\text{cylindric}} \end{aligned}$$

$$BM := I_{\text{semi}} / (\text{submp} + \text{submb} + \text{submwl}):$$

KG:

$$\begin{aligned} V[\text{call}] &:= l[c] * b[c] * h[\text{all}]: & V[\text{ccall}] &:= 3.1416 * r[\text{cc}]^2 * h[\text{all}] \\ V[\text{deck}] &:= h[\text{deck}] * l[\text{deck}] * b[\text{deck}]: \end{aligned}$$

$$V[\text{derrick}] := (1/2) * t[\text{derrick}] * h[\text{derrick}] * b[\text{derrick}]:$$

Volumes of ice and snow on elements:

$$\begin{aligned} V[\text{ice}] &:= m[\text{ice}] / \rho[\text{ice}]: & V[\text{snow}] &:= m[\text{snow}] / \rho[\text{snow}]: \\ V[\text{cwind}] &:= m[\text{cwind}] / \rho[\text{ice}]: & V[\text{cnwind}] &:= m[\text{cnwind}] / \rho[\text{ice}]: \end{aligned}$$

$V[\text{ccwind}] := m[\text{ccwind}]/\rho[\text{ice}]$; $V[\text{cnowind}] := m[\text{cnowind}]/\rho[\text{ice}]$;
 $V[\text{deckice}] := m[\text{deckice}]/\rho[\text{ice}]$;
 $V[\text{snowupperdeck}] := m[\text{snowupperdeck}]/\rho[\text{snow}]$;
 $V[\text{icederrick}] := m[\text{icederrick}]/\rho[\text{snow}]$

Heights:

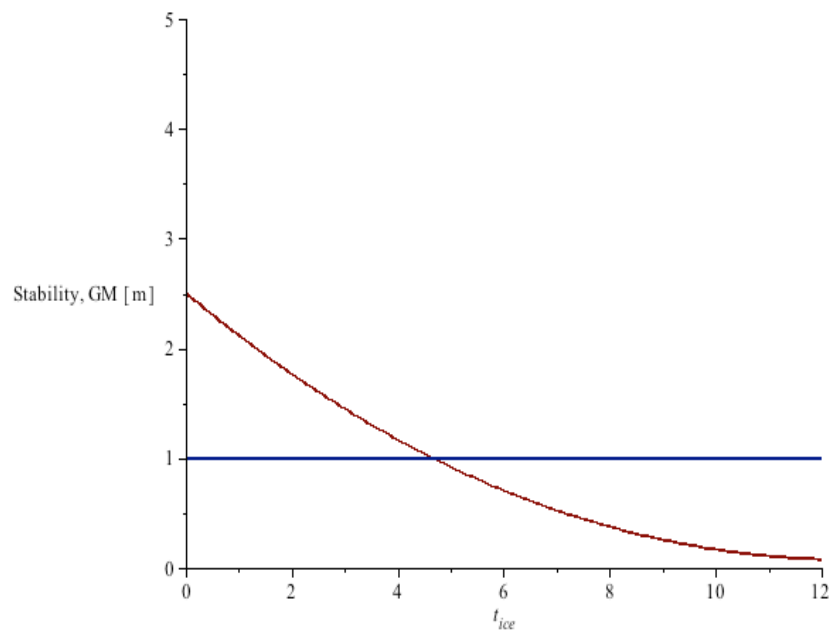
$y[\text{all}] := h[\text{p}] + (1/2) * h[\text{all}]$; $y[\text{deck}] := h[\text{p}] + h[\text{all}] + (1/2) * h[\text{deck}]$
 $y[\text{cwind}] := h[\text{p}] + (1/2) * h[\text{all}]$; $y[\text{cnowind}] := y[\text{cwind}]$;
 $y[\text{ccwind}] := y[\text{cwind}]$; $y[\text{ccnowind}] := y[\text{cwind}]$;
 $y[\text{deckice}] := h[\text{upperdeck}] + (1/2) * t[\text{ice}]$
 $y[\text{snowupperdeck}] := h[\text{upperdeck}] + (1/2) * t[\text{snow}]$; $y[\text{derrick}] := (2/3) * h[\text{derrick}]$:

KG :=

$(2 * V[\text{p}] * y[\text{p}] + 2 * V[\text{bracing}] * y[\text{bracing}] + 4 * V[\text{call}] * y[\text{all}] + 2 * V[\text{ccall}] * y[\text{all}] + V[\text{deck}] * y[\text{deck}] + 4 * V[\text{icederrick}] * y[\text{derrick}] + 4 * V[\text{derrick}] * y[\text{derrick}] + 2 * V[\text{cwind}] * y[\text{cwind}] + 2 * V[\text{cnowind}] * y[\text{cnowind}] + V[\text{ccwind}] * y[\text{ccwind}] + V[\text{ccnowind}] * y[\text{ccnowind}] + V[\text{deckice}] * y[\text{deckice}] + V[\text{snowupperdeck}] * y[\text{snowupperdeck}]) / (2 * V[\text{p}] + 4 * V[\text{call}] + 2 * V[\text{ccall}] + V[\text{deck}] + 2 * V[\text{bracing}] + V[\text{ice}] + V[\text{snow}] + 4 * V[\text{icederrick}] + 4 * V[\text{derrick}]$:

GM := KB + BM - KG:

plot([GM, 1], t[ice] = 0 .. 12, y = 0 .. 5)



GMlimit = fsolve(GM = 1.0, t[ice] = 0 .. 13)

4.666220238

Static heeling angle

$x[\text{deckice}] := (1/4) * b[\text{deck}] * (1/2)$; $x[\text{snowmaindeck}] := 70 * (1/2)$;
 $x[\text{snowupperdeck}] := 70 * (1/2)$; $x[\text{cwind}] := 6.5$;
 $x[\text{ccwind}] := x[\text{cwind}]$; $x[\text{pwind}] := x[\text{cwind}]$;
 $x[\text{cnowind}] := 63.5$; $x[\text{ccnowind}] := x[\text{cnowind}]$

$x[\text{pnowind}] := x[\text{cnowind}]$
 $x[\text{deck}] := 70 \cdot (1/2)$

$x[\text{bwind}] := 2.5$; $x[\text{bnowind}] := 67.5$:

$\text{KGtop} :=$

$2 \cdot V[\text{c}] \cdot (x[\text{cwind}] + x[\text{cnowind}]) + V[\text{cc}] \cdot (x[\text{ccwind}] + x[\text{ccnowind}]) + V[\text{p}] \cdot (x[\text{pwind}] + x[\text{pnowind}]) + V[\text{deck}] \cdot x[\text{deck}] + V[\text{bracing}] \cdot (x[\text{bwind}] + x[\text{bnowind}]) + 2 \cdot V[\text{cwind}] \cdot x[\text{cwind}] + 2 \cdot V[\text{cnowind}] \cdot x[\text{cnowind}] + V[\text{ccwind}] \cdot x[\text{ccwind}] + V[\text{ccnowind}] \cdot x[\text{ccnowind}] + V[\text{deckice}] \cdot x[\text{deckice}] + V[\text{snowupperdeck}] \cdot x[\text{snowupperdeck}] + 4 \cdot V[\text{derrick}] \cdot x[\text{deck}] + 4 \cdot V[\text{icederrick}] \cdot x[\text{deck}]$:

$\text{KGbelow} :=$

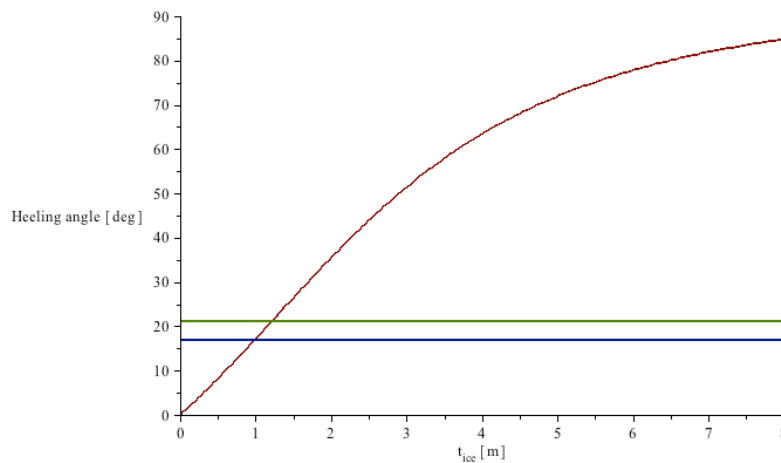
$4 \cdot V[\text{c}] + 2 \cdot V[\text{cc}] + 2 \cdot V[\text{p}] + V[\text{deck}] + 2 \cdot V[\text{bracing}] + V[\text{snow}] + V[\text{ice}] + 4 \cdot V[\text{derrick}]$:

$\text{KGnewice} := \text{KGtop} / \text{KGbelow}$:

$\text{KGnewice2} := 35 - \text{KGnewice}$

$\text{heel} := \arctan(\text{KGnewice2} / \text{GM}) \cdot \text{evalf}(180 / (3.1416))$

$\text{plot}([\text{heel}(t[\text{ice}]), 17], t[\text{ice}] = 0 \dots 6, y = 0 \dots 110)$



$\text{fsolve}(\text{heel} = 21, t[\text{ice}] = 0 \dots 4)$

1.206988726

$\text{fsolve}(\text{heel} = 17, t[\text{ice}] = 0 \dots 4)$

0.9901213000

$\text{fsolve}(\text{heel} = 8, t[\text{ice}] = 0 \dots 4)$

0.4861945574